LIST OF ERRORS

Page	Line	Errata	Corrections
(viii)	1	Frustrum	Frustum
(x)	penultimate	were	was
1.1	15	Couchy	Cauchy
1.2	14	.., the lateral ... resultants are ...	..., the effect of lateral ... resultants on Strain Energy is ...
1.2	15	∴ neglected	... neglected (see last paragraph of page 1.10).
1.4	11	$= \delta\{e\}(...$	$= \delta\{e\}^T(...$
1.10	1	Fig. 3.5	Fig. 3.15
1.10	19	sheer	shear
Ref.Ch.1	Ref.11	23427	1,2342-7
Ref.Ch.1	Ref.13	Revolution".	Revolution",
Ref.Ch.1	Ref.16	Ergatudis	Ergatoudis
2.2	7	Fig. 1	Fig. 2.1
2.5	last	$...) + \frac{w}{R_1}$	$...)v + \frac{w}{R_1}$
2.6	1	$\frac{\partial R_1}{\partial \alpha} = 0$	$\frac{\partial R_1}{\partial \theta} = 0$
2.7	13	Fig. 12	Fig. 2.12
Ref.Ch.2	Ref.1	Procedures ... - Petterson	Proceedings ... - Patterson
3.3	19	$...)_i(\xi)\}$	$...)_i N_i'(\xi)\}$
3.6	3,7	$S_{N/2}$	$S_N/2$
3.7	penultimate	deformation	deformations
3.11	penultimate	3.3.4). There	3.3.4), there
3.12	16	length T	length {T}
3.13	20	depecited	depicted
3.14	18	fulfill	fulfil
3.17	8	ot	to
3.18	20	are	is
3.19	12	anomoly	anomaly
3.20	14	$\therefore \{\varepsilon\}^{\ell}...$	$\therefore \{\varepsilon_j\}^{\ell}...$

Page	Line	Errata	Corrections
3.22	10	... ω ...	... ω^2 ...
3.25	10	programme	program
3.26	25	to be	are
3.26	26	Fig. 3.2.5(a) and (b)	Fig. 3.25(a) and (b)
3.27	20	is	has
3.29	7	Storme	Strome
3.30	15	Kalanin	Kalnins
3.30	16	Liopins	Liepins
4.1	10	is resulted	results
4.4	18	i,j>1	$i,j \geq 1$
4.9	18	orthohopic	orthotropic
4.9	24	Et	$E_2 t$
4.10	3	are	is
4.11	15	r=-pcos	r=pcos
4.12	1	... $N_w[rRd\theta d_s]$	... $N_w[rRd\theta ds])$
4.17	18	Matrix B	Matrix $[B]$
4.25	12	Razzague	Razzaque
4.29	17	were	was
4.29	26	shown	shows
4.31	14	were	was
5.3	6	$[N_p]$	$[N_p]^T$
5.5	14	neglible	negligible
5.9	13	5.2	5.4
5.9	last	5.4	5.2
5.13	22	n>2	$n \geq 2$
5.15	2	Schnobirch	Schnobrich
Ref.Ch.5	Ref.19	Schnobirch	Schnobrich
6.10	5	Matrix K_σ	Matrix $[K_\sigma]$
7.4	2	frustrum	frustum

Page	Line	Errata	Corrections
7.7	22	$-\frac{\pi}{2} < \theta < \frac{\pi}{2}$	$-\frac{\pi}{2} \leq \theta \leq \frac{\pi}{2}$
7.9	3	reasonably	reasonable
9.7	17	0.1 p 100	$0.1 \leq p \leq 100.$
10.4	21	indicate	indicates

Fig. 3.11 should be labelled (a), (b), (c) and (d) respectively

Fig. 3.34 in Fig. 3.34(b), ϕ = ... should be altered to $\Delta\phi_i$ = ...

Fig. 3.35 in Fig. 3.35(b), ϕ = ... should be altered to $\Delta\phi_i$ = ...

Fig 5.5 $a = 6.0$ should be altered to $a = 10.0$

Fig. 5.10 in the graph, the value of m=2 should be altered to m=3

Fig. 5.11 vertical axis should read f Hz

Fig. 5.13 vertical axis should read Frequency Hz

Fig. 6.6 First table, line 4 : 115.% should be 11.5%

Fig. 6.13 On the sketch, positions of T_s and $T_{s\theta}$ should be interchanged

RÔLE OF THE CURVED PARAMETRIC ELEMENT IN LINEAR ANALYSIS OF THIN ROTATIONAL SHELLS

by

R. Delpak

Thesis presented in fulfilment of the requirement for the Degree of Doctor of Philosophy, Council for National Academic Awards, London, 1975.

Department of Civil Engineering and Building,
The Polytechnic of Wales, December 1975.

CERTIFICATION OF RESEARCH

This is to certify that, except when specific reference to other investigations is made, the work described in this Dissertation is the result of the investigation of the candidate.

R. Delpak
(Candidate)

(Director of Studies)

30.12.1975
(Date)

14.2.76
(Date)

B. W. Pace
(Supervisor)

30/12/75
(Date)

DECLARATION

This is to certify that neither this thesis, nor any part of it, has been presented, or is being currently submitted, in candidature for any degree at any other university.

R. Delpak.

(Candidate)

ACKNOWLEDGEMENTS

The author wishes to acknowledge the efforts of Professor O.C. Zienkiewicz, his director of studies and Mr. B.W. Preece, his supervisor for their many valuable suggestions and in checking the manuscript.

He is thankful to Professor B.M. Irons for his guidance and advice both in fundamental matters and in details pertaining to numerical work.

He is appreciative of Mr. R.D. McMurray, his Head of Department, for his encouragement and making all possible departmental facilities available for this candidature.

The cooperation of the staff of the Computer Centres at the Polytechnic of Wales, University College of Swansea and the Mid-Glamorgan County is acknowledged.

He is also thankful to Miss B.M. Miles to have typed a difficult script.

CONTENTS

PART III

SOME EXPERIMENTAL VERIFICATION OF THE LINEAR SHELL THEORY

PART IV

THE INFLUENCE OF INPLANE LOADS

SUMMARY

The candidate's previous research had been in developing a linear and a curved parametric element applied to axisymmetric oscillations of thin shells of revolution.

The current scheme was confined to applying the above curved parametric element to the axisymmetric static case and was then developed to static analysis with any harmonic variation of loading.

The vibration program was also extended to estimate the natural frequency of undamped systems with any number of diametral nodes.

The general strain-displacement relationships from the original derivations were taken and simplified in order to explore their use in the present work independently of other available sources. The above relationships were then applied to codify the buckling problem, arising generally from compression or shear inplane resultants.

Some perspex models in the shape of a cooling Tower were formed and tested in order to verify the existence of any correlation between theoretical and experimental results. These tests covered linear, small displacement response of the model for both static and dynamic cases.

Finally the influence of the inplane stress resultants on the behaviour of axisymmetric shells was investigated and some numerical examples for simple cases were attempted.

NOTATION

a	Radial measure in a shell of revolution, inner radius in an annulus.
[A],A	General matrix, radius of curvature, area.
dA	Elemental area.
b	Outer radius.
B	Basic function, radius of curvature.
[B]	Differential operator in matrix form producing strains from nodal variables.
c,C	Constant of integration, curvature, general constant.
[D]	Elastic matrix.
$\mathcal{D}$	Elastic constant in moment/curvature relationship.
e,{e}	Naperian base, displacement.
E	Young's Modulus.
f	Function, Frequency.
F	Force.
g	Gravitational acceleration.
G	Shear Modulus.
[G]	Differential Operator in matrix form producing rotations from nodal variables.
h	Height.
H	Hermitian polynomials.
i	Imaginary number, dummy suffix.
j	Dummy suffix.
J	Bessel Function.
k	General constant, dummy suffix.
[K]	Stiffness matrix.
ℓ	Dummy suffix, suffix to indicate local coordinates.
L	Length, lower triangle in a Choleski reduction.
m, [dm]	Mass, elemental mass, number of meridional waves, mode.

M	Moment.
n	Dummy suffix, number of circumferential waves.
$[N]$	Shape function, matrix operator producing displacements from nodal variables.
o	Origin.
p	Distributed pressure, angular frequency of a travelling wave or a rotating surface.
{P}	Force vector.
q	Dimensionless variable related to buckling pressures or loads.
Q	Torque.
r	General radius, variable in the radial direction, ring load along R-axis.
R	Radial axis in cylindrical coordinates.
s	Curve length of the generator.
t	Thickness, time.
T,{T}	Transpose,kinetic energy, stress resultant.
u,{u}	Displacement along the Z-axis.
U	Upper triangle in a Choleski reduction, strain energy.
v,{v}	Displacement along the circumference, velocity.
w	Displacement in the radial direction.
W	Potential energy, work done.
{x}	General variable.
{z}	Vector used in a Choleski reduction $\{z\} = [U]\{\delta\}$.
Z	Axis of symmetry in cylindrical coordinates.
α	Angle between the tangent and the Z-axis.
β	Wave parameter along the shell generator, dimensionless variable related to plate buckling pressure.
γ	Constant involved in integration which could assume values of 2π or π.
$\{\delta\},\delta$	Displacement, Kronecker's delta.
$\{\varepsilon\}$	Strain.

θ	Circumferential angle.
Θ	Nodal rotations.
λ	Wave parameter along the shell generator, eigen-root.
ν	Poisson's ratio.
ξ	Parametric variable relating the parent element and the shell.
π	Circular constant.
ρ	Density.
σ,τ	Stress.
ϕ	Functional.
χ	Change in curvature.
$\{\psi\}$	Pseudo momentum term.
ω	Angular frequency.

PART I

STATIC ANALYSIS

CHAPTER 1

GENERAL CONCEPTS

1.1 Historical

Curved surfaces and shells of revolution have been favoured for structural purposes since ancient times. Aesthetic appearance together with the astonishing strength found through practice, encouraged the ancient engineers to create the historical structures that are widely scattered in Europe and Asia.

The development of the Elastic Shell Theory has proceeded in parallel with the evolution of the Theory of Elasticity by dedicated engineer-mathematicians. Different schools of thought were established in Britain, France, Germany, Russia, Switzerland and other European Faculties of Applied Mathematics and Applied Science. Among the early workers in this field one could recall the efforts of Kirchhoff, Lord Rayleigh, Lamé, Cauchy, Reissner and Love.

1.2 The Functional Approach

The analytical methods of determining the elastic stresses and deformations in a shell of revolution under a given set of loads have been extensively studied and perfected with mathematical elegance for simple shapes[1],[2],[3]. The finite difference[4] and the finite element [5] methods have also been applied in recent times for determining the above unknowns. The numerical method adopted in this text will be that of finite elements, introducing some developments with shape functions[6]. In the mathematical theory of shells, irrespective of the manner of solution, there are certain sets of relationships that have to

be devised.

a) The differential equation of equilibrium of an element of the shell is written down in terms of the stress resultants and the load components, e.g. gravity, pressure etc. In the case of the membrane shells, the three equations of equilibrium in the tangential, circumferential and normal directions, provide a unique solution for the stress resultants T_s, T_θ and $T_{s\theta}$ and subsequently yield the corresponding membrane displacements u, v and w. This is known as the primary or the statically determinate system. When considering the bending theory, two more equations of equilibrium about the tangential and circumferential axes provide the moments M_s, M_θ and $M_{s\theta}$. For thin shells of revolution, the effect of lateral shear resultants on Strain Energy are normally neglected. (see last paragraph of Page 1.10) The equation of equilibrium about the normal axis does not provide fresh information but merely expresses the equality of the complementary shear resultants.

b) Since the number of variables in the bending case exceeds the number of independent equations, there becomes a need for obtaining further information with the aid of compatibility conditions. This is achieved by relating the six strain components (three inplane strains and three curvatures) to displacements u, v and w. The use of these kinematic relationships is not confined to the mathematical theory for they play a pivotal role in the finite element approach. As a result of this an entire part of the text (Chapter 2) is devoted to their derivation and appreciation.

c) The two sets of equations discussed in a) and b), apparently unconnected, are then married through Hookean relationships. These equations express a linearised stress-strain (and moment-curvature) behaviour by the constituent material of the shell.

d) The above sets of equations are then subjected to a process of differentiation and elimination in order to arrive at the governing differential equation of the shell. The small order quantities are withdrawn in this process to enable a clearer and a relatively simpler final analysis.

The popular manner of solving the governing equation is to obtain a solution (where possible) for a discrete loading such as an edge ring-moment or a ring-force and thus evaluate the resulting displacements. The shell is then analysed with membrane action only, determining the primary (membrane) stresses and displacements. If this does not result in a satisfactory set of boundary conditions, then a corrective set of edge moments and forces are applied. The final stresses and displacements would result from a unique combination of the primary and the corrective systems[7].

1.3 The Finite Element Approach

In this section the virtual work derivation is adopted; for an alternative statement, reference (8) may be consulted. The nomenclature used is due to Zienkiewicz.

Let $\{e\}$ be any parameter, if the displacement is represented as,

$$\{u\} = [N]\{e\} , \qquad \ldots\ldots \text{ eqn. 1.1}$$

then the virtual displacement is given by,

$$\delta\{u\} = [N]\delta\{e\} , \qquad \ldots\ldots \text{ eqn. 1.2(a)}$$

and

$$\delta\{u\}^T = \delta\{e\}^T[N]^T. \qquad \ldots\ldots \text{ eqn. 1.2(b)}$$

The virtual work done externally by the 'body forces' $\{p\}$ and by the traction $\{F\}$ are given by the volume and the surface integrals below,

$$(\text{Work Done})_{ext} = \int_V \delta\{u\}^T\{p\}d(vol) + \int_S \delta\{u\}^T\{F\}d(surf),$$

$$(\text{Work Done})_{ext} = \delta\{e\}^T\left(\int_V [N]^T\{p\}d(vol) + \int_S [N]^T\{F\}d(surf) \right).$$

Similar to the displacements, the strains are represented in a familiar form by,

$$\{\varepsilon\} = [B]\{e\}, \qquad \ldots\ldots \text{ eqn. 1.3}$$

the virtual strains are then given by,

$$\delta\{\varepsilon\} = [B]\delta\{e\}, \qquad \ldots\ldots \text{ eqn. 1.3(a)}$$

and

$$\delta\{\varepsilon\}^T = \delta\{e\}^T[B]^T . \qquad \ldots\ldots \text{ eqn. 1.3(b)}$$

The stresses follow from Hooke's law, namely,

$$\{\sigma\} = [D]\{\varepsilon\} \qquad \ldots\ldots \text{ eqn. 1.4(a)}$$

$$\{\sigma\} = [D][B]\{e\}. \qquad \ldots\ldots \text{ eqn. 1.4(b)}$$

The virtual work done internally by the stresses on the virtual strains $\delta\{e\}$ is estimated from the integral given below,

$$(\text{Work Done})_{int} = \int_V \delta\{\varepsilon\}^T\{\sigma\}d(vol)$$

$$= \int_V (\lfloor B \rfloor \delta\{e\})^T . (\lfloor D \rfloor \lfloor B \rfloor \{e\}) d(vol)$$

$$(\text{Work Done})_{int} = \delta\{e\}^T \int_V \lfloor B \rfloor^T \lfloor D \rfloor \lfloor B \rfloor d(vol)\ \{e\}.$$

For equilibrium it necessitates that,

$$(\text{Work Done})_{int} - (\text{Work Done})_{ext} = 0 \qquad \ldots\ldots \text{ eqn. 1.5}$$

$$\delta\{e\}^T \left[\int_V \lfloor B \rfloor^T \lfloor D \rfloor \lfloor B \rfloor d(vol)\{e\} - \int_V \lfloor N \rfloor^T \{p\} d(vol) - \int_S \lfloor N \rfloor^T \{F\} d(surf) \right] = 0,$$

which is valid for any $\delta\{e\}^T$. It then follows that the expression in the square brackets must be zero. Upon comparison with the familiar expression,

$$\lfloor K \rfloor \{e\} = \{P\}, \qquad \ldots\ldots \text{ eqn. 1.6(a)}$$

or

$$\lfloor K \rfloor \{e\} - \{P\} = 0, \qquad \ldots\ldots \text{ eqn. 1.6(b)}$$

it can be seen that,

$$\lfloor K \rfloor = \int_V \lfloor B \rfloor^T \lfloor D \rfloor \lfloor B \rfloor d(vol), \qquad \ldots\ldots \text{ eqn. 1.7}$$

and

$$\{P\} = \int_V \lfloor N \rfloor^T \{p\} d(vol) + \int_S \lfloor N \rfloor^T \{F\} d(surf) \qquad \ldots\ldots \text{ eqn. 1.8}$$

The displacement $\{e\}$ is determined by solving eqn. 1.6(a) which is symbolically represented in the familiar notation of,

$$\{e\} = \lfloor K \rfloor^{-1} \{P\} .$$

These displacements indicate the formed pattern of the structure at the selected (nodal) points. The deformations, strains and stresses elsewhere may be calculated using equations 1.1, 1.3 and 1.4.

1.4 Terms and Definitions

With the increased subtlety in mathematical formulation of the recent elements, the understanding of the differences and merits of the existing elements is advantageous. In view of this and the review presented in the next section, it was thought appropriate to outline some of the relevant terminology. It is also hoped that the structures depicted in Figures 1.1(a)* and 1.1(b) would contribute towards the visualisation of certain aspects of the finite elements as applied to curved shells.

1. If the nodes were no longer regarded as the contact points of two or more elements but were associated more generally with degrees of freedom, it would then be possible to think of internal (or hierarchical) nodes which could be completely severed from the outside boundary of the element.

2. A straight element would appear as a truncated cone since the generator is a straight line.

3. A curved element would appear similar to that in 2 with the generator curved, i.e. a surface of revolution is 'sandwiched' between two planes with the axis of revolution perpendicular to both.

4. If continuity of slopes can be maintained at the junction of two elements before and after the application of the load then the elements are known as conforming; otherwise they are known as non-conforming.

---

* Figure 1.1(a) is a sketch taken from Baha'i House of Worship in Panama.

5. If the coordinates of the element could be given explicitly in terms of certain nodes, then the representation is explicit; similar facilities could be considered for displacements.

6. The order of the interpolating polynomial is known as the order of representation; this definition also applies to displacements.

7. If the same shape functions were to be used to define the geometry as well as the functional, the element would be called isoparametric.

8. The parametric representation of the coordinates could be significantly separate from that of displacements, but if the representation has some common areas between the coordinates and the displacements then special properties are mobilised. The reader is referred to Chapters 3 and 4 where this aspect is covered as required within the scope of this work.

9. Most of the numerical examples are calculated for the displacements with a higher order parameter representation than the geometry, thus making the element sub-parametric (by defn.).

1.5 Past Work

The development of finite elements as applied to thin shells of revolution has evolved from the original concept that constant strains and curvatures must prevail within each element so that the overall stress variation could be assessed by "averaging" the neighbouring stresses in an acceptable manner [9],[10].

One of the first elements developed was the straight truncated cone by Grafton and Strome[11] with linear tangential displacement and a cubic normal displacement which solved axisymmetric problems. The formulation for harmonic variation was extended by Klein and Sylvester[12] and subsequently for dynamic analysis.

Webster[13] used curved elements for static and dynamic work; the elements entailed the option of choosing a quartic term for normal displacements and a parabolic variation for the in-plane displacements.

Gianini and Miles[14] produced a parametric element capable of solving axisymmetric problems in which the geometry was related to the nodal conditions explicitly but the order of displacements depended on the nature of the problem. The maximum order of the parameter was a cubic which gave slope conformity.

A similar conforming curved element was used by Chan and Firmin[15] with a fifth order Hermitian polynomial. Both the geometry and the displacements had the same order of polynomials and formulation contained both axisymmetric and harmonic cases.

Ergatudis[16] and Ahmad[17] formulated conforming parametric elements to yield both thin and thick shell solutions which were used for axisymmetric and harmonic cases.

The majority of the above authors have used numerical integration successfully with surprising similarity of technique and application.

1.6 Existing Features

This scheme of work has been designed to cater for the needs of those engineers who have access to small computers - as generally used in a consulting firm or other offices - for which core capacity becomes critical. It was thought that in these circumstances emphasis should be on an efficient formulation which would have more degrees of freedom per element and subsequently it would dramatically reduce the number of elements needed in a conventional solution.

To cater accurately for the geometrical representation a parametric type element was chosen for which the position vectors Z and R (in cylindrical coordinates) were functions of the parameter ξ and the parametric representation was a cubic to permit slope conformity before deformation. In practice it was found that this representation is generally accurate for all the geometrical configurations encountered. The nodal displacements followed an identical pattern which added theoretical* and practical** advantages.

In addition to the basic shape functions for displacement fields, it was thought essential to have surplus shape functions coupled to nodeless variables (see hierarchical nodes above). This is especially used for normal displacements which generate bending terms involving derivatives of higher order than the in-plane strain terms. For this reason the surplus functions

---

* As it will be shown later rigid-body-motions are accurately produced as a consequence.

** The same interpolation function could be used for geometry and displacements, thus shorter and simpler program codification results.

were formulated so as to be locally directed as in Fig. 3.15 of Chapter 3, so that the choice of in-plane and normal displacements could be made independently. The intention was that for a given problem one element could be made different from the others. This implies that the change in element characteristics should be made a matter of change of input rather than a change in the program (formulation). Fortunately as it transpired, surplus displacements have no adverse effect on the essential criteria for the element convergence.

Numerical integration constituted the prominent tool of investigating the above requirements and in fact no explicit integration was carried out in this scheme of work. Quadrature had the added bonus that non-uniform thickness and pressure along the meridian could be incorporated without additional problems. This might have increased the computing time fractionally but the flexibility and versatility offered as a result was invaluable.

Finally any energy contributions due to lateral sheer stresses were thought to be negligible and as such were eliminated from the calculations. It is interesting to note that some workers had included the effect of the lateral shear to some extent, either in its implied form[15] from equilibrium equations or linked to displacements with internal nodes*. However there appear to be no corresponding degrees of freedom at any external node of the shell element, associated with the lateral shear in the above formulations.

---

* L.J. Brombolich, P.L. Gould, "A High Precision Curved Shell Finite Element", Proc. of the 12th Structures, Structural Dynamics and Materials Conf. of the Am. Inst. of Aer. and Astro. and the Am. Soc. of Mech. Eng., Anaheim, Calif., April, 1971.

REFERENCES

1. S.P. Timoskenko, S. Woinowsky-Krieger, Theory of Plates and Shells, McGraw-Hill, 2nd Ed, 1959.
2. V.V. Novozhilov, Theory of Thin Shells, (Translation), P. Noordhoff, 1959.
3. A.E.H. Love, A. Treatise on the Mathematical Theory of Elasticity. Dover Pub, 1944.
4. A.C. Cassel, Shells of Revolution under arbitrary loading and the use of Fictitions Densities in Dynamic Relaxation, Proc.I.C.E. Jan. 1970.
5. P.E. Grafton and D.R. Strome, "Analysis of axisymmetric shells by the Direct Stiffness Method", J.A.I.A.A., 23427, 1963.
6. O.C. Zienkiewicz, The Finite Element Method in Engineering Science, McGraw-Hill, 1971.
7. W. Flügge, Stresses in Shells, Springer-Verlag, 1960.
8. O.C. Zienkiewicz, The Finite Element Method in Engineering Science, P. 13-24, McGraw-Hill, 1971.
9. M.J. Turner, R.W. Clough, H.C. Martin and L.J. Topp, "Stiffness and Deflection analysis of Complex Structures", J. Aero. Science, 23,805-23, 1956.
10. Zienkiewicz, The Finite Element Method in Engineering Science, P. 59-61, McGraw-Hill, 1971.
11. P.E. Grafton and D.R. Strome, "Analysis of axisymmetric shells by the Direct Stiffness Method", J.A.I.A.A., 23427, 1963.
12. S. Klein and R.J. Sylvester, "The linear elastic, dynamic analysis of Shells of Revolution by the matrix Displacement method", Proc. Conf. on Matrix Methods in Struct. Mech., Air Force Inst. of Tech., Wright-Patterson A.F. Base, Ohio, Oct. 1965.
13. J.J. Webster, "The accuracy of Finite Element solutions for modal characteristics of Shells of Revolution".

14. M. Gianini and G.A. Miles, "A Curved Element in the analysis of Axisymmetric Thin Shells", Int.Jour. of Num. Methods in Eng. Oct.1970.

15. A.S.L. Chan and A. Firmin, "The Analysis of Cooling Towers by the Matrix Finite Element Method", The Aero. Jour., Vol. 74, Oct. 1970.

16. I. Ergatudis, Isoparametric Finite Elements in two and three dimensional stresss analysis. University of Wales, Ph.D. Thesis, 1968.

17. S. Ahmad, Curved Finite Elements in the analysis of solid shells and Plate Structures, University of Wales, Ph.D. Thesis, 1969.

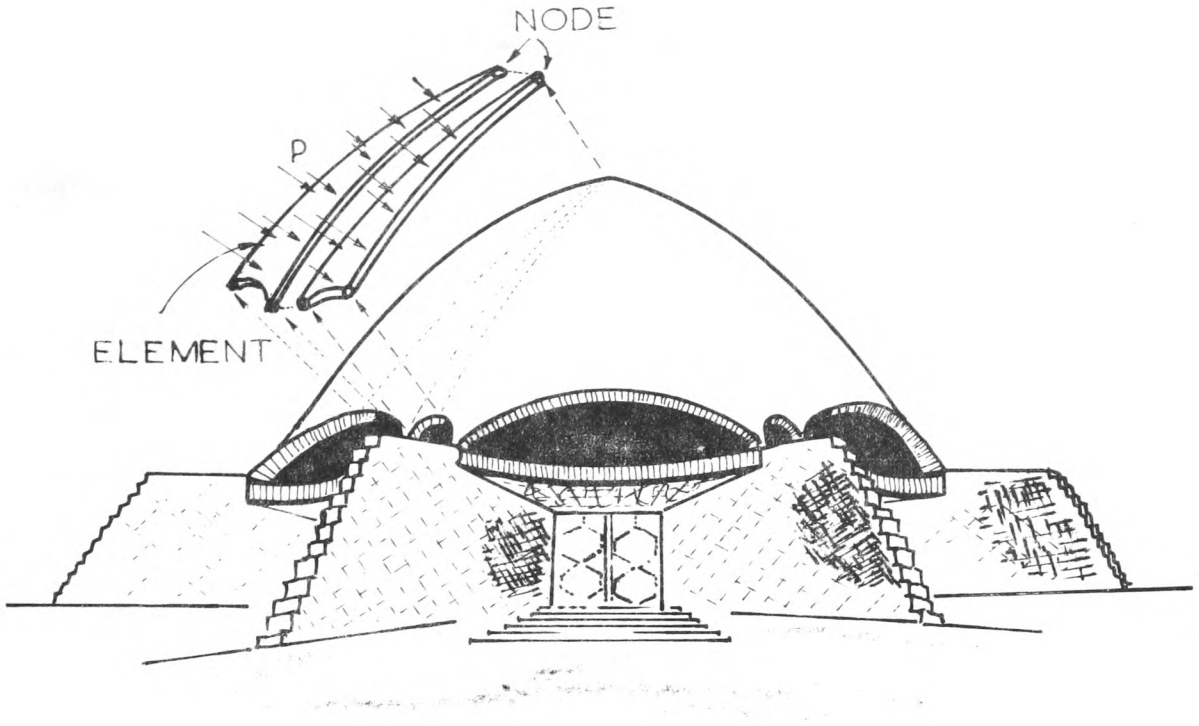

(a)

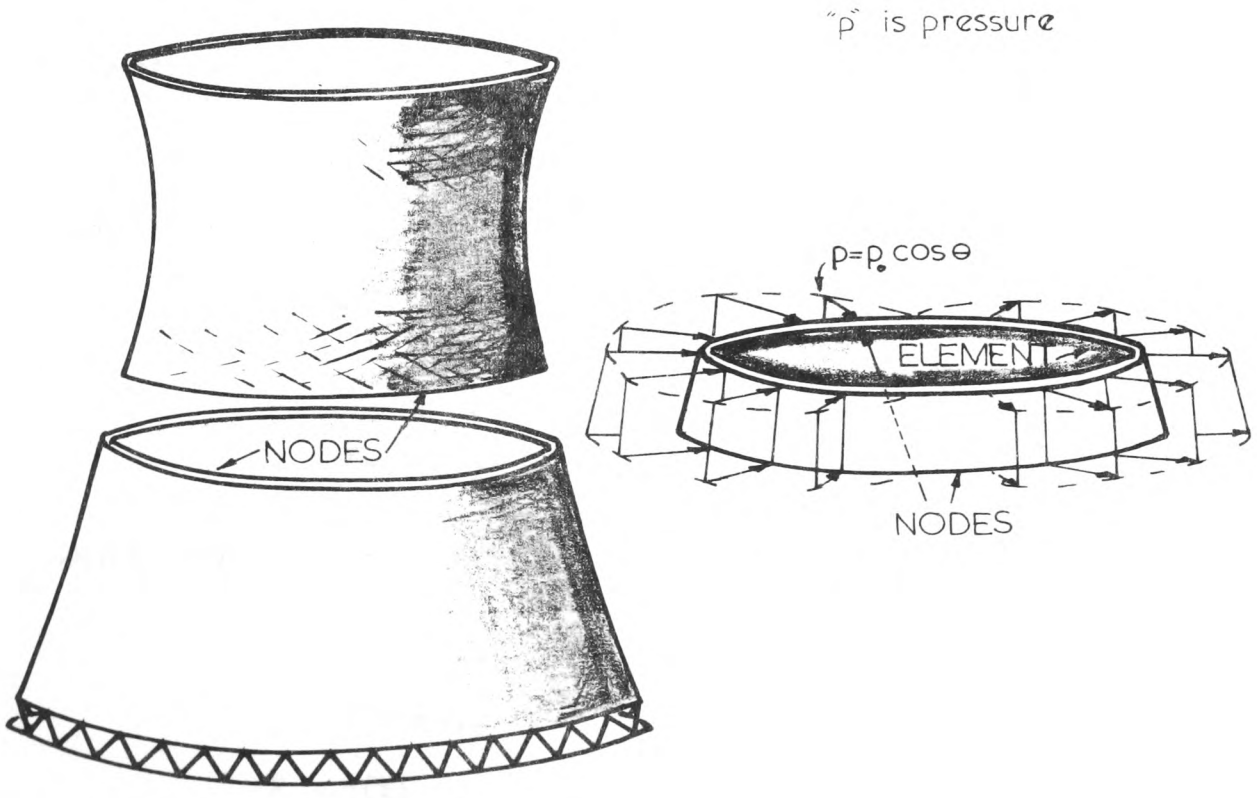

(b)

FIGURE 1-1

CHAPTER 2

GENERAL STRAIN-DISPLACEMENT RELATIONSHIPS

2.1 Synopsis

The general displacement-strain equations produced by Novozhilov have been taken and simplified for the particular case of a shell of revolution. The simplified form, with one exception, agrees with those obtained by Klein[1]. Each of the expressions produced has been investigated in an effort to attach a physical significance to each of the terms.

The equations have finally been transferred from a set of local coordinates system to a global system. This form is ideally suited to numerical procedures[2].

2.2 Geometry

Novozhilov[3] gives the cartesian equations of a general surface in terms of the parameters α_1 and α_2 as

$$\begin{aligned} x &= f_1(\alpha_1,\alpha_2) \\ y &= f_2(\alpha_1,\alpha_2) \\ z &= f_3(\alpha_1,\alpha_2) \end{aligned} \qquad \ldots\ldots \text{ eqn. 2.1}$$

which simplify for a surface of revolution to

$$\begin{aligned} x &= R \text{ Cos } \alpha_2 \\ y &= R \text{ Sin } \alpha_2 \\ R &= \rho(z) \\ z &= f(\alpha_1) \end{aligned} \qquad \ldots\ldots \text{ eqn. 2.2a}$$

where R and α_2 are defined as in Fig. 2.1. By substitution,

$$x = \rho\{f_1(\alpha_1)\} \text{ Cos } \alpha_2$$
$$y = \rho\{f_1(\alpha_1)\} \text{ Sin } \alpha_2 \qquad \ldots\ldots \text{ eqn. 2.2b}$$
$$z = f(\alpha_1)$$

The surface of revolution can also be represented using the well known vector notation, i.e.

$$r = ix + jy + kz \qquad \ldots\ldots \text{ eqn. 2.3}$$

where (as shown in Fig.2.1) i, j and k are the unit vectors along the x, y and z axes respectively. The radius vector is not to be confused with the principal radii of curvature R_1 and R_2 whose geometrical representation is given in Fig. 2.2.

Lame's parameters E and G are represented by A_1 and A_2 respectively and are defined by Novozhilov as

$$A_1 = \left|\frac{\partial r}{\partial \alpha_1}\right|$$
$$A_2 = \left|\frac{\partial r}{\partial \alpha_2}\right| \qquad \ldots\ldots \text{ eqn. 2.4}$$

which are now to be evaluated;

$$\left\{\frac{\partial r}{\partial \alpha_1}\right\} = \begin{Bmatrix} \frac{\partial x}{\partial \alpha_1} \\ \frac{\partial y}{\partial \alpha_1} \\ \frac{\partial z}{\partial \alpha_1} \end{Bmatrix}$$

$$= \begin{Bmatrix} \text{Cos } \alpha_2 \ \frac{\partial R}{\partial z} \ \frac{\partial z}{\partial \alpha_1} \\ \text{Sin } \alpha_2 \ \frac{\partial R}{\partial z} \ \frac{\partial z}{\partial \alpha_1} \\ \frac{\partial z}{\partial \alpha_1} \end{Bmatrix}.$$

thus

$$A_1 = \sqrt{\left\{\frac{\partial R}{\partial z}\cdot\frac{\partial z}{\partial \alpha_1}\right\}^2 + \left\{\frac{\partial z}{\partial \alpha_1}\right\}^2}$$

$$= \frac{\partial z}{\partial \alpha_1}\sqrt{\left\{\frac{\partial R}{\partial z}\right\}^2 + 1}$$

or

$$A_1\,\delta\alpha_1 = \delta z\sqrt{\left\{\frac{\partial R}{\partial z}\right\}^2 + 1}. \qquad \ldots\ldots \text{ eqn. 2.5a}$$

Similarly,

$$\left\{\frac{\partial r}{\partial \alpha_2}\right\} = \begin{Bmatrix} -R \text{ Sin } \alpha_2 \\ R \text{ Cos } \alpha_2 \\ 0 \end{Bmatrix},$$

therefore,

$$A_2 = \sqrt{\{-R \text{ Sin } \alpha_2\}^2 + \{R \text{ Cos } \alpha_2\}^2 + 0^2}$$

$$A_2 = R \qquad \ldots\ldots \text{ eqn. 2.5b}$$

Choose $\alpha_2 = \theta$ to be the circumferential variable and $\alpha_1 = \Phi$ the angle between the principal radii and the z-axis as shown in Fig.2.3.

In the newly defined cylindrical co-ordinates $\frac{\partial R}{\partial z}$ is the tangent and $\delta z\sqrt{\left\{\frac{\partial R}{\partial z}\right\}^2 + 1} = \delta s$, the arc length.

Substituting for $\delta\alpha_1$ as $\delta\Phi$ in equation (2.5a), it becomes

$$A_1\delta\Phi = \delta z\sqrt{\left\{\frac{\partial R}{\partial z}\right\}^2 + 1}$$

$$= \delta s$$

and

$$\lim_{\delta\Phi \to 0} \frac{\delta s}{\delta \Phi} = R_1$$

thus

$$\left.\begin{aligned} A_1 &= R_1 \\ A_2 &= R \end{aligned}\right\} \quad \ldots\ldots \text{ eqn. 2.6}$$

We can now justifiably adopt the following notation, i.e.

$$\frac{\partial(\ldots)}{A_1 \partial \alpha_1} = \frac{\partial(\ldots)}{\partial s} \quad \ldots\ldots \text{ eqn. 2.7}$$

$$\frac{\partial(\ldots)}{A_2 \partial \alpha_2} = \frac{1\partial(\ldots)}{R \ \partial \theta} \quad \ldots\ldots \text{ eqn. 2.8}$$

The displacement and co-ordinate systems are consistently right-handed and shown in Figs. 2.4 and 2.5.

Equations (2.7) and (2.8) will be used extensively in the formulation of the strain-displacement equations for shells of revolution.

2.3 General strain (and curvature) displacement relations

The general relations produced by Novozhilov follow, where the strains and curvatures have their usual meaning which will be given fully in Section 2.4.

$$\varepsilon_s = \frac{1}{A_1}\frac{\partial u}{\partial \alpha_1} + \frac{v}{A_1 A_2}\frac{\partial A_1}{\partial \alpha_2} + \frac{w}{R_1} \qquad \ldots\ldots \text{eqn. 2.9}$$

$$\varepsilon_\theta = \frac{1}{A_2}\frac{\partial v}{\partial \alpha_2} + \frac{u}{A_1 A_2}\frac{\partial A_2}{\partial \alpha_1} + \frac{w}{R_2} \qquad \ldots\ldots \text{eqn. 2.10}$$

$$\varepsilon_{s\theta} = \frac{A_2}{A_1}\frac{\partial}{\partial \alpha_1}\left(\frac{v}{A_2}\right) + \frac{A_1}{A_2}\frac{\partial}{\partial \alpha_2}\left(\frac{u}{A_1}\right) \qquad \ldots\ldots \text{eqn. 2.11}$$

$$\chi_s = -\frac{1}{A_1}\frac{\partial}{\partial \alpha_1}\left(\frac{1}{A_1}\frac{\partial w}{\partial \alpha_1} - \frac{u}{R_1}\right) - \frac{1}{A_1 A_2}\frac{\partial A_1}{\partial \alpha_2}\left(\frac{1}{A_2}\frac{\partial w}{\partial \alpha_2} - \frac{v}{R_2}\right) \qquad \ldots\ldots \text{eqn. 2.12}$$

$$\chi_\theta = -\frac{1}{A_2}\frac{\partial}{\partial \alpha_2}\left(\frac{1}{A_2}\frac{\partial w}{\partial \alpha_2} - \frac{v}{R_2}\right) - \frac{1}{A_1 A_2}\frac{\partial A_2}{\partial \alpha_1}\left(\frac{1}{A_1}\frac{\partial w}{\partial \alpha_1} - \frac{u}{R_1}\right) \qquad \ldots\ldots \text{eqn. 2.13}$$

$$\chi_{s\theta} = -\frac{1}{A_1 A_2}\left(\frac{\partial^2 w}{\partial \alpha_1 \partial \alpha_2} - \frac{1}{A_1}\frac{\partial A_1}{\partial \alpha_2}\frac{\partial w}{\partial \alpha_1} - \frac{1}{A_2}\frac{\partial A_2}{\partial \alpha_1}\frac{\partial w}{\partial \alpha_2}\right) \qquad \ldots\ldots \text{eqn. 2.14}$$

$$+ \frac{1}{R_1}\left(\frac{1}{A_2}\frac{\partial u}{\partial \alpha_2} - \frac{1}{A_1 A_2}\frac{\partial A_1}{\partial \alpha_2}u\right) + \frac{1}{R_2}\left(\frac{1}{A_1}\frac{\partial v}{\partial \alpha_1} - \frac{1}{A_1 A_2}\frac{\partial A_2}{\partial \alpha_1}v\right)$$

2.4 Strain-displacement relations for shells of revolution

Each of the above expressions (2.9) - (2.14) is now taken and reduced to the form applicable to shells of revolution. The physical interpretation of each of the terms in the expressions is then given.

2.4.1 Meridional strain ε_s

$$\varepsilon_s = \frac{1}{A_1}\frac{\partial u}{\partial \alpha_1} + \frac{1}{A_1 A_2}\frac{\partial A_1}{\partial \alpha_2}v + \frac{w}{R_1}$$

$$= \frac{\partial u}{\partial s} + \frac{1}{R_1}\left(\frac{1}{R}\frac{\partial R_1}{\partial \theta}\right)v + \frac{w}{R_1}$$

Now $\frac{\partial R_1}{\partial \theta} = 0$ and $\frac{w}{R_1} = w(\frac{1}{R_1})$ is neglected since the curvature $(\frac{1}{R_1})$ is regarded as a small quantity (i.e. the curvature does not change too abruptly), thus

$$\varepsilon_s = \frac{\partial u}{\partial s} \qquad \ldots\ldots \text{ eqn. 2.15}$$

This is possibly the simplest case encountered as can be seen from Fig.2.6.

2.4.2 Circumferential strain ε_θ

$$\varepsilon_\theta = \frac{1}{A_2}\frac{\partial v}{\partial \alpha_2} + \frac{1}{A_1 A_2}\frac{\partial A_2}{\partial \alpha_1} u + \frac{w}{R_2}$$

$$= \frac{1}{R}\frac{\partial v}{\partial \alpha} + \frac{1}{R}\frac{\partial R}{\partial s} u + \frac{w}{R_2}$$

From Figs.2.7 and 2.8 $\frac{\partial R}{\partial s} = \text{Cos } \Phi$ and $R_2 = R/\text{Sin } \Phi$

Hence:

$$\varepsilon_\theta = \frac{1}{R}\frac{\partial v}{\partial \theta} + \frac{u}{R}\text{Cos } \Phi + \frac{w}{R}\text{Sin } \Phi \qquad \ldots\ldots \text{ eqn. 2.16}$$

The above terms are all easily explained as follows: Term $\frac{1}{R}\frac{\partial v}{\partial \theta}$ is the equivalent of $\frac{\partial u}{\partial s}$ in the circumferential direction. The terms containing Sin Φ and Cos Φ when transformed to global axes yield

$$(\frac{\text{Cos } \Phi}{R}\ \frac{\text{Sin } \Phi}{R}) \begin{Bmatrix} u \\ w \end{Bmatrix} = (\frac{\text{Cos } \Phi}{R}\ \frac{\text{Sin } \Phi}{R}) \begin{bmatrix} \text{Cos}(90-\Phi) & \text{Sin } (90-\Phi) \\ -\text{Sin}(90-\Phi) & \text{Cos } (90-\Phi) \end{bmatrix} \begin{Bmatrix} u \text{ global} \\ w \text{ global} \end{Bmatrix}$$

$$= \frac{1}{R}\left((\text{Cos } \Phi \text{ Sin } \Phi - \text{Sin } \Phi \text{ Cos } \Phi)\ (\text{Cos}\Phi\ \text{Cos}\Phi + \text{Sin}\Phi\ \text{Sin}\Phi)\right) \begin{Bmatrix} u \text{ global} \\ w \text{ global} \end{Bmatrix}$$

$$= \frac{1}{R}\ (0 \quad 1) \begin{Bmatrix} u \text{ global} \\ w \text{ global} \end{Bmatrix}$$

$$= \frac{w \text{ global}}{R}$$

This is clearly the term associated with the hoop-strain represented in Figs. 2.3 and 2.10.

2.4.3 Mid-surface shear strain $\varepsilon_{s\theta}$

$$\varepsilon_{s\theta} = \frac{A_2}{A_1}\frac{\partial}{\partial\alpha_1}\left(\frac{v}{A_2}\right) + \frac{A_1}{A_2}\frac{\partial}{\partial\alpha_2}\left(\frac{u}{A_1}\right)$$

$$= R\frac{\partial}{\partial s}\left(\frac{v}{R}\right) + \frac{R_1}{R}\frac{\partial}{\partial\theta}\left(\frac{u}{R_1}\right)$$

$$= R\left\{\frac{1}{R}\frac{\partial v}{\partial s} + v(-1)\left(\frac{\partial R}{\partial s} / R^2\right)\right\} + \frac{R_1}{R}\left\{\frac{1}{R_1}\frac{\partial u}{\partial\theta} + u(-1)\left(\frac{\partial R}{\partial\theta} / R_1^{\,2}\right)\right\}$$

$$= \left(\frac{\partial v}{\partial s} - \text{Cos}\Phi.\frac{v}{R}\right) + \left(\frac{\partial u}{R\partial\theta} + 0\right)$$

$$\varepsilon_{s\theta} = \frac{\partial v}{\partial s} - \text{Cos}\Phi.\frac{v}{R} + \frac{1}{R}\frac{\partial u}{\partial\theta} \qquad \ldots\ldots \text{ eqn. 2.17}$$

The terms $\frac{\partial v}{\partial s} + \frac{1}{R}\frac{\partial u}{\partial\theta}$ are the equivalent of $\left(\frac{\partial v}{\partial x} + \frac{\partial u}{\partial y}\right)$ which is the shear strain in two dimensional elasticity. The explanation of Cos $\Phi.\frac{v}{R}$ is however more subtle. As seen from Fig. 2.11 the meridions are inclined towards each other. If A as datum is assumed initially to possess zero inclination, after a displacement v the inclination becomes $\omega = \frac{v}{\rho}$.

Now from Fig.2.12,

$$\rho = \frac{R}{\text{Cos}\Phi}$$

Hence,

$$\omega = \frac{v}{R/\text{Cos}\Phi} = \text{Cos}\Phi\,\frac{v}{R}$$

As it is seen, this is a geometrical rotation and not a mechanical one; therefore it is subracted from the original shear $\left(\frac{\partial v}{\partial s} + \frac{1}{R}\frac{\partial u}{\partial\theta}\right)$.

2.4.4 Meridional bending χ_s

$$\chi_s = -\frac{1}{A_1}\frac{\partial}{\partial\alpha_1}\left(\frac{1}{A_1}\frac{\partial w}{\partial\alpha 1} - \frac{u}{R_1}\right) - \frac{1}{A_1A_2}\frac{\partial A_1}{\partial\alpha_2}\left(\frac{1}{A_2}\frac{\partial w}{\partial\alpha_2} - \frac{v}{R_2}\right)$$

$$= -\frac{\partial}{\partial s}\left(\frac{\partial w}{\partial s} - \frac{u}{R_1}\right) - \frac{1}{R_1}\frac{\partial R_1}{\partial\theta}\left(\frac{1}{R}\frac{\partial w}{\partial\theta} - \frac{v}{R_2}\right)$$

$$= -\frac{\partial^2 w}{\partial s^2} + \frac{\partial}{\partial s}\left(\frac{u}{R_1}\right) - 0$$

Again, if the curvature $\left(\frac{1}{R_1}\right)$ does not change abruptly then the second term may be neglected and

$$\chi_s = -\frac{\partial^2 w}{\partial s^2} \qquad \ldots\ldots \text{ eqn. 2.18}$$

This obviously is identical with $-\frac{d^2y}{dx^2}$ which is the well-known curvature of simple bending theory.

2.4.5 Circumferential bending χ_θ

$$\chi_\theta = -\frac{1}{A_2}\frac{\partial}{\partial\alpha_2}\left(\frac{1}{A_2}\frac{\partial w}{\partial\alpha_2} - \frac{v}{R_2}\right) - \frac{1}{A_1A_2}\frac{\partial A_2}{\partial\alpha_1}\left(\frac{1}{A_1}\frac{\partial w}{\partial\alpha_1} - \frac{u}{R_1}\right)$$

$$= -\frac{1}{R}\frac{\partial}{\partial\theta}\left(\frac{1}{R}\frac{\partial w}{\partial\theta} - \frac{\mathrm{Sin}\Phi v}{R}\right) - \frac{1}{R}\frac{\partial R}{\partial s}\left(\frac{\partial w}{\partial s} - \frac{u}{R_1}\right)$$

$$= -\frac{1}{R^2}\frac{\partial^2 w}{\partial\theta^2} + \frac{\mathrm{Sin}\Phi}{R^2}\frac{\partial v}{\partial\theta} - \frac{1}{R}\mathrm{Cos}\Phi\left(\frac{\partial w}{\partial s}\right) + \frac{\mathrm{Cos}\Phi}{R} \cdot u \cdot \left(\frac{1}{R_1}\right)$$

neglecting any product of $\left(\frac{1}{R_1}\right)$. (.....), we arrive at

$$\chi_\theta = -\frac{1}{R^2}\frac{\partial^2 w}{\partial\theta^2} + \frac{\mathrm{Sin}\Phi}{R^2}\frac{\partial v}{\partial\theta} - \frac{1}{R}\mathrm{Cos}\Phi\frac{\partial w}{\partial s} \qquad \ldots\ldots \text{ eqn. 2.19}$$

The term $-\frac{1}{R^2}\frac{\partial^2 w}{\partial\theta^2}$ is the equivalent of $-\frac{\partial^2 w}{\partial s^2}$ in the meridional direction. The third term can be interpreted as follows: the tangent to meridians A and B meet on the z-axis, Fig. 2.11. The rotation $\frac{\partial w}{\partial s}$ at A can be resolved about meridian B. In Fig. 2.13 the two components are labelled $ROT(B_1)$ and $ROT(B_2)$ for convenience.

$$ROT(B_1) = \frac{\partial w}{\partial s} \text{ Cos } d\omega$$

$$ROT(B_2) = \frac{\partial w}{\partial s} \text{ Sin } d\omega,$$

which reduce to $\frac{\partial w}{\partial s} \cdot 1$ and $\frac{\partial w}{\partial s} d\omega$ respectively. Activating these components on the side B, we observe that meridian B rotates the same amount $\frac{\partial w}{\partial s}$ as A but there is a 'bending' change of slope of magnitude $\frac{\partial w}{\partial s} d\omega$ along B due to A. The amount of curvature per length $Rd\theta$ of the circumference is thus

$$(\frac{\partial w}{\partial s} d\omega)/Rd\theta = \frac{1}{R}\frac{\partial w}{\partial s}\frac{\partial \omega}{\partial \theta}$$

From a well-known theorem in solid geometry, Fig. 2.14

$$d\omega = d\theta \text{ Cos}\Phi \text{ or } \frac{d\omega}{d\theta} = \text{Cos}\Phi$$

and thus the curvature due to meridional rotation is $\frac{\text{Cos}\Phi}{R}\frac{\partial w}{\partial s}$. The last constituent term to be dealt with is $\frac{\text{Sin}\Phi}{R^2}\frac{\partial v}{\partial \theta}$. The increase in circumferential angle due to stretch v and $v + \delta v$ is $\frac{(v+\delta v)-v}{R} = \frac{\delta v}{R}$. The increase in curvature is the increase in slope per unit length of the element Fig. 2.15. The increase in slope $\delta\alpha$ along the second principal radius R_2 is obtained using the same theorem in solid geometry, i.e. $\delta\alpha = (\frac{\delta v}{R})$ Cos $(90-\Phi)$. Thus the contribution to increase in curvature due to δv is

$$\lim_{\partial\theta\to 0} \frac{\delta\alpha}{R\delta\theta} = \frac{1}{R}\frac{\partial}{\partial\theta}(\frac{\text{Sin}\Phi}{R} \cdot v)$$

$$= \frac{\text{Sin}\Phi}{R^2}\frac{\partial v}{\partial\theta}$$

2.4.6 Mid-surface twist $\chi_{s\theta}$

$$\chi_{s\theta} = -\frac{1}{A_1A_2}\left(\frac{\partial^2 w}{\partial\alpha_1\partial\alpha_2} - \frac{1}{A_1}\frac{\partial A_1}{\partial\alpha_2}\frac{\partial w}{\partial\alpha_1} - \frac{1}{A_2}\frac{\partial A_2}{\partial\alpha_1}\frac{\partial w}{\partial\alpha_2}\right) +$$

$$\frac{1}{R_1}\left(\frac{1}{A_2}\frac{\partial u}{\partial\alpha_2} - \frac{1}{A_1A_2}\frac{\partial A_1}{\partial\alpha_2}u\right) + \frac{1}{R_2}\left(\frac{1}{A_1}\frac{\partial v}{\partial\alpha_1} - \frac{1}{A_1A_2}\frac{\partial A_2}{\partial\alpha_1}v\right),$$

$$\chi_{s\theta} = -\frac{\partial^2 w}{R\partial\theta\partial s} + \frac{\cos\Phi}{R^2}\frac{\partial w}{\partial\theta} + \frac{1}{R_1}\frac{\partial u}{R\partial\theta} + \frac{\sin\Phi}{R}\frac{\partial v}{\partial s} - \frac{\sin\Phi\cos\Phi}{R^2}v$$

Neglecting $\frac{1}{R_1}\left(\frac{\partial u}{R\partial\theta}\right)$

$$\chi_{s\theta} = -\frac{\partial^2 w}{R\partial\theta\partial s} + \frac{\cos\Phi}{R^2}\frac{\partial w}{\partial\theta} + \frac{\sin\Phi}{R}\frac{\partial v}{\partial s} - \frac{\sin\Phi\cos\Phi}{R^2}v \quad \ldots\ldots \text{ eqn. 2.20}$$

Let us consider each term individually bearing in mind the notation of Figs. 2.4 and 2.5.

The term $\frac{\partial^2 w}{R\partial\theta\partial s}$ is self-explanatory since it corresponds to the twist in the plate bending problem. For the second term $\frac{\cos\Phi}{R^2}\frac{\partial w}{\partial\theta}$ consider the displacement w on an element shown in Fig. 2.16. The slope at A due to an increase of w along the circumference is $\frac{\partial w}{R\partial\theta}$. This is now resolved at B to components ROT(B_2) and ROT(B_1) which are $\frac{\partial w}{R\partial\theta}\,d\omega$ and $\frac{\partial w}{R\partial\theta}$. 1 respectively. The first component $\frac{\partial w}{R\partial\theta}\,d\omega$ on meridian B has a twisting effect and the twist per unit length is $\frac{\partial w}{R\partial\theta}\frac{\partial\omega}{R\partial\theta} = \frac{\cos\Phi}{R^2}\frac{\partial w}{\partial\theta}$. For the term $\frac{\sin\Phi}{R}\frac{\partial v}{\partial s}$ consider the rates of stretch along A and B which are $\left(\frac{\partial v}{\partial s}\right)_A$ and $\left(\frac{\partial v}{\partial s}\right)_B$ respectively, shown in Fig. 2.17. The rates of stretch would represent rotation about the normals which subtend an angle α on the z-axis. Again, ROT(B_2) and ROT(B_1) are $\frac{\partial v}{\partial s}\,d\alpha$ and $\frac{\partial v}{\partial\alpha}$. 1 respectively, $\left(\frac{\partial v}{\partial s}\right)_A$ being $\frac{\partial v}{\partial s}$. The component

ROT(B_2) represents a positive twist at B per unit length of element which along the circumference is

$$\frac{\partial v}{\partial s}\frac{\partial \alpha}{R\partial \theta} = \frac{\text{Sin}\Phi}{R}\frac{\partial v}{\partial s}$$

The final contribution is due to v as can be seen from Fig.2.18(a). The extension along the circumference is v and the angle subtended at I is given by $\omega = \frac{\text{Cos}\Phi v}{R}$. Now consider in Fig.2.18(b) the circumscribing cone IABC. The meridians B and C are rotating relative to A at a rate of ω subtended at the vertex of the cone I. These rotations are on the parallel circle ABC, but relative to the local meridians B and C; thus can be represented as a vector normal to the surface which would be the continuation of R_2, the second principal radius of curvature. It is clear that we can resolve these to obtain $\omega_{B_1} = \omega_A = \frac{\text{Cos}\Phi v}{R}$ and $\omega_{B_2} = \omega_A \alpha = \frac{\text{Cos}\Phi v}{R}\alpha$. This again represents a twist about B and the rate per unit length of circumference is $\frac{\text{Cos}\Phi v}{R}/R\theta$

$$= \frac{\text{Cos}\Phi\ \text{Sin}\Phi\ v}{R^2}$$

2.5 Practical applications

The strain-displacement relations obtained in the previous sections are given below with the co-ordinate parameters changed in accordance with those shown in Fig.2.19(a). The relations then become:

$$\varepsilon_s = \frac{\partial u}{\partial s}$$

$$\varepsilon_\theta = \frac{1}{R}\frac{\partial v}{\partial \theta} + \frac{1}{R}(\text{Sin}\Phi u + \text{Cos}\Phi w)$$

$$\varepsilon_{s\theta} = \frac{1}{R}\frac{\partial u}{\partial \theta} + \frac{\partial v}{\partial s} - \frac{v}{R}\text{Sin}\Phi$$

$$\chi_s = -\frac{\partial^2 w}{\partial_s{}^2}$$

$$\chi_\theta = -\frac{1}{R^2}\frac{\partial^2 w}{\partial\theta 2} - \frac{\sin\Phi}{R}\frac{\partial w}{\partial s} + \frac{\cos\Phi}{R^2}\frac{\partial v}{\partial\theta}$$

$$\chi_{s\theta} = -\frac{\partial^2 w}{R\partial\theta\partial s} + \frac{\sin\Phi}{R^2}\frac{\partial w}{\partial\theta} + \frac{\cos\Phi}{R}\frac{\partial v}{\partial s} - \frac{\sin\Phi\cos\Phi v}{R^2}$$

The set of equations above are in the local displacement system whereas for practical applications[4] it is necessary to transform them to the global system shown in Fig. 2.19(b). To obtain the equations in global co-ordinates we use the transformation

$$\begin{Bmatrix} u \\ w \\ v \end{Bmatrix}_\ell = \begin{bmatrix} \cos\Phi & \sin\Phi & 0 \\ -\sin\Phi & \cos\Phi & 0 \\ 0 & 0 & 1 \end{bmatrix} \begin{Bmatrix} u \\ w \\ v \end{Bmatrix}_g$$

where subscripts ℓ and g refer to local and global systems respectively.

$$\begin{Bmatrix} \varepsilon_s \\ \varepsilon_\theta \\ \varepsilon_{s\theta} \\ \chi_s \\ \chi_\theta \\ \chi_{s\theta} \end{Bmatrix} = \left[\begin{array}{c|c|c} \frac{\partial}{\partial s} & & \\ \sin\Phi/R & \cos\Phi/R & \frac{1}{R}\frac{\partial}{\partial\theta} \\ \frac{1}{R}\frac{\partial}{\partial\theta} & & -\sin\Phi/R + \frac{\partial}{\partial s} \\ & -\frac{\partial^2}{\partial s^2} & \\ & -\frac{1}{R^2}\frac{\partial^2}{\partial\theta^2} - \frac{\sin\Phi}{R}\frac{\partial}{\partial s} & \frac{\cos\Phi}{R^2}\frac{\partial}{\partial\theta} \\ & -\frac{1}{R}\frac{\partial^2}{\partial\theta\partial s} + \frac{\sin\Phi}{R^2}\frac{\partial}{\partial\theta} & \frac{\cos\Phi}{R}\frac{\partial}{\partial s} - \frac{\sin\Phi\cos\Phi}{R^2} \end{array}\right] \begin{bmatrix} \cos\Phi & \sin\Phi & 0 \\ -\sin\Phi & \cos\Phi & 0 \\ 0 & 0 & 1 \end{bmatrix} \begin{Bmatrix} u \\ w \\ v \end{Bmatrix}_g$$

or

$$\begin{Bmatrix} \varepsilon_s \\ \varepsilon_\theta \\ \varepsilon_{s\theta} \\ \chi_s \\ \chi_\theta \\ \chi_{s\theta} \end{Bmatrix} = \left[\begin{array}{c|c|c} \cos\Phi\frac{\partial}{\partial s} & \sin\Phi\frac{\partial}{\partial s} & \\ & \frac{1}{R} & \frac{1}{R}\frac{\partial}{\partial\theta} \\ \frac{\cos\Phi}{R}\frac{\partial}{\partial\theta} & \frac{\sin\Phi}{R}\frac{\partial}{\partial\theta} & -\frac{\sin\Phi}{R}+\frac{\partial}{\partial s} \\ \sin\Phi\frac{\partial 2}{\partial s^2} & -\cos\Phi\frac{\partial^2}{\partial s^2} & \\ \frac{\sin\Phi}{R^2}\frac{\partial^2}{\partial\theta^2}+\frac{\sin\Phi}{R}\frac{\partial}{\partial s} & -\frac{\cos\Phi}{R^2}\frac{\partial^2}{\partial\theta^2}-\frac{\cos\Phi}{R}\frac{\partial}{\partial s} & \frac{\cos\Phi}{R^2}\frac{\partial}{\partial\theta} \\ \frac{\sin\Phi}{R}\frac{\partial^2}{\partial\theta\partial s}-\frac{\sin^2\Phi}{R^2}\frac{\partial}{\partial\theta} & -\frac{\cos\Phi}{R}\frac{\partial^2}{\partial\theta\partial s}+\frac{\cos\Phi\sin\Phi}{R^2}\frac{\partial}{\partial\theta} & \frac{\cos\Phi}{R}\frac{\partial}{\partial s}-\frac{\sin\Phi\cos\Phi}{R^2} \end{array}\right] \begin{Bmatrix} u \\ w \\ v \end{Bmatrix}_g$$

The equations are presented in the differential operator notation so that matrix transformation operations can be manipulated easily. In the above equations u_g is along the axis of symmetry, w_g along the radius R (in the cylindrical co-ordinate) and v_g along the meridian.

2.6 Conclusions

It is felt that the physical interpretation of the terms in each of the relationships is helpful in understanding the behaviour of shells.

The final equations have been presented in a form suitable for numerical applications. To confirm the use of the equations a number of examples have been investigated, each of which has been compared with known solutions. Plane and curved surfaces under in plane and normal loading under static and dynamic conditions have

been considered. Where possible, both uniform thickness and variable thickness have been analysed.

REFERENCES

1. S. Klein, Proceedings Conf. Matrix Methods in Structural Mechanics, Institute of Technology, Wright-Petterson, A.F. Base, Ohio, Oct. 1965.
2. O.C. Zienkiewicz, The Finite Element Method in Engineering Science (2nd Ed.), McGraw-Hill, 1971.
3. V.V. Novozhilov, Thin Shell Theory, P. Noordhoff, 1959.
4. R. Delpak, Axisymmetric Vibrations of Shells of Revolution By The Finite Element Method, University of Wales M.Sc. Thesis, 1968.

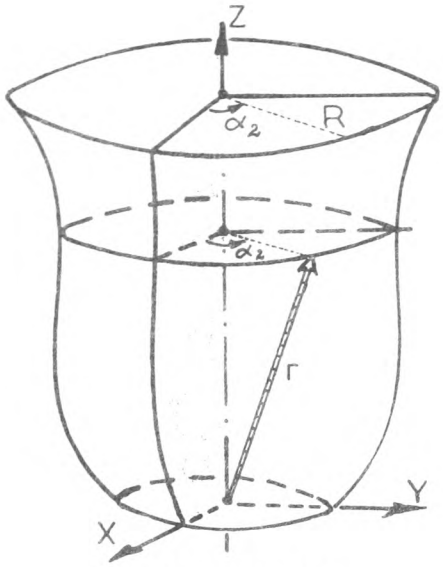

FIGURE 2.1

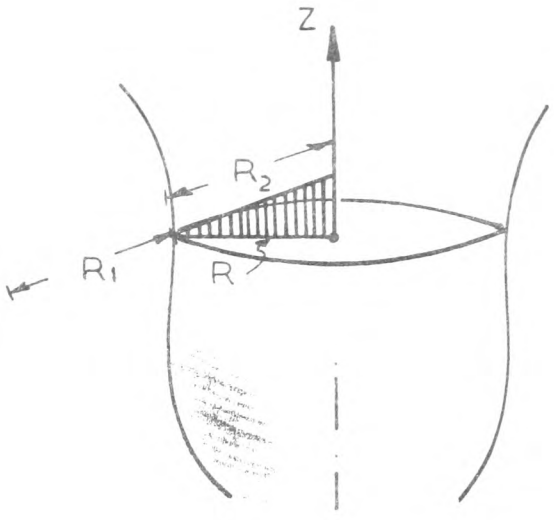

FIGURE 2.2

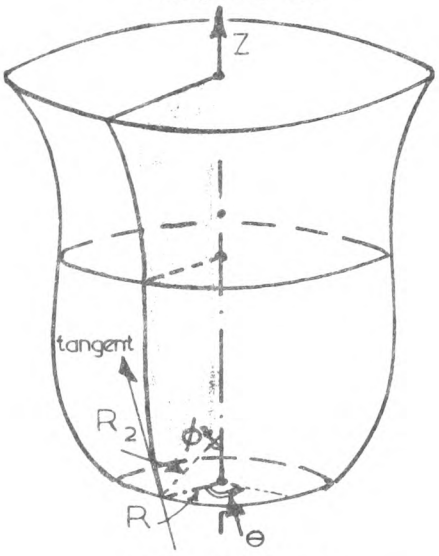

FIGURE 2.3

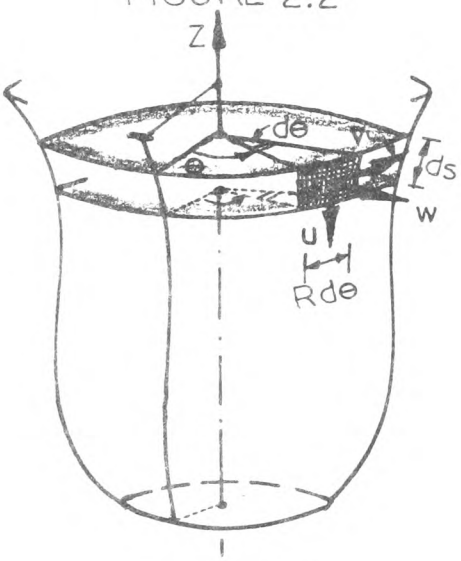

FIGURE 2.4

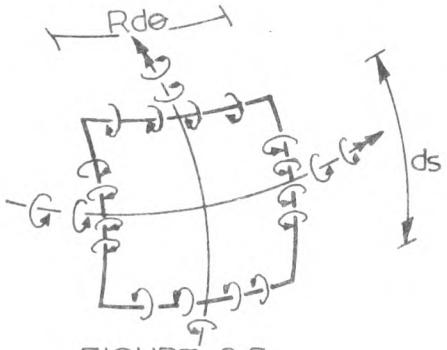

FIGURE 2.5

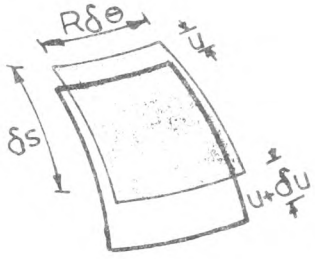

FIGURE 2.6

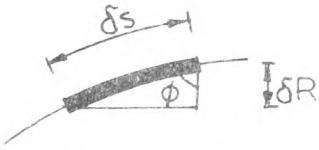

FIGURE 2.7

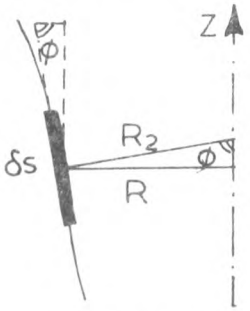

FIGURE 2.8

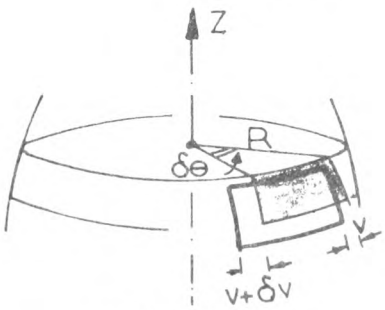

FIGURE 2.9

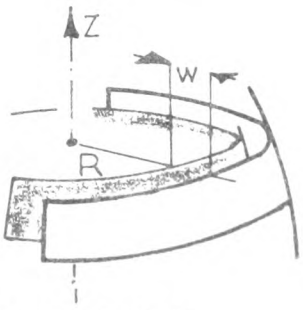

FIGURE 2.10

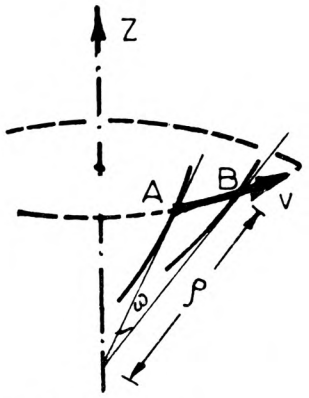

FIGURE 2.11

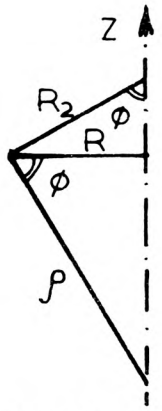

FIGURE 2.12

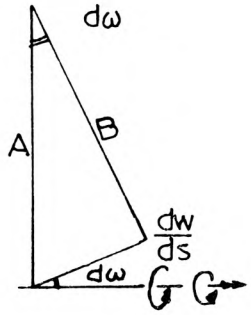

(a)

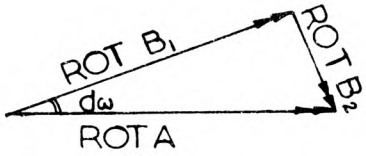

(b)

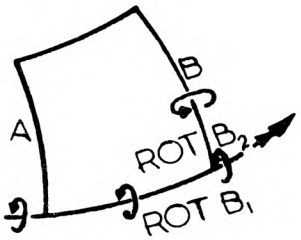

(c)

FIGURE 2.13

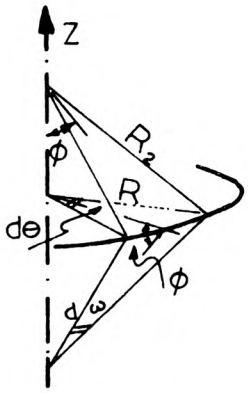

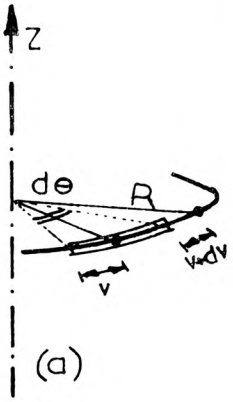

FIGURE 2.14

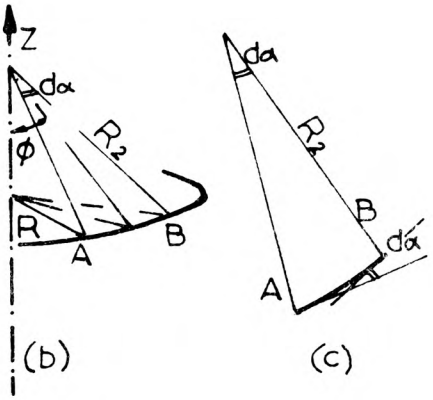

FIGURE 2.15

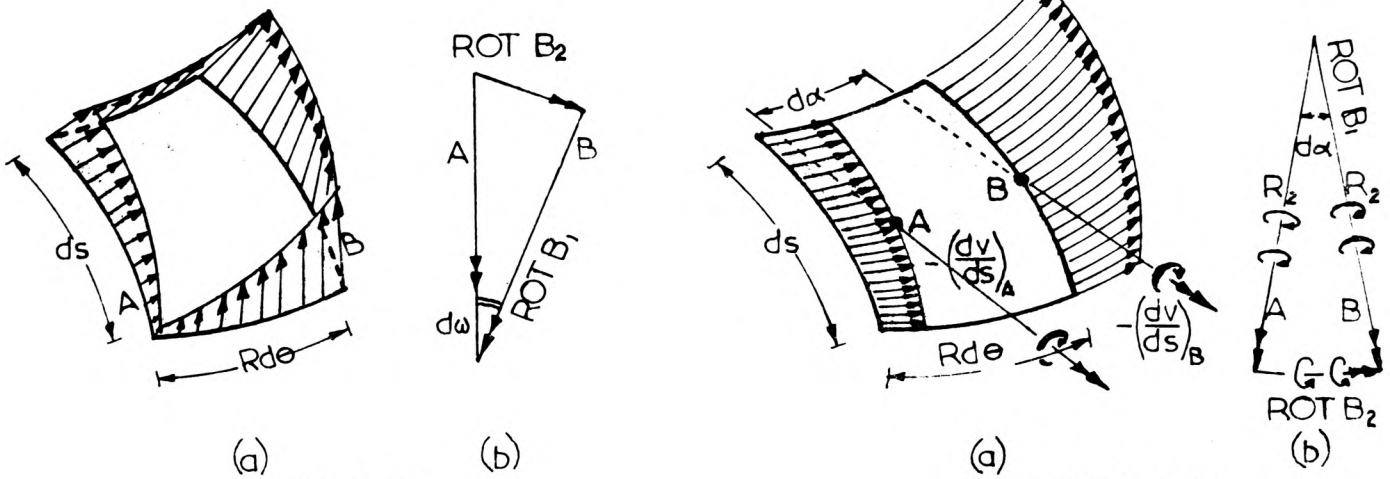

(a) (b) (a) (b)

FIGURE 2.16 FIGURE 2.17

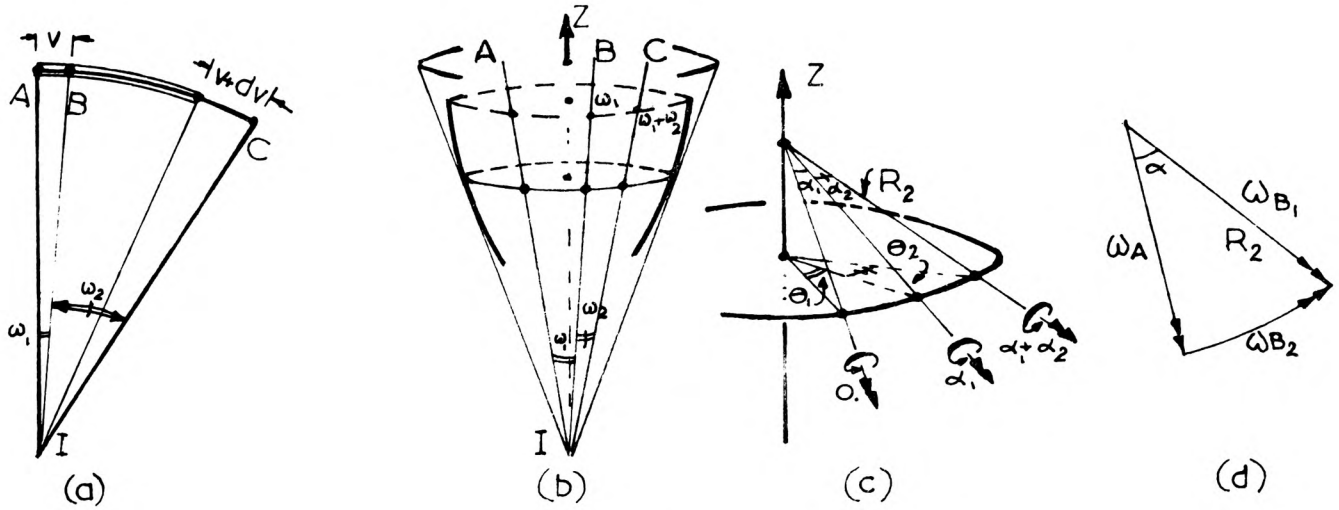

(a) (b) (c) (d)

FIGURE 2.18

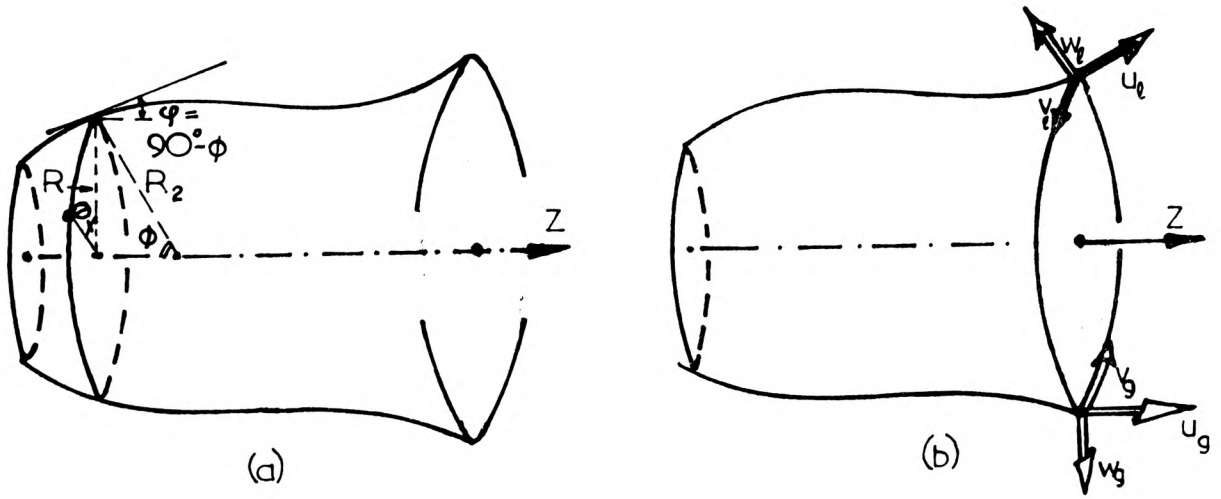

(a) (b)

FIGURE 2.19

CHAPTER 3

THE AXISYMMETRIC THIN SHELL

3.1 Introduction

The fundamental finite element equation as applied to small displacements of linear elastic structures was derived in general terms, in Chapter 1. This equation related the force vector $\{P\}$ and the displacement vector $\{\delta\}$ via the stiffness matrix $[K]$ as given by,

$$\{P\} = [K]\{\delta\}.$$

For thin shells of revolution the possible displacement pattern is somewhat specialised and a sketch of the type of displacements possible is given in Fig. 2.19. Since displacements are one of the prime factors in the finite element analysis they need full consideration. Examination of the nature and the type of displacement has received attention in some detail later in the text. The load vector $\{P\}$ which can include concentrated nodal forces and moments, the forces distributed over the surface of the shell or the body forces (Fig. 1.1), is calculated with the understanding that the nodal values involve appropriate integration round the circumference.

The stiffness matrix $[K]$ being presented in its usual form,

$$[K] = \int [B]^T [D][B]\, d(\text{vol}) ,$$

is really a matrix of surface integrals with d(vol) being t(thickness) x d(surface), and this reduces the integral for thin shells, to summation along the meridian and circumference which further reduces to a single integral. All the details of the finite element formulation and that of the factors particularly relevant to thin shells of revolution are fully discussed in Chapter 3 and Chapter 4.

3.2 Geometry

3.2.1 Consider a linear element P with the variable ξ defined in the domain $-1 \leqslant \xi \leqslant +1$, with both extremities regarded as the nodes of the element. Let us label the nodes corresponding to $\xi = -1$ and $\xi = +1$ as nodes 1 and 2 respectively, as shown in Fig. 3.1. Further consider a nodal variable ϕ_i which assumes a value of unity at a particular node and possesses an interpolated value $\phi_{\xi i}$ at the point ξ on the element as defined by Hermitian-type polynomial $N_i(\xi)$. Thus $\phi_{\xi i} = \phi_i N_i(\xi)$, where subscript i refers to the nodes 1 and 2 by assuming such values. Other Hermitian-type polynomials with unit slope of $\left(\frac{d\phi}{d\xi}\right)_i$ and interpolation function of $N_i'(\xi)$ have to be included to maintain continuity, the contribution of which at the point ξ on the element would be $\phi'_{\xi i} = \left(\frac{d\phi}{d\xi}\right)_i N_i'(\xi)$ (for a detailed account of these polynomials refer to Section 3.3.2). Incorporating these two nodal variables we have:

$$\bar{\phi}_i = \phi_{\xi i} + \phi'_{\xi i}$$

or

$$\bar{\phi}_i = \phi_i N_i(\xi) + \left(\frac{d\phi}{d\xi}\right)_i N_i'(\xi)$$

The latter equation can be represented more aptly as:

$$\phi(\xi) = \sum_{i=1}^{2} \{\phi_i N_i(\xi) + \left(\frac{d\phi}{d\xi}\right)_i N_i'(\xi)\} \qquad \ldots\ldots \text{ eqn. 3.1(a)}$$

Substituting from Hermitian polynomials for $N(\xi)$ and $N_i'(\xi)$,

$$\phi(\xi) = \{\phi_1 \tfrac{1}{4}(\xi^3 - 3\xi + 2) + \left(\frac{d\phi}{d\xi}\right)_1 \tfrac{1}{4}(1-\xi)^2(1+\xi)$$

$$+ \phi_2 \cdot \tfrac{1}{4}(-\xi^3 + 3\xi + 2) + \left(\frac{d\phi}{d\xi}\right)_2 \tfrac{1}{4}(1-\xi)(\xi+1)^2\} \qquad \ldots\ldots \text{ eqn. 3.1(b)}$$

Equation 3.1(a) and (b) represent the variation of the functional $\phi(\xi)$ in terms of two nodal variables and two nodal slopes[1]. The above element P with the defined domain and the shape function is known as the PARENT ELEMENT. This approach to element formulation was first made by Taig[2], then independently by Irons[3] and subsequently was applied to some problems by a number of workers [4],[5],[6]. For application to shells of revolution the following procedure is adopted.

A shell of revolution is proposed to be defined whose axis of symmetry signifies a height relative to a given datum and the radius traces the parallel circles at every position, Fig. 3.2. The geometrical co-ordinates of the mid-surface of the shell are given in terms of Z and R which are in turn defined in terms of some "NODAL" value, namely:

$$Z(\xi) = \sum_{i=1}^{2} \{ Z_i N_i(\xi) + \left(\frac{dZ}{d\xi}\right)_i N_i'(\xi) \} \qquad \ldots\ldots \text{ eqn. 3.2}$$

$$R(\xi) = \sum_{i=1}^{2} \{ R_i N_i(\xi) + \left(\frac{dR}{d\xi}\right)_i N_i'(\xi) \} \qquad \ldots\ldots \text{ eqn. 3.3}$$

The thickness t of the shell along the generator+ is considered to vary identically as the coordinates Z and R, thus:

$$t(\xi) = \sum_{i=1}^{2} \{ t_i N_i(\xi) + \left(\frac{dt}{d\xi}\right)_i N_i'(\xi) \} \qquad \ldots\ldots \text{ eqn. 3.4}$$

+ The current theories of shells of revolution generally deal with thin shells. Attempts have been made to attach numerical values as a test of "thickness" involving the thickness t and some other geometrical property such as the radius R. The formulation in this article is based purely on thin shell theory. It is therefore quite legitimate for a shell to be thin and yet of varying thickness.

Comparing these sets of equation with eqns. 3.1 we define: <u>If the variation in the coordinates Z and R of an element are represented in the same manner as the variation of the unknown function $\phi(\xi)$ of the PARENT ELEMENT, then the former is known as the ISOPARAMETRIC ELEMENT[7].</u>

3.2.2 Equations 3.2, 3.3 and 3.4 will yield the "coordinates" Z, R and t of the element for each value of the parameter ξ provided that the quantities Z_i, $\frac{dZ_i}{d\xi}$, R_i, $\frac{dR_i}{d\xi}$, t_i and $\frac{dt_i}{d\xi}$ (for i = 1,2) are known, this is shown in Fig. 3.3, (a) to (c). These quantities are input for each element and they determine the degree of representation of the mathematical model to the actual shell, as shown in Fig. 3.4.

The result of the introduction of the above quantities presents some interesting features as follows:

a) The slope of the tangent to the generator is given by $\frac{dR}{dZ}$ or in terms of the parameter by $\frac{dR}{d\xi} / \frac{dZ}{d\xi}$. The values of the nodal slopes are then governed by the ratio of $\frac{dR_i}{d\xi}$ and $\frac{dZ_i}{d\xi}$. A true slope conformity between two neighbouring elements N and N + 1 becomes possible by the equality $\left(\frac{dR_2}{d\xi} / \frac{dZ_2}{d\xi}\right)_N = \left(\frac{dR_1}{d\xi} / \frac{dZ_1}{d\xi}\right)_{N+1}$, Fig. 3.5. It must be noted that for neighbouring elements of unequal generator length, the Z and R derivatives on both sides of the node will be unequal.

b) An abrupt change in the slope of the generator can be dealt with in a like manner. Assume that slopes corresponding to nodes 2 and 1 of the neighbouring elements N and N + 1 are given by $\tan\alpha_N$ and $\tan\alpha_{N+1}$.

This change in slope can be incorporated by expressing $\tan\alpha_N = \left(\frac{dR_2}{d\xi} / \frac{dZ_2}{d\xi}\right)_N$ and $\tan\alpha_{N+1} = \left(\frac{dR_1}{d\xi} / \frac{dZ_1}{d\xi}\right)_{N+1}$, as shown in Fig. 3.6.

c) The treatment of shells of revolution with branching is along the lines expressed in the above sections. The coordinates Z and R will be common but the gradients must be prescribed to provide for the slope orientations. Fig. 3.7 is indicative of the above condition.

d) A shell with an abrupt change in thickness can be accommodated at the common node of two elements N and N + 1 with an appropriate choice of the value of thickness $(t_2)_N$ and $(t_1)_{N+1}$, see Fig. 3.8. For any other change of thickness along any given element a maximum variation of up to a cubic (vide eqn. 3.4) is allowed.

3.2.3 Calculation of the Z and R derivatives for input deserves some considerations. In many familiar geometrical shapes it can be written down by inspection. However in unfamiliar cases the calculation consists of the following steps:

i) The scalar length S_N along the generator of the Nth element is calculated numerically or measured directly from a graph, Fig. 3.9.

ii) By considering the distance $S_N/2$ from a node, the mid-point of the element generator is made to correspond with $\xi = 0$ of the parent element.

iii) The value of the tangent to the curve[+] at any node i of the element is assumed to be half the generator length i.e. $\left(\frac{dS}{d\xi}\right)_i = \frac{1}{2}S_N$ (for i=1,2), see Fig. 2.10.

iv) The Z and R derivatives are then determined by solving the following four simultaneous equations:

$$\left.\begin{aligned} (\mathrm{Tan}\alpha_i)_N &= \left(\frac{dR_i}{d\xi} \Big/ \frac{dZ_i}{d\xi}\right)_N \\ \frac{1}{2}S_N &= \sqrt{\left(\frac{dZ_i}{d\xi}\right)^2 + \left(\frac{dR_i}{d\xi}\right)^2} \end{aligned}\right\} \quad i = 1,2$$

see Fig. 3.10.

+ This part of the analysis can be found in most standard text on Differential Geometry. The radius vector $\underset{\sim}{r}$ is given in terms of its components as $\underset{\sim}{r} = \begin{Bmatrix} Z \\ R \end{Bmatrix}$ by differentiation of which with respect to the curve length the tangent $\underset{\sim}{t}$ to the curve is found to be $\underset{\sim}{t} = \frac{d\underset{\sim}{r}}{ds}$ where $\underset{\sim}{t}$ is a unit vector. A scalar product of the tangent would then reveal the value of the curve length derivative, namely

$$\begin{aligned} 1 &= \underset{\sim}{t} \cdot \underset{\sim}{t} \\ &= \frac{d\underset{\sim}{r}}{ds} \cdot \frac{d\underset{\sim}{r}}{ds} \\ &= \left(\frac{d\underset{\sim}{r}}{d\xi} \Big/ \frac{ds}{d\xi}\right) \cdot \left(\frac{d\underset{\sim}{r}}{d\xi} \Big/ \frac{ds}{d\xi}\right) \\ &= \left(\frac{dZ}{d\xi} \Big/ \frac{ds}{d\xi} \quad \frac{dR}{d\xi} \Big/ \frac{ds}{d\xi}\right) \begin{Bmatrix} \frac{dZ}{d\xi} / \frac{ds}{d\xi} \\ \frac{dR}{d\xi} / \frac{ds}{d\xi} \end{Bmatrix} \\ &= \left(\frac{dZ}{d\xi} \Big/ \frac{ds}{d\xi}\right)^2 + \left(\frac{dR}{d\xi} \Big/ \frac{ds}{d\xi}\right)^2 \\ &= \left[\left(\frac{dZ}{d\xi}\right)^2 + \left(\frac{dR}{d\xi}\right)^2 \Big/ \left(\frac{ds}{d\xi}\right)^2\right]. \end{aligned}$$

It can be seen that the curve length derivative is $\frac{ds}{d\xi} = \sqrt{\left(\frac{dZ}{d\xi}\right)^2 + \left(\frac{dR}{d\xi}\right)^2}$.

The bold letters $\underset{\sim}{r}$ and $\underset{\sim}{t}$ refer to vector quantities.

3.3 Displacements

3.3.1 Reference was made to the geometry of the ISOPARAMETRIC element in the last section. The equations defining the geometry were (eqn. 3.2 and eqn. 3.3):

$$Z(\xi) = \sum_{i=1}^{2} \{Z_i N_i(\xi) + \frac{dZ_i}{d\xi} N_i'(\xi)\}$$

$$R(\xi) = \sum_{i=1}^{2} \{R_i N_i(\xi) + \frac{dR_i}{d\xi} N_i'(\xi)\}$$

The definition of the ISOPARAMETRIC element can now be utilized to yield the global displacements u (replacing Z and in the direction of Z) and w (replacing R and in the direction of R), thus:

$$u(\xi) = \sum_{i=1}^{2} \{u_i N_i(\xi) + \frac{du_i}{d\xi} N_i'(\xi)\} \qquad \ldots\ldots \text{ eqn. 3.5(a)}$$

$$w(\xi) = \sum_{i=1}^{2} \{w_i N_i(\xi) + \frac{dw_i}{d\xi} N_i'(\xi)\} \qquad \ldots\ldots \text{ eqn. 3.5(b)}$$

These equations are termed BASIC FUNCTIONS and are shown in Fig. 3.11. The very formulation of these displacements implies the compatibility at the common node of two (or more) adjacent elements. These properties of geometrical conformity and mechanical compatibility are some of the desirable features of the isoparametric family.

The above Basic functions would describe correctly the actual displacement pattern of the shell when the physical size of the element becomes infinitesimal. For an element of 'FINITE' size however, compatibility at the nodes is a necessary but not a sufficient condition. Additional displacements independent of the above are needed to ensure that the element deformations are sufficiently close to the actual structure. These internal

displacements which can be regarded as being associated with internal (or hierarchical) degrees of freedom, would then have to possess zero value and zero derivative at the nodes. the term applied to "Additional displacements" is SURPLUS FUNCTIONS shown in Fig. 3.12 and sufficient discussion is devoted to them in future sections. It is felt that the displacements devised in this element indicate a significant breakthrough in this field. These shape functions are due to Irons[8].

3.3.2 BASIC FUNCTIONS - Third-order Hermitian-type polynomials are thought to represent the Basic Functions quite adequately. They consist of two pairs of shape functions having "unit value" and "unit slope" at each node and are listed below:

$$B_1 = N_1(\xi) = \tfrac{1}{4}\{\xi^3 - 3\xi + 2\} \quad \ldots\ldots \text{eqn. 3.6(a)}$$

$$B_2 = N_1'(\xi) = \tfrac{1}{4}\{(1-\xi)^2(1+\xi)\} \quad \ldots\ldots \text{eqn. 3.6(b)}$$

$$B_3 = N_2(\xi) = \tfrac{1}{4}\{-\xi^3 + 3\xi + 2\} \quad \ldots\ldots \text{eqn. 3.6(c)}$$

$$B_4 = N_2'(\xi) = \tfrac{1}{4}\{(1-\xi)(\xi+1)^2\} \quad \ldots\ldots \text{eqn. 3.6(d)}$$

Figures 3.11(a) - (d) are graphical representations of the Basic functions and Fig. 3.13(a) and (b) show the deformation of the generator when the first of the Basic Functions is applied to the generator of the element. Some care must be taken when dealing with slope functions B2 and B4 for two completely different reasons. Firstly the length of the PARENT element is 2 units and if the slope functions B2 and B4 are stretched to the new length s_N - the length of the element generator - then the slope will reduce by a value of $\frac{ds}{d\xi}$ everywhere along the generator. Attention is given to this problem when dealing with strains and curvatures and remedial measures are taken (Section 3.5.6). The second point arises when the mechanical deformation of the generator due to rotations are

considered. The slope functions B2 and B4 become meaningless when applied as global displacements since the only physical rotation is the rotation of the generator relative to itself in the undeformed position as the local coordinates. This difficulty is overcome by a simple transformation of axis.

The final point regarding the Basic Functions is that by reason of being cubic polynomials they are better suited for numerical processing than power series[8],[9].

3.3.3 SURPLUS FUNCTIONS - The independence of the surplus functions from the Basic is fully satisfied if the former has zero values and zero derivatives at the nodes. This is achieved through a set of functions shown in Fig. 3.12 and are given below:

(a) $S_0 = Q_0 = D^0(\xi^2 - 1)^2 = (\xi^2 - 1)^2$

(b) $S_1 = Q_1 = D^1(\xi^2 - 1)^3 = (\xi^2 - 1)^2 6\xi$

(c) $S_2 = Q_2 = D^2(\xi^2 - 1)^4 = 8(7\xi^2 - 1)(\xi^2 - 1)^2$

(d) $S_3 = Q_3 = D^3(\xi^2 - 1)^5 = 240\ (3\xi^2 - 1)(\xi^2 - 1)^2$

$\vdots$

(n) $S_N = Q_N = D^N(\xi^2-1)^{N+2}$

The functions above are polynomials with their actual formulation and generation being designed to eliminate numerical ill-conditioning. The full derivation of the function is discussed in Appendix (1).

The use of the above functions as displacements are two-fold, global and local. There are provisions for the use of both alternatives. The same term Q_n can be used for both u and w displacements. It was found that in forming the strains and curvatures w displacements were differentiated to one higher order than u displacements, thus an

additional term of Q_n was thought to be desirable. In Fig. 3.14(a) and (b) global displacements are shown for the term Qo. Diagramatic representation of local in-plane displacements (u_{local}) becomes more difficult where as the local normal displacement (w_{local}) is more easily achieved. Figures 3.15(a) and (b) show the local in-plane and normal displacement for the term Q1 of surplus functions.

3.3.4 SUBROUTINE SHPFN - (SHaPe FunctioN) - This is basically a service subroutine providing the Basic and Surplus functions. The variables influencing the operation of the subroutine are ξ at which point the shape functions are computed and the integer NQ which is the total number of Basic and Surplus Functions required. The shape functions and their first, second and third derivatives are generated in the $Q[4 \times NQ]$ matrix with values and the derivatives being positioned in the first, second, third and fourth rows respectively. The "KICK-OFF" values Q'_{-1}, Q''_{-1}, Q'''_{-1}, Q_0, Q'_0, Q''_0 and Q'''_0 are written in fourth and fifth columns of $[Q]$ as shown in Fig. 3.16(a) and using these, the values of Q_n for $n \geq 1$ are generated. The first four columns are over-written by the Basic Functions abbreviated as H (for Hermitian-type) and the final form is indicated in Fig. 3.16(b). The point ξ is a stress sampling point and when integration is carried out it could be a Gauss-point.

3.4 Strain/Displacement and Stress/Strain relationships in the axisymmetric case

3.4.1 The method of approach in this Chapter is greatly simplified since only the effects of the axisymmetric loading on the structure are examined. This in turn brings about the opportunity of projecting certain features of the element formulation which

otherwise might have been obscured by the intricacies of the full Kinematic relationships. As a result of this simplification, the following derivatives and quantities contributing to the Kinematic equations of Section 2.5 would become zero; these involve the variables and the terms along the circumference. Thus,

$$\frac{1}{R}\frac{\partial(\ldots)}{\partial\theta} \quad , \quad \frac{1}{R^2}\frac{\partial^2(\ldots)}{\partial\theta^2} \quad \text{and} \quad \frac{1}{R}\frac{\partial^2(\ldots)}{\partial\theta\partial s} = 0,$$

and similarly,

$$v,\ \varepsilon_{s\theta},\ \chi_{s\theta},\ T_{s\theta} \text{ and } M_{s\theta} = 0.$$

It is hoped that Figures 3.17(a),(b) and (c) illustrate the above simplification graphically, while Fig. 3.18 provides a visual summary of the stress resultants on an infinitesimal element of the shell. The simplified matrix equation of Chapter 2 would then appear as,

$$\begin{Bmatrix} \varepsilon_s \\ \varepsilon_\theta \\ \chi_s \\ \chi_\theta \end{Bmatrix} = \left[\begin{array}{c|c} \cos\alpha\,\frac{\partial}{\partial s} & \sin\alpha\,\frac{\partial}{\partial s} \\ 0 & \frac{1}{R} \\ \sin\alpha\,\frac{\partial^2}{\partial s^2} & -\cos\alpha\,\frac{\partial^2}{\partial s^2} \\ \frac{\sin\alpha}{R}\,\frac{\partial}{\partial s} & -\frac{\cos\alpha}{R}\,\frac{\partial}{\partial s} \end{array}\right] \begin{Bmatrix} u \\ w \end{Bmatrix}_{\text{global}} \quad \ldots\ldots \text{ eqn. 3.8}$$

As can be observed, no shear or twist term appears in the above equation.

In the actual program the strain components produced are not arranged in a vector form since each vector corresponds to a given displacement and its derivatives, thus for "NT" arbitrary displacements (H.functions and Q-functions, see 3.3.4). There are NT strain vectors. The whole collection of strain vectors

$\{\varepsilon\}$ is computed at a particular value of ξ - the parameter for the Parent Element - and as can be seen from 3.5.2, this corresponds to a Gauss-point or an integrating point.

3.4.2 To enumerate the elastic matrix $[D]$ some standard equations, especially those presented for plane-stress by Zienkiewicz (ref.(1), P.53) are directly applicable, namely,

$$[D] = \frac{E}{1-\nu^2} \begin{bmatrix} 1 & \nu & 0 \\ \nu & 1 & 0 \\ 0 & 0 & \text{no shear} \end{bmatrix} .$$

But since the material properties meridionally, could be different from corresponding properties circumferentially (i.e. different nature of reinforcement in concrete, plastics, etc.), a more general relationship was thought to be convenient resulting in,

$$[D] = \frac{E_2}{1-n\nu_2^2} \begin{bmatrix} n & n\nu_2 \\ n\nu_2 & 1 \end{bmatrix} , \quad \text{where } n = \frac{E_1}{E_2} .$$

In most analyses since the force per unit length $[T]$ is preferred to force per unit area $\{\sigma\}$, it is customary to multiply the elastic matrix at the point by the corresponding thickness $t(\xi)$, so that the product $[D]\{\varepsilon\}$ results in $\{T\}$ directly and not in $\{\sigma\}$. Similar relationships could be written (ref.(17),P.432) for moments $\{M\}$ and curvatures $\{\chi\}$ which with a slight change in notation and convention is given as,

$$M_s = \mathscr{D}(\chi_s + \nu\chi_\theta)$$
$$M_\theta = \mathscr{D}(\nu\chi_s + \chi_\theta) \quad \text{or} \quad \begin{Bmatrix} M_s \\ M_\theta \end{Bmatrix} = [\mathscr{D}] \begin{Bmatrix} \chi_s \\ \chi_\theta \end{Bmatrix}$$

where $\mathscr{D}$ is equal to $\frac{Et^3}{12(1-\nu^2)}$. Taking orthotropy in bending into account and presenting the in-plane and moment elements of the

elastic matrix in a unified form the following equation is obtained

$$[D] = \frac{E_2 t}{1-n\nu_2^2} \begin{bmatrix} n & n\nu_2 & 0 & 0 \\ n\nu_2 & 1 & 0 & 0 \\ 0 & 0 & \frac{nt^2}{12} & \nu_2\frac{nt^2}{12} \\ 0 & 0 & \nu_2\frac{nt^2}{12} & \frac{t^2}{12} \end{bmatrix} \quad \ldots\ldots \text{ eqn. 3.9}$$

If the material is isotropic then $E_1 = E_2$ and $n = 1$ and the above reduces to the equation given in reference (1), page 139.

The stress and moment components $\{T\}$ calculated from $[D]$ and $\{\varepsilon\}$ are in a similar manner to strains namely they are collection of NT stress vectors each obtained individually from the product $[D]\{\varepsilon\}$ and without any modifications they are stresses corresponding to unit nodal variables. To obtain the correct stress at a given sampling point the summation,

$$\{T\} = [D](\{\varepsilon\}_1\delta_1^e + \{\varepsilon\}_2\delta_2^e + \ldots\ldots \{\varepsilon\}_{NT}\delta_{NT}^e) , \quad \ldots\ldots \text{ eqn. 3.10}$$

must be carried out, where δ_i^e is equal to i-th displacement vector, after the "correct" displacements have been determined. The stresses and moments on an infinitesimal element would appear as depicted in Fig. 3.18.

In forming the stiffness matrix $[K]$, the actual value of stress $\{T\}$ defined in eqn. 3.10 is not required but the stresses resulting from shape functions namely,

$$\{T\} = [D]\{\varepsilon\} = [D][B]\{\delta\},$$

are used.

3.5 Details of Calculations of Axisymmetric Case

3.5.1 Multiplication of Quantities - Owing to the nature of the isoparametric formulation, namely the expression of the shape functions in terms of ξ, most of the other variables which are constantly up-dated in the program, are either in terms of ξ or its derivatives. Therefore when the product of two quantities or their derivatives of their product are required, a simple multiplication would not suffice. With this in mind the following equations resulting from the product of two general quantities $A(\xi)$ and $B(\xi)$ are written down, using elementary laws of differentiation.

$$C = A.B \qquad \ldots\ldots \text{ eqn. 3.11(a)}$$

$$\frac{dC}{d\xi} = \frac{d}{d\xi}(A.B) = A\frac{dB}{d\xi} + B\frac{dA}{d\xi} \qquad \ldots\ldots \text{ eqn. 3.11(b)}$$

$$\frac{d^2C}{d\xi^2} = \frac{d^2}{d\xi^2}(A.B) = A\frac{d^2B}{d\xi^2} + 2\frac{dA}{d\xi}\cdot\frac{dB}{d\xi} + B\frac{d^2A}{d\xi^2} \qquad \ldots\ldots \text{ eqn. 3.11(c)}$$

The above relations can be applied to calculate a wide range of quantities such as products, squares and ratios, as can be seen from the following sections. A special Subroutine was devised to fulfil this requirement when called which was labelled Shape Function MULTiplier, SFMULT.

3.5.2 Differentiation with Respect to s - The differentiation carried out when using the Kinematic and other relations should be made with respect to s, the intrinsic variable, whereas all the available terms contain ξ as explained before. It is therefore essential that a systematic generation and grouping of terms in terms of s is made with ξ still as the parameter. Typical sets of quantities needed for calculation of strains would be $\sin[\alpha(\xi)]$,

$\cos[\alpha(\xi)]$, $R(\xi)$, $\frac{\partial(\ldots)}{\partial s(\xi)}$, $\frac{\partial^2(\ldots)}{\partial s(\xi)^2}$ and $\frac{\partial}{\partial s(\xi)}\left\{\frac{\cos[\alpha(\xi)].w(\xi)}{R(\xi)}\right\}$, etc.

Formation of $R(\xi)$ and its derivatives are through equations 3.1(b) and eqn. 3.3. The derivatives R_ξ, $R_{\xi\xi}$ and $R_{\xi\xi\xi}$ are calculated and retained in a Column form without any difficulties using Hermitian (Basic) functions H_1, ..., H_4 (Fig. 3.16(b)). In an identical manner $Z(\xi)$ and its derivatives Z_ξ, $Z_{\xi\xi}$, and $Z_{\xi\xi\xi}$ are calculated and stored in a vector form.

The formation of derivatives with respect to curve length $\frac{\partial(\ldots)}{\partial s}$ is a natural development from the above paragraph and involves both $Z(\xi)$, $R(\xi)$ and their derivatives (vide foot-note on page 3.6). The function s is never calculated in its explicit value but always retained in the differential form.

From

$$\left(\frac{ds}{d\xi}\right)^2 = \left(\frac{dZ}{d\xi}\right)^2 + \left(\frac{dR}{d\xi}\right)^2 ,$$

$\left(\frac{ds}{d\xi}\right)$ is calculated in four stages.

(i) $\left(\frac{dZ}{d\xi}\right)^2$, $\frac{d}{d\xi}\left[\left(\frac{dZ}{d\xi}\right)^2\right]$ and $\frac{d^2}{d\xi 2}\left[\left(\frac{dZ}{d\xi}\right)^2\right]$ are obtained by double application of Subroutine SFMULT on the column containing $Z(\xi)$ and its derivatives. Similarly $\left(\frac{dR}{d\xi}\right)^2$, $\frac{d}{d\xi}\left[\left(\frac{dR}{d\xi}\right)^2\right.$ and $\frac{d^2}{d\xi 2}\left[\left(\frac{dR}{d\xi}\right)^2\right]$ are obtained using the same Subroutine twice on the column containing $R(\xi)$ and its derivatives.

(ii) The term by term addition of the corresponding elements of the columns generated in (i) results in $\left(\frac{ds}{d\xi}\right)^2$ and its derivatives $\frac{d}{d\xi}\left[\left(\frac{ds}{d\xi}\right)^2\right]$ and $\frac{d^2}{d\xi}2\left[\left(\frac{ds}{d\xi}\right)^2\right]$, since the law of adding derivatives is commutative.

Now the following short-hand is adopted.

$$F = (s_\xi)^2,\ F_\xi = \frac{d}{d\xi}\left[(s_\xi)^2\right] \text{ and } F_{\xi\xi} = \frac{d^2}{d\xi}2\left[(s_\xi)^2\right]$$

(iii) Since the first derivative of any functional ϕ with respect to s can be calculated easily in the parametric form,

$$\frac{d\phi}{ds} = \frac{\phi_\xi}{s_\xi} = \phi_\xi \cdot s_\xi^{-1} ,$$

it was found more useful to find the higher order derivatives also in the parametric form along the following lines. Use additional short-hand in the form,

$$G = (1/s_\xi),\ G_\xi = \frac{d}{d\xi}(1/s_\xi) \text{ and } G_{\xi\xi} = \frac{d^2}{d\xi}2\ (1/s_\xi).$$

The quantities F are available in a vector form, then the G quantities can be calculated as,

$$G = 1/s_\xi$$
$$= 1/(F)^{\frac{1}{2}}$$
$$G = F^{-\frac{1}{2}} \qquad \ldots\ldots \text{ eqn. } 3.12(a)$$

also,

$$G_\xi = \frac{d}{d\xi}(F^{-\frac{1}{2}})$$
$$= -\tfrac{1}{2}F_\xi/F^{3/2}$$
$$\therefore\ G_\xi = -\tfrac{1}{2}F_\xi G/F \qquad \ldots\ldots \text{ eqn. } 3.12(b)$$

and finally,

$$G_{\xi\xi} = \frac{d}{d\xi}(G_\xi)$$

$$= -\tfrac{1}{2}\left(\frac{F_{\xi\xi}}{F^{3/2}} - \frac{3}{2}\frac{F_\xi^2}{F^{5/2}}\right)$$

$$= \frac{3}{4}\frac{F_\xi^2}{F^{5/2}} - \tfrac{1}{2}\frac{F_{\xi\xi}}{F^{3/2}}$$

$$G_{\xi\xi} = 3G_\xi^2/G - \tfrac{1}{2}F_{\xi\xi}G/F \qquad \ldots\ldots \text{ eqn. 3.12(c)}$$

The values of G in a vector form replace those of F since there would be no further need for the latter.

(iv) The derivatives with respect to s of any functional ϕ can now be calculated as shown,

$$\frac{\partial\phi}{\partial s} = \phi_\xi.(1/s_\xi)$$

$$\therefore \quad \frac{\partial\phi}{\partial s} = \phi_\xi.G \qquad \ldots\ldots \text{ eqn. 3.13(a)}$$

$$\frac{\partial^2\phi}{\partial s^2} = \frac{d}{ds}(\phi_\xi.G)$$

$$= \frac{d}{d\xi}(\phi_\xi.G).\frac{d\xi}{ds}$$

$$= (\phi_{\xi\xi}G + \phi_\xi G_\xi)G$$

$$= \phi_{\xi\xi}G^2 + \phi_\xi G_\xi G \qquad \ldots\ldots \text{ eqn. 3.13(b)}$$

and similarly derivatives of any order could be found if required.

Note that the Subroutine SFMULT is really used to form the s derivatives of the functional ϕ by apparently forming the products of the appropriate G and ϕ columns.

3.5.3 Calculation of Trignometric terms with view to Rotation of Axis

Once s_ξ^{-1} and its derivatives are prepared, the trignometric terms could then be generated. It is helpful to refer to Fig. 2.7 and Fig. 2.8 and by substituting for $\alpha = 90-\phi$, the following expressions can be written,

$$\cos\alpha = \frac{dZ}{ds}$$

$$= \frac{Z_\xi}{s_\xi}$$

$$\cos\alpha = Z_\xi.G,$$

and similarly,

$$\sin\alpha = R_\xi.G.$$

The separate operations of SFMULT on {Z}, {G} and {R}, {G} result in ($\cos\alpha$ $\frac{d}{d\xi}\cos\alpha$ $\frac{d^2}{d\xi^2}\cos\alpha$) and ($\sin\alpha$ $\frac{d}{d\xi}\sin\alpha$ $\frac{d2}{d\xi^2}\sin\alpha$).

3.5.4 Displacement Transformation - It was pointed out (Section 3.3) that it was ideal to have a choice of local or global system of displacements with surplus degrees of freedom (Q-functions), at the formulation stage. However, prior to the formation of strains all displacements must consistently be one or the other. In this scheme of work since the rigid body motions (discussed in Chapter 4) are in the global system of coordinates, a global system of displacements is also chosen. There might be a slight ambiguity in the meaning of the term "global system of displacements". It is meant that the displacements fed into the kinematic relationships are expressed in terms of the global coordinates. This does not mean that all the displacements generated must necessarily be global. Thus the necessity arises that the locally orientated displacements must first be processed into the global system so that subsequently they can be operated upon by the [B]matrix.

The transformation is standard and is carried out as follows:-

$$u_i^g = u_i^\ell(\cos\alpha)_i - w_i^\ell(\sin\alpha)_i$$

$$w_i^g = u_i^\ell(\sin\alpha)_i + w_i^\ell(\cos\alpha)_i \qquad \ldots\ldots \text{ eqn. 3.14(a)}$$

or $$\begin{Bmatrix} u \\ w \end{Bmatrix}_i^g = \begin{bmatrix} \cos\alpha & -\sin\alpha \\ \sin\alpha & \cos\alpha \end{bmatrix} \begin{Bmatrix} u \\ w \end{Bmatrix}_i^\ell \qquad \ldots\ldots \text{ eqn. 3.14(b)}$$

where superscript g and ℓ refer to global and local displacement systems and suffix i can assume symbols 0, ξ and $\xi\xi$ denoting zeroth, first and second derivatives. Subroutine SFMULT is again applied to individual columns e.g. $\{u\}^\ell$,$\{\cos\alpha\}$to result the product in the expected column form.

3.5.5 <u>The Variables associated with the Slopes at the Nodes</u> - Having converted all the displacements to global system one anomaly remains. The derivatives obtained from the slope functions B2 and B4, unless expressed relative to the generator and its normal have little physical significance, since the genuine rotation of the shell must be expressed locally. In actual practice it is just as easy to perform a rotation towards local axes of the strains and curvatures as it is to convert the displacements initially. This is illustrated for the variables resulting from B2 and B4 (Fig. 3.11) as follows:

$$[L]_\alpha = \begin{bmatrix} \cos\alpha & -\sin\alpha \\ \sin\alpha & \cos\alpha \end{bmatrix}, \quad [L]_0 = \begin{bmatrix} 1 & 0 \\ 0 & 1 \end{bmatrix}, \quad [L]_{90} = \begin{bmatrix} 0 & -1 \\ 1 & 0 \end{bmatrix},$$

$$\{\delta\}^g = [L]_\alpha \{\delta\}^\ell \quad , \{\delta\}^g = \{{}^{u}_{w}\}^g \quad , \quad \{\varepsilon\} = [B]\{\delta\}^g \quad ,$$

$$\{\varepsilon_j\}_{B2,B4} = [B_{j1} \quad B_{j2}][L]_\alpha \{\delta\}^\ell = [B_{j1} \quad B_{j2}] \begin{Bmatrix} u\cos\alpha - w\sin\alpha \\ u\sin\alpha + w\cos\alpha \end{Bmatrix} \quad j=1,4$$

$$= \{B_{j1}u\cos\alpha - B_{j1}w\sin\alpha + B_{j2}w\cos\alpha + B_{j2}u\sin\alpha\}$$

$$= \{\cos\alpha [B_{j1} B_{j2}] \{{}^{u}_{w}\} + \sin\alpha [B_{j1} B_{j2}] \{{}^{-w}_{u}\}$$

now

$$\{{}^{u}_{w}\} = [L]_0 \{{}^{u}_{w}\} \quad , \quad \{{}^{-w}_{u}\} = [L]_{90} \{{}^{u}_{w}\}$$

$$\therefore \{\varepsilon_j\}^L_{B2,B4} = \{\cos\alpha [L]_0 \{\varepsilon_j\} + \sin\alpha [L]_{90} \{\varepsilon_j\}\}$$

$$= \left(\begin{bmatrix} \cos\alpha & 0 \\ 0 & \cos\alpha \end{bmatrix} + \begin{bmatrix} 0 & -\sin\alpha \\ \sin\alpha & 0 \end{bmatrix} \right) \{\varepsilon_j\}$$

$$= \begin{bmatrix} \cos\alpha & -\sin\alpha \\ \sin\alpha & \cos\alpha \end{bmatrix} \{\varepsilon_j\}$$

$$\therefore \{\varepsilon_j\}^\ell_{B2,B4} = [L]\{\varepsilon\} \qquad \ldots\ldots \text{ eqn. 3.15}$$

Now strains from B2 and B4 functions for w_ℓ become "genuine" where as the degrees of freedom from B2 and B4 for u_ℓ have no significance and could be regarded as surplus.

3.5.6 Scaling of Slopes - The gradient of the functions B2 and B4 which possessed unit slopes with the Parent Element no longer remains unity when stretched to a new length s*, shown in Fig. 3.21. Therefore a final adjustment of $\left(\frac{ds}{d\xi}\right)_i$ in slopes becomes essential, to restore the nodal value of the slopes to the desired amount of unity. All the quantities such as the strains and the external work terms are modified for "genuine" slopes for B2 and B4 functions only.

---

* see footnote of page 3.21

Points discussed in Section 3.4.5 and here are implemented together i.e. at the same time when some displacements are turned back into local coordinates, their slopes are also scaled up to unity.

3.5.7 Derivation of the Elements of Loading - The following cases are treated for the work done by external actions.

i) Meridionally varying pressure p(s):

The force on a ring length ds normal to the surface = $p(2\pi R)ds$ or globally,

$$\begin{Bmatrix} dF_z \\ dF_R \end{Bmatrix} = \begin{Bmatrix} -\sin\alpha \\ \cos\alpha \end{Bmatrix} p(2\pi R)ds$$

Work done on the ring = $(u \quad w)_g \begin{Bmatrix} dF_z \\ dF_R \end{Bmatrix}$

$$\text{Work done} = 2\pi pR(-u_g \sin\alpha + w_g \cos\alpha)ds$$

See Fig. 3.20(a).

For any finite element a maximum of linear variation of loads along the meridian is allowed.

---

* This point can be illustrated by considering the trivial case of a beam element of length L, the variation of the lateral displacement of which is assumed to be $w = \frac{1}{4}\left\{\left[1-(\frac{2x}{L})^2\right]\left[1+(\frac{2x}{L})\right]\right\}$ where $\xi = \frac{2x}{L}$. The slope $\theta = \frac{dw}{dx}$ can be calculated from $\theta = \frac{1}{4} \cdot \frac{2}{L} \cdot \left[-1-2(\frac{2x}{L})+3(\frac{2x}{L})^2\right]$ for $-\frac{L}{2} \leq x \leq \frac{L}{2}$. It can be seen that the slope at $x = -\frac{L}{2}$ is not unity but $\theta = \frac{2}{L}$. A simple corrective measure in this case would be to retain the function w in its original form but multiply the slopes by a factor of $(\frac{2}{L})^{-1}$ when any slope calculations are required. The extension of this adjustment to the curvilinear case should now be obvious, Fig. 3.21.

ii) Constant Gravitational Field g:

Taking the same elemental ring, the force along the Z-axis is

$$dF_z = \rho tg(2\pi R)ds,$$

$$\therefore \quad \text{work done} = (2\pi Rt)\rho g u_g ds.$$

This is shown in Fig. 3.20(b).

iii) Centripetal forces from constant angular frequencies:

Force on the ring shown in Fig. 3.20(c) due to ω is given by,

$$dF_R = \left[(2\pi R)tds\right]\rho(\omega^2 R),$$

$$\therefore \quad \text{work done} = 2\pi R^2 \rho\, tds.\omega^2.w_g.$$

iv) Concentrated Nodal Loads:

These loads are added at the nodal points only. The work done is numerically equal to the actual forces, since they suffer unit deflections or rotations at the nodes, see Fig. 3.20(d).

Other type of loading such as thermal forces are not included presently but could be incorporated at a later date.

3.5.8 Quadrature - When determining the stiffness matrix and the load vector, integration was extended over the surface and the volume of the shell. For the axisymmetric case, the integral extending to the circumference and the generator reduces as shown,

$$\iint (\ldots)Rd\theta ds = \int(\ldots)2\pi Rds.$$

For the reduced integral to be in a workable form, it must be represented parametrically in terms of ξ, since the "sampling" points extend from -1 to +1 on the parent element. The following

representations are made for the area and the volume integrals, for any functional ϕ,

$$\int_A \phi.(2\pi R)ds = \int_{-1}^{+1} \phi.(2\pi R)\frac{ds}{d\xi}\, d\xi,$$

$$\int \phi.(2\pi R)tds = \int_{-1}^{+1} \phi.(2\pi R)t\frac{ds}{d\xi}d\xi.$$

The R.H.S. of both equations can be integrated numerically using Gaussian Quadrature with the appropriate symbols and factors being replaced, thus;

$$\int_{-1}^{+1} \phi.(2\pi R)\frac{ds}{d\xi}d\xi = \sum_{i=1}^{n} \phi_i.(2\pi R_i)(\frac{ds}{d\xi})_i W_i, \quad \ldots\ldots \text{ eqn. 3.16(a)}$$

$$\int_{-1}^{+1} \phi.t(2\pi R)\frac{ds}{d\xi}d\xi = \sum_{i=1}^{n} \phi_i(2\pi R_i t_i)(\frac{ds}{d\xi})_i W_i, \quad \ldots\ldots \text{ eqn. 3.16(b)}$$

where W_i is the weighting constant at a Gauss-Point and n is the number of points used for integration.

The number of Gauss-points is found to be dependent on the order of the surplus functions and the latter being a variable in each problem and even differ from one element to the next for the same problem. A rough guide of n = 2(N+4)-1 was considered where N is the order of the highest surplus term Q_N. A subroutine was written to provide the Gauss-Points and the corresponding weighting constants of required order for integration and sampling purposes.

Needless to say that the quantities sometimes labelled with the suffix i, indicate that they have been calculated at a Gauss-point; sometimes the suffix is omitted for brevity. Examples of the use of the sampling points are given in the next section.

3.5.9 Formation of Stiffness Matrix and Load Vector - Preparation for Gaussion Quadrature is made in this section (see 3.5.2). Because of the provisions for variation in thickness, the latter is calculated at the Gauss-point ξ to yield $t(\xi_i)$ or simply t_i from equation 3.4.

Since the variable required is ds and the Gauss-points available are in terms of ξ_i, a change of variable $\left(\frac{ds}{d\xi}\, d\xi\right)_i$ is made. The weighting constant W_i is thus modified to $\left(\frac{ds}{d\xi}\right)_i W_i$ which is now in a usable form.

One of the first items to be modified are the elements of the elastic matrix $[D]_{kj}$ which when multiplied by the weighting factor will appear as,

$$(2\pi R_i).\left(\frac{ds}{d\xi_i}\right)W_i[D_i] = \frac{\left[(2\pi R_i)\left(\frac{ds}{d\xi_i}\right)W_i\right]E_2 t_i}{(1-n\nu_2{}^2)} \left[\begin{array}{cc:cc} n & n\nu_2 & 0 & 0 \\ n\nu_2 & 1 & 0 & 0 \\ \hdashline 0 & 0 & \frac{nt_i^2}{12} & \frac{\nu_2 nt_i^2}{12} \\ 0 & 0 & \frac{\nu_2 nt_i^2}{12} & \frac{t_i^2}{12} \end{array}\right] \quad \text{eqn.3.17}$$

As it may have been noticed the area and volume integrals are now replaced by

$$\left[(2\pi R_i).\left(\frac{ds}{d\xi}\right)_i W_i\right] \text{ and } \left[(2\pi R_i).\left(\frac{ds}{d\xi}\right)_i W_i t_i\right] \text{ respectively.}$$

The stress term $\{T\} = [D]\{\varepsilon\}$ will now contain,

$$\{T_i\} = (2\pi R_i)\left(\frac{ds}{d\xi}\right)_i W_i\, [D_i]\{\varepsilon_i\} \quad .$$

The accumulation of the product of which with $\{\varepsilon_i\}^T$ will result in generation of stiffness matrix $[K]$ for the element which is,

$$[K] = \int_A \{\varepsilon\}^T \{T\} dA = \sum_{i=1}^{n} \{\varepsilon_i\}^T [D_i] \{\varepsilon_i\} (2\pi R_i) \left(\frac{ds}{d\xi}\right)_i W_i \quad \ldots\ldots \text{eqn. 3.18}$$

The Potential energy terms of 3.5.7(i), (ii) and (iii) resulting in consistent load vector, are obtained similarly by a symbolic representation of,

$$\{P\} = \int [N]^T \{p\} dA = \sum_{i=1}^{n} [N_i]^T \{p_i\} (2\pi R_i) \left(\frac{ds}{d\xi}\right)_i W_i \quad \ldots\ldots \text{eqn. 3.19}$$

3.5.10 The stiffness matrix and the stresses are generated in a SUBROUTINE called SHELL, the block diagram of which is laid out in Fig. 3.22.

3.6 Some Examples

The program was tested for some of the cases for which an analytical solution existed. It was felt that a remarkable accuracy was inherent in the Element of the present formulation as can be observed from the presented results. For almost every problem the number of elements required to satisfy the geometry was few and the numbers of surplus degrees of freedom required were also surprisingly low.

3.6.1 "Long cylindrical shell of uniform thickness" - In stressing a shell of this nature, there are various loading alternatives. A concrete storage tank was thought to be a suitable example. Some theoretical values were given by Billington[10] for a tank with the following set of dimensions.

$Z = 20.0$ ft. $\quad E = 2.88 \times 10^8$ lbf/ft^2

$R = 27.0$ ft.

$t = 1.25$ ft. $\quad \nu = 1/6$

(a) Firstly the tank was subjected to an edge moment to investigate the rate of decay of the "ripples" along the generator, Fig. 3.23 (b) and (c).

Secondly, the effect of shifting the point $\xi = 0$ to an off-centric position was examined. It can be noticed that the value of M_s improves when, $\xi = 0$ is nearer to the loaded edge. It appears that this interference causes more integrating points to be concentrated in the left half of the shell and thus integrate that portion more closely. Figure 3.23(a) indicates the convergence of the variation with surplus degrees of freedom and also indicates the effect of $\xi = 0$ not being central.

(b) Again the shell was subjected to circumferential moments but supported by a hinge and afterwards to a uniform radial shear. In both cases the approximation was regarded satisfactorily. The last experiment is interesting since there is no lateral shear stress component contribution to strain energy. The slight increase in T_θ may be viewed in the light of the above observation and in the mean time illustration of the negligible contribution of the lateral shear in this case.

Figures 3.24(a) and (b) indicate the variations in stresses due to loads discussed above.

3.6.2 Long cylinder with non-uniform thickness - This example was considered from Flügge[11] with the view that the influence of surplus degrees of freedom could be examined. It appears that 4 Surplus lateral displacements are perfectly adequate to represent the moments and displacements, see Fig. 3.2 5 (a) and (b).

A comparison was then made between the two cylindrical tanks whose Z and R coordinates were identical but the thicknesses

were different in a way that one possessed uniform thickness and the other had a uniformly increasing thickness in the manner shown in Fig. 3.25 and Fig. 3.26. The percentage difference obtained in fixing moments between uniform and non-uniform tanks (both theoretical and F.E.) is less than 1.0% but the difference increases with distance from the point of fixity as shown in Fig. 3.2 6 (a) and (b). The difference in T_θ can be seen to be insignificant.

3.6.3 Lame' problem - This experiment is designed to verify the Element sensitivity to complicated in-plane stress variation. Timoshenko and Goodier[12] were used as reference.

(a) The first example is an annulus subjected to internal pressure. The stress variation depends on a $\frac{1}{r2}$ factor; Fig. 3.27(a).

(b) The second example is from the same reference with the difference that it is a disc subjected to axial rotation. This time the factor influencing the stress variation is r^2, see Fig. 3.27(b).

The numerical data in each case is indicated in the appropriate graphs.

3.6.4 Bending of circular plates - This example is again originated from Billington[11]. The initial choice of loading was made to indicate the bending moments due to a uniformly distributed load and an additional edge moment due to plate-cylinder interaction. In both cases (a) and (b) the plate is hinged round the rim, Fig. 3.28. One element was used with 3 surplus "w" displacements. Details are as follows:

R = 27.0 ft. $\qquad$ E = 288.0 x 10^6

t = 1.0 ft. $\qquad$ ν = 1/6

3.6.5 Tapering Annulus - This is the tapering annulus also given by Gianini and Miles[13]. Because of the fairly complicated lateral pressure distribution 20 elements were used to simulate a cubic variation of the loading in the above reference, see Fig. 3.29(a). Since the program used in the existing work could incorporate a linear variation of external pressures, it was found that 4 elements appeared to suffice with no apparent loss in accuracy - The stresses were sampled at the points $\xi = (-1, 0, +1)$, the extremities being the common nodes between the neighbouring elements, Fig. 3.29(b) and (c).

3.6.6 Pressurised Fixed Cone - It was thought that the axisymmetric analysis would be augmented by including a conical shell. Thus a 45^{o} shell was arbitrarily chosen with convenient dimensions. The theoretical values were obtained from ref.(14). Satisfactory convergence is obtained taking 2 elements with moderate number of surplus d.o.f. (3 u's and 4 w's). The circumferential and meridional stress components and moments are shown in Fig. 3.30 (a), (d).

3.6.7 Rotating sphere - This example is again compared with that given in reference[13] where 10 elements were used and the numerical results were checked against the theoretical example of Lure. Because of the certain inconsistency in the radial displacements a similar set of theoretical values using the Membrane theory was obtained. These results are included below should a future possible reference be required, symbols have their usual meaning.

$$c = \frac{\omega^2 \rho a^2}{E}, \qquad w = c \cos^3\alpha,$$

$$T_\theta = \frac{Etc}{a} \cos^2\alpha, \qquad u = c\sin\alpha(\nu + \sin^2\alpha)$$

Four equal elements were used in this example which were sampled at the points (-1, 0, +1) similar to 3.5.5 and the results are shown in Fig. 3.31(a) and (b).

3.6.8 Hemispherical Dome with a sky-light - Unlike the previous case where the membrane strength was mobilised, this example examines bending response of the structure. It was originally analysed using 28 unequal elements by Grafton and Strome [15] and subsequently discussed by Zienkiewicz[16] and Kraus[14]. This structure was used in an experiment to investigate the improved convergence with the number of elements. Up to 3 elements, the results appear significantly in error and the increase in surplus degrees of freedom is of little help. It was thought that the inadequacy in geometrical representation could be the main contributor to the observed errors. This improves beyond comparison just by doubling the elements. Using 6 elements both the moment M_s and the displacement w are satisfactory. Using 7 elements the difference between the theoretical and numerical results appear indistinguishable, Fig. 3.32(a), (f).

It is interesting to note that no improvement is achieved by increasing surplus degrees of freedom beyond 3 in the last two cases.

3.6.9 The spherical cap - This example is given by Timoshenko and Wienowsky-Krieger[7] which is a 35^o concrete cap subject to radial pressure and rigidly fixed round the rim and the computed results from Fig. 3.33(a) and (b) appear satisfactory with 5 equal elements.

It was decided to investigate the salient values of additional forces and moments required due to lack of support (e.g. inadequate

ring-beam etc). By inserting a hinge to allow circumferential rotation, the overall values of T_θ do not appear to vary significantly only the peak value of the moment reduces by about 4-times, see Fig. 3.34(a) and (b). But dramatic changes take place by resting the shell freely (with the pin and the lateral support both removed). The hoop-stress T_θ appears to magnify by(minus) 5-fold, indicating the tearing of the rim and the peak value of the moment doubles. So with adequate factor of safety considered for moments against the ring-beam failure, the hoop-stress becomes the main factor influencing total failure, shown in Fig. 3.35(a) and (b).

3.6.10 Toroidal Shell under internal pressure - This particular example has been given by two independent sources namely Chan and Firmin[18] and Gianini and Miles[13] where reference has been made to previous calculations made by Kalanins, Jordan, Sanders and Liepins by the above authors. As it was found from experience the correct geometrical representation for this structure is critical. Eighteen elements with geometrically increasing element size (1^o, 2^o, 4^o, 8^o, 15^o, ... 15^o) were used in this example until some moderate agreement was obtained, see Fig. 3.36. It was realised later that the exclusion of the lateral shear in forming the Strain Energy counted for a sizable fraction of the total Strain Energy. This, is speculated to be carried by the elements bending further, thus causing bending moments with slightly more amplified peaks and fractionally larger bending stresses manifested in hoop stress (about 10%). The meridional stress being statically determinate is unaffected, Fig. 3.36(a),(c).

3.6.11 Branching - To examine the behaviour of the program when branching takes place, the example given by Kraus[14] is quite edifying. This basically is the displacement analysis in the

pressure vessel shown in Fig. 3.37(a) with theoretical and numerical results available (29 points, each implying an element appear on the original representation). In the present analysis a total 7 elements were used both in the cylindrical and the spherical sections with encouraging results shown in Fig. 3.37(b).

3.5.11 CONVERGENCE - Constant stress conditions - In the next Chapter statements regarding a practical method of inferring convergence will be quoted. In the axisymmetric case it is sufficient to mention that, it is necessary to determine that whether the element is capable of producing a constant stress, when the loading and the support conditions require it to produce one; this being some measure of convergence. Two experiments were considered to examine this.

(a) A "long" cylinder with roller supports at the loaded end subject to a hydrostatic pressure meridionally. Using even 1 element a satisfactory linearly increasing hoop-stress is obtained.

(b) This time a spherical shell is subjected to internal pressure where meridional and hoop-stress become equal. Symmetry was used in this case and 3 elements represented the geometry of a quadrant adequately. All details regarding the two cases are given in Fig. 3.38(a) and (b). Membrane equations used were from Ref. (17).

REFERENCES

1. O.C. ZIENKIEWICZ
   The Finite Element Method in Eng. Science, McGraw-Hill, 1971.
2. I.C. TAIG
   "Structural analysis by the displacement method", English Electric Aviation Ltd., Report SO17(1961), unpublished.
3. B.M. IRONS
   "Numerical integration applied to Finite Element Methods", Internal report C/E161/71, Civil Eng. Dept., University of Swansea.
4. S. AHMAD
   "Psudo-Isoparametric Finite Elements for Shell and Plate Analysis", paper submitted to Joint British Committee for Stress Analysis, London 1968.
5. I. ERGATOUDIS, B.M. IRONS, O.C. ZIENKIEWICZ
   "Curved Iso-parametric Element for Finite Element Analysis", J. of Solids and Structures, Jan. 1968.
6. G.C. NAYAK
   Plasticity and Large Deformation Problems by the Finite Element Method", University of Wales Ph.D. Thesis, Jan. 1971.
7. R. DELPAK
   "Axisymmetric Vibrations of Shells of Revolution by the Finite Element Method", University of Wales, M.Sc. Thesis, Feb. 1968.
8. B.M. IRONS
   "Shape functions for Elements with Point Conformity", A.S.M. 1204, Rolls-Royce Library.
9. B.M. IRONS
   "Numerical integration applied to Finite Element Methods", paper submitted to International Symposium "The use of Electronic Digital Computers in Structural Engineering", University of Newcastle upon Tyne, Dept. of Civil Engineering.

10. D.P. BILLINGTON

"Thin Shell Concrete Structures", McGraw-Hill, 1965.

11. W. FLÜGGE

"Stresses in Shells", Springer - Verlag, 1967.

12. TIMOSHENKO and GOODIER

"Theory of Elasticity", McGraw-Hill, 1951.

13. M. GIANNINI, G.A. MILES

"A Curved Element Approximation of Axi-symmetric Thin Shells", Jour. of Solids and Structures, 1969.

14. H. KRAUS

"Thin Elastic Shells", J. Wiley & Son Inc. 1967.

15. P.E. GRAFTON and D.R. STORME

"Analysis of axi-symmetric shells by the direct stiffness method", J.A.I.A.A. 1. pp. 2342-47, 1963.

16. O.C. ZIENKIEWICZ

"The Finite Element Method in Eng. Science", McGraw-Hill, 1971.

17. TIMOSHENKO and WIENOWSKY-KRIEGER

"Theory of Plates and Shells", McGraw-Hill, 1959.

18. A.S.L. CHAN and A. FIRMIN

"The analysis of Cooling Towers by the Matrix Finite Element Method", Aeronautical Journal, Oct. 1970.

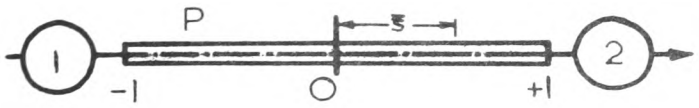

FIGURE 3.1

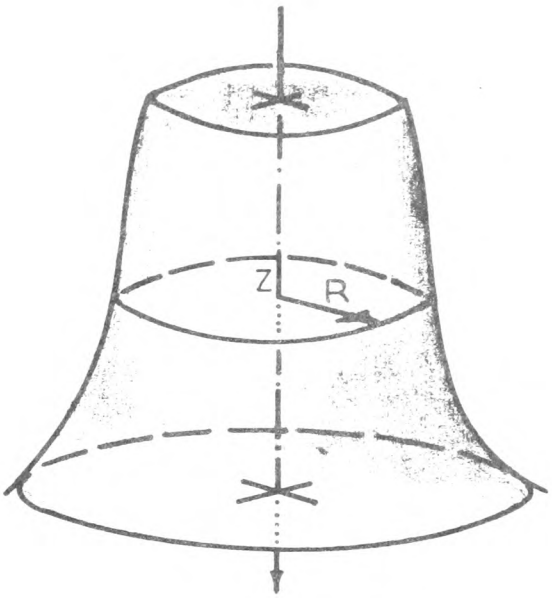

FIGURE 3.2

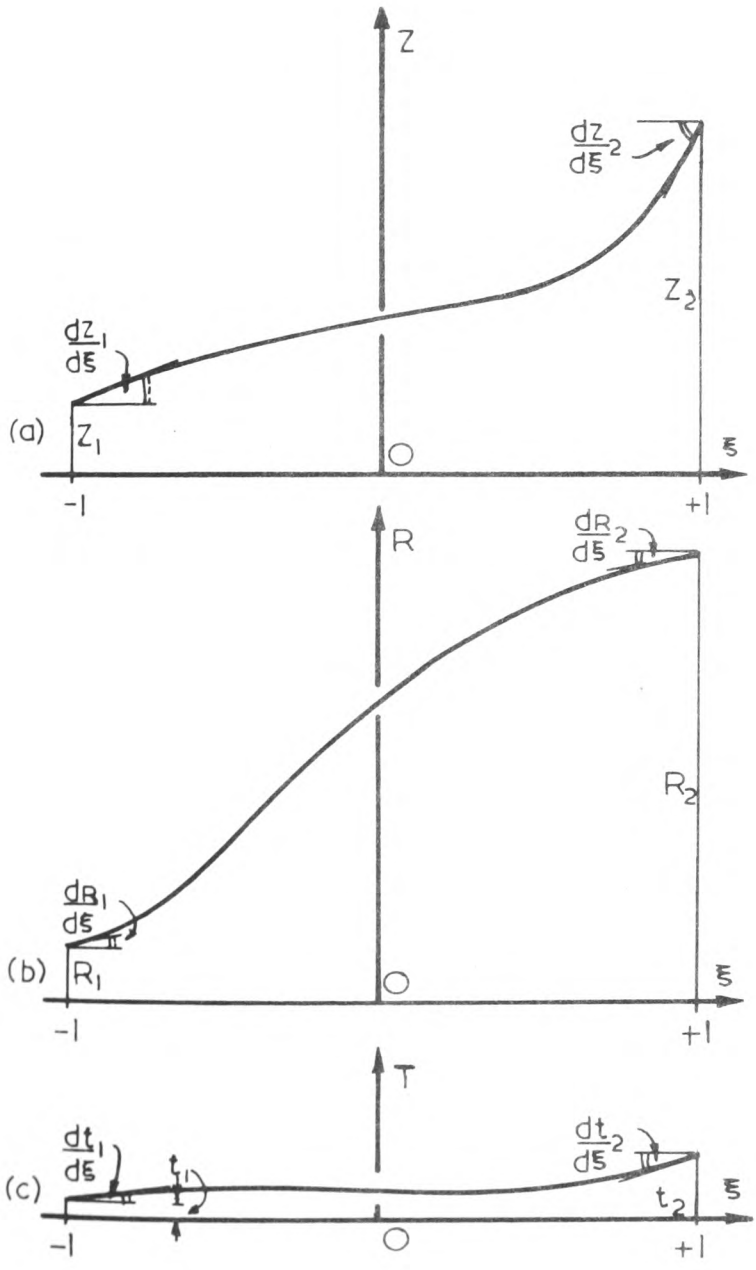

FIGURE 3.3

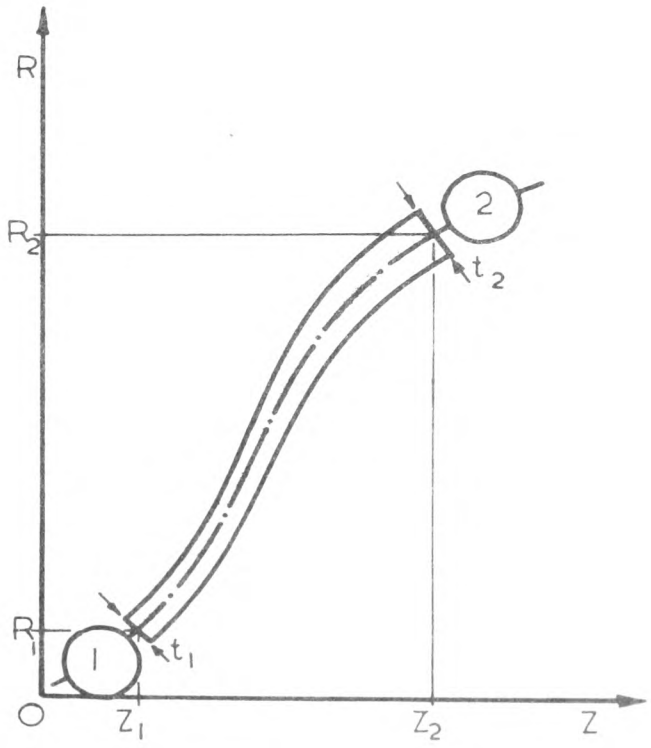

FIGURE 3.4

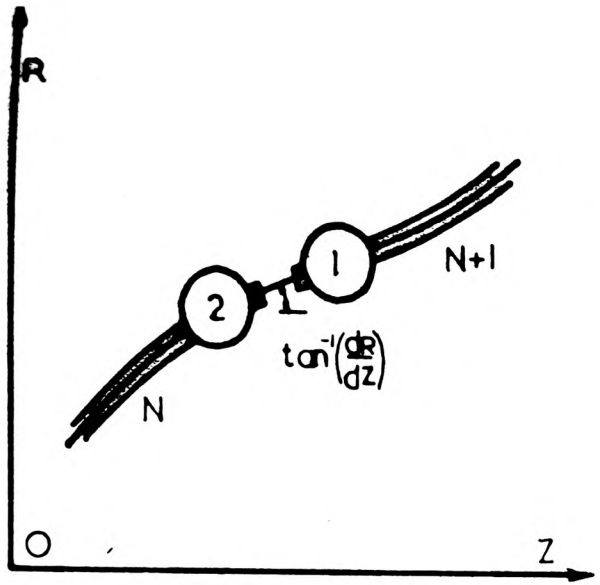

FIGURE 3.5

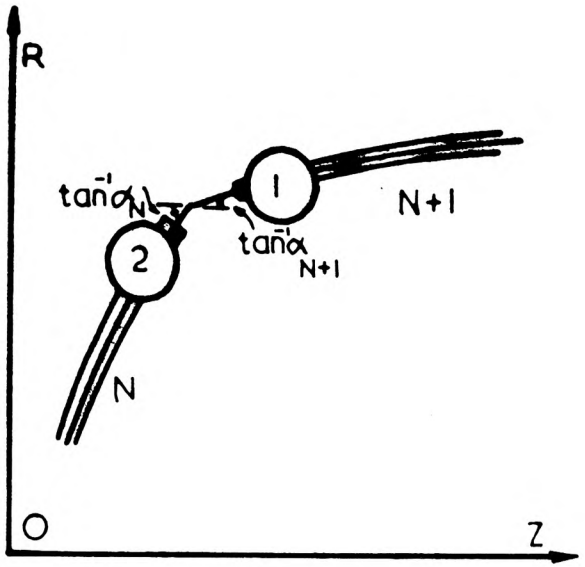

FIGURE 3.6

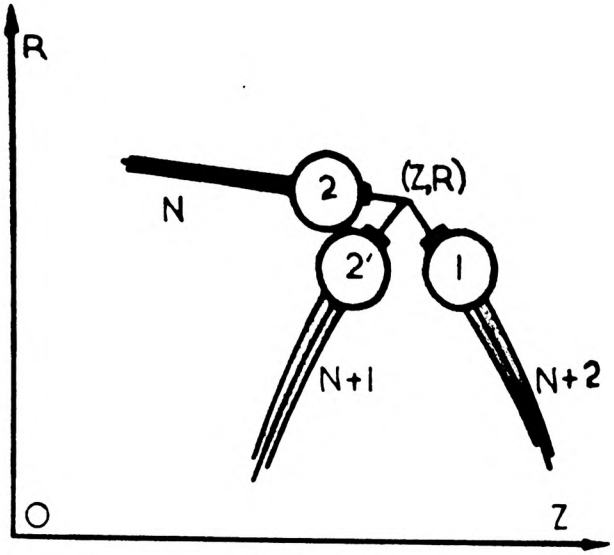

FIGURE 3.7

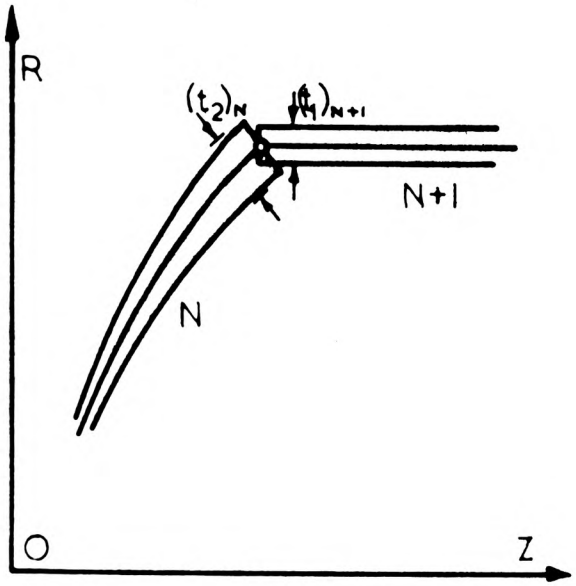

FIGURE 3.8

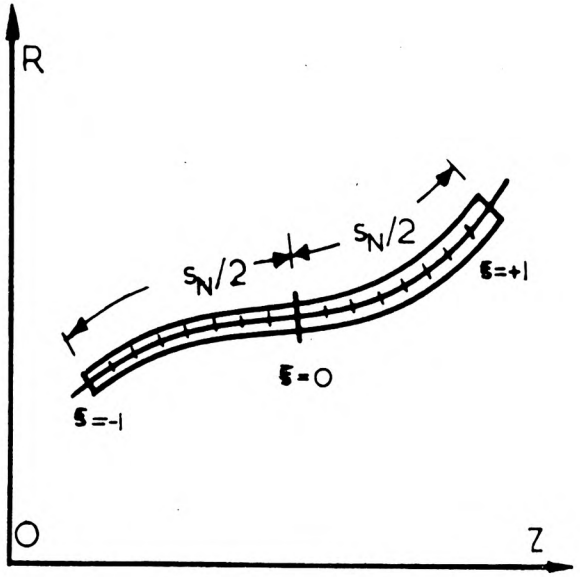

FIGURE 3.9

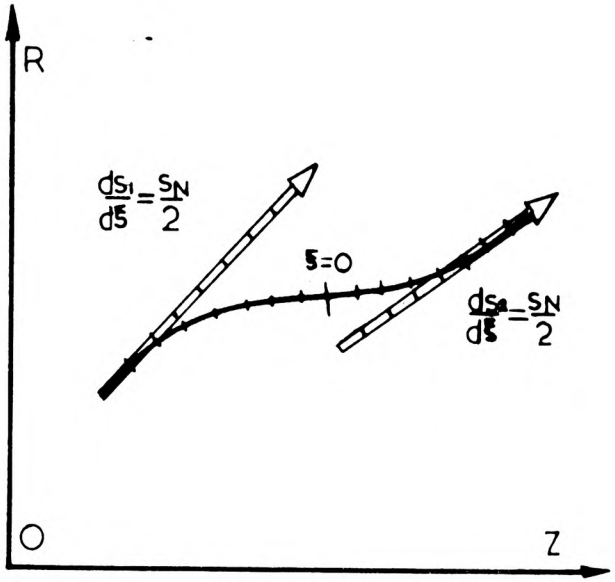

FIGURE 3.10

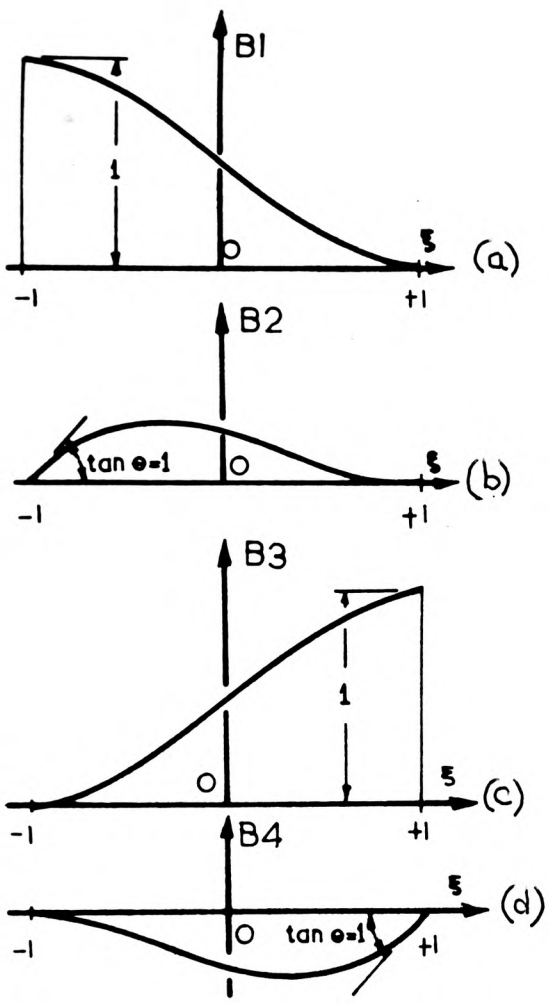

HERMITIAN–TYPE

$$H = A_0 + A_1\xi + A_2\xi^2 + A_3\xi^3$$

FIGURE 3.11

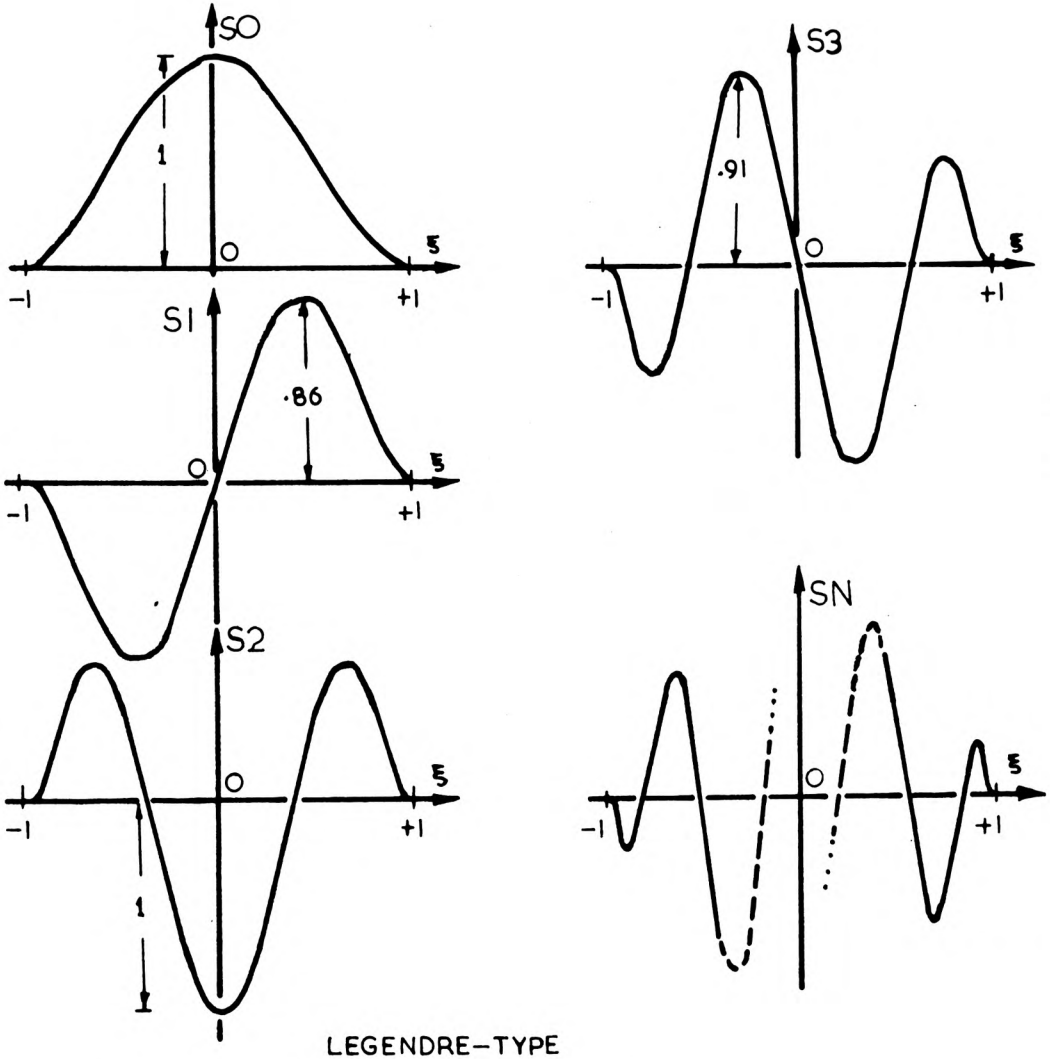

B1-B4 ARE BASIC FUNCTIONS

SO-SN ARE SURPLUS FUNCTIONS

LEGENDRE–TYPE

$$(\xi^2-1)Q_N'' - 2\xi Q_N' - (N+1)(N+4)Q_N = 0.$$

FIGURE 3.12

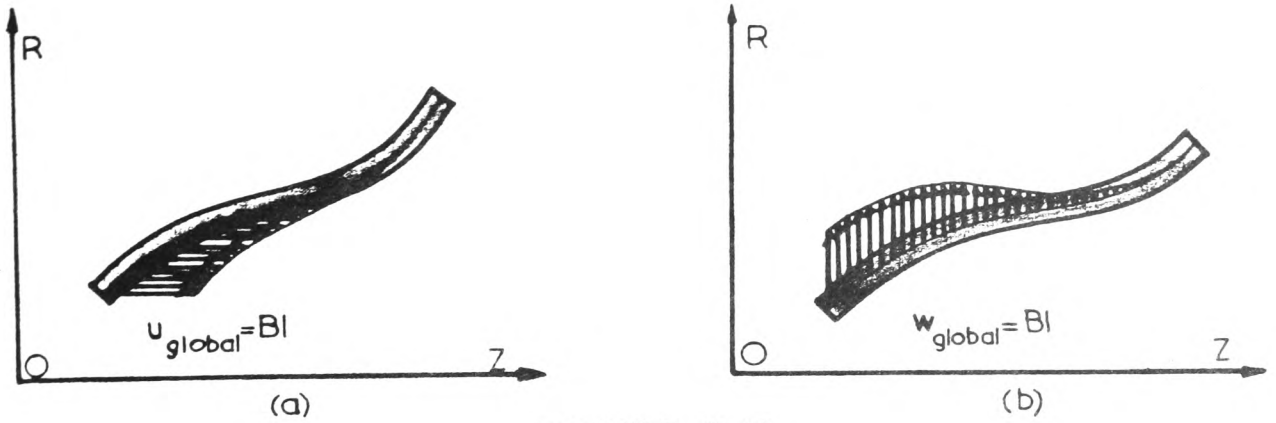

FIGURE 3.13

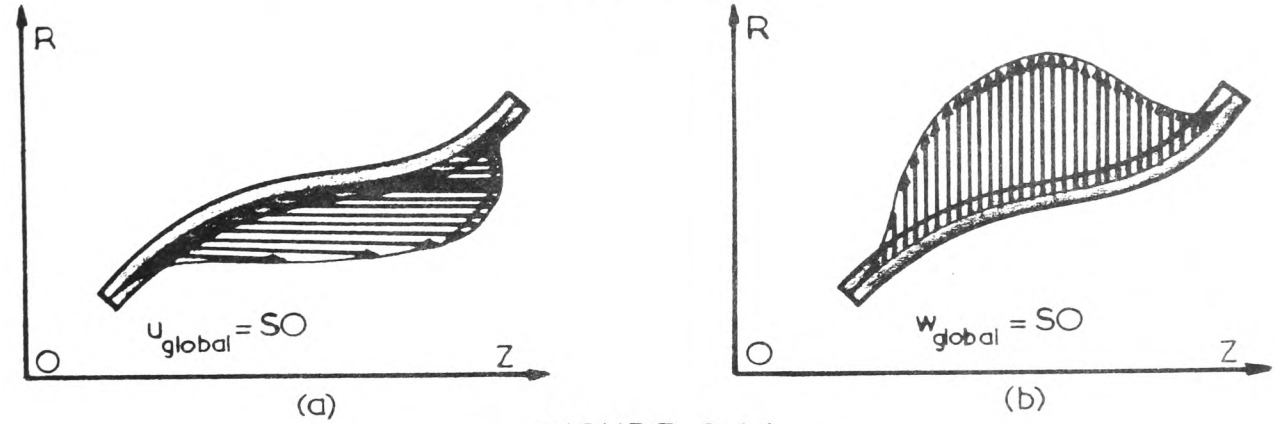

FIGURE 3.14

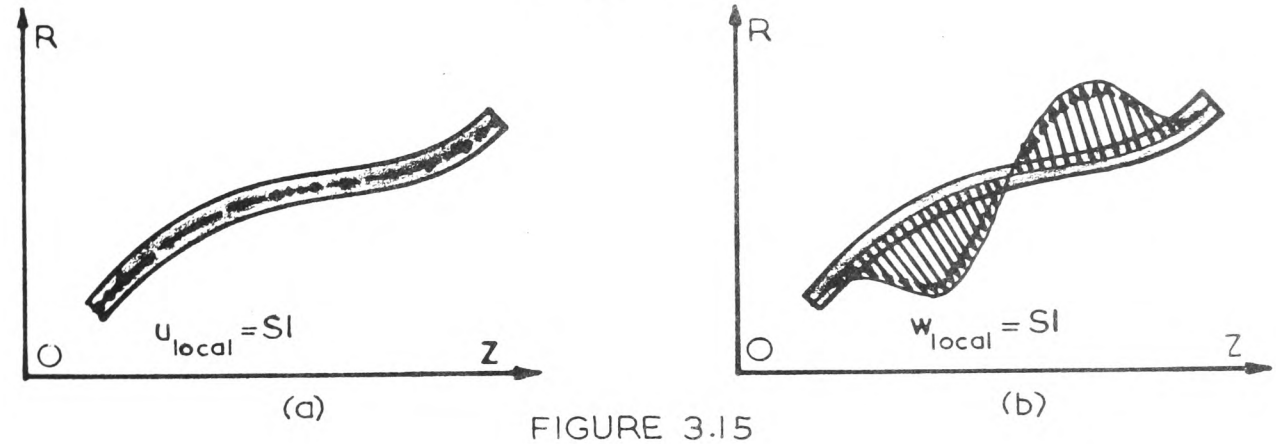

FIGURE 3.15

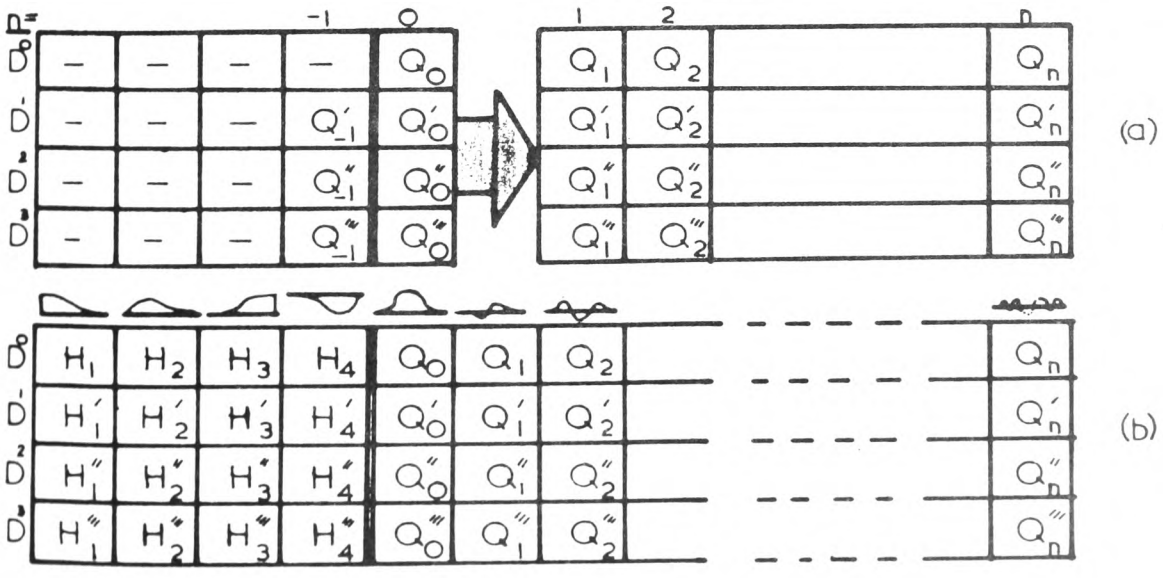

FIGURE 3.16

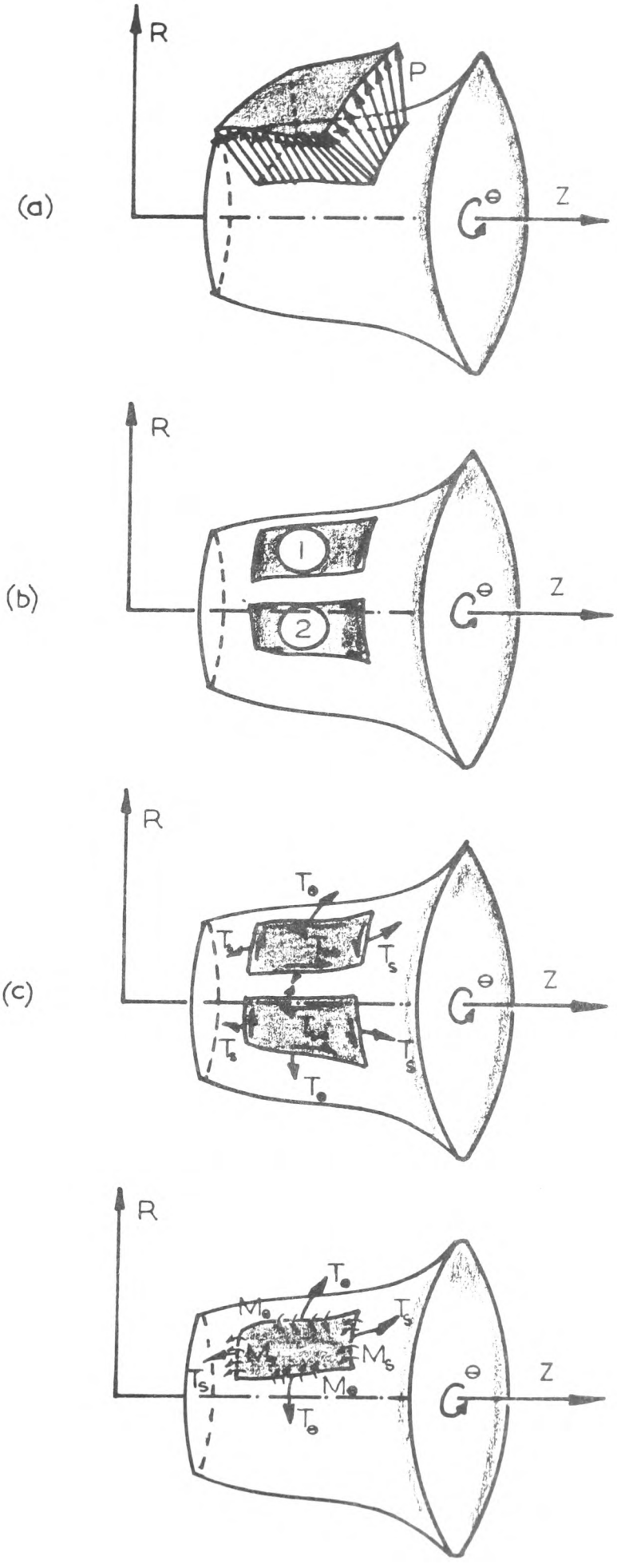

FIGURE 3.17

FIGURE 3.18

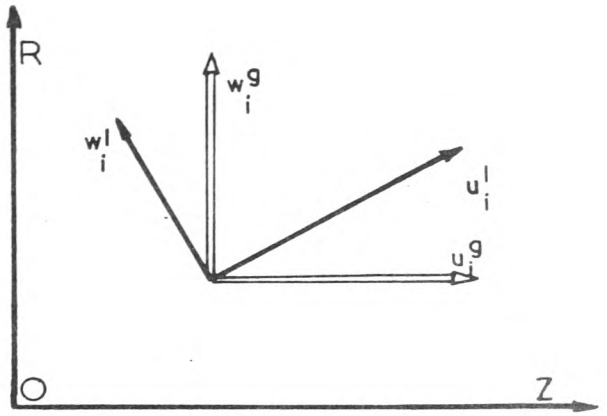

FIGURE 3.19

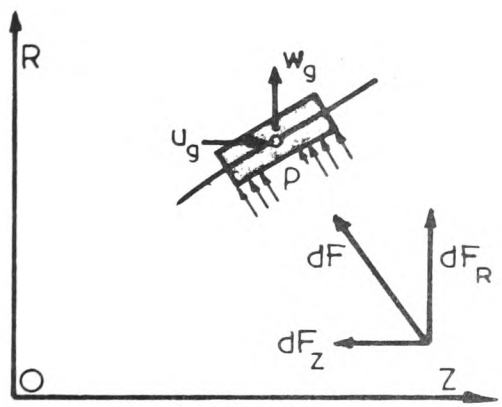

(a)

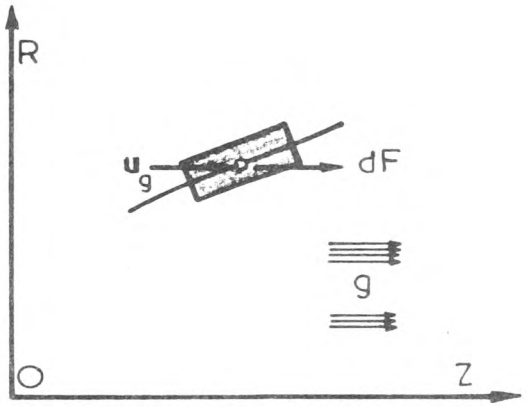

(b)

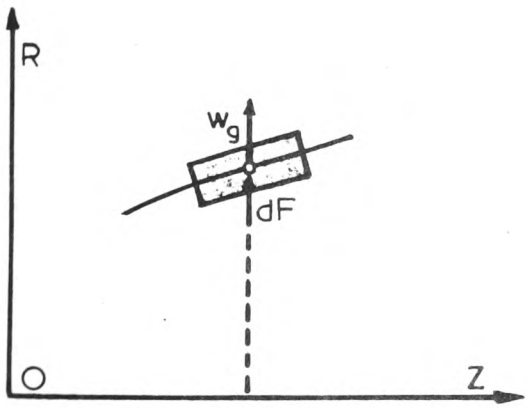

(c)

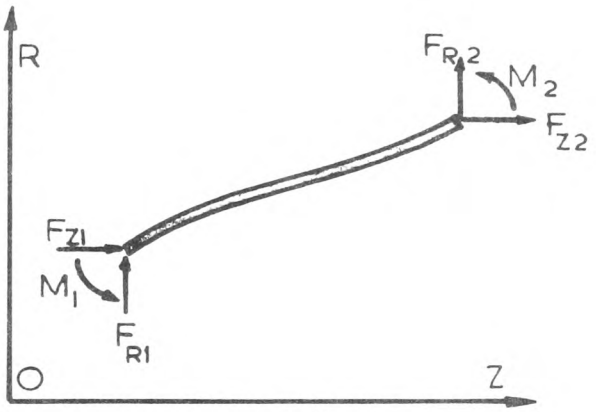

(d)

FIGURE 3.20

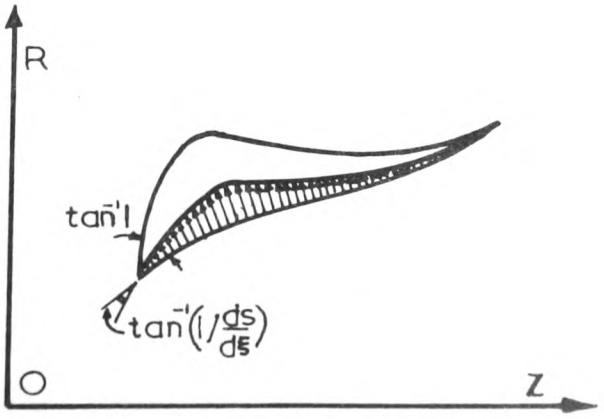

FIGURE 3.21

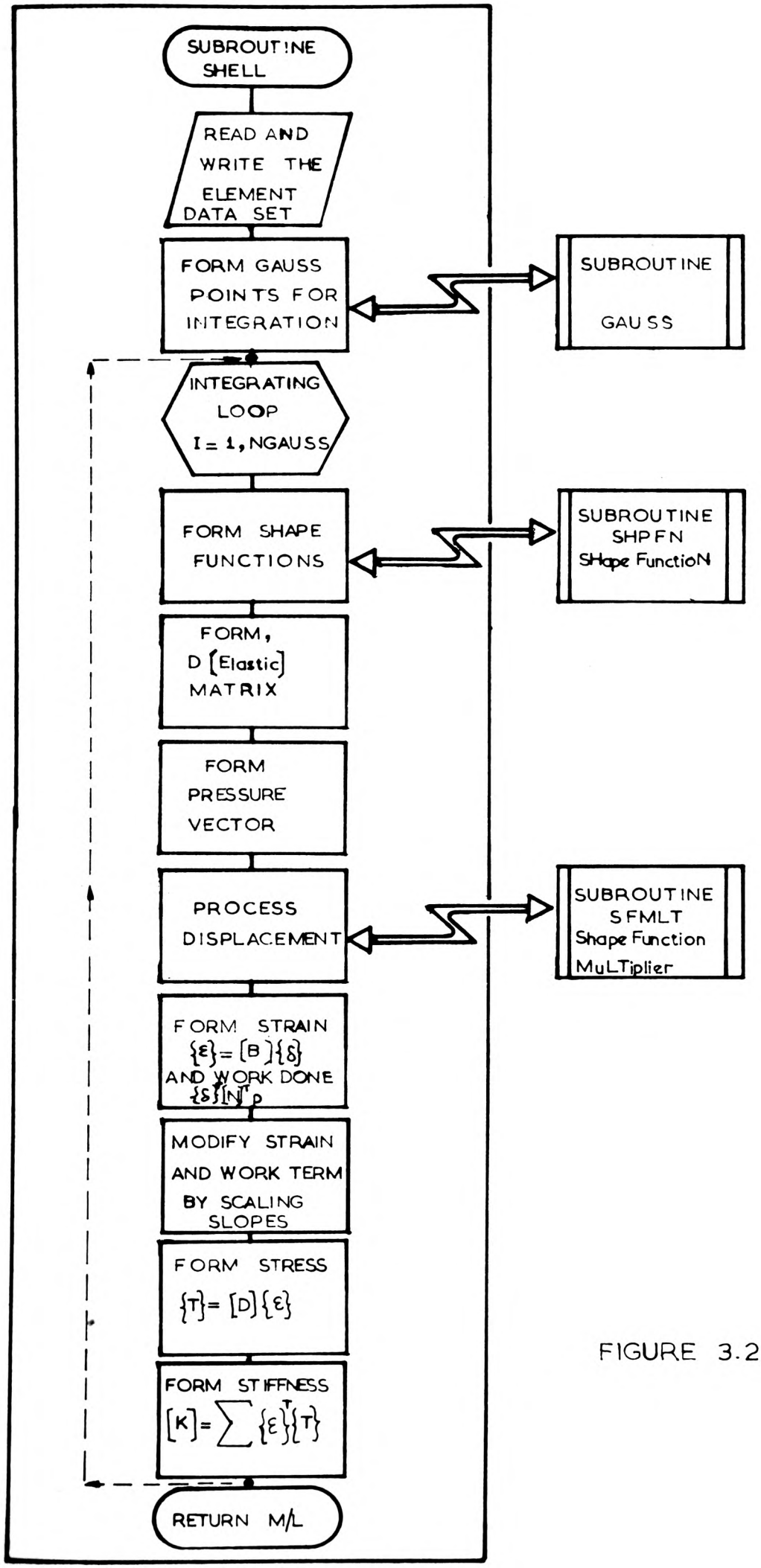
SUBROUTINE SHELL
READ AND WRITE THE ELEMENT DATA SET
FORM GAUSS POINTS FOR INTEGRATION
SUBROUTINE GAUSS
INTEGRATING LOOP I = 1, NGAUSS
FORM SHAPE FUNCTIONS
SUBROUTINE SHPFN SHape FunctioN
FORM, D [Elastic] MATRIX
FORM PRESSURE VECTOR
PROCESS DISPLACEMENT
SUBROUTINE SFMLT Shape Function MuLTiplier
FORM STRAIN {ε} = [B]{δ} AND WORK DONE {δ}{N}^T p
MODIFY STRAIN AND WORK TERM BY SCALING SLOPES
FORM STRESS {T} = [D]{ε}
FORM STIFFNESS [K] = Σ {ε}^T {T}
RETURN M/L

FIGURE 3.22

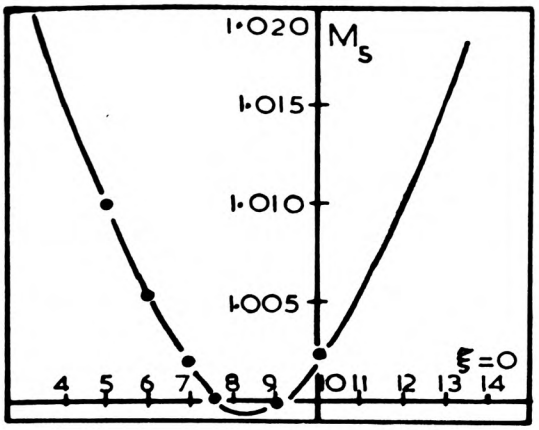

(a)

GRAPH OF M_s VERSUS THE POSITION OF ξ = 0, ALONG THE TANK GENERATOR.

ONE ELEMENT IS USED WITH 5 SURPLUS W'S

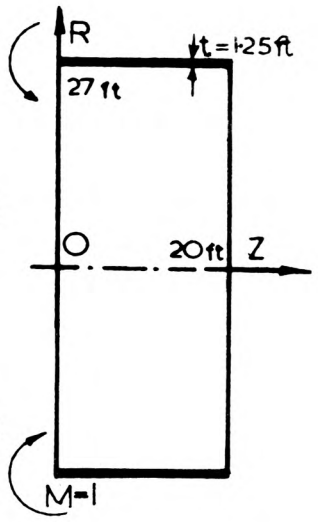

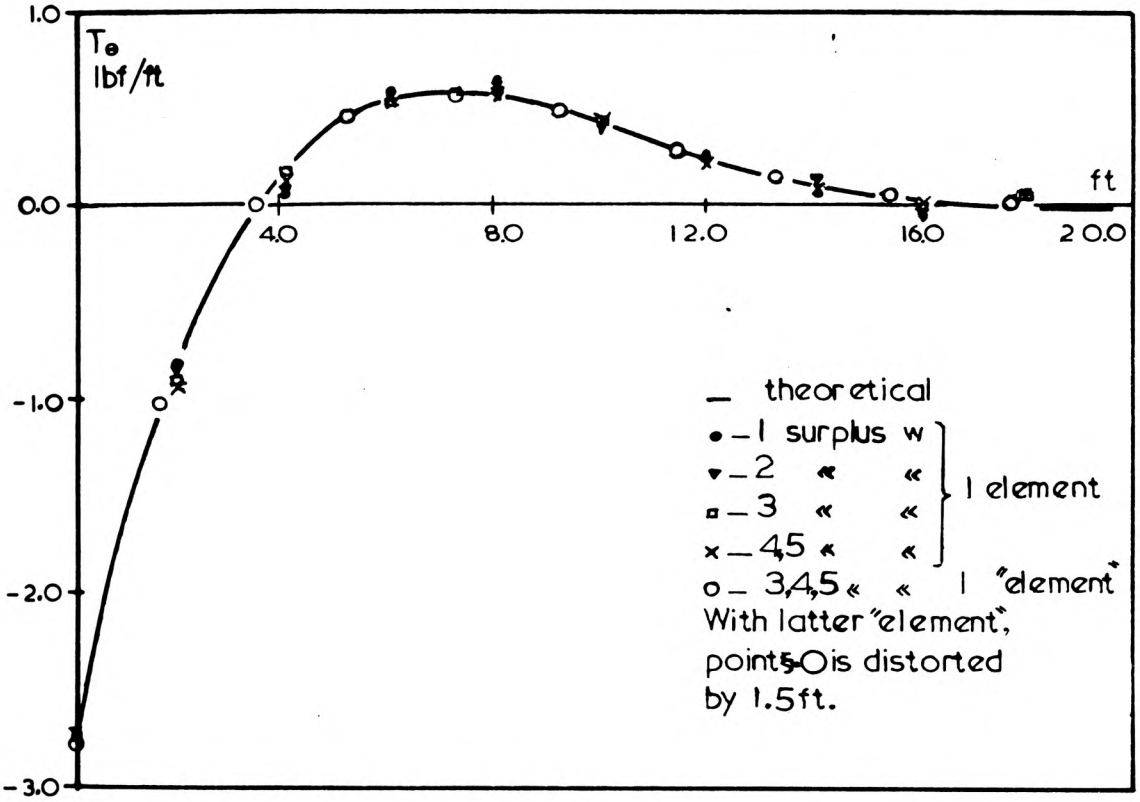

(b)

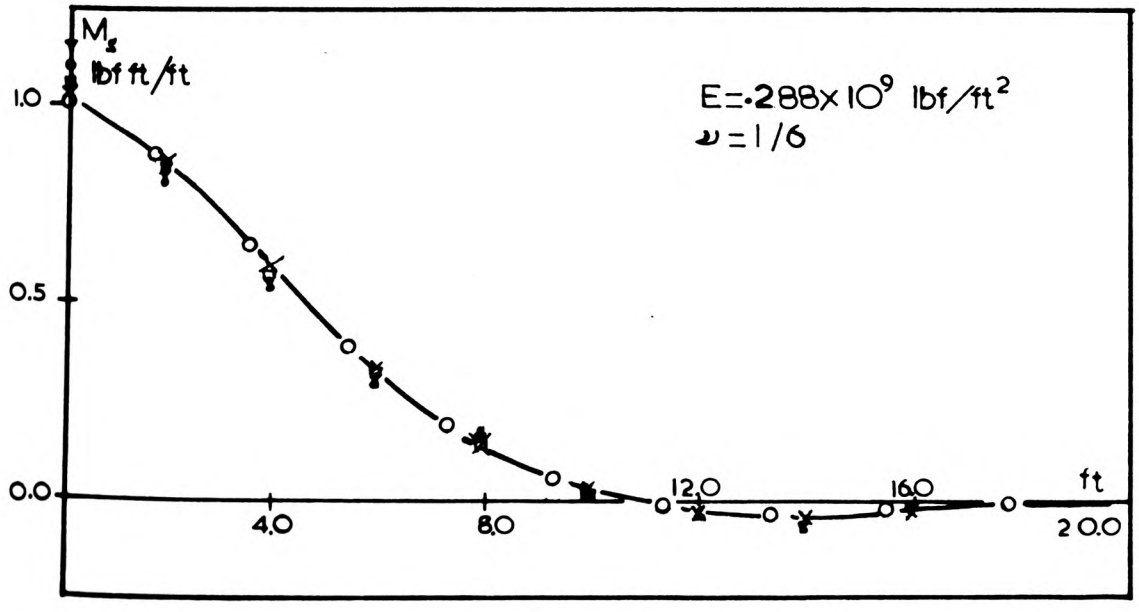

(c)

FIGURE 3.23

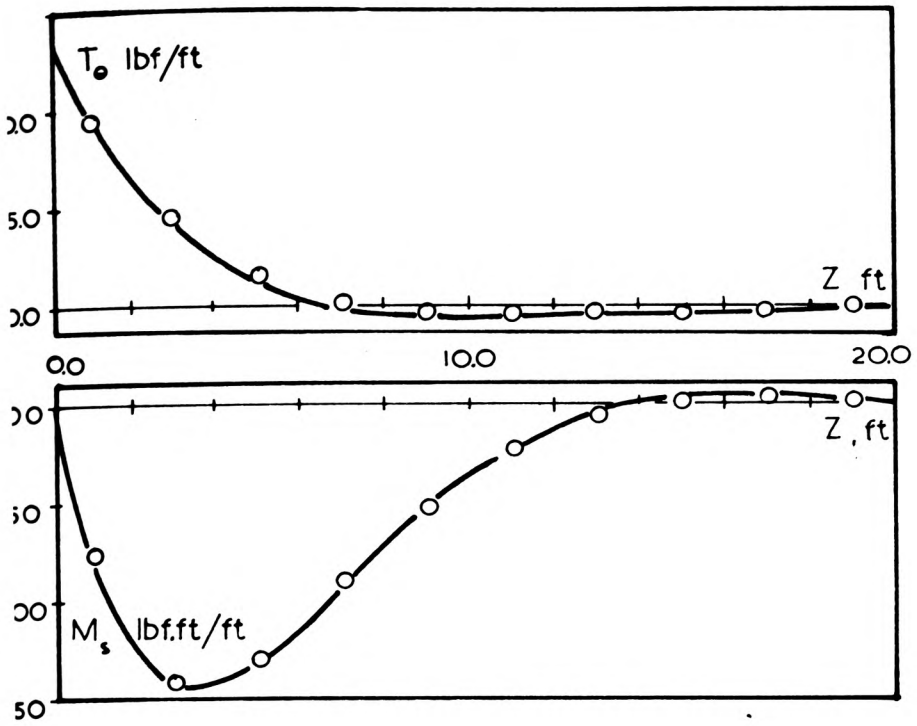

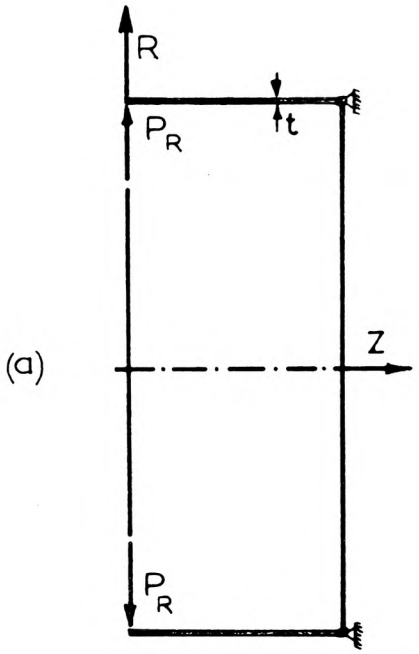

(a)

Z = 20.0 ft
R = 27.0 ft
t = 1.25 ft

$E = 2.88 \times 10^8$ lbf/ft^2
$\nu = 1/6$

— Theoretical
-O- Finite Element
1 element
3 Surplus "w"

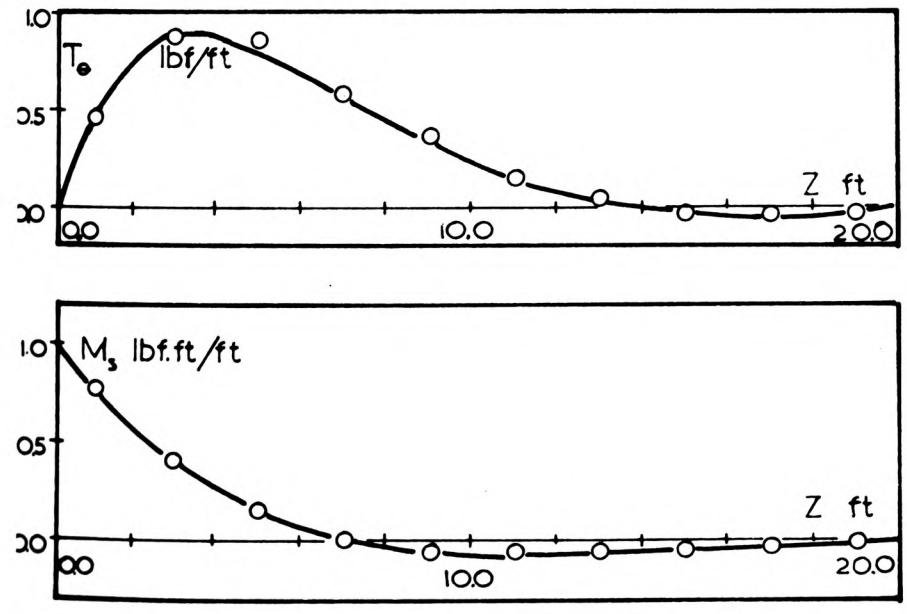

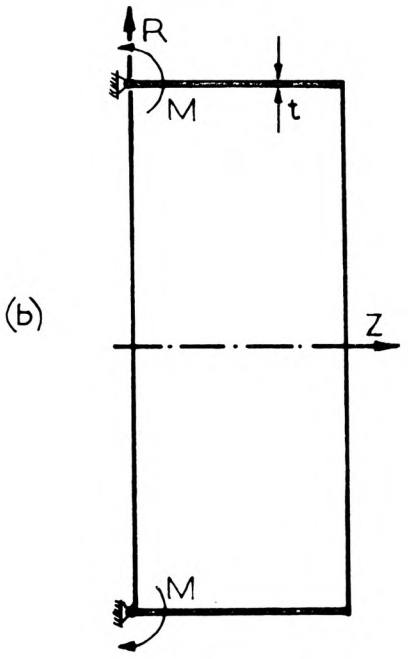

(b)

FIGURE 3.24

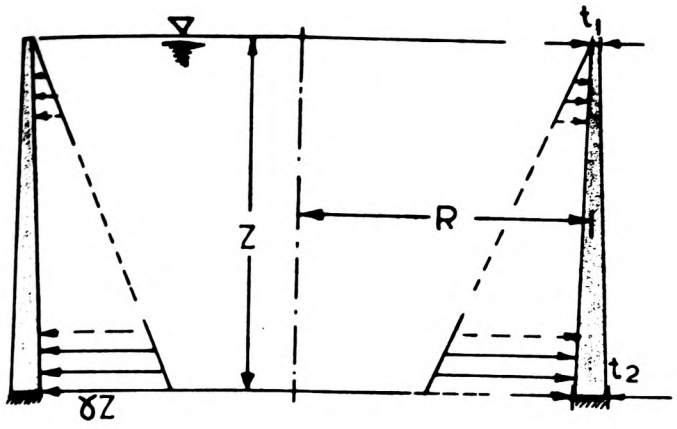

Z = 12. ft
R = 9. ft
t_1 = .25 ft
t_2 = .9167 ft
E = .288 x 10^9 lbf/ft^2
ν = .0
γ = 62.4 lbf/ft^3

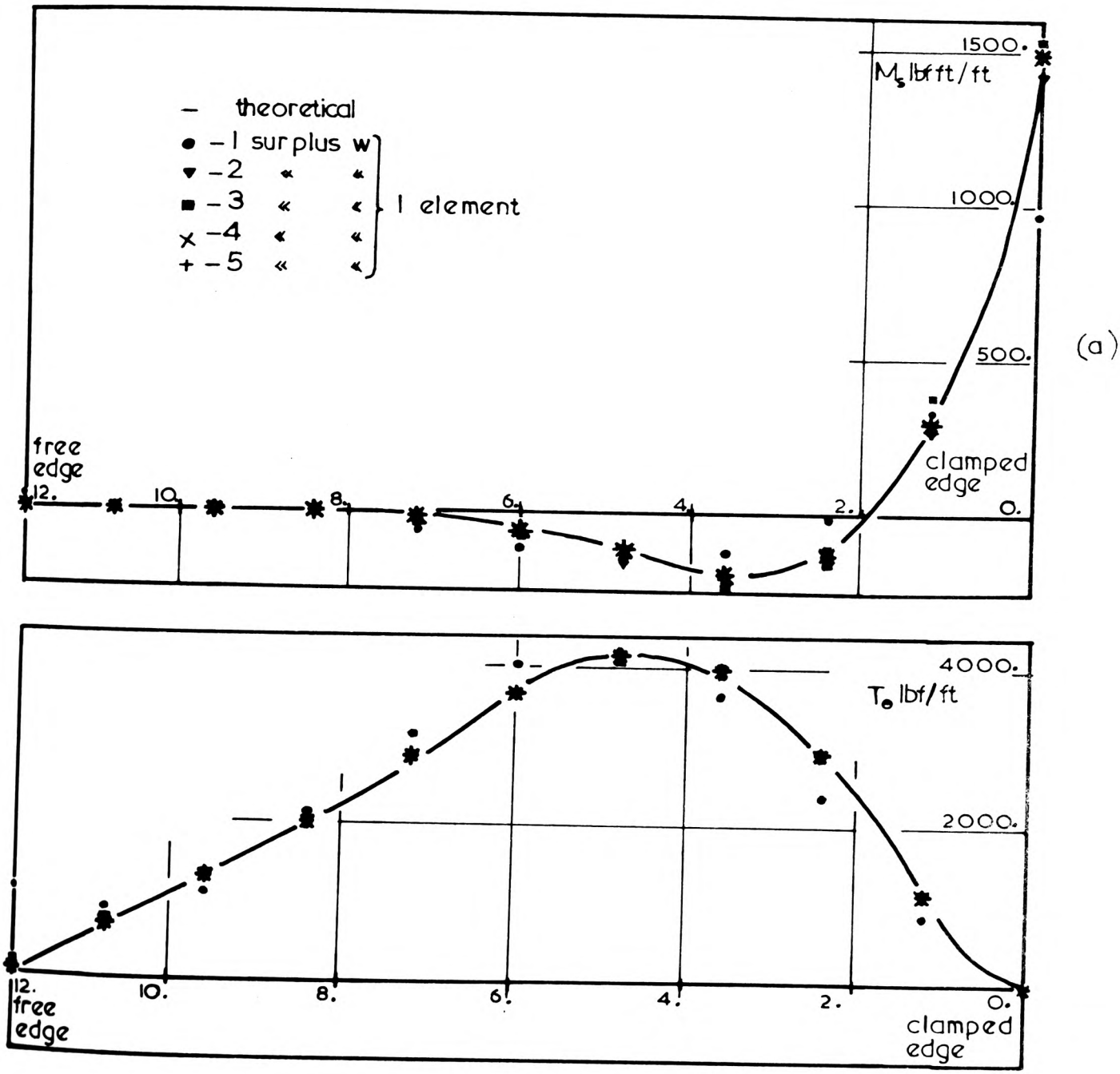

(a)

FLÜGGE TANK

FIGURE 3.25

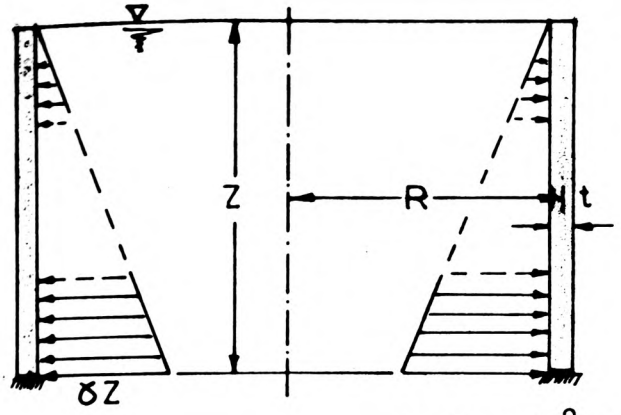

Z= 12. ft
R= 9. ft
T=.9167 ft

E= 288x 10^9 lbf/ft^2
ν =.0
δ = 62.4 lbf/ft^3

Principal values:

		M_s	T_θ
Non-uniform	theo.	1470.	4180.
	F.E.	1480.	4200.
Uniform	theo.	1458.	4000.
	F.E.	1474.	4000.

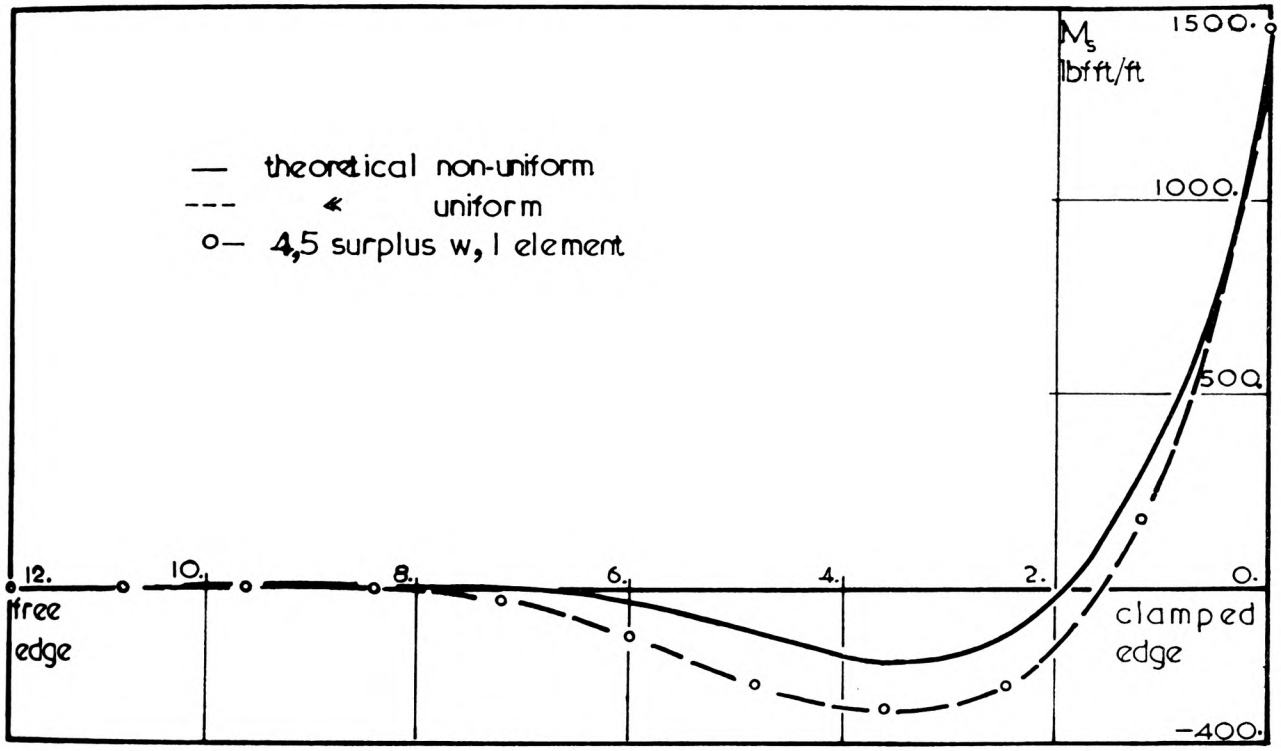

(a)

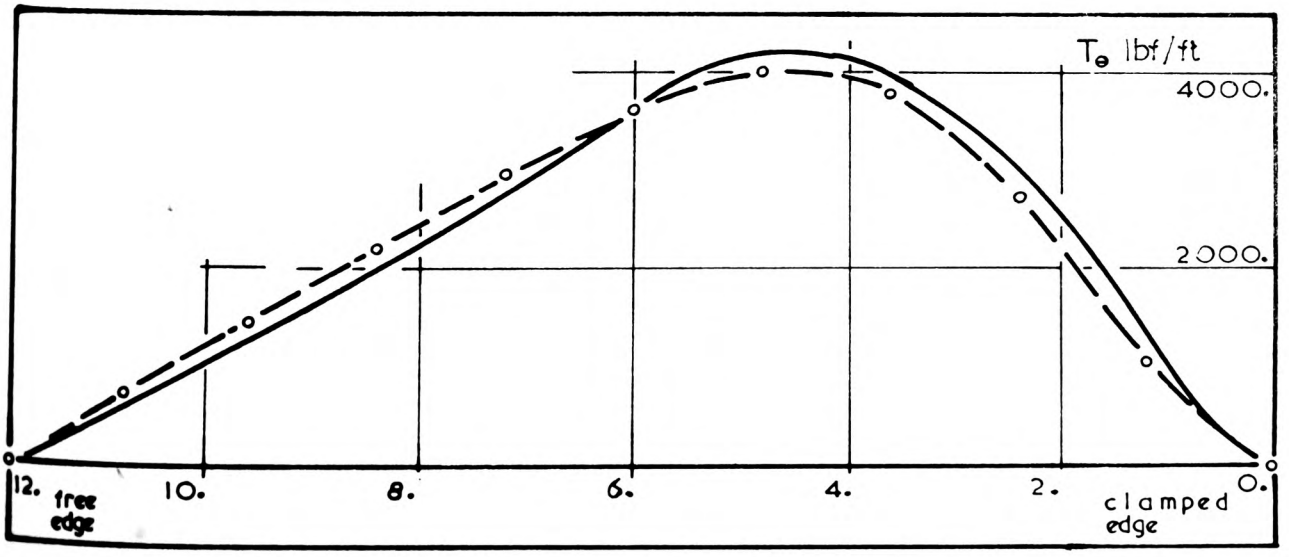

(b)

READ IN CONJUNCTION WITH FIG. 3.25

FIGURE 3.26

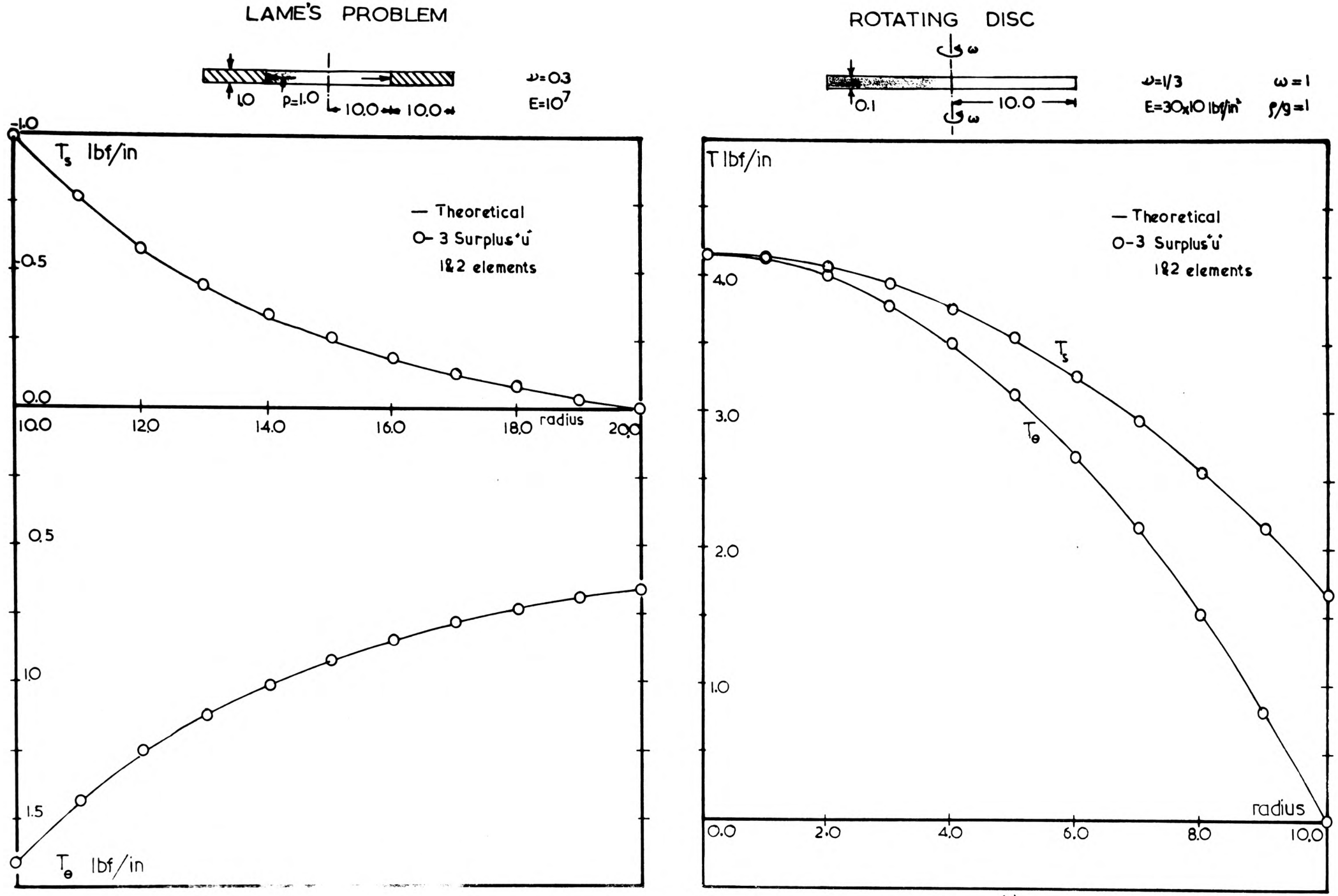
LAME'S PROBLEM
1.0
p=1.0
10.0
10.0
ν=0.3
E=10^7
-1.0
T_s lbf/in
— Theoretical
O- 3 Surplus "u"
1&2 elements
-0.5
0.0
10.0
12.0
14.0
16.0
18.0
radius
20.0
0.5
1.0
1.5
T_θ lbf/in
ROTATING DISC
ω
0.1
10.0
ω
ν=1/3
ω=1
E=30x10 lbf/in²
ρ/g=1
T lbf/in
— Theoretical
O-3 Surplus "u"
1&2 elements
4.0
3.0
2.0
1.0
T_s
T_θ
radius
0.0
2.0
4.0
6.0
8.0
10.0
(b)

FIGURE 3.27

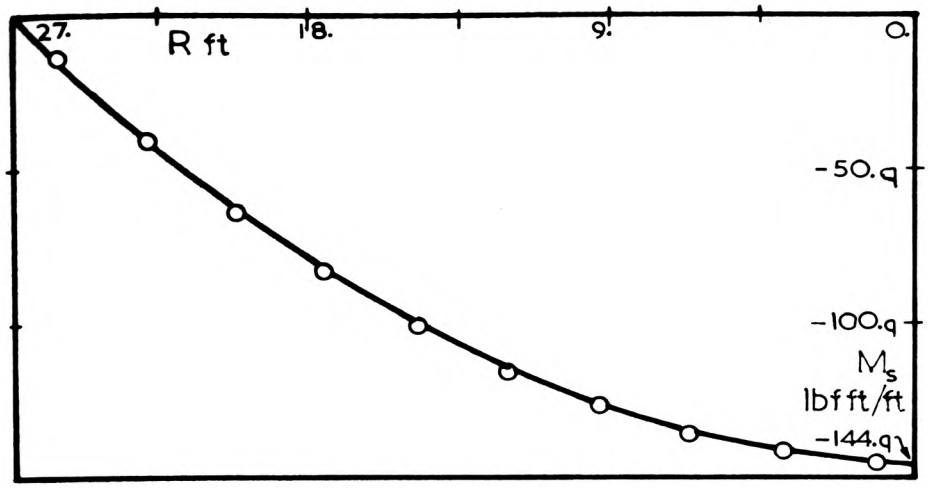

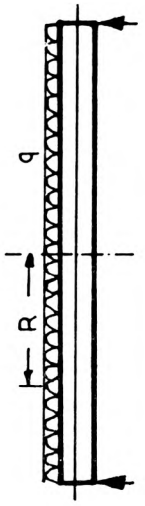

(a)

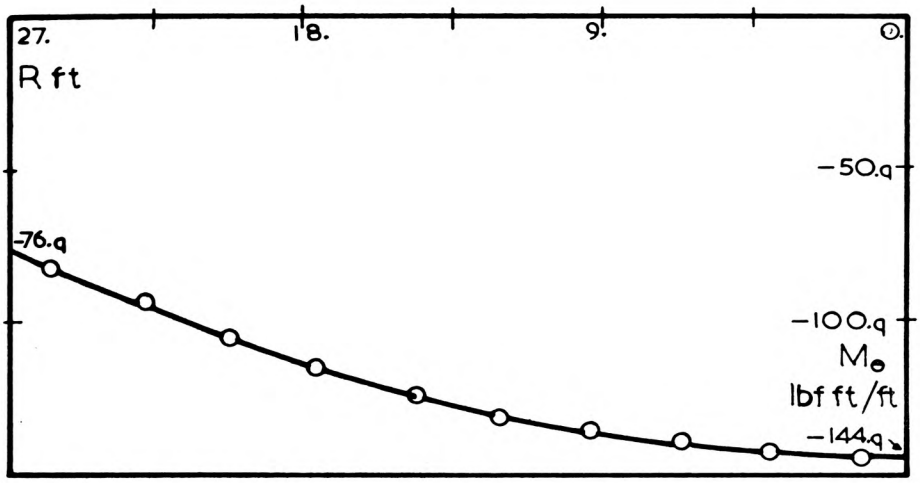

FIGURE 3.28

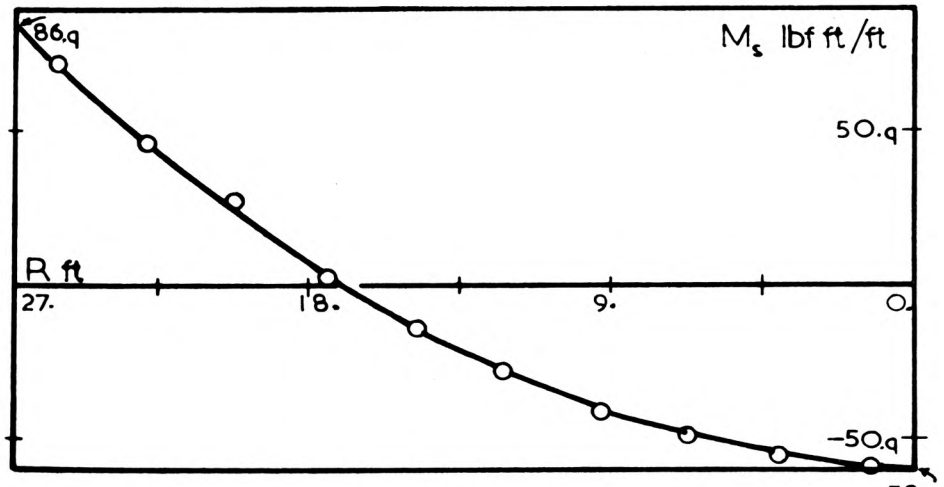

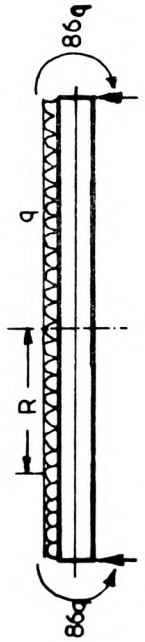

(b)

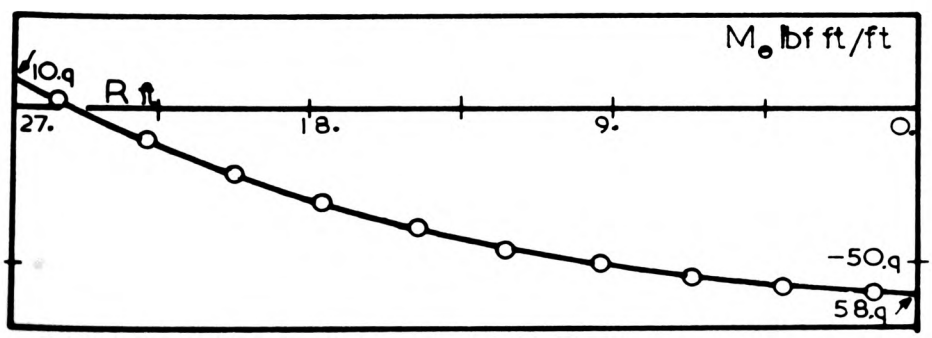

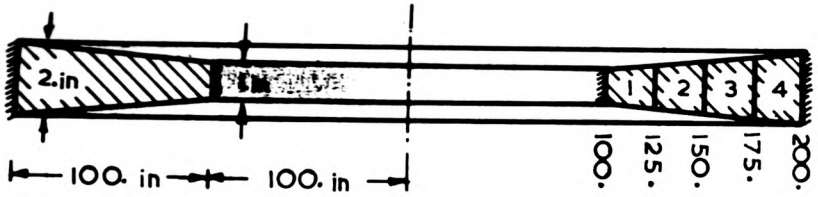

INNER AND OUTER EDGES ARE RIGIDLY FIXED

4 EQUAL ELEMENTS USED, DIVISIONS SHOWN ABOVE

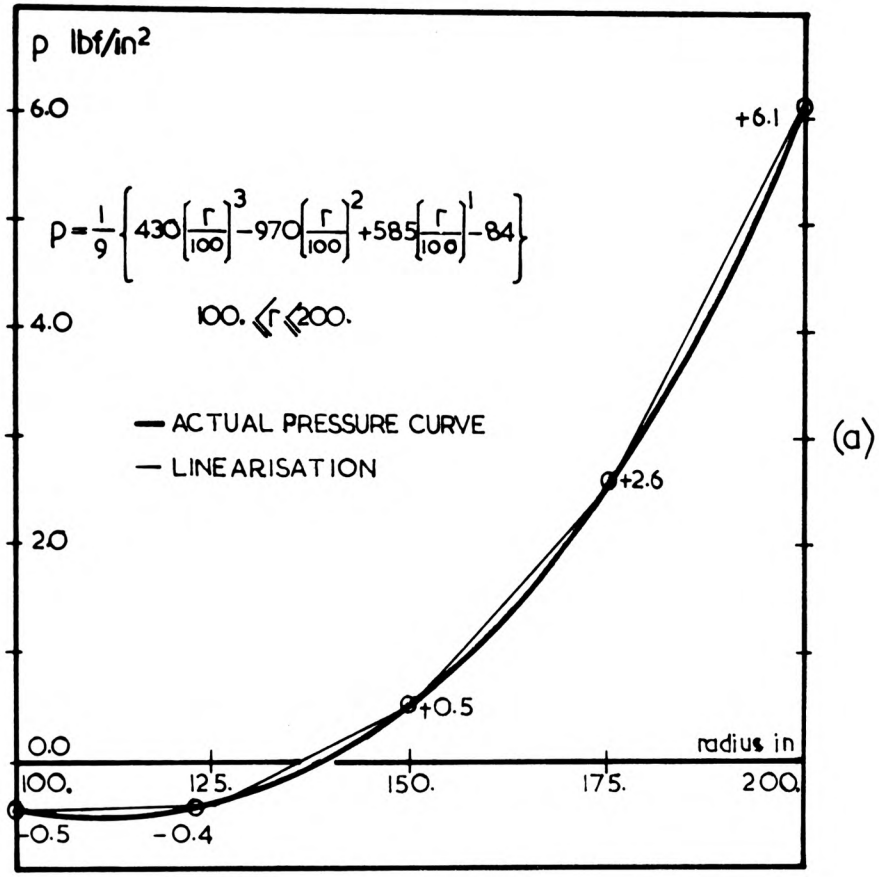

(a)

$E = 9 \times 10^6$

$\nu = 0.5$

FIGURE 3.29

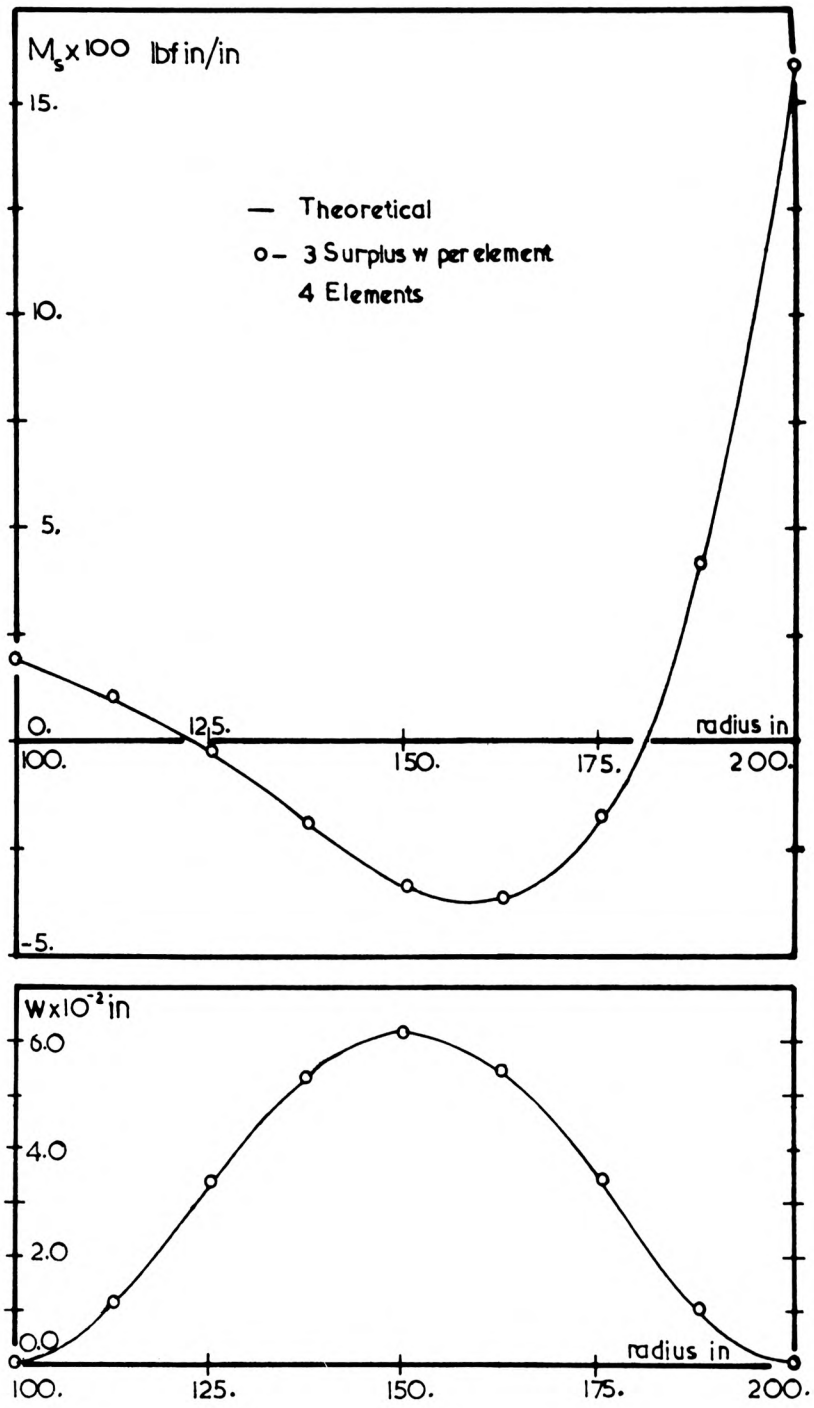

(b)

(c)

PRESSURISED FIXED CONE

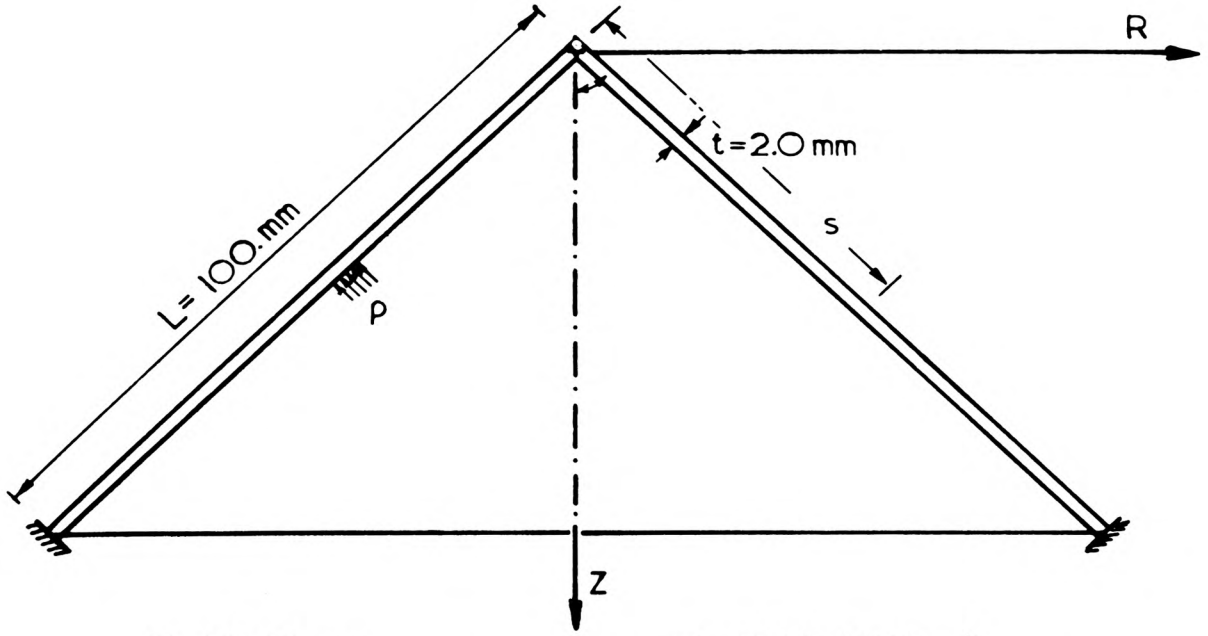

Z = 70.71 mm
R = 70.71 mm
t = 2.0 mm

E = 200. KN/mm²
ν = 0.3
p = 1.0 N/mm²

LEGEND:

— Theoretical
—o— 1 Element, Surplus: 3u & 4w
—▽— 2 Equal Elements, Surplus: 3u & 4w

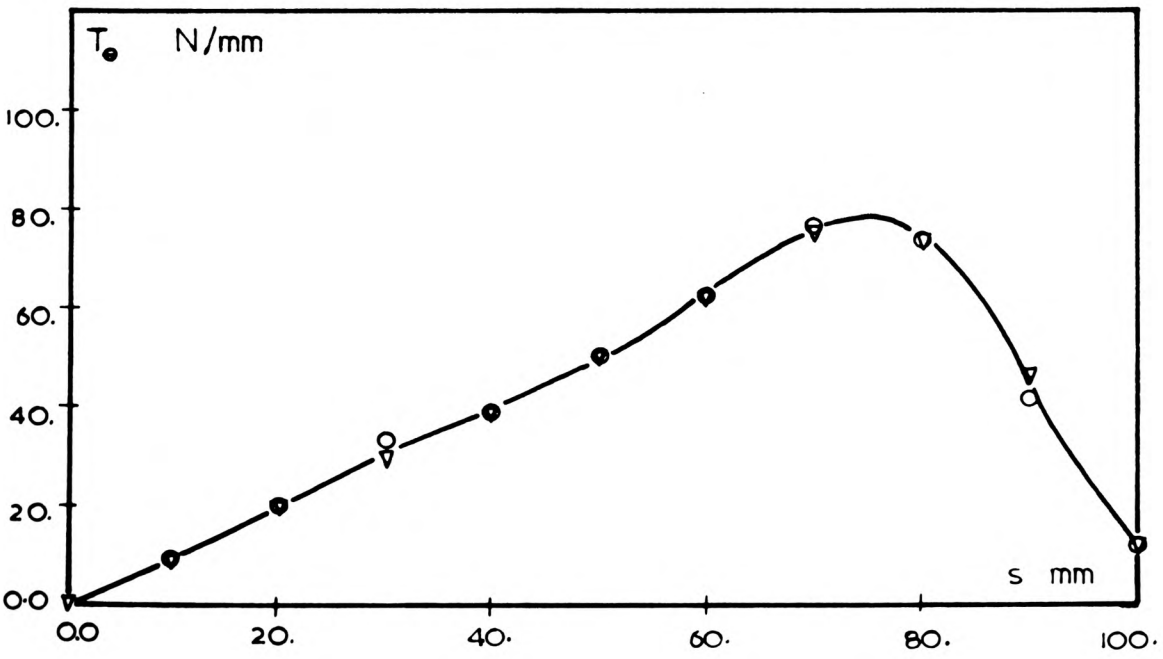

(a)

FIGURE 3.30

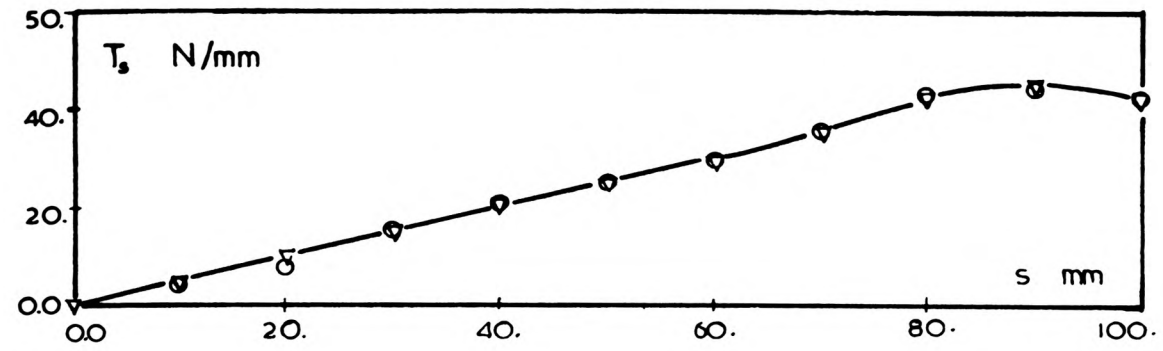

(b)

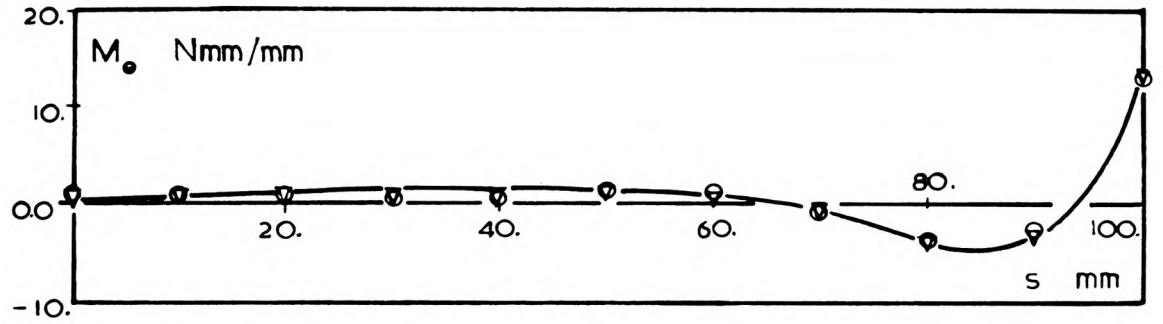

(c)

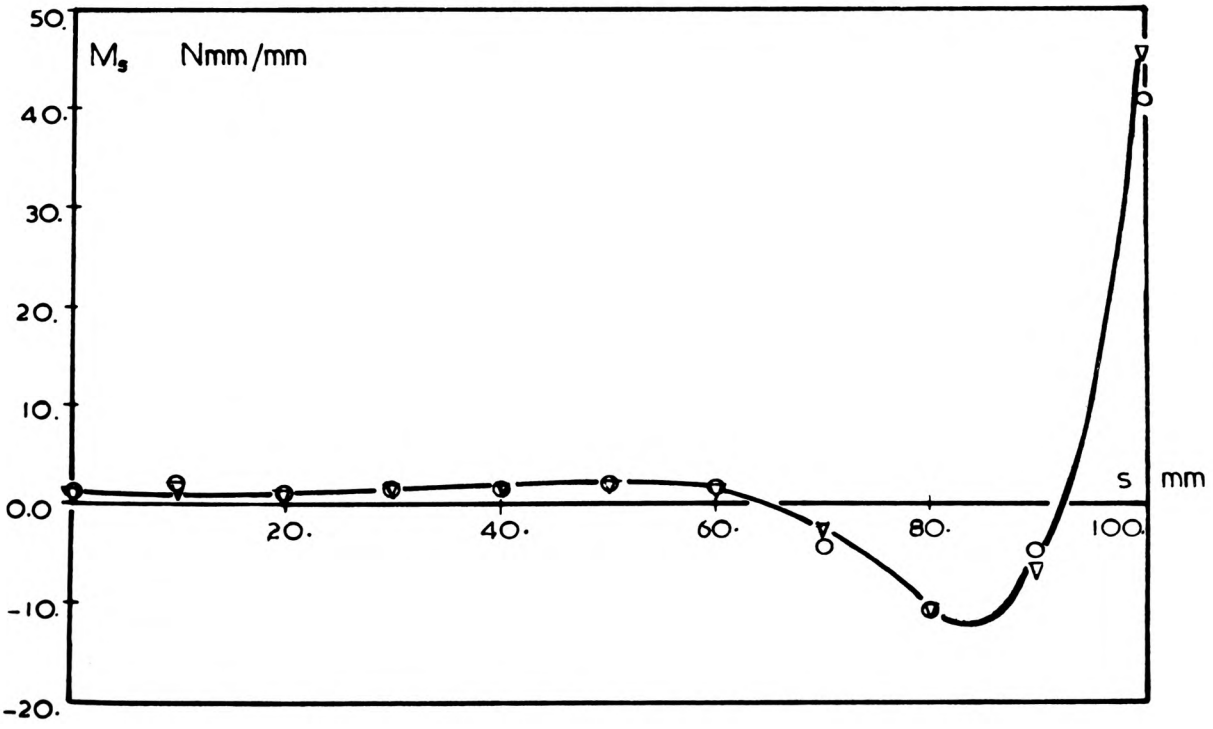

(d)

FIGURE 3.30

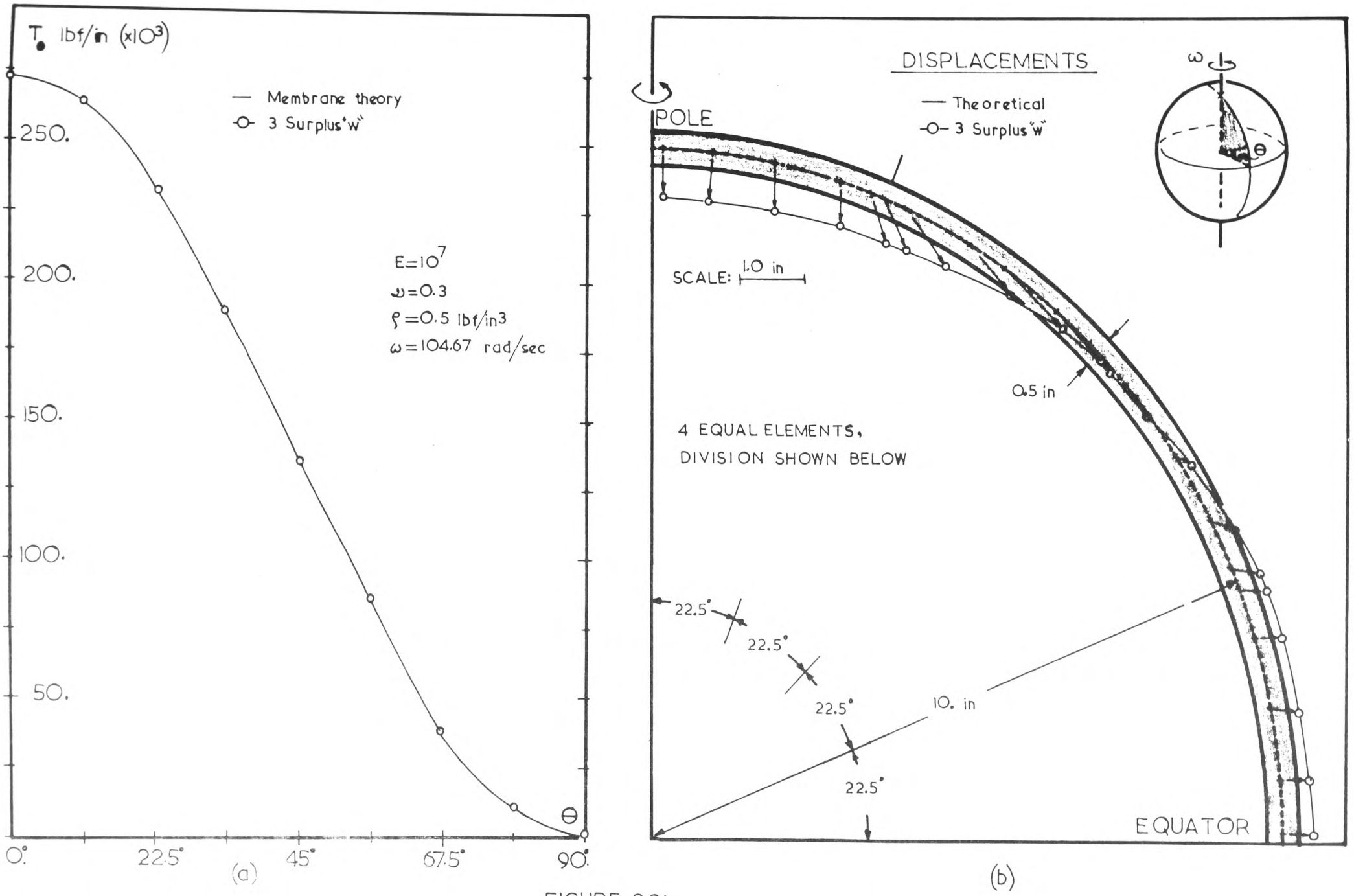
T_θ lbf/in (x10³)
Membrane theory
3 Surplus "w"
250.
200.
150.
100.
50.
E=10⁷
ν=0.3
ρ=0.5 lbf/in3
ω=104.67 rad/sec
θ
0°
22.5°
45°
67.5°
90°
(a)
DISPLACEMENTS
Theoretical
3 Surplus "w"
POLE
ω
θ
SCALE: 1.0 in
0.5 in
4 EQUAL ELEMENTS,
DIVISION SHOWN BELOW
22.5°
22.5°
22.5°
22.5°
10. in
EQUATOR
(b)

FIGURE 3.31

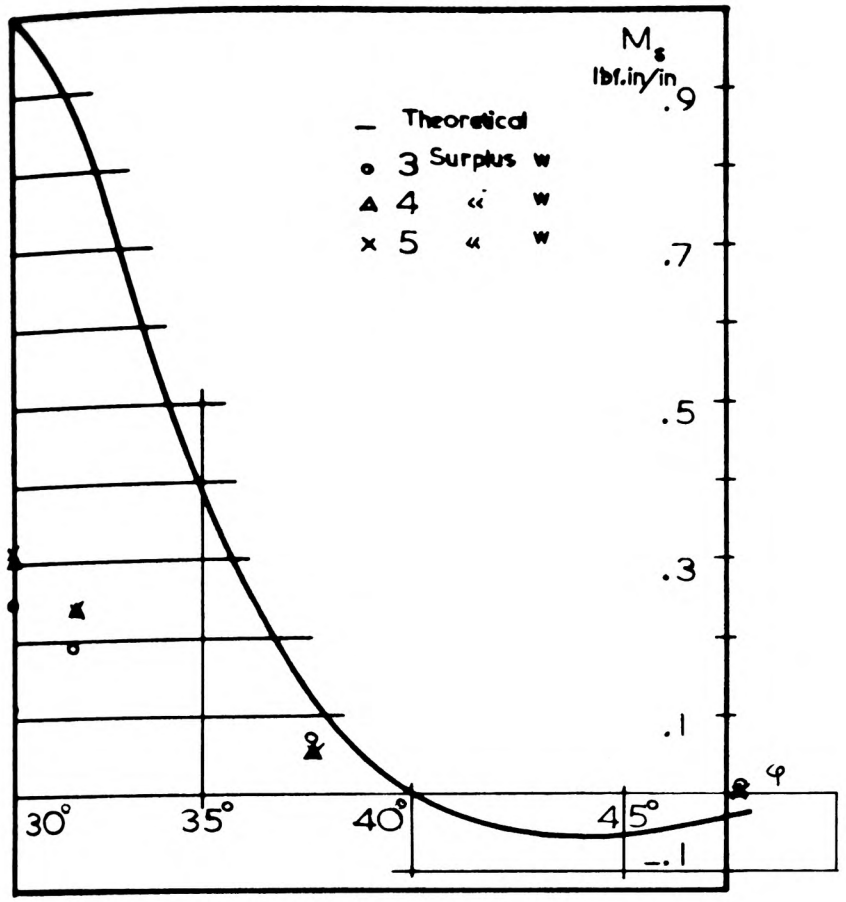

(a)

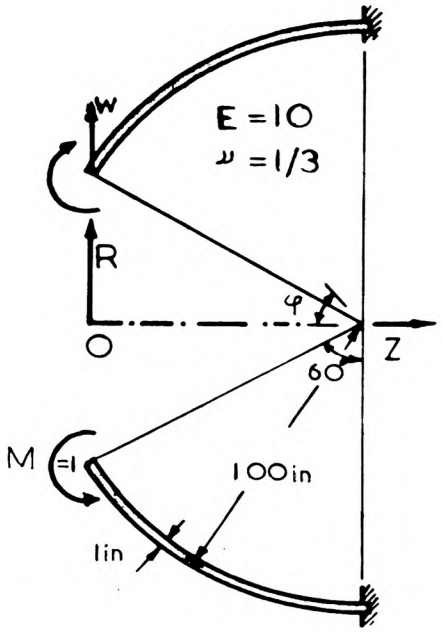

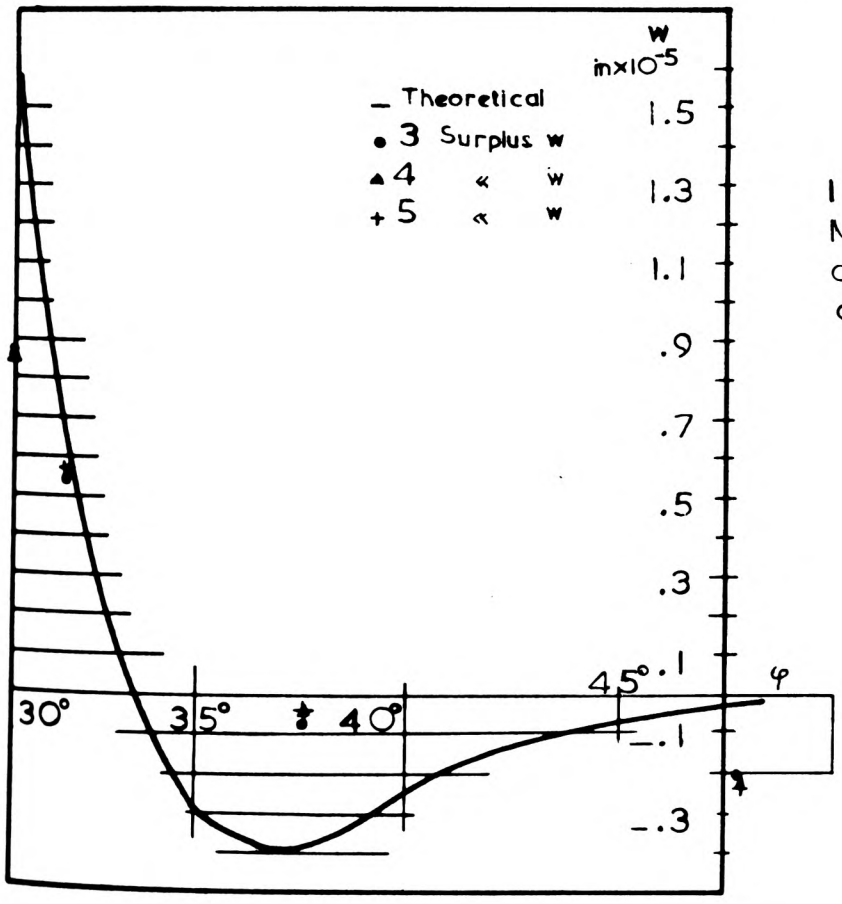

(b)

1 Element spanning 60°
Moments and displ-
acements sampled
at Gauss points

FIGURE 3.32

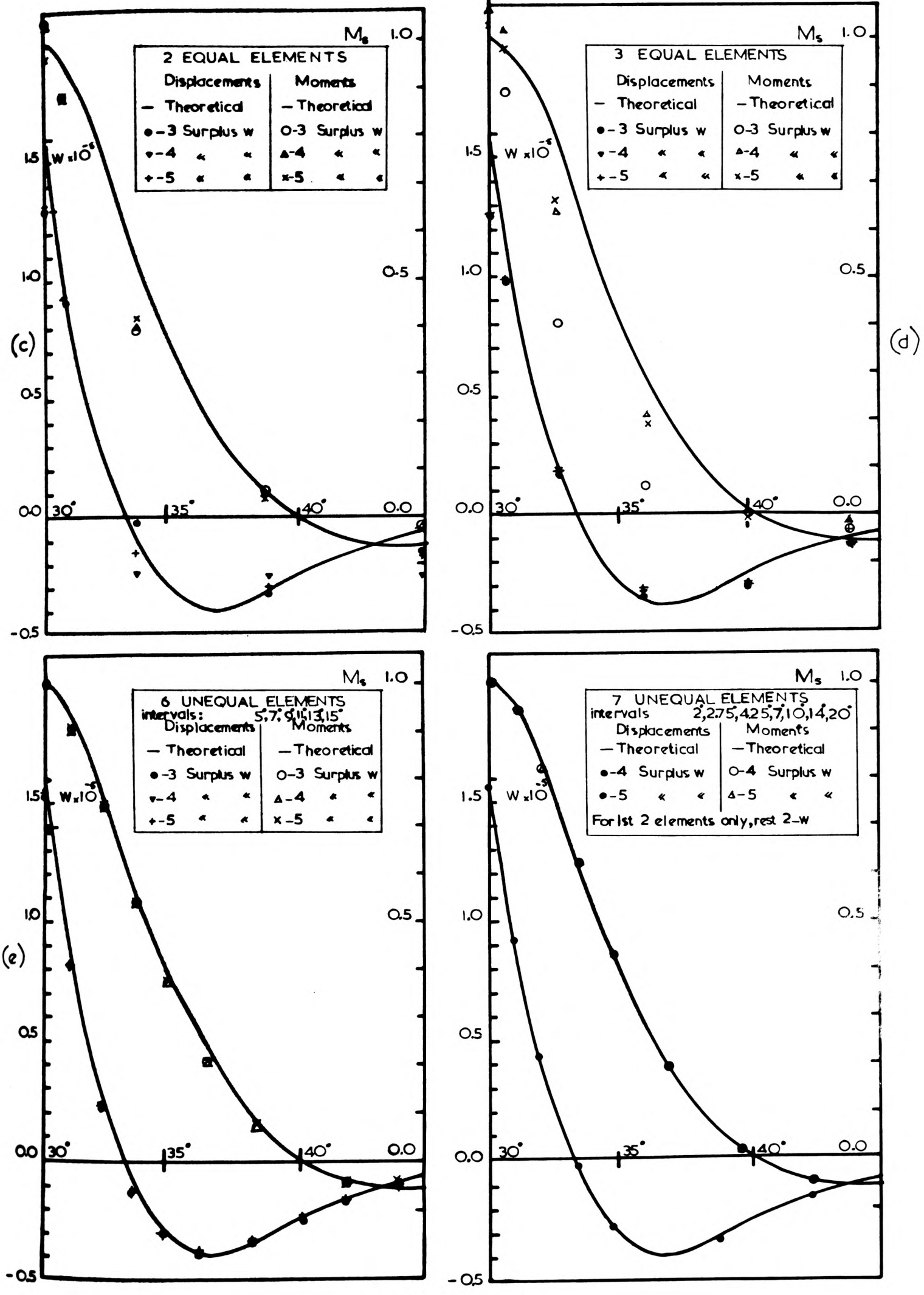
(c)
2 EQUAL ELEMENTS
Displacements
— Theoretical
●-3 Surplus w
▼-4 « «
+-5 « «
Moments
— Theoretical
○-3 Surplus w
△-4 « «
×-5 « «
(d)
3 EQUAL ELEMENTS
Displacements
— Theoretical
●-3 Surplus w
▼-4 « «
+-5 « «
Moments
— Theoretical
○-3 Surplus w
△-4 « «
×-5 « «
(e)
6 UNEQUAL ELEMENTS
intervals: 5°,7°,9°,11°,13°,15°
Displacements
— Theoretical
●-3 Surplus w
▼-4 « «
+-5 « «
Moments
— Theoretical
○-3 Surplus w
△-4 « «
×-5 « «
7 UNEQUAL ELEMENTS
intervals 2°,2.75°,4.25°,7°,10°,14°,20°
Displacements
— Theoretical
●-4 Surplus w
●-5 « «
Moments
— Theoretical
○-4 Surplus w
△-5 « «
For 1st 2 elements only, rest 2-w
W x10⁻⁵
Ms
1.0
0.5
0.0
-0.5
30°
35°
40°

FIGURE 3.32

CONCRETE SPHERICAL CAP

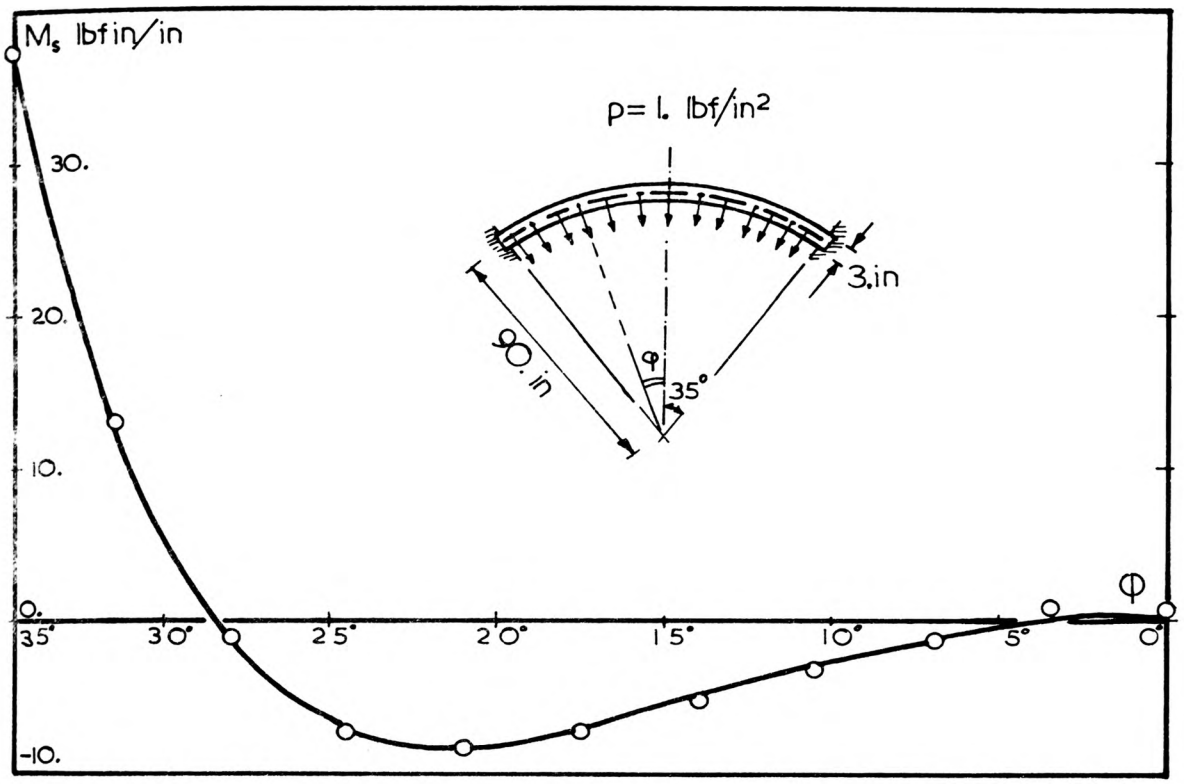

(a)

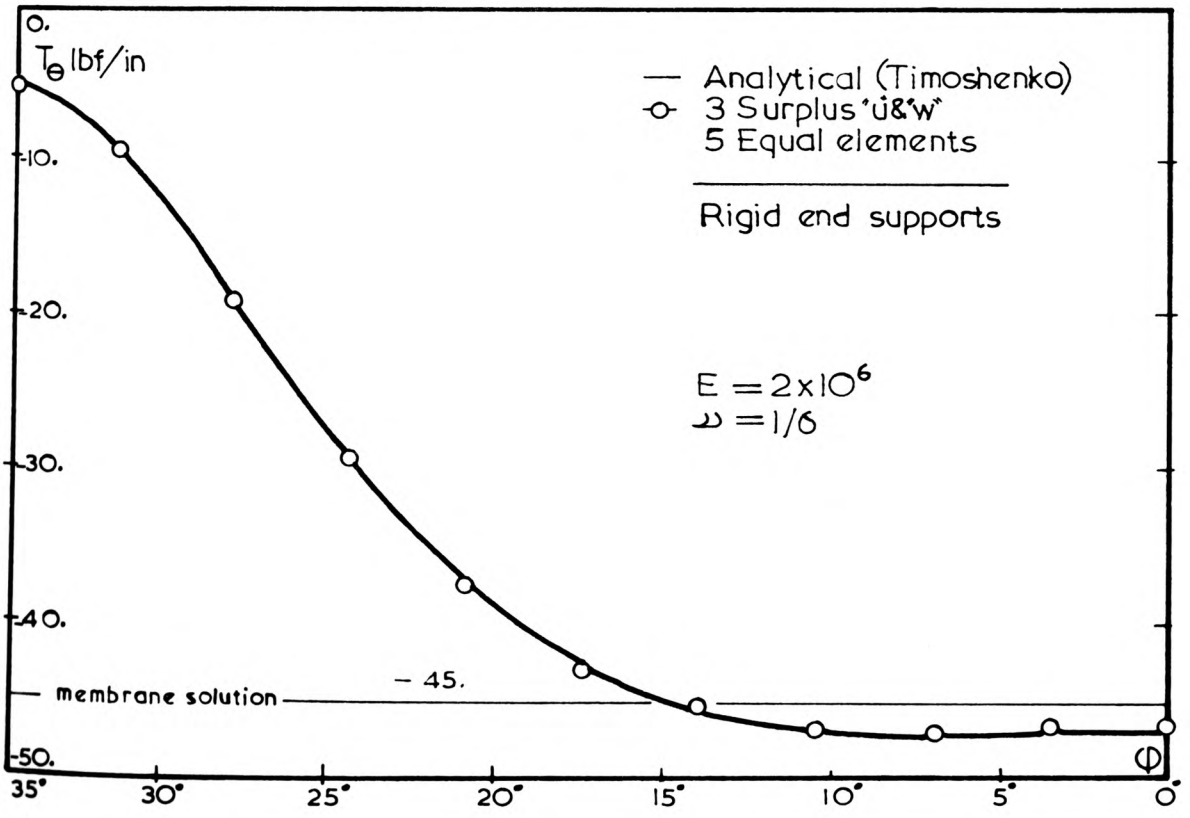

(b)

FIGURE 3.33

CONCRETE SPHERICAL CAP

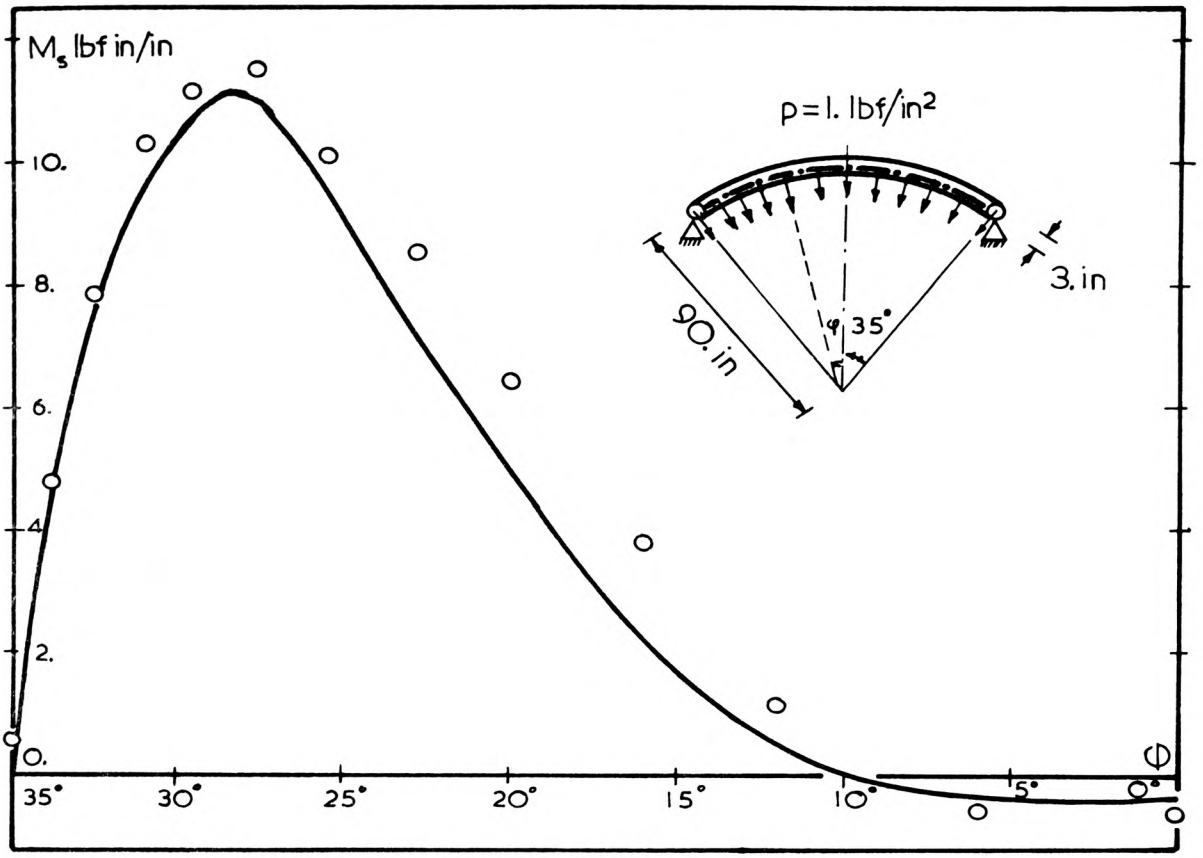

(a)

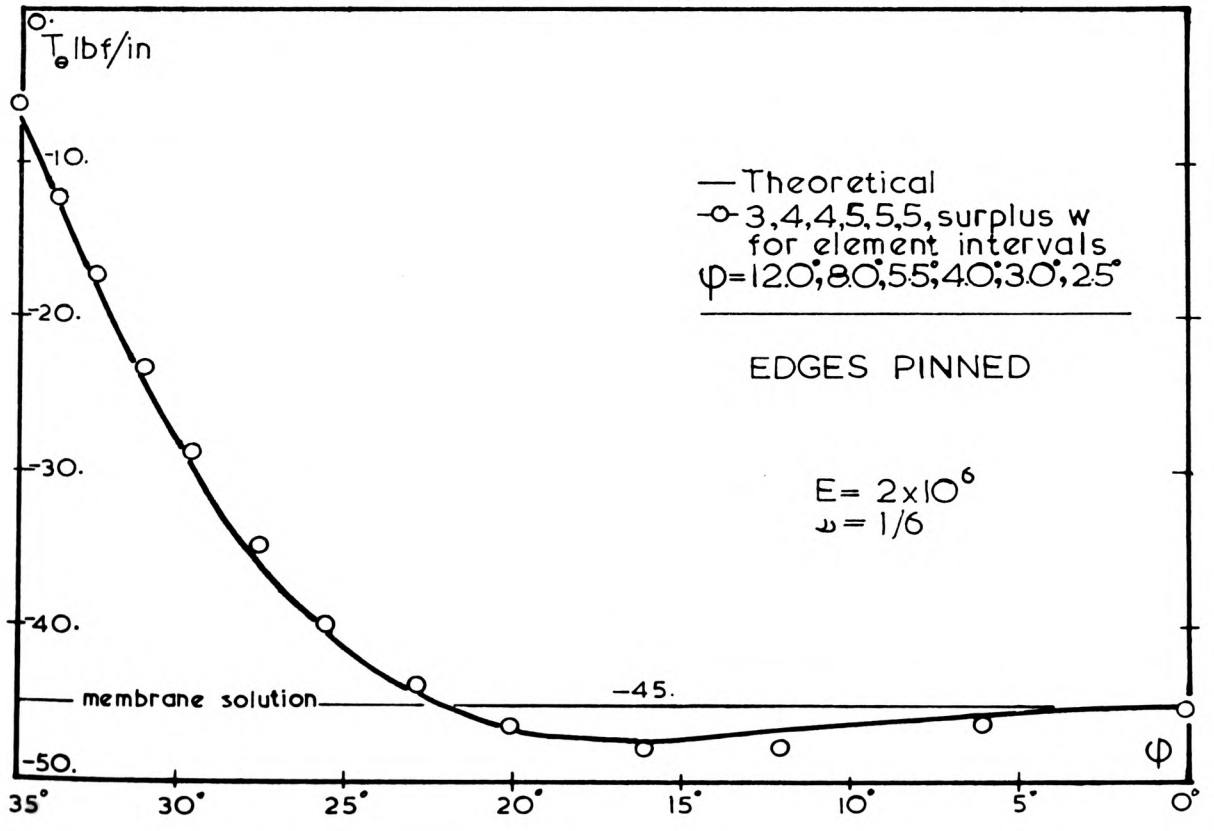

(b)

FIGURE 3.34

CONCRETE SPHERICAL CAP

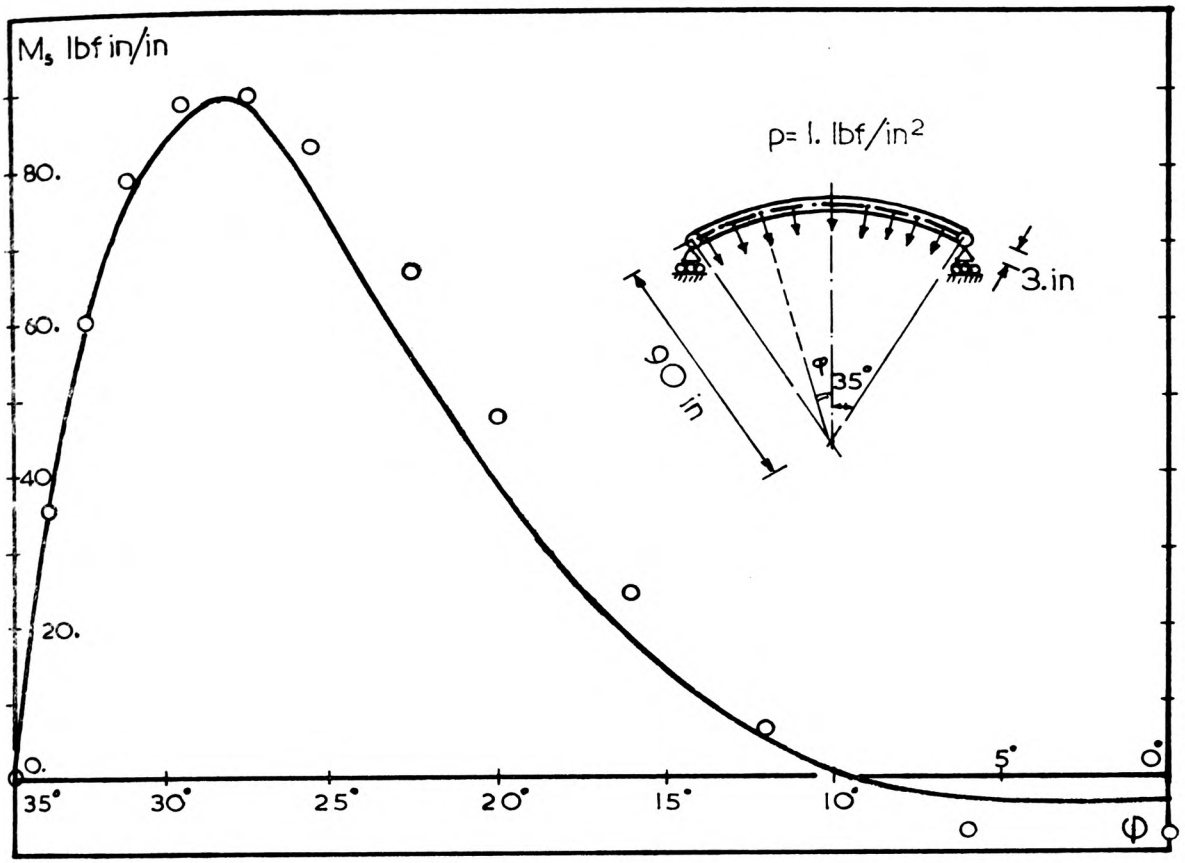

(a)

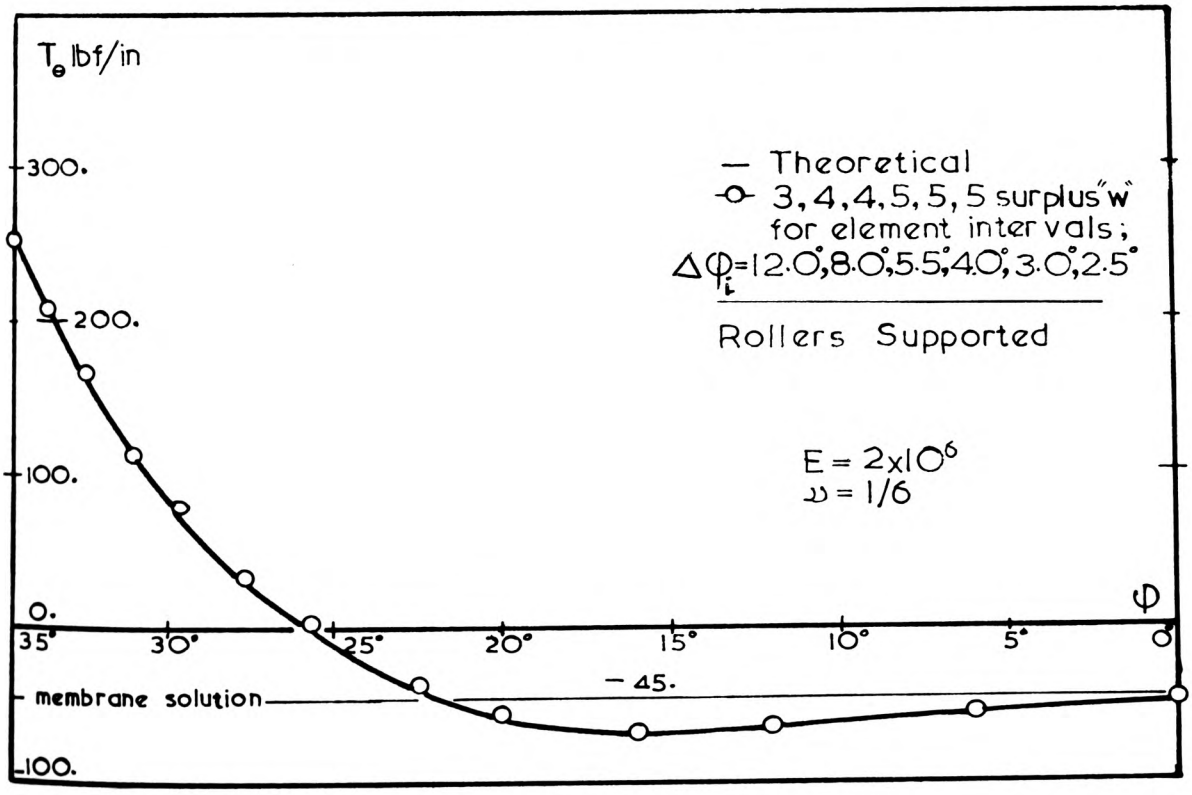

(b)

FIGURE 3.35

THE TOROIDAL SHELL

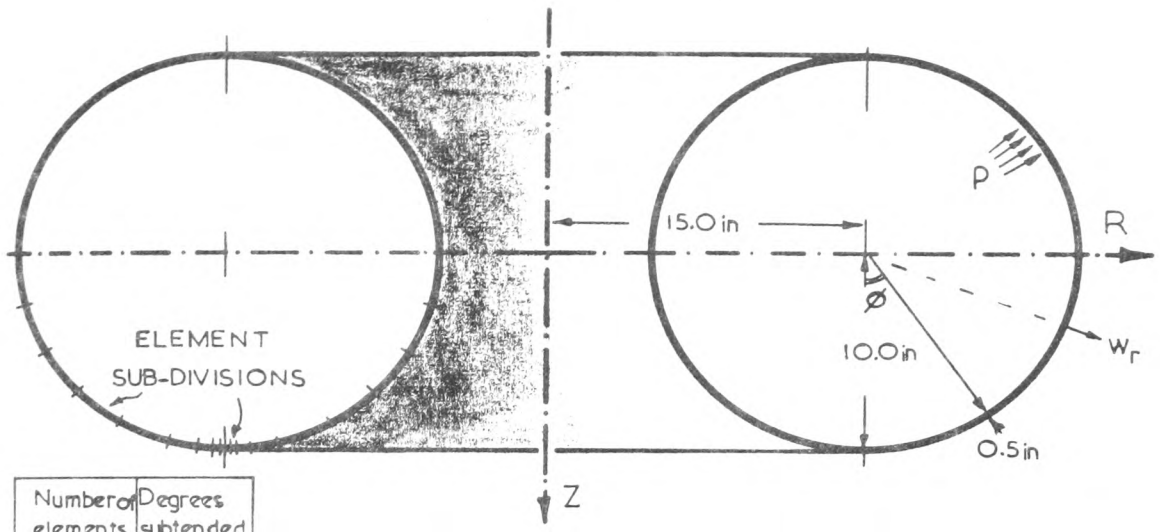

Number of elements	Degrees subtended
10	15°
2	8°
2	4°
2	2°
2	1°
Total 18	180°

$E = 10. \times 10^6$ lbf/in^2

$\nu = 0.3$

$p = 1.0$ lbf/in^2

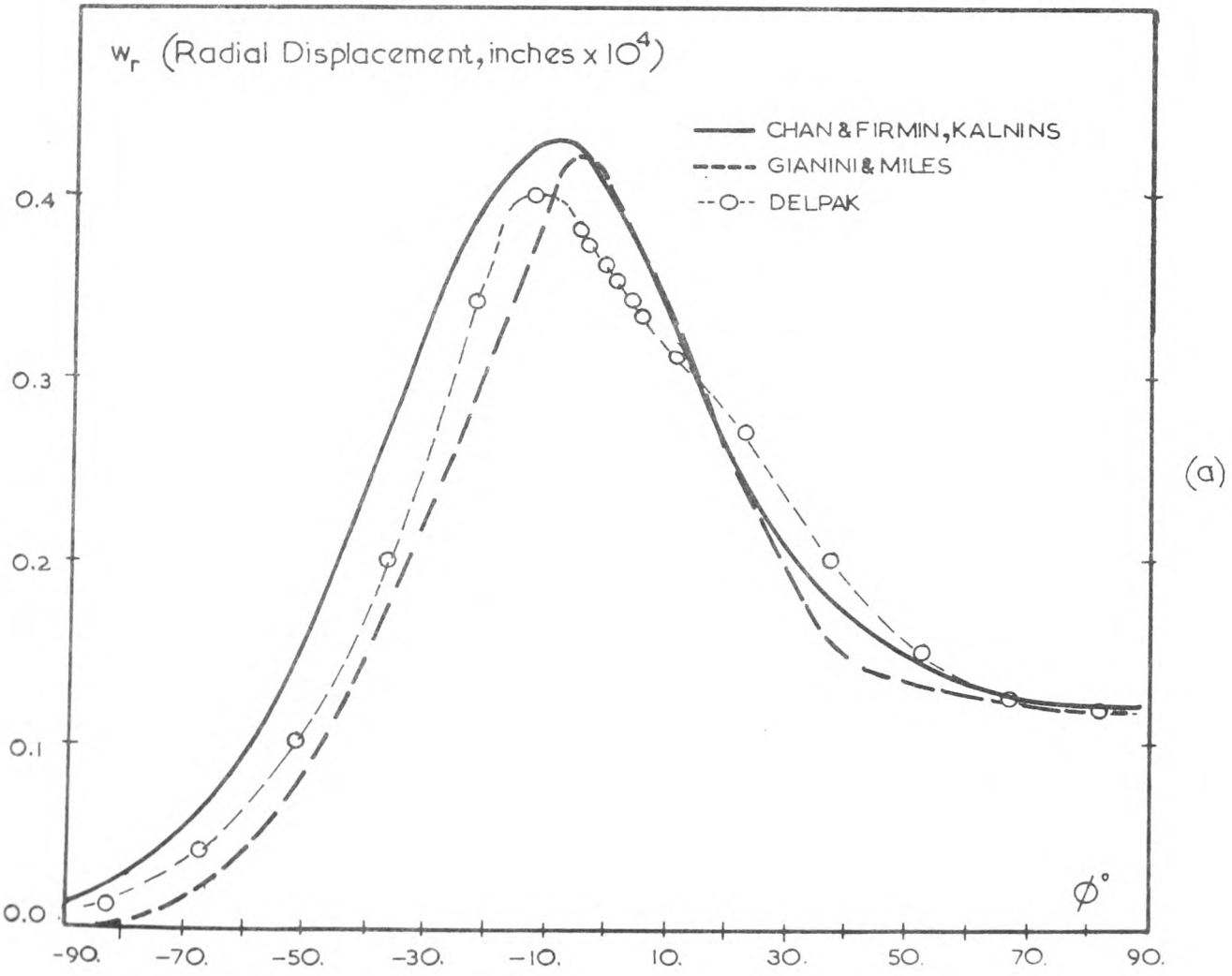

(a)

FIGURE 3.36

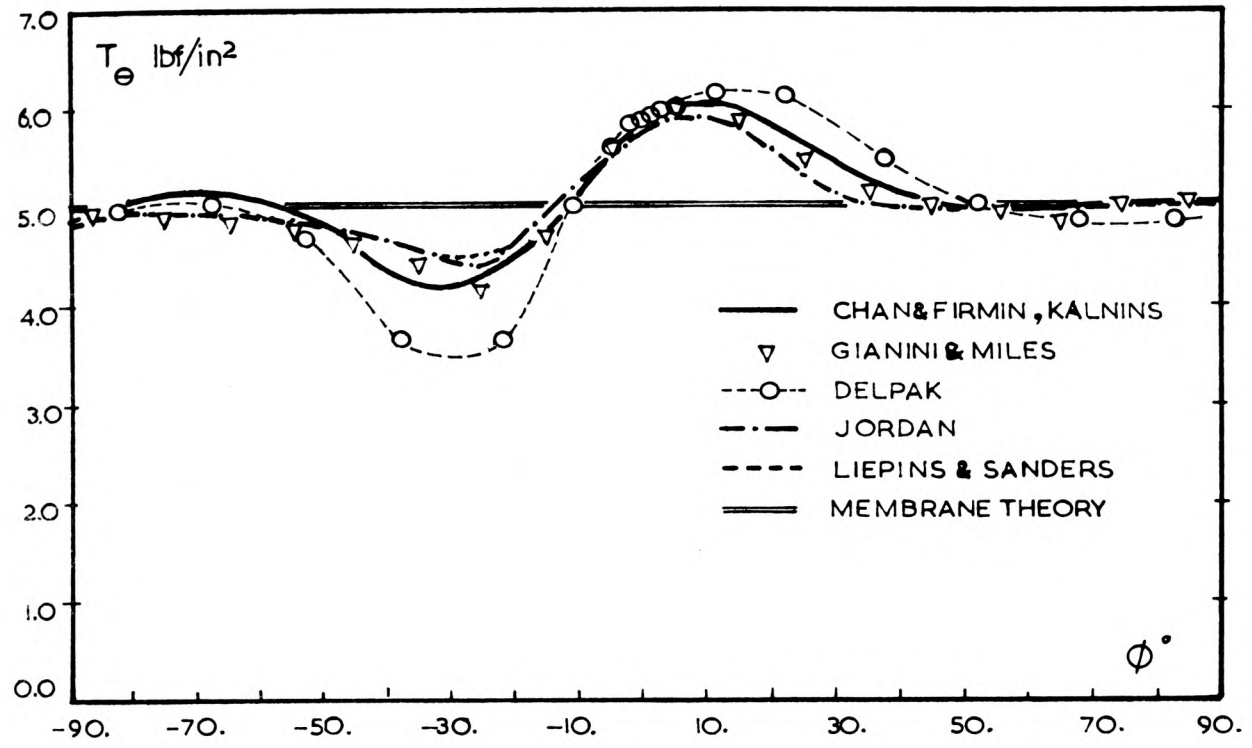

(b)

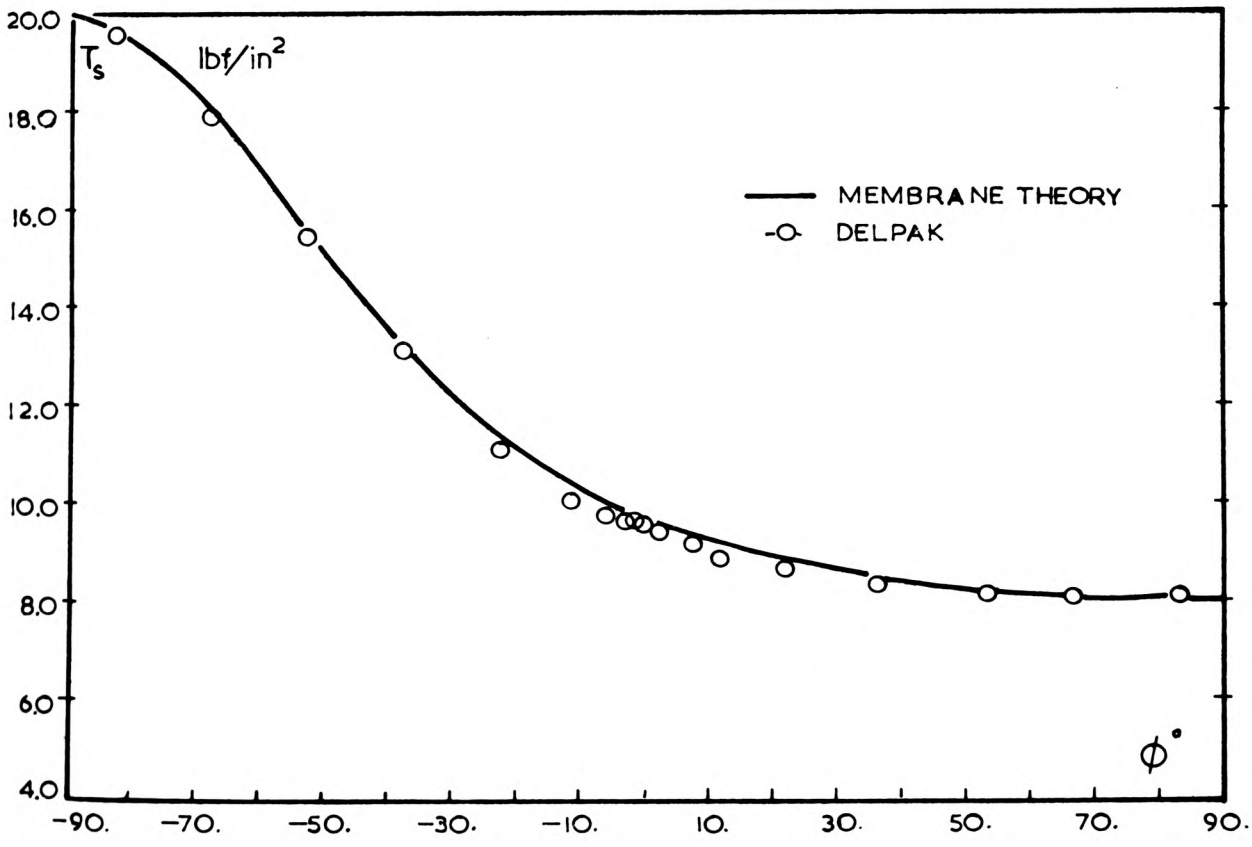

(c)

FIGURE 3.36

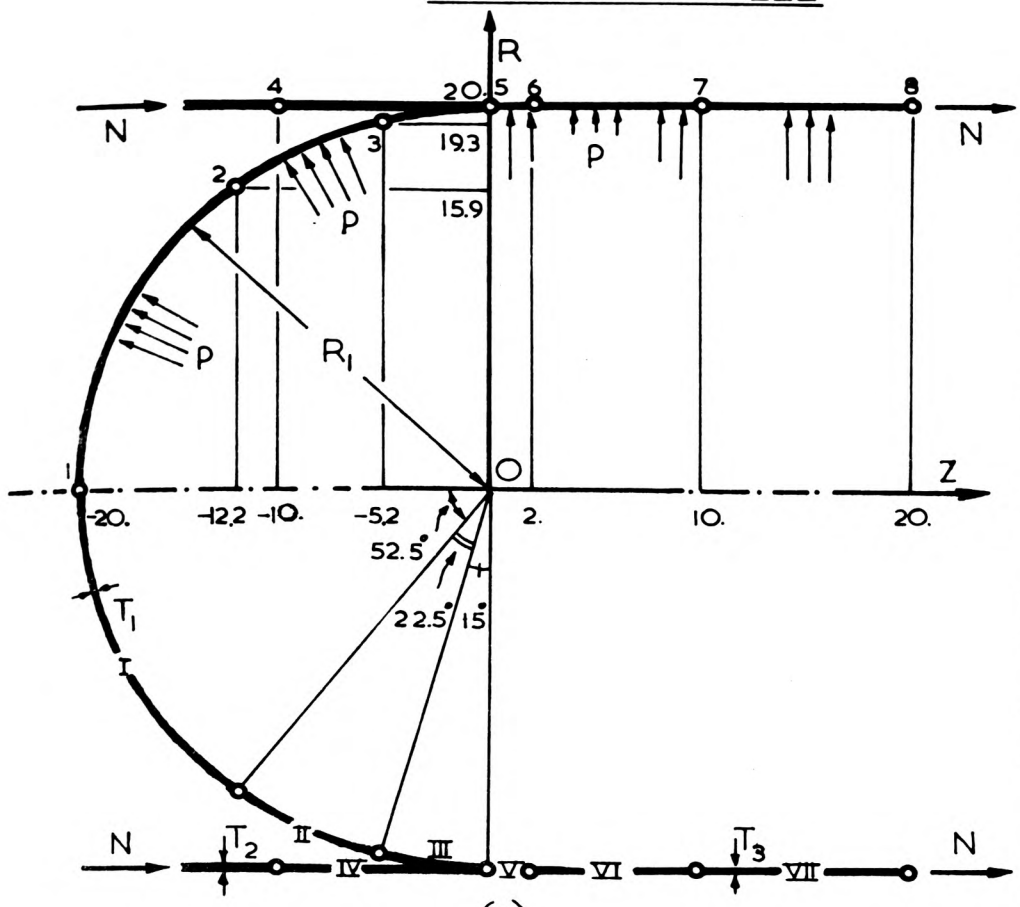

R_1=20. in
T_1=.4 in
T_2=.5 in
T_3=.3 in

p=1000. lbf/in^2
N=5000. lbf/in

E=10x10^6 lbf/in^2
ν=.3

Nodes shown by figures

7 Elements used shown by Roman letters

FIGURE 3.37

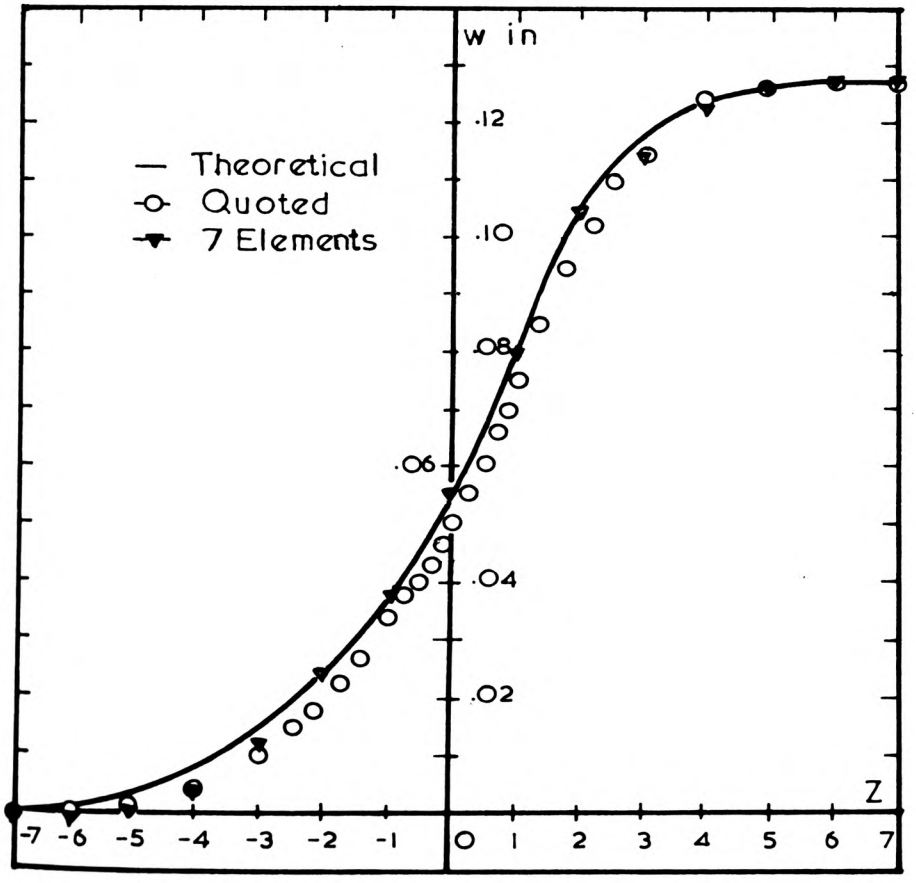

w is global radial displacement of cylinders

PURE MEMBRANE EXAMPLES

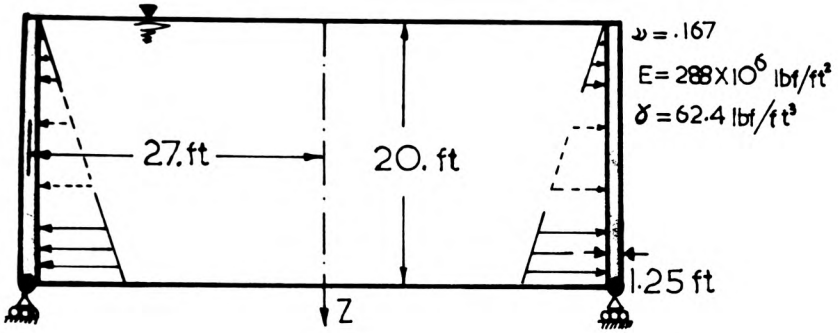

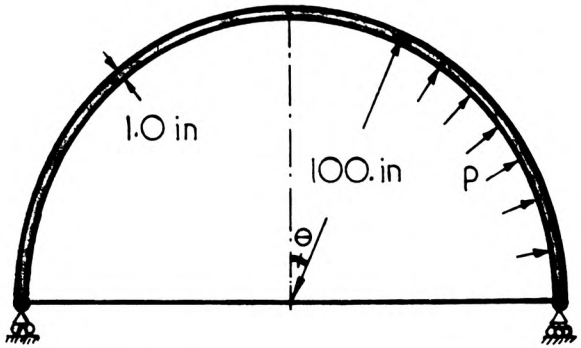

ν = .333
E = 10^7 lbf in
p = 50. lbf in

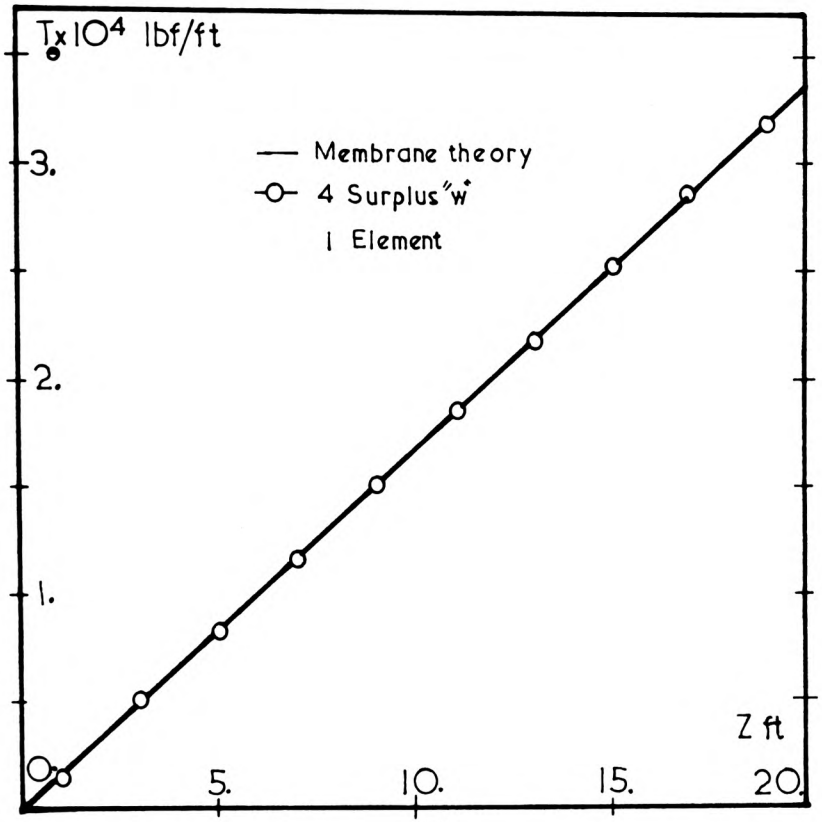

(a)

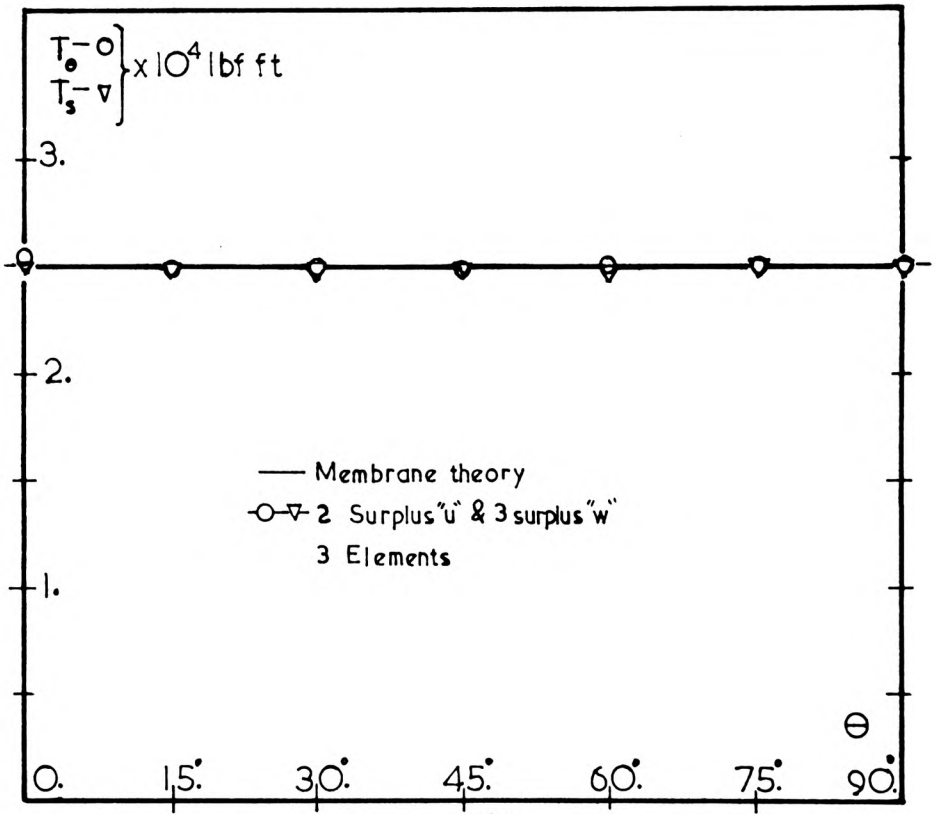

(b)

FIGURE 3.38

CHAPTER 4

THE ASYMMETRIC ANALYSIS

4.1 INTRODUCTION

The development of the program from axisymmetric shell problems to asymmetric analysis of thin shells is discussed in this Chapter. The above process of extension is not fundamentally difficult but a great deal of care is required both in understanding the problem and in correctly preparing all the relevant ingredients.

The strain-displacement relationship from which the [B] matrix results was derived in Chapter 2 and can be used directly with only minor adjustments.

The elastic matrix [D] now required, should be in its general form for orthotropic plane-stress conditions which in addition to the axisymmetric case should include a mid-surface shear and a curvature-twist term.

Another important aspect in the current extension is a suitable choice of displacements so that certain simplifying properties become manifest. It is hoped that the manner of use of all these factors will become clear in the following sections.

4.2 DISPLACEMENTS

4.2.1 The "simplification" referred to above reduces the problem to one of processing the displacements in the plane of Z and R axes only, which then makes the problem effectively two-dimensional. The development takes place in two stages.

The first is the evaluation of the loads. This is achieved using the well known technique of expressing the loads in terms of a Fourier Series, where the circumferential line force $F = f(\theta)$ acting round a truncated cone of generator length 'ds', can be represented in the expanded form of,

$$\left.\begin{aligned} F = F_0 + F_1 \cos\theta + F_2 \cos 2\theta + \ldots\ldots F_n \cos n\theta \\ + F_1' \sin\theta + F_2' \sin 2\theta + \ldots\ldots F_n' \sin n\theta \end{aligned}\right\}. \quad \text{eqn. 4.1}$$

This is depicted in Fig. 4(a) and (b). It is preferable to express the line loads in terms of Z, R and θ components as F_Z, F_R and F_θ. The following are two alternatives of representing the i-th term of the above directional components,

a) the θ-symmetric set, i.e. $\begin{cases} F_Z \cos i\theta \\ F_R \cos i\theta \\ F_\theta \sin i\theta \end{cases}$, eqn. 4.2(a)

and b) the anti-symmetric set, i.e. $\begin{cases} F_Z \sin i\theta \\ F_R \sin i\theta \\ F_\theta \cos i\theta \end{cases}$. eqn. 4.2(b)

The above representation of the forces at this stage is not in itself significant. However, the ensuing conclusions are of paramount importance. It has been shown (Novozhilov[1] and Zienkiewicz[2]), that a solution to the displacement pattern of an axisymmetric shell resulted from loading by the i-th term of the forces given in eqn. 4.1, is indeed a set of displacements of a similar circumferential variations. It is the existence and the nature of these displacements which are significant and particularly relevant. The discussion regarding the enumeration of a given term of the applied loads can now be postponed to the appropriate section (4.5), whereas attention is focussed towards further development in the area of

displacement representations.

Corresponding to the set of forces labelled under eqn. 4.2(a) and (b) the displacements are listed as follows,

a) the θ-symmetric set, i.e. $\begin{cases} u \cos i\theta \\ w \cos i\theta \\ v \sin i\theta \end{cases}$, eqn. 4.3(a)

and b) the antisymmetric set, i.e. $\begin{cases} u \sin i\theta \\ w \sin i\theta \\ v \cos i\theta \end{cases}$. eqn. 4.3(b)

respectively. For non-zero values of i, the general problem associated with the i-th term of these displacements is solved. On the other hand for zero values of i, the first set of loads and displacements result in a solution for the axially symmetrical problem (Chapter 3), while the second set yield the solution to torsional loading.

4.2.2 Uncoupling of Harmonics

The next stage is the analysis of the interrelationship between the various components. The forms of approach to the above problem appear to be manifold but the outcome is identical[3],[4],[5]. The approach adopted here and in subsequent work is a modification of references (4) and (5) and is particularly suited for numerical work. In forming the stiffness matrix for the element $[k]^e$, the (i,j)-th component is considered which, when expressed using the Zienkiewicz[2] nomenclature reads as:

$$\{\delta_i\}^T [k_{ij}] \{\delta_j\} = \int_V \{\varepsilon_i\}^T [D] \{\varepsilon_j\} dv \qquad \ldots\ldots \text{ eqn. 4.4}$$

where $\{\varepsilon_i\} = [B_i]\{\delta_i\}$ and $\{\varepsilon_j\} = [B_j]\{\delta_j\}$. $\{\delta_i\}$ and $\{\delta_j\}$ are nodal variables linked with i-th and j-th harmonics respectively and the rest of the symbols have their usual meaning. Thus,

$$\{\delta_i\} = \begin{Bmatrix} u_0 \cos i\theta \\ w_0 \cos i\theta \\ v_0 \sin i\theta \end{Bmatrix} \quad \text{and} \quad \{\delta_j\} = \begin{Bmatrix} u_0 \cos j\theta \\ w_0 \cos j\theta \\ v_0 \sin j\theta \end{Bmatrix} ,$$

upon substitution and "simplification" of which the (i,j)-th element and the integral are reduced to,

$$[K_{ij}] = \int_v [B_i]^T [D][B_j] dv . \qquad \ldots\ldots \text{ eqn. 4.5}$$

Now $[B_i]$ operating on nodal variables would result in typical terms shown below:-

$$[B_i] = [B_{i1} \cos i\theta + B_{i2} \sin i\theta],$$

thus the element $[K_{ij}]$ of the stiffness matrix would contain terms such as,

$$[K_{ij}] = \int_v [B_{i1} \cos i\theta + B_{i2} \sin i\theta]_K^T [D_{k\ell}] [B_{j1} \cos j\theta + B_{j2} \sin j\theta]_\ell dv. \quad \text{eqn. 4.6}$$

It is clear that products such as $\int \sin i\theta \cos j\theta d\theta$ would vanish identically and the following results are obtained.

$$\begin{Bmatrix} \int_0^{2\pi} \cos i\theta \cos j\theta d\theta \\ \int_0^{2\pi} \sin i\theta \sin j\theta d\theta \end{Bmatrix} = \begin{Bmatrix} \pi\delta_{ij} & \text{for } i,j \geq 1 \\ 2\pi & \text{for } i,j = 0 \end{Bmatrix} , \qquad \ldots\ldots \text{ eqn. 4.7}$$

δ_{ij} being Kronecker Delta. This is a clear indication that a complete element stiffness matrix $[K]^e_{1:n}$ * is diagonal, i.e. $K_{ij}=0$ for unequal values of i and j.

---

* The representation $[K]^e_{1:n}$ is a shorthand notation for $[K]^e_{1,1}$, $[K]^e_{1,2}, \ldots [K]^e_{1,n}, \ldots . [K]^e_{n,n}$.

A possible representation of the entire element stiffness matrix is as follows,

$$[K]^e_{1:n} = \begin{array}{|c|c|c|c|c|} \hline K_{11} & K_{12}=0 & & & K_{1n}=0 \\ \hline K_{21}=0 & K_{22} & & & \\ \hline & & & & \\ \hline & & & & \\ \hline K_{n1}=0 & & & & K_{nn} \\ \hline \end{array} \quad \ldots\ldots \text{ eqn. 4.8}$$

The disappearance of the off-diagonal terms shown above proves the uncoupling or independence of the various harmonic components and in turn facilitates the separate formation of each stiffness matrix $[K_{11}]$ to $[K_{nn}]$.

Now the work done by the load on the displacements of element "e" is examined. Let the loads of the j-th harmonic be $\{p_j\}$ and be given as,

$$\{p_j\} = \begin{Bmatrix} p_Z \cos j\theta \\ p_R \cos j\theta \\ p_\theta \sin j\theta \end{Bmatrix}$$

The virtual work done $\{\overset{*}{\delta}\}^T \int [N]^T \{p\} dA$ by the individual terms on displacements $\{\delta_i\}$ is then,

$$\{\overset{*}{\delta}_i\}^T \int\int_0^{2\pi} (p_Z N_u)\cos i\theta \cos j\theta d\theta ds,\ \{\overset{*}{\delta}_i\} \int\int_0^{2\pi} (p_R N_w)\cos i\theta \cos j\theta d\theta ds,$$

and $\{\overset{*}{\delta}_i\} \int\int_0^{2\pi} (p_\theta N_v)\sin i\theta \sin j\theta d\theta ds,$

which indicate that the integrals such as $\int_0^{2\pi} \cos i\theta \cos j\theta d\theta$ follow the pattern discussed in the previous paragraph and that the loads of the unlike harmonics would also uncouple.

It is now evident that the structure can be analysed for the individual harmonics under a particular load term and that the total strain and displacement at a point will be obtained by super-imposing the various harmonic components.

4.3 THE DERIVATION OF THE MATRIX $[B_n]$

The task of producing the operating matrix $[B_n]$ is greatly simplified since the general {strain, curvature} / {displacement} relationships taken from Novozhilov[6] have already been modified to cylindrical coordinates. Due to the globally orientated nature of the displacement $\{\delta_n\}$, a further local to global transformation of the terms of the $[B]$ matrix is required to yield the strains and the curvatures instantly. Similar rules of differentiation to Chapter 3 must be observed, namely $\frac{\partial(\ldots)}{\partial s}$ is the derivative with respect to the curve length and that '$\cos\alpha$' and '$\sin\alpha$' are constants at a given Gauss-point and thus escape differentiation. A new variable, circumferential angle θ, is now introduced and must be taken into account. Thus on differentiation with respect to the curve length along the parallel circle, namely $\frac{1}{R}\frac{\partial(\ldots)}{\partial\theta}$ the following rules are observed:

$$\frac{\partial}{R\partial\theta}\{f(u_0,w_0)\cos n\theta\} = (-\frac{n}{R})\{f(u_0,w_0)\sin n\theta\},$$

$$\frac{\partial}{R\partial\theta}\{f(v_0)\sin n\theta\} = (\frac{n}{R})\{f(v_0)\cos n\theta\},$$

$$\frac{\partial^2}{\partial s R\partial\theta}\{f(u_0,w_0)\cos n\theta\} = (-\frac{n}{R})\frac{\partial}{\partial s}\{f(u_0,w_0)\sin n\theta\},$$

$$\frac{\partial^2}{\partial s R\partial\theta}\{f(v_0)\sin n\theta\} = (\frac{n}{R})\frac{\partial}{\partial s}\{f(v_0)\cos n\theta\},$$

$$\frac{\partial^2}{R^2\partial\theta^2}\{f(u_0,w_0)\cos n\theta\} = (-\frac{n}{R})(\frac{n}{R})\{f(u_0,w_0)\cos n\theta\},$$

$$\frac{\partial^2}{R^2\partial\theta^2}\{f(v_0)\sin n\theta\} = (\frac{n}{R})(-\frac{n}{R})\{f(v_0)\sin n\theta\}.$$

..... eqn. 4.9

Thus the detailed relationship of $\{\overset{\varepsilon}{\chi}_n\} = [B_n]\{\delta_n\}$ given in Chapter 2 simplifies further when the above rules are applied. The {strain, curvature}/ {displacement} relationship now appears as,

$$
\begin{Bmatrix} \varepsilon_s \\ \varepsilon_\theta \\ \varepsilon_{s\theta} \\ \chi_s \\ \chi_\theta \\ \frac{\chi_{s\theta}}{2} \end{Bmatrix}_n =
\left[\begin{array}{c|c|c|c}
(\cos\alpha\frac{\partial}{\partial s} & \sin\alpha\frac{\partial}{\partial s} & 0\ ) & \cos n\theta \\
(0 & \frac{1}{R} & \frac{n}{R}\ ) & \cos n\theta \\
((-\frac{n}{R})\cos\alpha & (-\frac{n}{R})\sin\alpha & -\frac{\sin\alpha}{R}+\frac{\partial}{\partial s}\ ) & \sin n\theta \\
(\sin\alpha\frac{\partial^2}{\partial s^2} & -\cos\alpha\ \frac{\partial^2}{\partial s^2} & 0) & \cos n\theta \\
((-\frac{n}{R})(\frac{n}{R})\sin\alpha+\frac{\sin^2\alpha}{R}\ \frac{\partial}{\partial s} & -(-\frac{n}{R})(\frac{n}{R})\cos\alpha-\frac{\sin\alpha\cos\alpha}{R}\ \frac{\partial}{\partial s} & (\frac{n}{R})\frac{\cos\alpha}{R}\ ) & \cos n\theta \\
((-\frac{n}{R})\sin\alpha\frac{\partial}{\partial s} - (-\frac{n}{R})\frac{\sin^2\alpha}{R} & -(-\frac{n}{R})\cos\alpha\frac{\partial}{\partial s} + (-\frac{n}{R})\frac{\sin\alpha\cos\alpha}{R} & \frac{\cos\alpha}{R}\ \frac{\partial}{\partial s} - \frac{\sin\alpha\cos\alpha}{R^2}) & \sin n\theta
\end{array}\right]
$$

$$
X \begin{Bmatrix} u_0 \\ w_0 \\ v_0 \end{Bmatrix}_n . \qquad \ldots\ldots \text{ eqn. 4.10}
$$

By taking the second displacement system of eqn. 4.1 (which is chosen from considering the torsional aspect of displacements), a change in the order of appearance of $\cos n\theta$ and $\sin n\theta$ results which in turn causes an appropriate change in the sign of $(\frac{n}{R})(\ldots) = \frac{1}{R}\frac{\partial}{\partial\theta}(\ldots)$. It is interesting to note that, with the first displacement system of eqn. 4.1, the quantities ε_s, ε_θ, χ_s and χ_θ are multiplied by a $\cos n\theta$ factor, whereas $\varepsilon_{s\theta}$ and $\chi_{s\theta}$ are multiplied by $\sin n\theta$. When the displacements are changed to the second group of eqn. 4.1 displacements,

the multiplying factors, cosnθ and sinnθ suffer a reversal of positions. The existence of these factors indicates the nature of the strains, i.e. whether the resulting strain and curvature components are θ-symmetric, skew-symmetric or asymmetric for a given problem.

4.4 CALCULATION OF THE STRESSES AND THE MOMENTS

Since in analysing thin shells of revolution the normal stress σ_z and the radial shears Q_s and Q_θ are normally neglected a simplified version of the elastic matrix is used. The remaining terms are two strains (ε_s, ε_θ), two curvatures (χ_s, χ_θ), a mid-surface shear($\varepsilon_{s\theta}$) and a twist ($\chi_{s\theta}$) which result in a 6x6 matrix given[7] below,

$$[D] = \frac{Et}{(1-\nu^2)} \left[\begin{array}{ccc|ccc} 1 & \nu & 0 & & & \\ \nu & 1 & 0 & & 0 & \\ 0 & 0 & \left(\frac{1-\nu}{2}\right) & & & \\ \hline & & & \frac{t^2}{12} & \frac{\nu t^2}{12} & 0 \\ & 0 & & \frac{\nu t^2}{12} & \frac{t^2}{12} & 0 \\ & & & 0 & 0 & \frac{t^2}{12}\left(\frac{1-\nu}{2}\right) \end{array}\right] \quad \text{..... eqn. 4.11}$$

or if the material is orthotropic with principal axes directed in the meridional and circumferential directions (possibly due to steel reinforcements in a concrete shell), then,

$$[D] = \frac{Et}{(1-n\nu_2^2)} \left[\begin{array}{ccc|ccc} n & n\nu_2 & 0 & & & \\ n\nu_2 & 1 & 0 & & 0 & \\ 0 & 0 & m(1-n\nu_2) & & & \\ \hline & & & \frac{nt^2}{12} & \frac{n\nu_2 t^2}{12} & 0 \\ & 0 & & \frac{n\nu_2 t^2}{12} & \frac{t^2}{12} & 0 \\ & & & 0 & 0 & \frac{mt^2}{12}(1-n\nu_2^2) \end{array}\right] \quad \text{..... eqn. 4.12}$$

where $n = \frac{E_1}{E_2}$ and $m = \frac{G_2}{E_2}$. Equations 4.11 and 4.12 are clearly plane-stress elastic matrices for obvious reasons. The outcome of the product $[D]\{\varepsilon\}$ is not actually the stresses $\{\sigma\}$ but the forces $\{T\}$ and moments (per unit length) $\{M\}$ better expressed as,

$$\left\{\begin{array}{c} T \\ \hline M \end{array}\right\} = \left[\begin{array}{c|c} D_T & \\ \hline & D_M \end{array}\right] \left\{\begin{array}{c} \varepsilon \\ \hline \chi \end{array}\right\} \qquad \ldots\ldots \text{ eqn. 4.13}$$

Some further practical points relevant to the calculation of strains and stress resultants are given in Section 4.6.3. Figure 4.8 illustrates the position and the direction of each of the above resultants acting on an infinitesimal element of a finite element. Moments are represented by double headed arrows as customary.

4.5 EVALUATION OF EXTERNAL LOADS

The derivation of the expressions for external loads can be more conveniently considered if divided into the groups discussed below.

a) External loads peculiar to the first harmonic (n=1), with special attention being paid to forces causing deformations along the R-axis.

The derivation of expressions for this class of loading is initiated by considering a radial ring load $r=r_0\cos\theta$ which is assumed to act around the circumference of an infinitesimal truncated cone, shown in Fig. 4.2(a) and (b). The elemental virtual work d(V.W.), done by the above force at an angle θ on the circumference is expressed in the familiar notation as,

$$d(V.W.) = \{\overset{*}{\delta}\}^T \int_0^{2\pi} (N_w[(Rd\theta ds).r] - N_v[(Rd\theta ds).0])$$

$$= \{\overset{*}{\delta}\}^T \int_0^{2\pi} [(N_w)_0 \cos\theta][r_0 \cos\theta] Rd\theta ds$$

$$\therefore \quad d(V.W.) = \{\overset{*}{\delta}\}^T (N_w)_0 r_0 \pi ds,$$

where the following short-hand was used to represent the above displacements and to incorporate eqns. 3.1 and 4.3, namely,

$$w(\xi) = [N_w]\{\delta\}$$

or

$$w(\xi) = [(N_w)_0 \cos\theta]\{\delta\} \quad .$$

The expressions for u and v-displacements would have a similar appearance. As a slight extension of the loading discussed above, let the pressure $p=p_0\cos\theta$ be the external load acting along the normal of the infinitesimal truncated cone. This can be resolved into the following global components shown in Fig. 4.3(a) and (b),

$$z = -p \sin\alpha$$

$$r = p \cos\alpha,$$

where

$$z = z_0 \cos\theta$$

$$r = r_0 \cos\theta$$

The elemental Virtual Work done round the circumference (Fig.4.3(c)) can be found as follows,

$$d(V.W.) = \{\overset{*}{\delta}\}^T \int_0^{2\pi} (N_u[-zRd\theta ds] + N_w[rRd\theta ds])$$

$$= \{\overset{*}{\delta}\}^T \left(\int_0^{2\pi} [(-p_0 \sin\alpha . \cos\theta)((N_u)_0 \cos\theta) + (p_0 \cos\alpha . \cos\theta)((N_w)_0 \cos\theta)] Rd\theta \right) ds$$

$$d(V.W.) = \{\overset{*}{\delta}\}^T p_0 [(N_w)_0 \cos\alpha - (N_u)_0 \sin\alpha] R\pi ds \qquad \ldots\ldots \text{ eqn. 4.14}$$

The Virtual Work done by gravity loads is dealt with in an identical manner. Assume an upward, uniform, radial gravity field of intensity g_R to act upon the elemental cone shown in Fig. 4.4(a) and (b). The elemental force dF along the R-axis is thus,

$$dF = g_R[\rho t(Rd\theta ds)] .$$

This force is resolved normal to and along the shell circumference at an angle θ. The Virtual Work done by the infinitesimal cone is then obtained by adding the individual components, namely,

$$d(V.W.) = \{\overset{*}{\delta}\}^T \int_0^{2\pi} [(g_R . Rd\theta \rho t)\cos\theta (Nw)_0 -$$

$$(g_R \cdot Rd\theta \rho t)\sin\theta (N_v)_0] ds$$

$$\therefore \quad d(V.W.) = \{\overset{*}{\delta}\}^T g_R . R\rho t[(N_w)_0 - (N_v)_0]\pi ds. \qquad \ldots\ldots \text{ eqn. 4.15}$$

The last loading case regarding the first harmonic, concerns the concentrated moment M which acts about an axis normal to both Z and R axes. This loading presents an interesting case, since the moment can effectively be applied by two different methods.

(i) by applying a total moment of M given by

$$M = \int_0^{2\pi} (M_0 \cos\theta) . \cos\theta Rd\theta = m_0 R\pi \qquad \ldots\ldots \text{ eqn. 4.16(a)}$$

or

(ii) by applying a couple caused by the forces in the direction of Z-axis, i.e. $z = z_0 \cos\theta$ which results in,

$$M' = \int_0^{2\pi} (z_0 \cos\theta) R d\theta . (R\cos\theta) = z_0 R^2 \pi . \qquad \ldots\ldots \text{ eqn. } 4.16(b)$$

The Virtual Work contribution of moments M and M' is numerically equal to expressions 4.16(a) and (b) respectively, since they do work by rotating through a unit angle at the node.

b) Distributed pressures generally encountered in the n-th harmonic, resulting from the usual expansion of the Fourier components.

When formulating class b) forces, only the normal pressures were thought worth considering. The external Virtual Work done was then written down in a like manner to the case given earlier,

$$d(V.W.) = \{\overset{*}{\delta}\}^T \Big(\int_0^2 \Big[((N_u)_0 \cos n\theta)(-p_0 \cos n\theta \sin\alpha) + ((N_w)_0 \cos n\theta)(p_0 \cos n\theta \cos\alpha) \Big] R d\theta \Big) ds,$$

$$\therefore \quad d(V.W.) = \{\overset{*}{\delta}\}^T R\pi \left[(N_w)_0 \cos\alpha - (N_u)_0 \sin\alpha \right] p_0$$

Despite the difference in the harmonic terms, this result is identical to eqn. 4.14.

c) Concentrated forces acting at the common node between two or more elements or acting at the free extremity of an element.

The forces arising from class c)-type loading when integrated circumferentially, exhibit identical form to the results of eqn. 4.16(a) and (b) above, since for all integer, positive values of j,

$$\int_0^{2\pi} \cos^2(j\theta) d\theta = \pi .$$

d) Concentrated loads causing torsional stresses.

The calculation of the external loads, especially using energy formulation deserves some attention[+]. The following analysis (although apparently irrelevant) is intended to clarify the situation.

Consider first the Virtual Work involved in compressing a thin vertical cylinder whose radius, length and thickness are R, L, and t respectively. If the cylinder displaces elastically by an amount u* under the ring load P_z, as shown in Fig. 4.5, the resulting external Virtual work done is given by,

$$(V.W.)_{ext.} = u^*(p_z.2\pi R) = u^*P_z$$

The internal Virtual Work is calculated in the normal manner as,

$$(V.W.)_{int} = \int_A \varepsilon^*_s \, T_s \, dA$$

$$= \left[\left(\frac{u^*}{L}\right)\left(Et.\frac{u}{L}\right)2\pi RL\right]$$

$$(V.W.)_{int} = u^* \, . \, \frac{2\pi RtE.u}{L}$$

Equating the two work equations

$$u^*p_z.2\pi R = u^*.\frac{2\pi Rt.E.u}{L} \qquad \ldots\ldots \text{ eqn. 4.17}$$

Now consider the same cylinder in torsion due to a twisting force P_θ, with the axis of the cylinder now horizontal as shown in Figure 4.6. Further assume that this force P_θ is due to edge shears p_θ.

+ It was observed that the magnitudes of the shear stresses obtained were double the expected values. After some consultations, Mr. Bruce Irons pointed out that the apparent inconsistency was due to miscalculation of the Work term for the applied torsional loads.

The Virtual Work expression is then,

$$(V.W.)_{ext.} = \int_0^{2\pi} (v^* \sin\theta).\left[(p_\theta \sin\theta) R d\theta\right]$$

$$(V.W.)_{ext.} = v^* p_\theta R\pi$$

Similarly the Virtual Work done internally is calculated as,

$$(V.W.)_{int} = \int_A \varepsilon^*_{s\theta} T_{s\theta} dA$$

$$= \left[\left(\frac{v^*}{L}\right)\left(Gt\frac{v}{L}\right)2\pi RL\right]$$

$$(V.W.)_{int} = v^* \frac{2\pi RtG.v}{L}$$

Equating these energies,

$$v^* p_\theta R\pi = v^* . \frac{2\pi RtG.v}{L} \qquad \ldots\ldots \text{ eqn. 4.18}$$

Comparing equations 4.17 and 4.18, it can be seen that term by term the external work done in torsion is half that normally required in cases where n=0. Thus for the same value of nodal displacement v(i.e. unity), only one half of the nodal force P_θ (= $2\pi R p_\theta$) need be assembled.

4.6 SOME PRACTICAL AND PROGRAMMING DETAILS

4.6.1 Integration

By extending the axisymmetric program it was meant that any individual case of axisymmetric or asymmetric problem could be solved on the same suite of programs. This meant that when integrating with respect to θ(along the circumference), the weighting (integrating) constant W_G had to be modified from a factor of 2π when n=0 to a factor of π when $n \geq 1$ which was an obvious use of eqns. 4.7. The integration with respect to volume $\int(\ldots)dv$, then reduced to,

v

$$\left.\begin{aligned} \int_V (\ldots)dv &= 2\pi \int_S (\ldots)t_\xi ds, \\ \int_V (\ldots)dv &= 2\pi \int_{-1}^{+1} (\ldots)t_\xi \frac{ds}{d\xi}\, d\xi\ , \end{aligned}\right\} \quad \text{for } n = 0,$$

and

$$\left.\begin{aligned} \int_V (\ldots)dv &= \pi \int_S (\ldots)t_\xi ds, \\ \int_V (\ldots)dv &= \pi \int_{-1}^{+1} (\ldots)t_\xi \frac{ds}{d\xi}\, d\xi \end{aligned}\right\} \quad \text{for } n \geqslant 1.$$

Gaussian Quadrature was used throughout, the process further simplified to,

$$\int_V (\ldots)dv = 2\pi \sum_{i=1}^{m} (\ldots)t_i \left(\frac{ds}{d\xi}\right)_i W_i \qquad \text{for } n = 0,$$

..... eqn. 4.19

and

$$\int_V (\ldots)dv = \pi \sum_{i=1}^{m} (\ldots)t_i \left(\frac{ds}{d\xi}\right)_i W_i \qquad \text{for } n \geqslant 1.$$

Numerical integration was explained at some length in Chapter 3 and the last of the eqn. 4.19 is only an indication of extension to the asymmetric case.

4.6.2 The Nodal Variable v

The displacement field due to the nodal variable v is similar to the fields obtained using u and w displacements which were discussed in Chapter 3, namely it is expressed in terms of ξ (the parameter in the Parent element) and consequently a function of s (the distance along the generator). It again consists of the two types of displacements available, i.e. the Basic (globally directed) and the Surplus (locally and globally directed) with optional number of

displacements. Figures 4.7(a) and (b) attempt to give a visual indication of the two types of displacements. All displacements along the θ-axis have the peculiar dual property of fulfilling a globally directed and a locally directed role which subsequently require no further reorientation. Again the basic displacements B1 and B3 ensure that continuity is maintained in the v-field at the junction of two or more elements, whereas the surplus functions improve the internal field variation. The Basic functions B1 and B3 being of unit nodal value are trouble free and need no adjustment due to variation of slopes when stretched. The functions B2 and B4 become trouble free for a different reason. Since the functions B2 and B4 indicate a rate of inplane stretch of v-displacement with respect to the generator "s", i.e. $(\frac{\partial v}{\partial s})$, they behave in a Surplus capacity, and no longer influence the inter-element displacement field which relieves the programmer of the task of normalising the above functions. (A similar point to this is covered in Chapter 3 regarding $\frac{\partial u}{\partial s}$ for functions B2 and B4).

4.6.3 The Modification of the Matrix [B]

The choice of the v-displacements discussed above presents a new difficulty when dealing with relationships such as eqn. 4.15, since the same shape functions at the point ξ are used for u, w and v-displacements. This implies that the value of $\left[(N_w)_0 - (N_v)_0\right]$ is numerically zero at every Gauss-point, and the elemental contribution to the external work done $g_R.R\rho t\left[(N_w)_0 - (N_v)_0\right]$ vanishes entirely during quadrature. This problem was overcome through a suggestion by Irons [8] that the difference (w_0-v_0) should be made non-trivial, e.g. equal to unity by choosing a suitable variable, say of w_0^+. Hence it was proposed to examine u_0, w_0 and $(v_0+w_0^+)$ displacement fields as a possible replacement for u_0, w_0 and v_0 displacements. To study the implication of this, the

general {strain, curvature}/displacement relationship is written down,

$$\varepsilon_i = \left[B_{ui}, B_{wi}, B_{vi}\right] \cdot \begin{Bmatrix} u \\ w \\ v+w^+ \end{Bmatrix}$$

$$= B_{ui}.u + B_{wi}.w + B_{vi}.(v+w^+)$$

$$= B_{ui}.u + (B_{wi}+B^+_{vi}).w + B_{vi}.v$$

$$\therefore \quad \varepsilon_i = \left[B_{ui}, B_{wi} + B^+_{vi}, B_{vi} \right] \cdot \begin{Bmatrix} u \\ w \\ v \end{Bmatrix} \qquad \ldots\ldots \text{ eqn. 4.20}$$

As can be seen the only adjustment required is that the $[B]$ matrix is augmented which involves a single column. For example consider the mid-surface shear given by eqn. 4.10,

$$\varepsilon_{s\theta} = \left[(-\frac{n}{R})\cos\alpha \;\vdots\; (-\frac{n}{R})\sin\alpha \;\vdots\; -\frac{\sin\alpha}{R} + \frac{\partial}{\partial s} \right] . \sin n\theta \begin{Bmatrix} u_0 \\ w_0 \\ v_0 \end{Bmatrix} ,$$

now when the augmentation of eqn. 4.20 becomes effective, $\varepsilon_{s\theta}$ then appears as,

$$\varepsilon_{s\theta} = \left[(-\frac{n}{R})\cos\alpha \;\vdots\; (-\frac{n}{R})\sin\alpha + (-\frac{\sin\alpha}{R} + \frac{\partial}{\partial s})^+ \;\vdots\; \frac{-\sin\alpha}{R} + \frac{\partial}{\partial s} \right] . \sin n\theta \begin{Bmatrix} u_0 \\ w_0 \\ v_0 \end{Bmatrix}$$

as can be seen the term $(-\frac{\sin\alpha}{R} + \frac{\partial}{\partial s})^+$ is the modification. The overall stiffness matrix $[K]^+$ obtained using the above method, is not the physical stiffness matrix $[K]$ but is a matrix into which a certain amount of numerical expedience is built. When the general matrix handling e.g. assembly and solution is completed, then the stresses obtained using the expression $\{T\} = [D][B]^+\{\delta\}$ of eqn. 4.13 are the genuine physical stresses, an appropriate correction having been made. Fig. 4.8 illustrates the stress resultants (also see Section 4.4). Since the gravity loads g_R along the R-axis are mainly responsible for the above

condition, the problem of trivial differences becomes critical for the first harmonic only.

4.6.4 The Choice of Displacements

It can be recalled that in the axisymmetric case, the in-plane displacements represented the axial loading condition and the transverse displacements contributed to bending. There appears to be a certain reversal of roles in the first harmonic, since the u-displacements - being stretched for one half and compressed for the other - represent bending and in contrast w and v-displacements ensure the freedom of deformation along the R-axis which is generally of the rigid body nature. Thus the choice and inclusion of the Surplus displacements for w and v must be simultaneous whereas the u-displacements could be reduced or increased according to the discretion of the engineer.

In dealing with harmonics $n > 1$, the considerations are more involved and each problem should be examined separately. The w and v-displacements in this case become more independent, with u and w-displacements contributing mostly to the Strain Energy in bending.

When torsion problems are considered n is set to zero and both u and w displacements are excluded, giving four Basic functions B1 to B4 with an optional number of Surplus functions, see Fig. 3.12 and Fig. 4.7.

4.7 SOME FUNDAMENTAL TESTS

The Finite Element method of analysis has been the subject of many discussions regarding its validity and reliability. In the past, certain methods which apparently gave a solution failed after further tests and sometimes with methods that proved workable consistently, no evidence of their validity was found. It is not within the scope of this work to attempt to provide proofs or postulate principles regarding the

mathematical legality of the technique but when the method is applied to Shells of Revolution, using the Isoparametric Element, there are certain areas of interest to confirm one's confidence in using the method and the Element. Two tests were considered to examine the behaviour of the Isoparametric Element; these tests will follow the discussions and the views presented. This part of the work appears to be most suitably dealt with in this section, since there are some discussions on Rigid Body Motions which involve u,w,v and $\frac{\partial w}{\partial s}$ degrees of freedom that are covered in this Chapter.

4.7.1 The Theorems Concerning the Isoparametric Element

It had been observed for some time that the Isoparametric Element appeared to have certain desirable properties apart from being one of the best suited for quadrature. These observations were formulated into lemmas by Irons[9]. The following are the simplified versions as applied to thin Shells of Revolution with a linear Parent Element. There is a slight difference in the order of presentation with the Theorems given in Chapter 8 of ref. (7).

1. Theorem - Isoparametric Elements always allow linear variations that are zero at the origin in Z and R coordinates. In terms of plane strain when nodal deflections such as $u_i = aZ_i + bR_i$ are imposed then the internal point (Z,R) experiences a deflection of $u = aZ + bR$.

For if (by definition, see Chapter 3), $Z = \Sigma N_i Z_i, R = \Sigma N_i R_i$ and $u = \Sigma N_i u_i$, then

$$\begin{aligned} u &= \Sigma N_i u_i \quad \text{(as above)} \\ &= \Sigma N_i (aZ_i + bR_i) \\ &= a\Sigma N_i Z_i + b\Sigma N_i R_i \\ \therefore \quad u &= aZ + bR \end{aligned}$$

Similarly $w = cZ+dR$ is also available. This property does not depend on Ni.

2. Theorem - If the Parent Element allows Rigid Body Translations, so does the Isoparametric Element.

With ordinary nodes when u_i = constant = k, it gives u=k at every other point and thus $k = \Sigma N_i k$ with $\Sigma N_i = 1$ everwhere and at hierarchical nodes $u_i = 0$, so that $\Sigma N_i = 1$ excludes such nodes. Thus if $u = \Sigma N_i u_i$ is constant for the Parent Element, then the same constant translation is obtained for the Isoparametric Element. This can also be extended for torsional Rigid Body Motions both for straight and curved Elements; since,

$$\begin{aligned} v &= \Sigma v_i N_i \\ &= \Sigma \theta R_i N_i \\ &= \theta \Sigma R_i N_i \end{aligned}$$

$$\therefore \quad v = \theta R,$$

so if a Rigid Body Rotation of θ is imposed, the torsional Rigid Body Motions become possible.

3. Theorem - The Isoparametric Element can reproduce any constant strain over the element.

Since at ordinary nodes $u_i = a + bZ_i + cR_i$ and the value of u elsewhere is $u = a + bZ + cR$. With special value of u_i the property also extends to hierarchical nodes.

4. Theorem - The Parent Elements are assumed to be straight so by suitable translation, rotation and perhaps linear stretching Parent Elements can be brought into contact at a node. If the Parent Elements then conform to any nodal displacement, i.e. no separation or overlapping takes place, then Isoparametric Elements conform before and after deformation.

It follows that N_i for nodes not at the junction is zero. This is clearly a one-dimensional simplification of a more generalised statement.

5. Consider the Parent Element and N_i at a particular node, it is possible to:-

a) choose internal points as if two or more elements were replacing the original larger element which would generally generate more nodes than the original element,

b) regard N_i as defining a new response on the subassembly,

c) provide the total response due to N_i in terms of the internal subelement nodes N_j for each subelement,

d) reproduce sometimes, the response due to N_i exactly by a suitable arrangement of the subelements. Melosh[10] argument can be stated as follows[9],

"a structure of large elements responds to loads with a certain total strain energy, and when any element is subdivided the original response remains available so that the total strain energy cannot increase. In this sense, convergence is monotonic when the mesh is refined".

Theorem - If Melosh subdivision (ref. (9) above) were to be performed on the parent element, the corresponding subdivision in the Isoparametric element also gives monotonic convergence.

The above is justified since the assembly of Isoparametric elements may be regarded as a single enlarged Isoparametric element.

6. Numerical integration has already been discussed (see sections 3.4 and 4.6) and the conversion formula for a functional ϕ was given by,

$$\int_{-1}^{+1} \phi_\xi \frac{ds}{d\xi}\, d\xi = \sum_{i=1}^{m} \phi(\xi_i) W_i \left(\frac{ds}{d\xi}\right)_i .$$

Theorem - If a rule is selected to integrate accurately the area of the Isoparametric Element for arbitrary coordinates (Z_i, R_i) a fine "string" of Isoparametric Elements will converge.

Since, for a fine string of elements, the stress variation will be small over any element, the variation over the Isoparametric Elements should also be small. Using Virtual Work it is possible to calculate the force F_i corresponding to u_i for a unit stress of say $\sigma_s = 1$,

$$F_i = \frac{\partial}{\partial u_i} \int (\sigma_s : \varepsilon_s)\, dA$$

$$= \int \left(1 . \frac{\partial \varepsilon_s}{\partial u_i}\right) dA$$

$$= \int \frac{\partial}{\partial u_i} \left[\frac{\partial}{\partial s} (N_i u_i) \right] . R\, d\theta\, ds$$

$$= \int \frac{\partial}{\partial u_i} \left[\frac{d(N_i u_i)}{d\xi} \cdot \frac{d\xi}{ds} \right] \cdot \left[R\, d\theta \right] \cdot \left(\frac{ds}{d\xi}\right) d\xi$$

$$= \int \left(\frac{dN_i}{d\xi}\right) . d\xi . R\, d\theta$$

$$\therefore \qquad F_i = \int \left(\frac{dN_i}{d\xi}\right) N_i\, d\xi (R_i\, d\theta),$$

where $N_i \left(\frac{dN_i}{d\xi}\right)$ is a polynomial containing ξ, this being integrable by the choice of integration rule. The force F_i obtained above is the influence on the neighbouring elements exerted by the Isoparametric Element. If the force F_i is nearly correct, the neighbours have no way of distinguishing between the approximately integrated element and a

perfectly integrated element. Thus if the perfect integration makes the problem converge, the approximate rule also guarantees convergence.

There is however a danger of making the integrating rule too approximate; it may lead to singularities in the stiffness matrix. It must be emphasised that these theorems are only modifications for the particular case of thin shell problems. For a more generalised approach the original paper should be consulted.

Within the elastic range, the existence of the above properties unfolds a whole range of possibilities for the Isoparametric Element upon which the future developments will be drawn. To examine the validity of some of the above statements all conceivable Rigid Body Motions were imposed individually and simultaneously where possible. The types of shells chosen in this case were a cylinder, a disc and a hemispherical shell. It was thought that any oddities due to geometry will be manifested as a result of the above choice of structures.

The case of bodily displacement along the Z-axis is a trivial one, it was exercised successfully using all three structures as was the case of bodily displacement along the R-axis. Translation along the R-axis by an amount "C" was achieved using the assignment $w_1 = -v_1 = C$ and $w_2 = -v_2 = C$, where suffices refer to the node numbers. Rotation was also carried out in the Z-R plane for all the above structures. Only "small" rotations are admissible, so that $\theta = \tan\theta = \sin\theta$. The difficult case was that of an R-axis translation together with a Z-R rotation which was achieved as follows. A structure was devised to contain a cylinder ABC and connected to a disc DCE, shown in Fig. 4.9. The point A was rigidly fixed and a uniformly distributed load with a circumferential variation of $p=p_0\cos\theta$ was applied transversely along AB, as the result of which the remaining part BC/DCE underwent a combined translation and rotation in the Z-R plane. In the last two

cases "n" was set to unity. The hemisphere also underwent this set of Rigid Body Motions successfully. The final test case was an arbitrary rotation ϕ about the Z-axis which consisted of setting n=0 and then specifying,

i) a displacement $v_1 = v_2 = R.\phi$ for a cylinder and

ii) a set of displacements $v_1 = R_1\phi$, $v_2 = R_2\phi$ to a thin truncated cone.

In both cases the Rigid Body Motions were achieved.

4.7.2 The Patch Test

As was discussed above, to prove the convergence in a Finite Element Solution, in the absence of a rigorously mathematical approach, other methods have been examined. Irons and Razzaque[11] provide the historical development of a numerical technique known as the PATCH-TEST as well as discussions on the practical applicability of the test upon which this section is heavily dependent. The original test was carried out on an assembly of plate bending elements with the structure subjected to pure bending. It was found out that providing a successful mesh was used even the non-conforming elements emulated their curvature and thus moment values. The experiment was successful for the conforming elements irrespective of the choice of the mesh. With the above experiments in mind the following statement could be quoted.

"... if the external nodes of any sub-assembly of a successful assembly of elements are given prescribed values corresponding to an arbitrary state of constant curvature, then the internal nodes must obediently take their correct values. (An internal node is defined as one completely surrounded by elements). Conversely, if two overlapping patches can reproduce any given state of constant curvature, they should combine into a larger successful patch, provided that every

external node lost is internal to one of the original patches, for such nodes are in equilibrium at their correct values, and should behave correctly as internal nodes of the extended patch".

It was decided to subject the Isoparametric Element to the patch test in tension (or compression), pure (in-plane) shear, pure bending and pure torque. The pure tension case is a trivial one and deserves no further comment except that the outcome was successful. In the pure shear experiment, Fig. 4.10, the chimney stack AB fixed at A was subjected to a transversely applied concentrated load in the form of a ring force given as $P_R = P_0\cos\theta$. The mid-surface shear $T_{S\theta}$ between BA improves dramatically by a further subdivision, shown in the same Figure. The pure bending case is another interesting experiment. The tube AB of Fig. 4.11 was subjected to constant bending in two distinct manners. When the moment was applied in the form of a varying in-plane force $P_z = P_0\cos\theta$ giving an effective moment of $M = P_0R^2\pi$, then the convergence is immediate and the displacements are correct even for one element representing the entire structure. When the moment M was applied directly at A, the correct displacements were obtained but for a considerable length of the tube, the in-plane stresses and moments were fluctuating. One's only reaction to this was that the fluctuations were due to an inadequate mesh size, and thus the size of the elements near the ends were decimated. Favourable results were then obtained as can be seen in Fig. 4.11(b) & (c) and the decay appears to be of the same order as the example 3.5.1(a) given in Chapter 3 for the axisymmetric case. The value of the meridional stress T_s soon converges to the steady state condition once the local anomalies due to the external loading are a short distance away. With the cylinder subjected to a pure torque the patch test is again successful as can be seen from Figs. 4.19 and 4.20. It is worth mentioning that in the pure tension and the pure torque cases, since the linear response required for

the strains $\varepsilon_s = \frac{\partial u}{\partial s}$ and $\varepsilon_{s\theta} = \frac{\partial v}{\partial s}$ were available the coefficients due to Surplus Functions corresponding to internal nodes were effectively zero (of the order 10^{-6} of the smallest displacement) which numerically verifies the statement quoted in the above section. The choice of non-cylindrical structures for the patch-test requires some attention. The only other geometrical representations tested were a disc and a hemispherical dome. The disc was subjected to a uniform edge moment M which automatically causes a constant meridional curvature and thus set $M_s = M$ throughout the plate. The hemispherical dome was roller supported and was subjected to internal pressure p; the meridional and hoop stresses both converged to a value of $T_s = T_\theta = \frac{pR}{2}$ for an adequate geometrical representation. Both of these examples are given in Chapter 3, Figs. 3.28 and 3.38. The only other test which was abandoned due to its triviality was the disc being subjected to an inplane tension (or compression) T, in this test again both stresses T_s and T_θ would have converged to a value of T. Finally a cylinder was subjected to hydrostatic pressure with the top end free and the other end roller supported. Although this is not a patch-test it shows the ability for linear response. The results are again shown in Fig. 3.38 of Chapter 3 and 1 element appears to respond satisfactorily.

4.8 EXAMPLES

It is now appropriate to indicate the ability of the element in dealing with different theoretical and practical problems. It must be admitted that the variety of the suitable examples were not as readily available as in the axisymmetric case. These examples have not been collected over a short period of time. Contact at various short courses with other co-workers has helped significantly.

4.8.1 Cylindrical Chimney Stack

The same cylinder had previously been subjected to Rigid Body Motions and patch-test in lateral shear, in-plane shear and edge moments. It was thought to impose a uniform lateral distributed load so as to verify if the linear shear T_S was available, the results are given in Fig. 4.12. The constant and linear response of the meridional stress resultant T_S, have been obtained from a pure moment and a concentrated edge force P, shown in Fig. 4.10, 4.11 and 4.9.

4.8.2 Cylinder with Harmonic edge moment

This example has been tried by various authors e.g. Ahmad[12]. The object is to compare the decay of the edge moment M and the lateral displacement w for different harmonics, n=0,2,...,20, see Fig. 4.13 and 4.14.

4.8.3 Asymmetrical Bending of Circular Plates

It was thought appropriate, to examine a linear geometry with a non-zero slope. The plate of Figure 4.15 was chosen which was subjected to a pressure $p = p_0 \frac{r}{R} \cos\theta$ and simply supported throughout. The relevant equations were taken from ref. (13). One element was chosen with a total of 12 degrees of freedom. The judgement of the outcome is left to the reader.

4.8.4 Natural Draught Cooling Tower

The analysis of cooling towers has been of some interest, before and after the recent disasters. Alternative means of estimating the various stresses and the energies involved have been proposed by some researchers. Albasiny and Martin[14] had used a total of 10 harmonics (n=0,...9) in order to simulate the pressure distribution circumferentially. The data used in this example is based on the above reference. Other workers have also adopted the same elastic and geometric particulars as

a basis of comparing the various axisymmetric shell elements, e.g. Ahmad[15] used 15 cubic elements whereas Chan and Firmin[16] had engaged 5 "SABA5" elements. In the present work also, 5 elements were used forming a total of 55 degrees of freedom which stretched the Polytechnic IBM 1130 (16K words) computer to its limit. The total computing time per harmonic was about 20 minutes. The final displacement and stress were obtained by summing the displacements and the stresses for each harmonic, punched on cards previously, as an output from the above mentioned analysis. It is fair to say that the results obtained from all the workers compare favourably. The meridional and circumferential variation of displacements, moments and stresses are shown in Figure 4.16(c), ... (g), whereas Figures 4.16(a) and (b) indicate the element arrangement and their circumferential pressure distribution respectively.

4.8.5 Hemisphere with Concentrated Diametral Moments

In the case of the Cooling Tower of the previous section a limited number of harmonics was used both by the functional and the numerical analysts and thus both analyses were comparable. In this example the theoretical solution resulting from the use of infinite series taken from Kraus[17] is compared with the numerical analysis of finite number of harmonics. The hemispherical shell shown in Fig. 4.17(a) with its centre at the origin, radius a and thickness t is subjected to a pair of diametral moments M_0. The points of application of the moments are at $\theta = 0^o$ and $\theta = 180^o$ on the great circle normal to the Z-axis. Upon harmonic analysis, only the even cosine terms are admissible, the super position of which shows the approximate value of the concentrated moment depicted in Figure 4.17(b). The shell itself is divided into 5 elements, the grading of which is signified in Figure 4.17(a). Firstly it was decided to use one surplus degree of

freedom for u, w and v for each of the elements. Then the edge values were slightly refined by re-distribution of surplus displacements so that elements 1 and 2 had no surplus functions whereas elements 4 and 5 had 2 sets of u, w and v surplus functions each. The total number of degrees of freedom again was limited to 55 owing to the size of the machine. Naturally, it is accepted that, the accuracy is dependant on the number of harmonics used but for the value of variables slightly away from the edge z=0, the ceiling of n=10 (a total of six harmonics) appears to be sufficient. It seems that the dependence of the overall convergence is more on the degrees of freedom of the mathematical model, than the simulation of correct loading.

4.8.6 Pinched Cylinder

At a locally held course, it was realised that the use of the pinched cylinder with those workers developing cylindrical elements was comparable to the repeated trials of the Albasiny and Martin Cooling Tower with the shells of revolution researchers. It was anticipated at this time that one could not expect dramatic results applying the shell of revolution to the above problem, since the former workers had the flexibility of refining the cylindrical panels near the concentrated load in both Z and θ directions, whereas the latter could only improve their subdivision along the Z-axis. Despite all the discouraging indications, two cylinders whose particulars are classified under the headings case (a) and case (b) were attempted. The first case which was presented by Professor Cantin[18] and Dr. Ashwell[19] emphasised the nature of convergence. The displacement w which was directly under the concentrated load was compared with the already available figures for two different values of thicknesses. The variation of w with the number of harmonics used is listed in Table (i). In the second case not only the displacement under the load is compared by other available values but the variation of

meridional and circumferential stress resultants are also provided by Edwards and Webster[20]. Only two harmonic limits of n=10 and n=20 are used with 4 equal elements, each consisting of 2 surplus u, v and w displacements. The outcome is not regarded as perfect but merely optimistic, see Fig. 4.18(b),(e). The results might have improved with a graded mesh. Symmetry was employed to save computer storage and time.

4.8.7 Torsion of Cylindrical and Conical Sections

These two sections were initially chosen so that the response of this element to rigid body motions about the Z-axis could be examined, see 4.7.2. The cylindrical shell proved to be more useful when experimenting with patch-test discussed in 4.7.2. The conical shell was tested by a pair of torques Q_1 and Q_2 applied in a manner shown by Figures 4.19 and 4.20. The variation of the shear stresses was found to be satisfactory but the displacement v along the circumference did not coincide with the elementary torsion theory ($\frac{Q}{J} = G.\frac{d\phi}{dZ}$) although the terminal values were almost exact.

4.8.8 Torsion of a thin spherical segment

In this example the response of the element to torsion having undergone a considerable curvature was being tested. Only one element subtending some 60^o was used with different surplus degrees of freedom being tried each time. The ratio of the shear stress $T_{s\theta}$ and the edge shear T was plotted against the azimuth angle ϕ. The outcome is plotted in Figure 4.21.

REFERENCES

1. V.V. NOVOZHILOV
"Theory of Shells", p. 120 and p. 306, P. Noordhoff Ltd., Netherlands 1964.

2. O.C. ZIENKIEWICZ
"The Finite Element Method in Engineering Science", p. 263, McGraw-Hill, England, 1971.

3. S. KLEIN
"A Study of the Matrix Displacement Method as Applied to Shells of Revolution", Wright-Patterson Air Force Base, December 1965.

4. S. AHMAD
"Curved Finite Elements in The Analysis of Solid, Shell and Plate Structures", University of Wales, Ph.D. Thesis, 1969.

5. A.S.L. CHAN, A. FIRMIN
"The Analysis of Cooling Towers by the Matrix Finite Element Method , Small Displacements", Part I, Jour. of Royal Aer. Soc., Vol. 74, October 1970.

6. V.V. NOVOZHILOV
"Theory of Shells", p. 23, P. Noordhoff Ltd., Netherlands 1964.

7. O.C. ZIENKIEWICZ
"The Finite Element Method in Engineering Science", p. 137, McGraw-Hill, England, 1971.

8. B.M. IRONS
Private communication.

9. B.M. IRONS
Civil Eng. Report (unidentified), Dept. of Civil Eng., University of Wales, Swansea.

10. R.J. MELOSH
"Basis for Derivation of Matrices for the Direct Stiffness Method", J.A.I.A.A., 2, 576, 1964.

11. B.M. IRONS, A. RAZZAQUE
"The Mathematical Foundations of the Finite Element Method with Applications to Partial Differential Equations", p. 557, 585, Academic Press, 1972, New York and London (Publication edited by A.K. Aziz).

12. S. AHMAD
"Curved Finite Elements in the Analysis of Solid Shell and Plate Structures", p. 142, Ph.D. Thesis, Univ. of Wales, Swansea, 1969.

13. S.P. TIMOSHENKO, S. WINOWSKY-KRIEGER
"Theory of Plates and Shells", p. 285, McGraw-Hill, New York, 1959.

14. E.L. ALBASINY, D.W. MARTIN
"Bending and Membrane equilibrium in Cooling Towers", Proc. Am. Soc. Civ. Eng., 93, EM3, 1-17, 1967.

15. S. AHMAD
"Curved Finite Elements in the Analysis of Solid Shell and Plate Structures", p. 143, Ph.D. Thesis, Univ. of Wales, Swansea, 1969.

16. A.S.L. CHAN, A. FIRMIN
"The Analysis of Cooling Towers by the Matrix Finite Element Method, Small Displacements", Part I, Jour. of Royal Roy. Soc. Vol. 74, Oct. 1970.

17. H. KRAUS
"Thin Elastic Shells", p. 253, John Wiley and Sons Ltd., New York, 1967.

18. G. CANTIN
"Rigid body motion and equilibrium in Finite Element Analysis", Conf. on Finite Elements for Thin Shells and Curved Members, Civil Eng. Dept., Univ. of Wales, Cardiff, 1974.

19. D.G. ASHWELL
"Strain Elements with applications to Arches, Rings and Cylindrical Shells", Conf. on Finite Elements for Thin Shells and Curved Members, Civil Eng. Dept., Univ. of Wales, Cardiff, 1974.

20. G. EDWARDS, J.J. WEBSTER
"Hybrid cylindrical shell elements", Conf. on Finite Elements for Thin Shells and Curved Members, Civil Eng. Dept., Univ. of Wales, Cardiff, 1974.

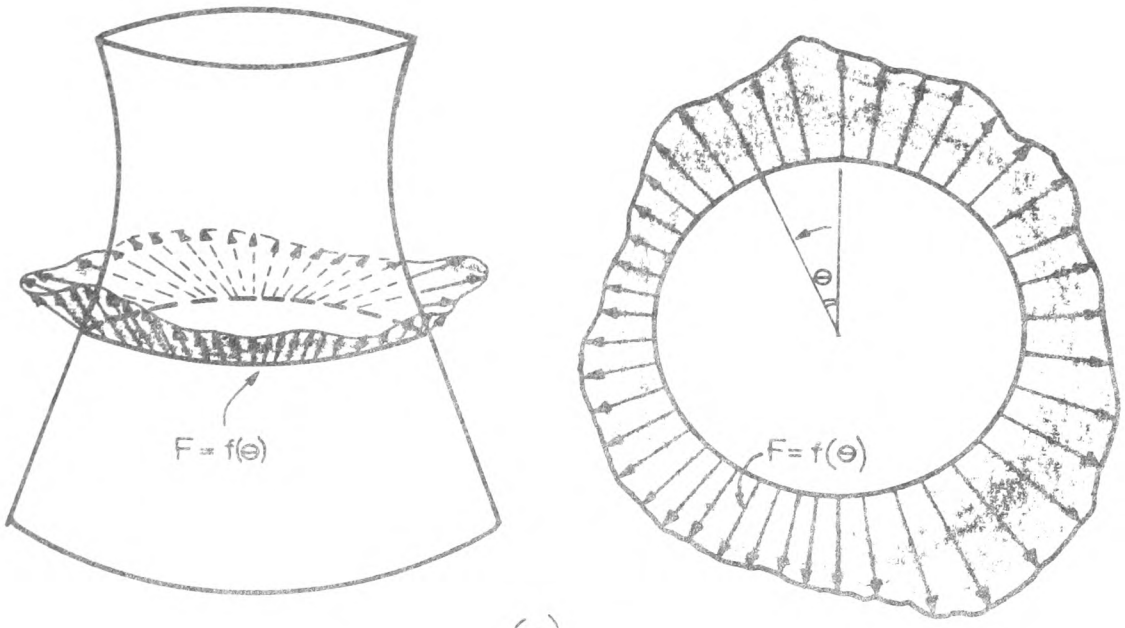

(a)

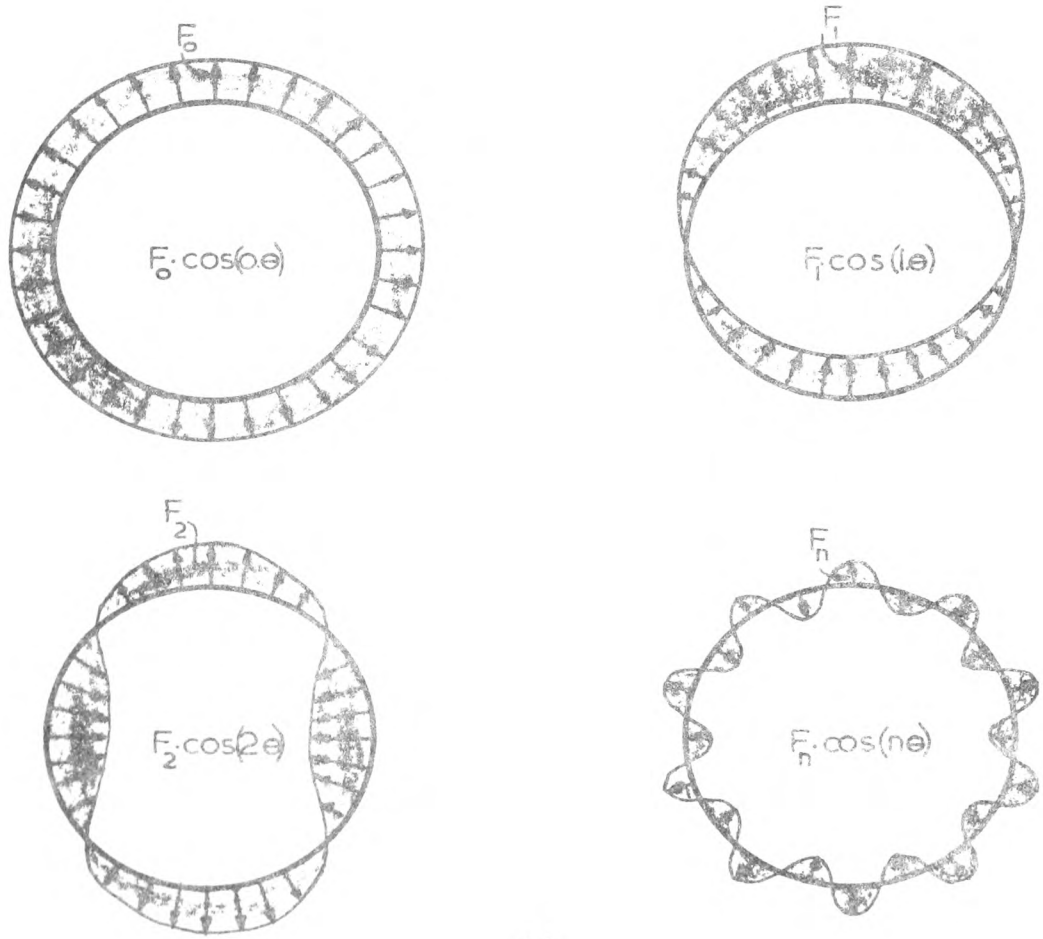

(b)

FIGURE 4.1

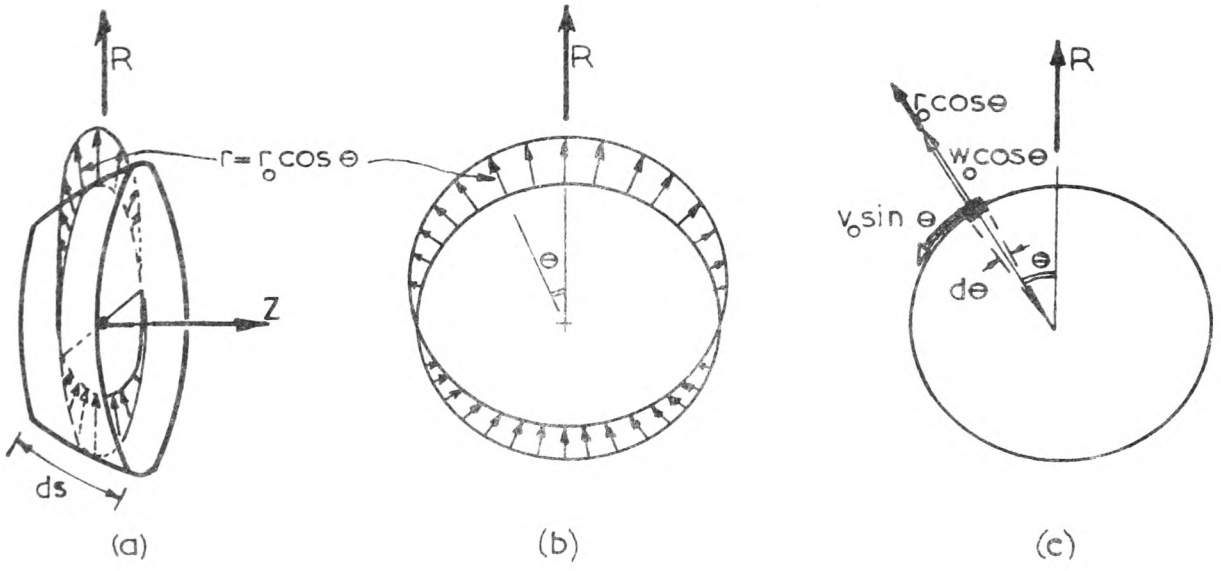

FIGURE 4.2

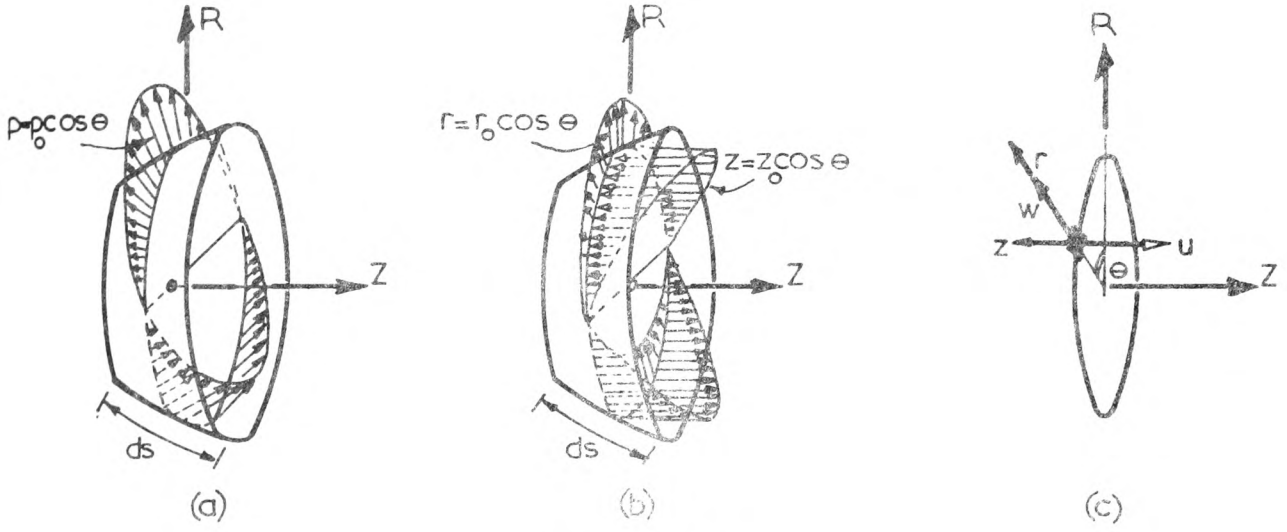

FIGURE 4.3

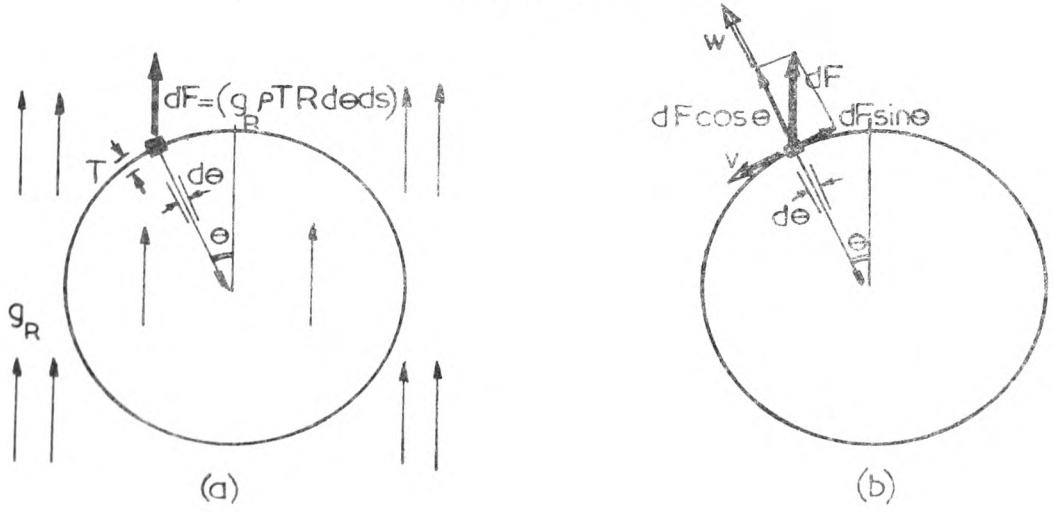

FIGURE 4.4

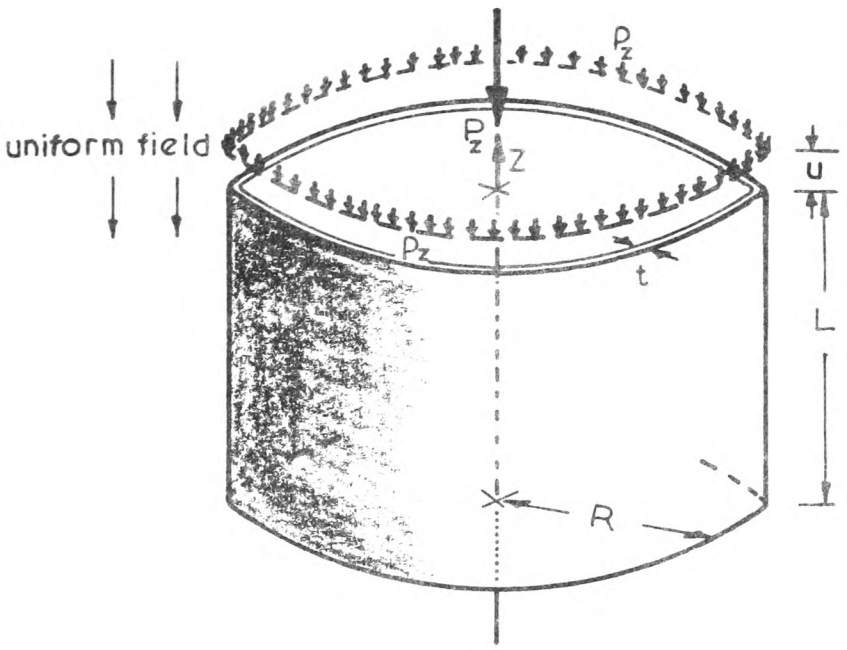

FIGURE 4.5

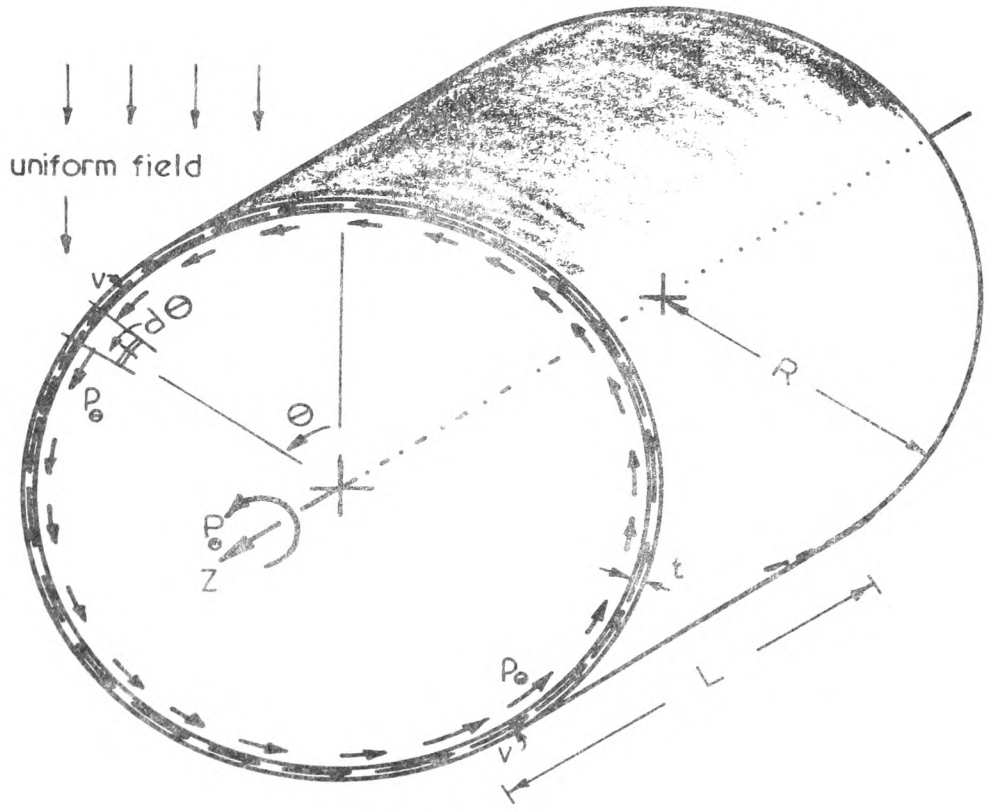

FIGURE 4.6

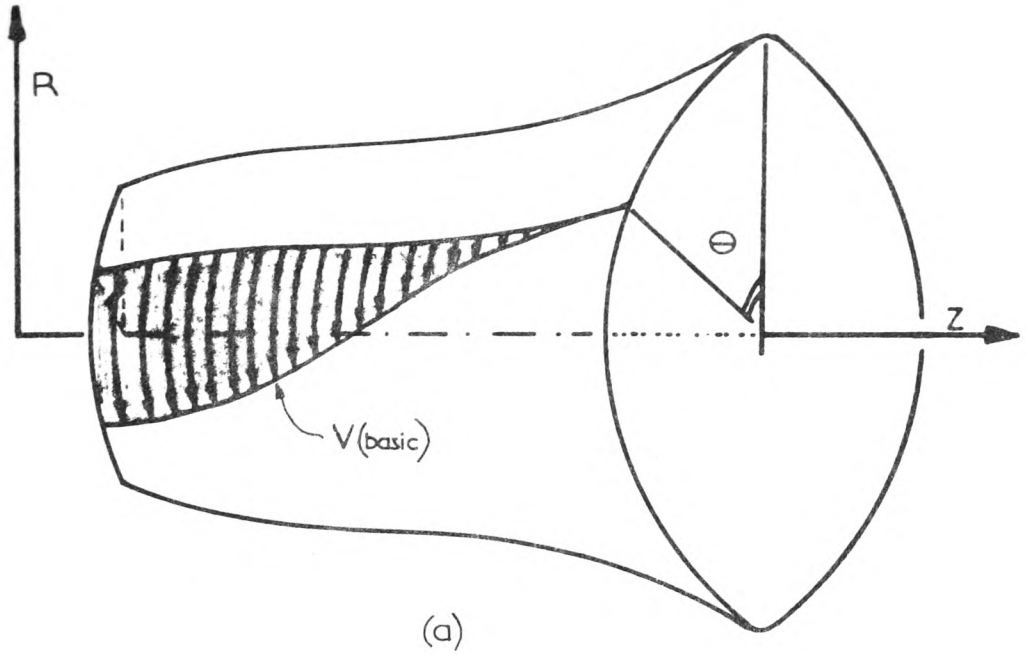

(a)

FIGURE 4.7

(b)

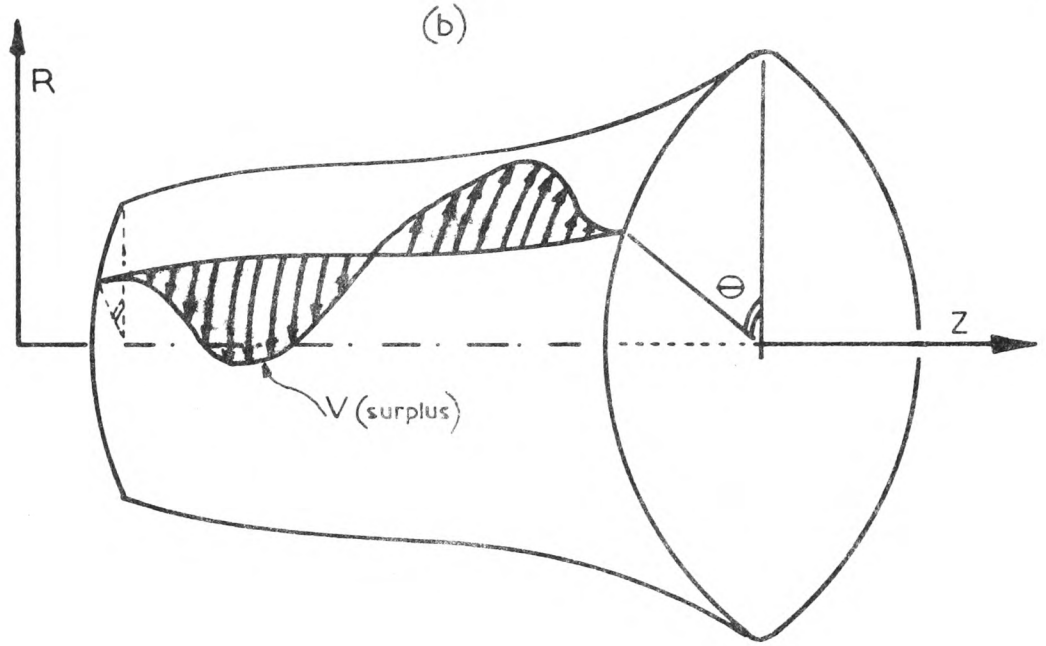

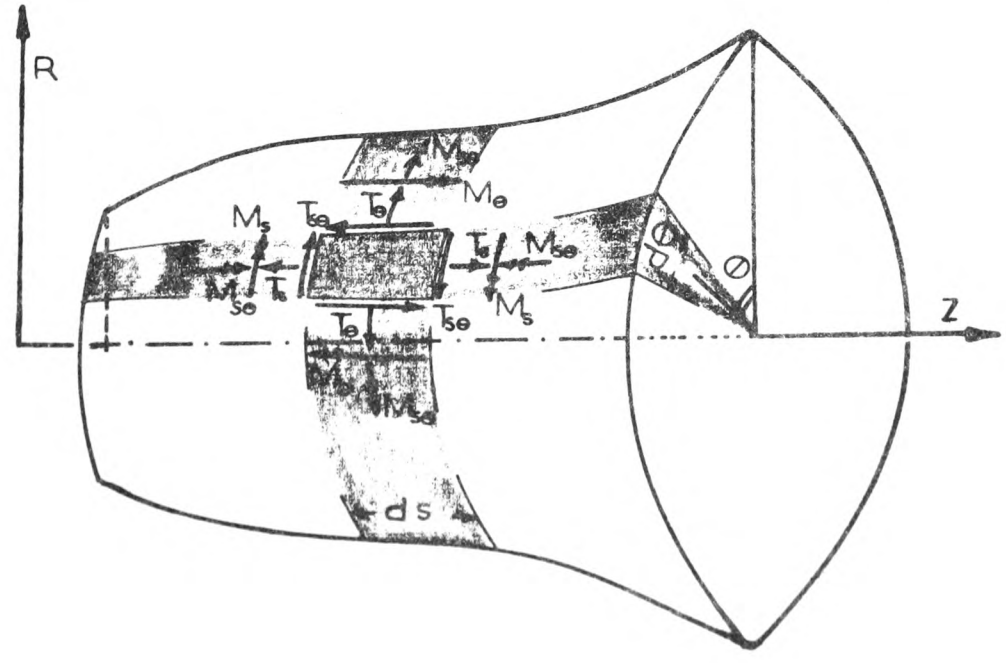

FIGURE 4.8

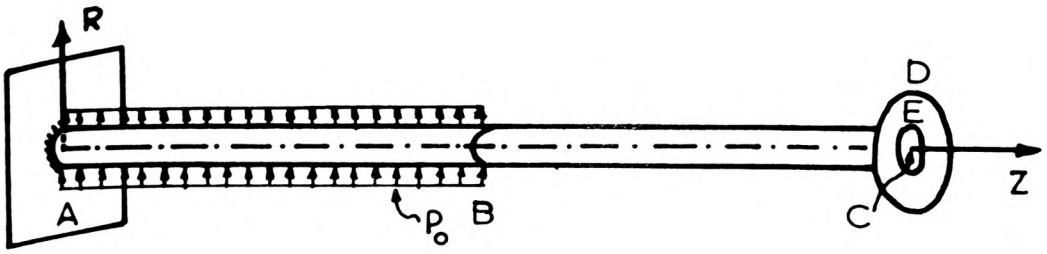

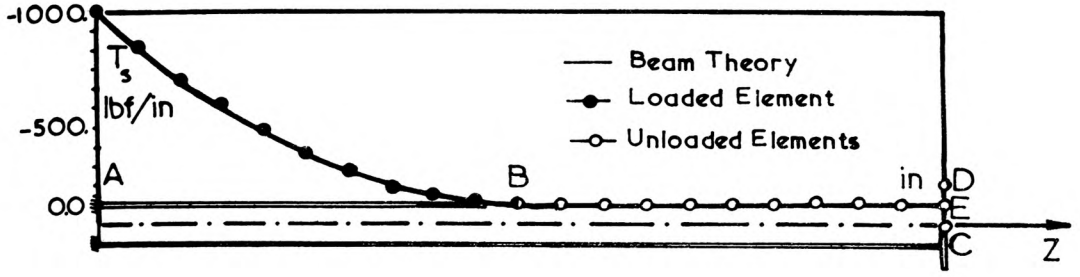

(a)

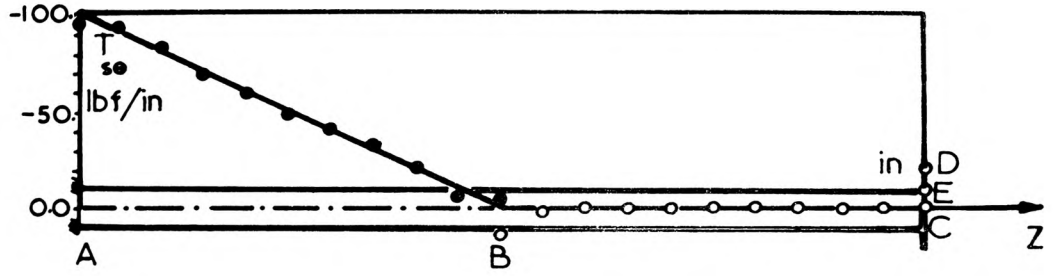

(b)

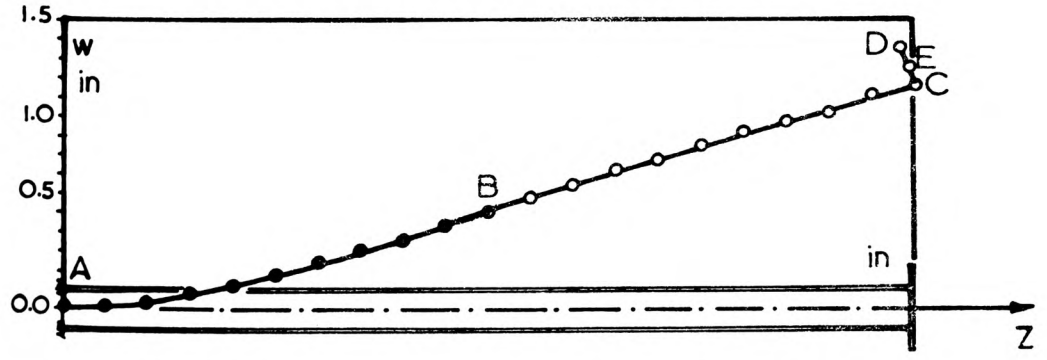

(c)

AB= BC= 100. in
E = 10 x10^6 lbf/in^2
G = 4 x10^6 lbf/in^2
ν = 25
t = 0.1 in

CE= ED= 5.0 in
E = 30 x10^6 lbf/in^2
G = 11.25x10^6 lbf/in^2
ν = 1/3
t = 0.1 in

p= 1.0 lbf/in^2

FIGURE 4.9

CHIMNEY STACK PROBLEM

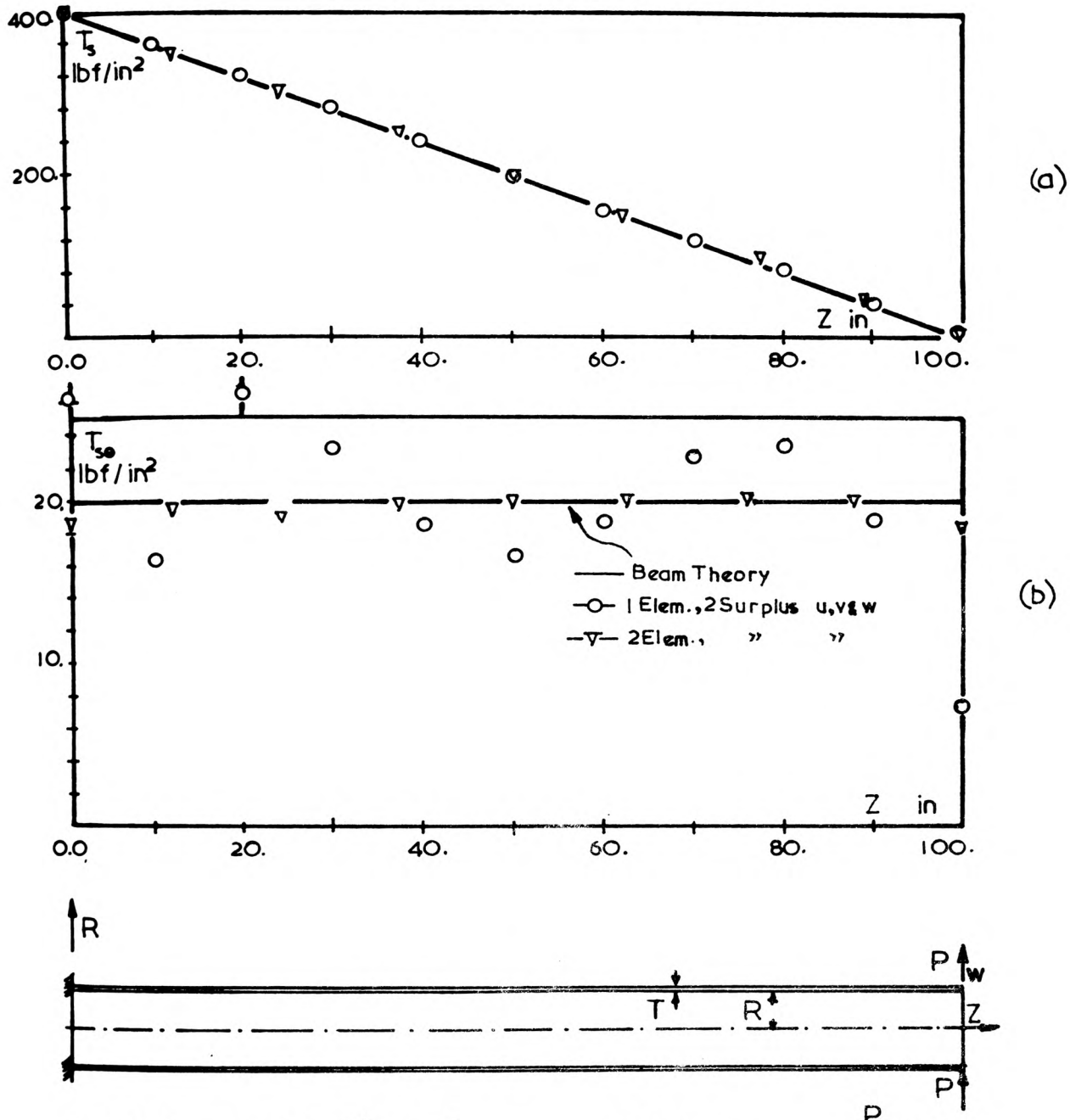

DISPL:	Beam Th.	1 Elem.	2 Elems.
$\frac{dw}{dz}$ rad	0.0040	0.00401	0.00425
W in	0.26667	0.26932	0.27109

TIP DISPLACEMENT

FIGURE 4.10

CIRCULAR BENDING OF LONG CYLINDERS

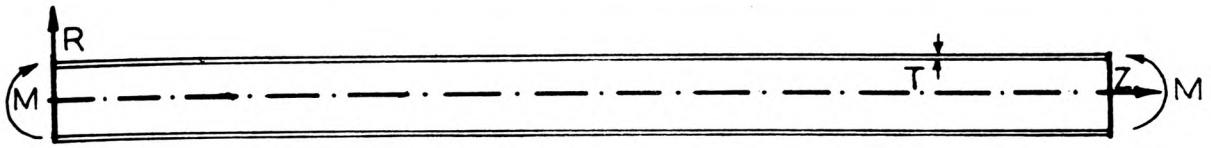

Z = 100.0 in
R = 5.0 in
T = 0.1 in

$E = 10 \times 10^6$ lbf/in^2
$G = 4 \times 10^6$ lbf/in^2
$\nu = 0.25$

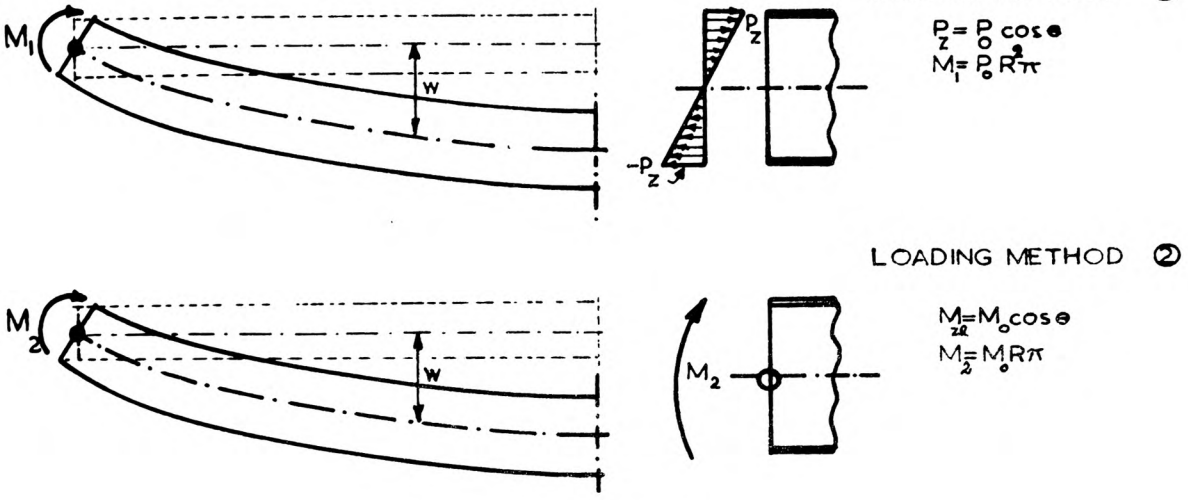

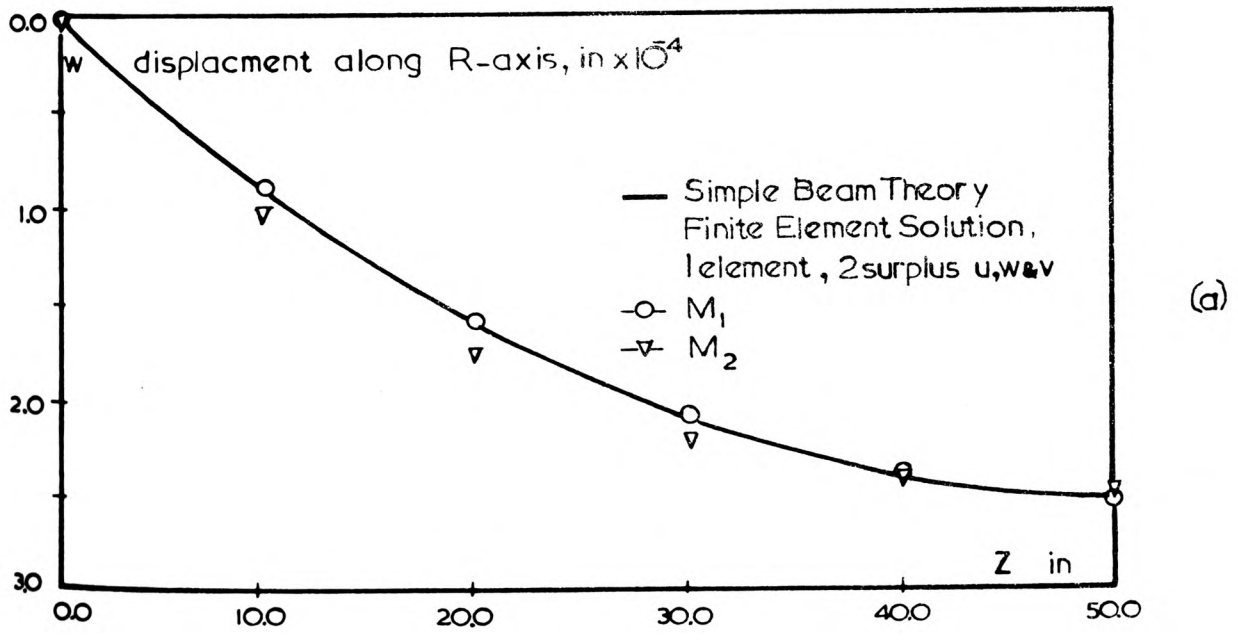

(a)

FIGURE 4.11

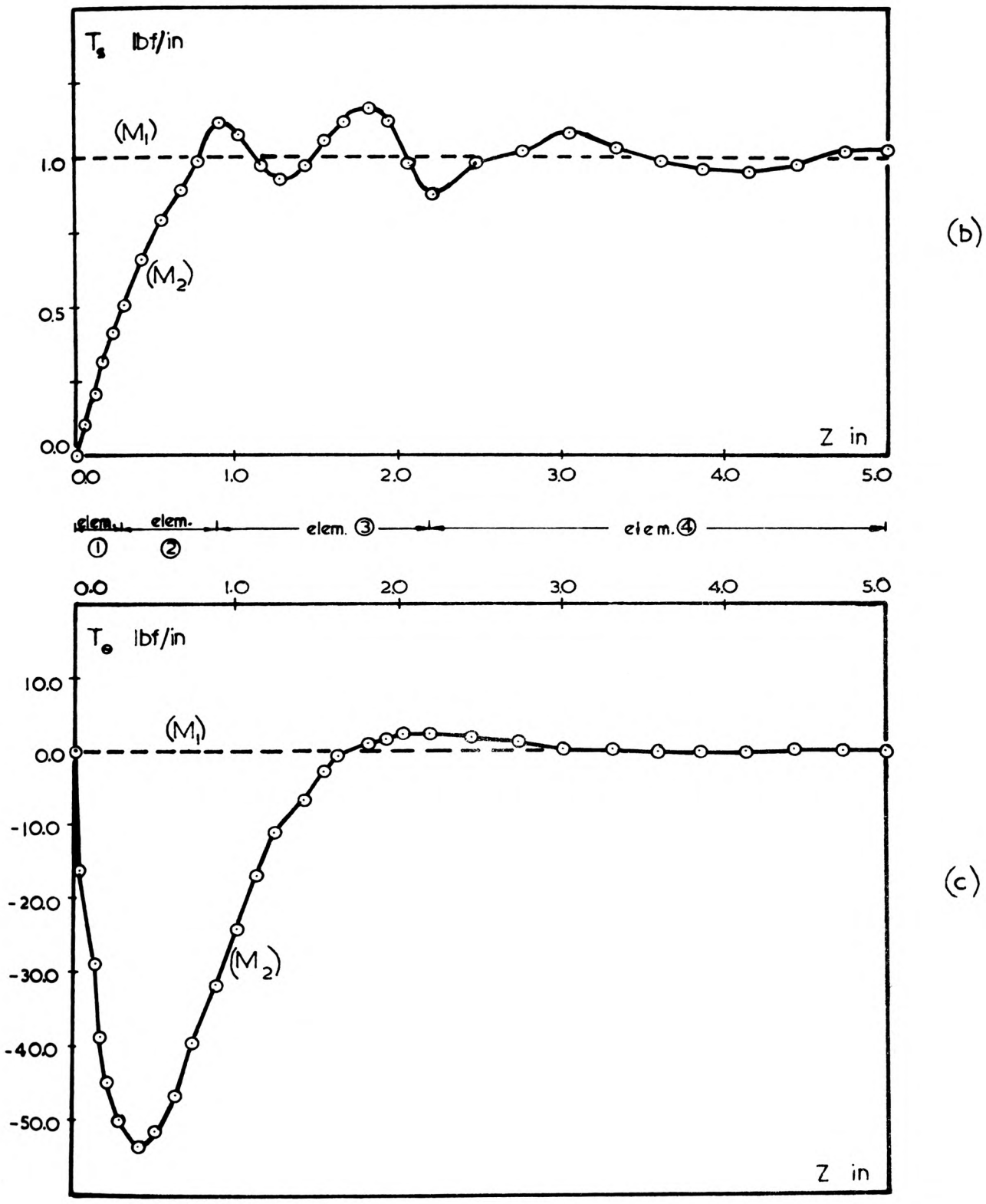

TOTAL OF 4 ELEMENTS,
INTERVALS SHOWN ABOVE,
2 SURPLUS u,w & v.

--- Theoretical (Simple beam) and when M_1 is applied

-⊙- Finite Element, when M_2 is applied

FIGURE 4·11

CHIMNEY STACK PROBLEM

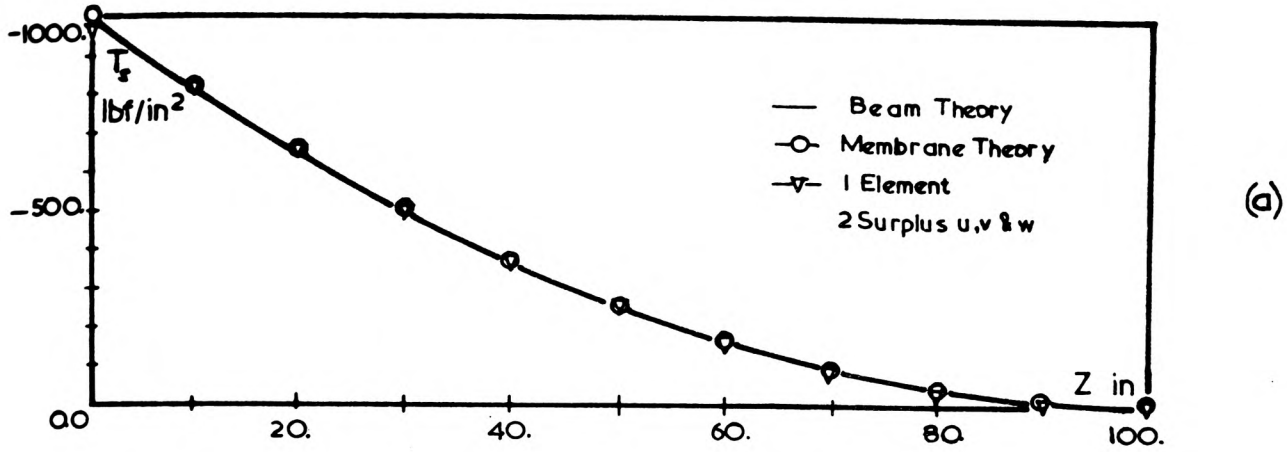

(a)

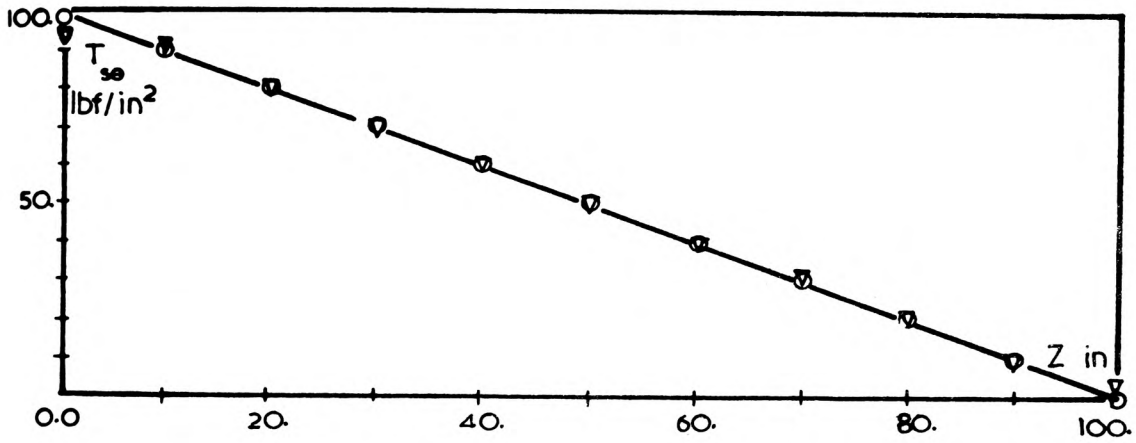

(b)

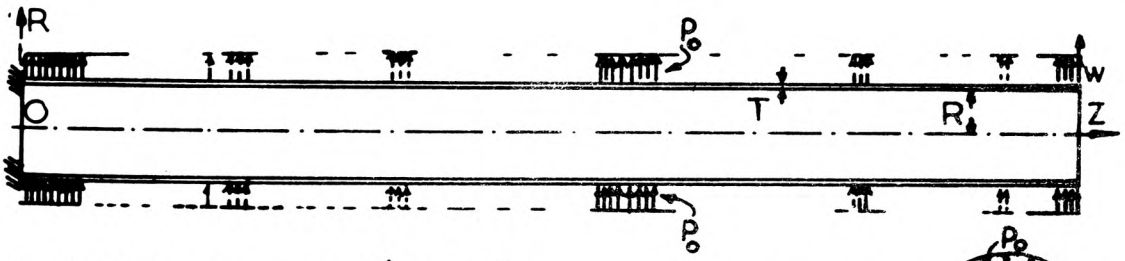

L = 100. in E = 10.×10⁶ lbf/in²
R = 5.0 in G = 4×10⁶ lbf/in²
t = 0.1 in ν = 0.25

$p = p_o \cos\theta$

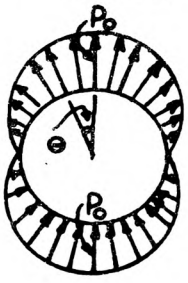

DISPL.	Beam Th.	Memb.Th.	F. Elem.
$\frac{\partial w}{\partial z}$ rad.	0.0067	.0066	.00657
W in	0.500	.5065	.5038

TIP DISPLACEMENTS

FIGURE 4.12

CYLINDER WITH HARMONIC EDGE MOMENT

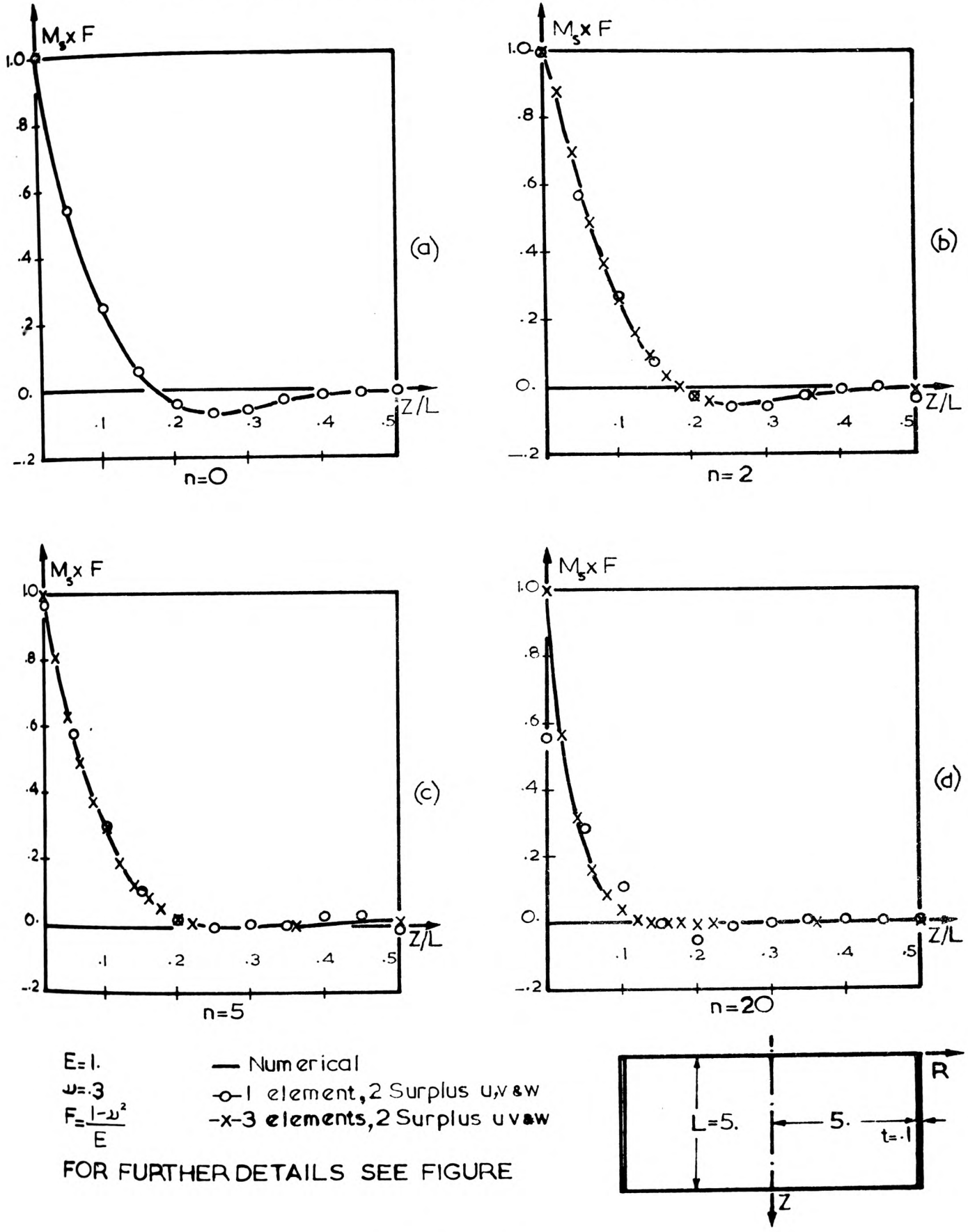

E=1.
ν=.3
$F=\frac{1-\nu^2}{E}$

— Numerical
-o- 1 element, 2 Surplus u,v & w
-x- 3 elements, 2 Surplus u v & w

FOR FURTHER DETAILS SEE FIGURE

FIGURE 4.13

CYLINDER WITH HARMONIC EDGE MOMENT

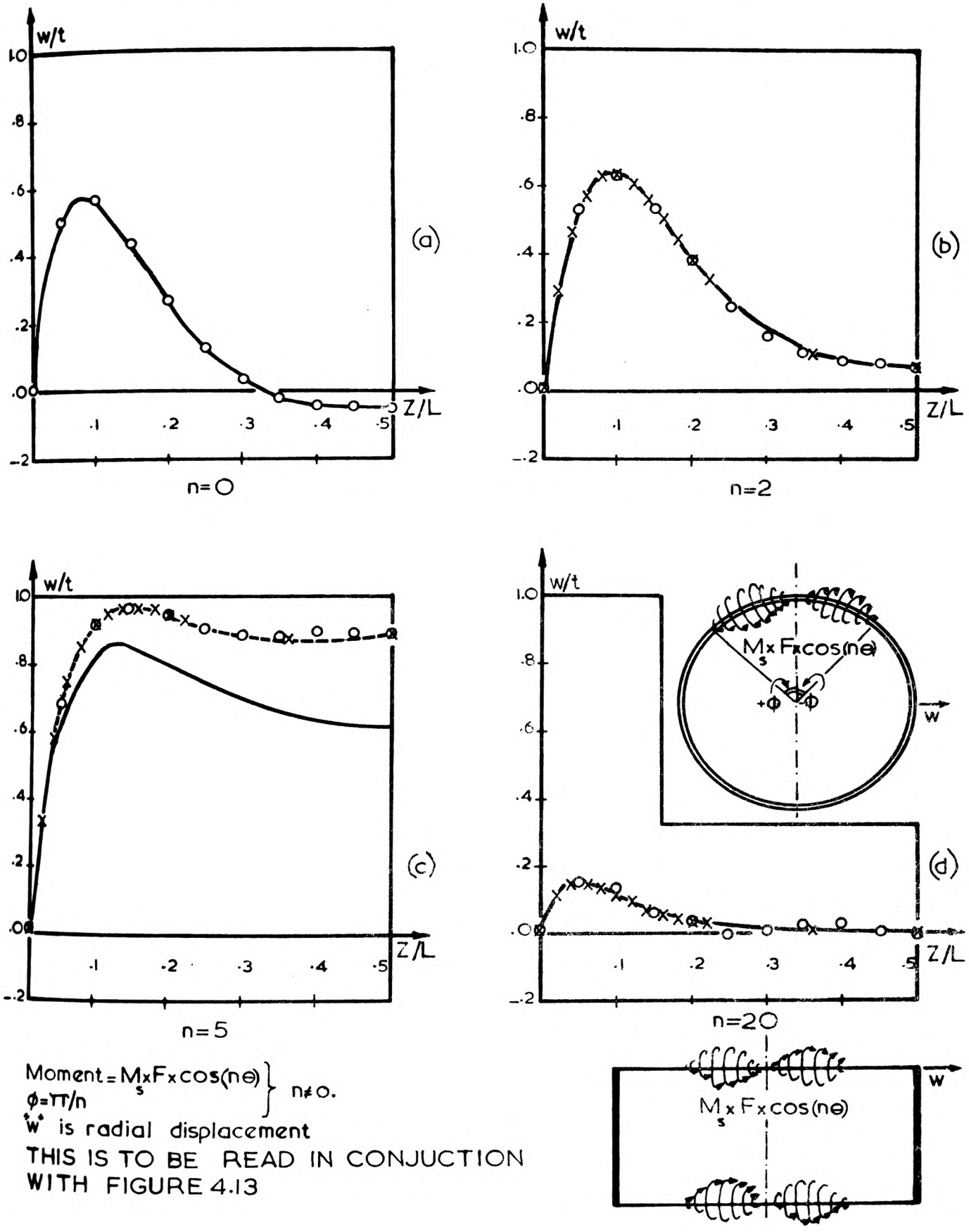

Moment = M_s x F x cos(nθ) } $n \neq 0$.
$\phi = \pi/n$

'w' is radial displacement

THIS IS TO BE READ IN CONJUCTION WITH FIGURE 4.13

FIGURE 4.14

ASYMMETRICAL BENDING OF CIRCULAR PLATE

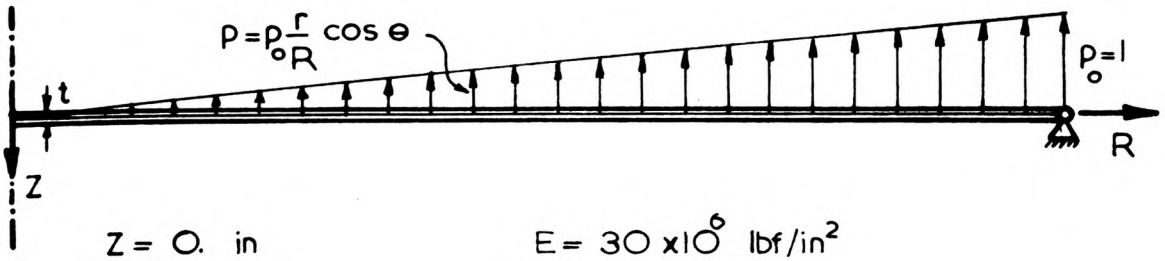

Z = 0. in
R = 10. in
t = 0.1 in

E = 30 x 10^6 lbf/in^2
ν = 0.3

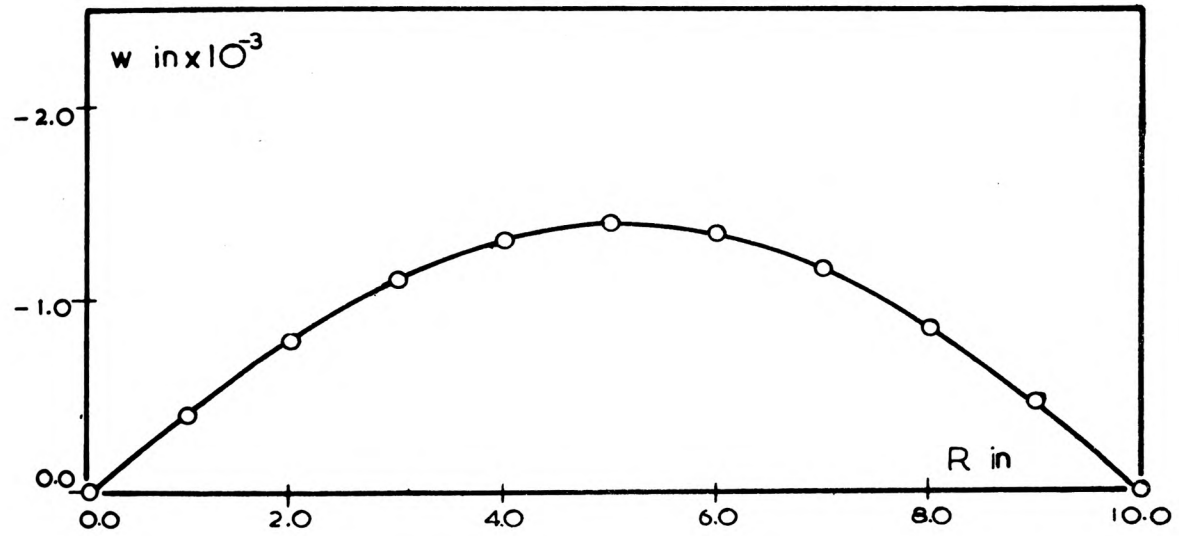

(a)

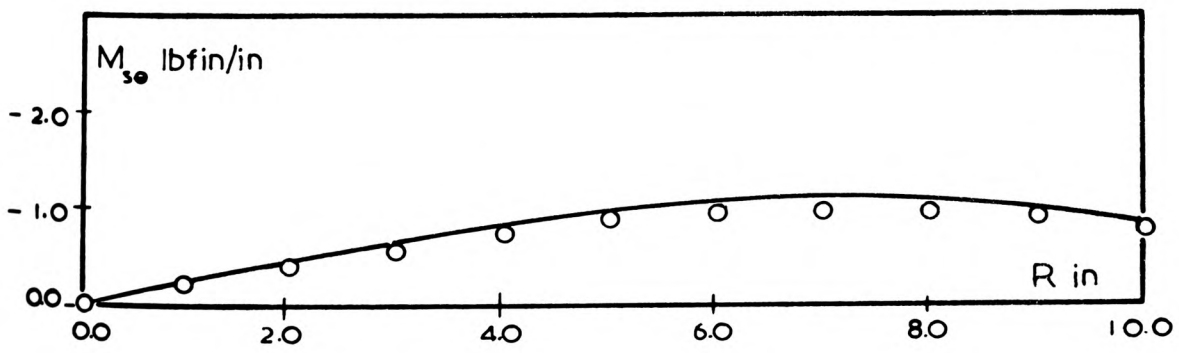

(b)

FIGURE 4.15

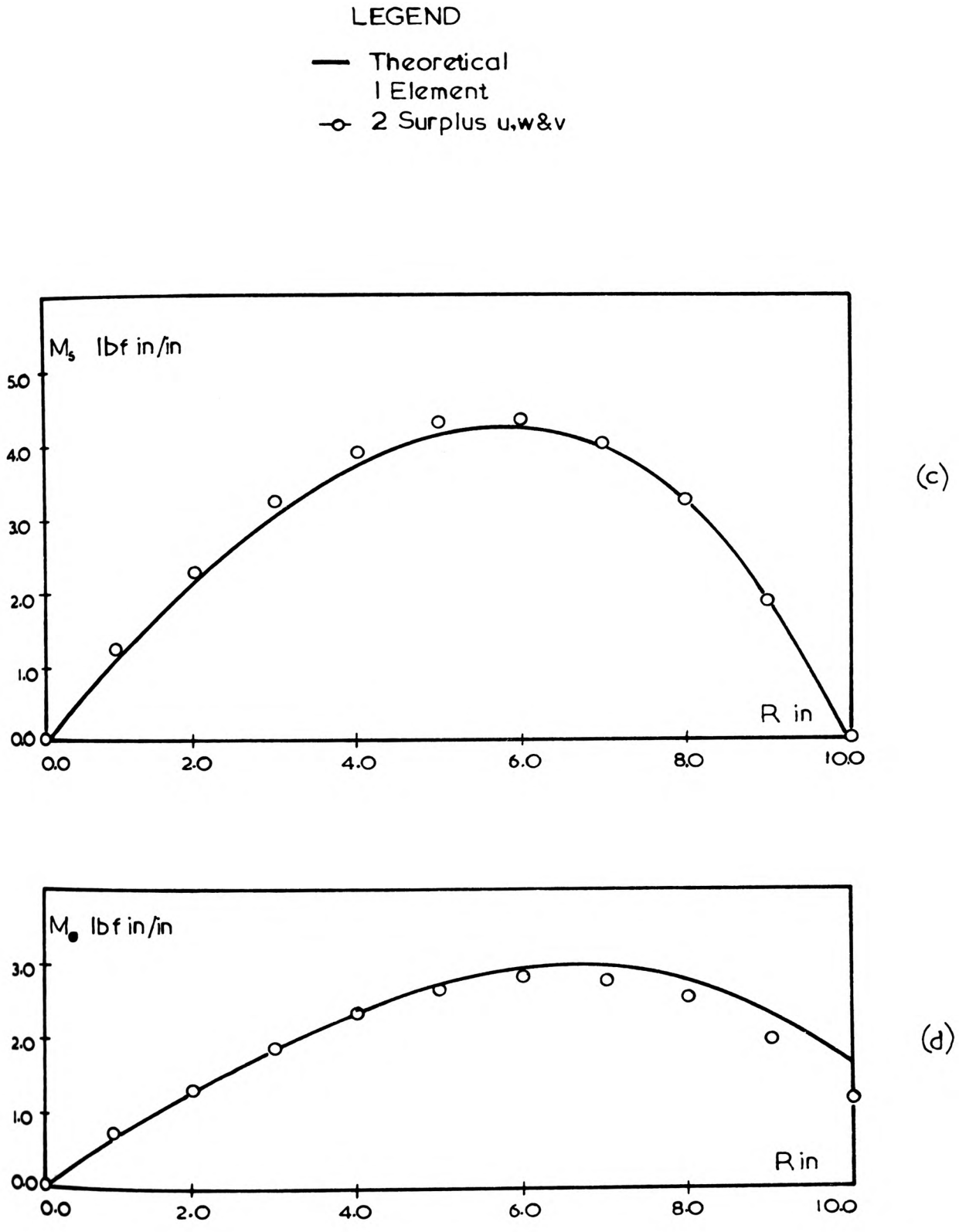
LEGEND
Theoretical
1 Element
2 Surplus u,w&v
M_s lbf in/in
5.0
4.0
3.0
2.0
1.0
0.0
R in
0.0
2.0
4.0
6.0
8.0
10.0
(c)
M_θ lbf in/in
3.0
2.0
1.0
0.0
R in
0.0
2.0
4.0
6.0
8.0
10.0
(d)

FIGURE 4·15

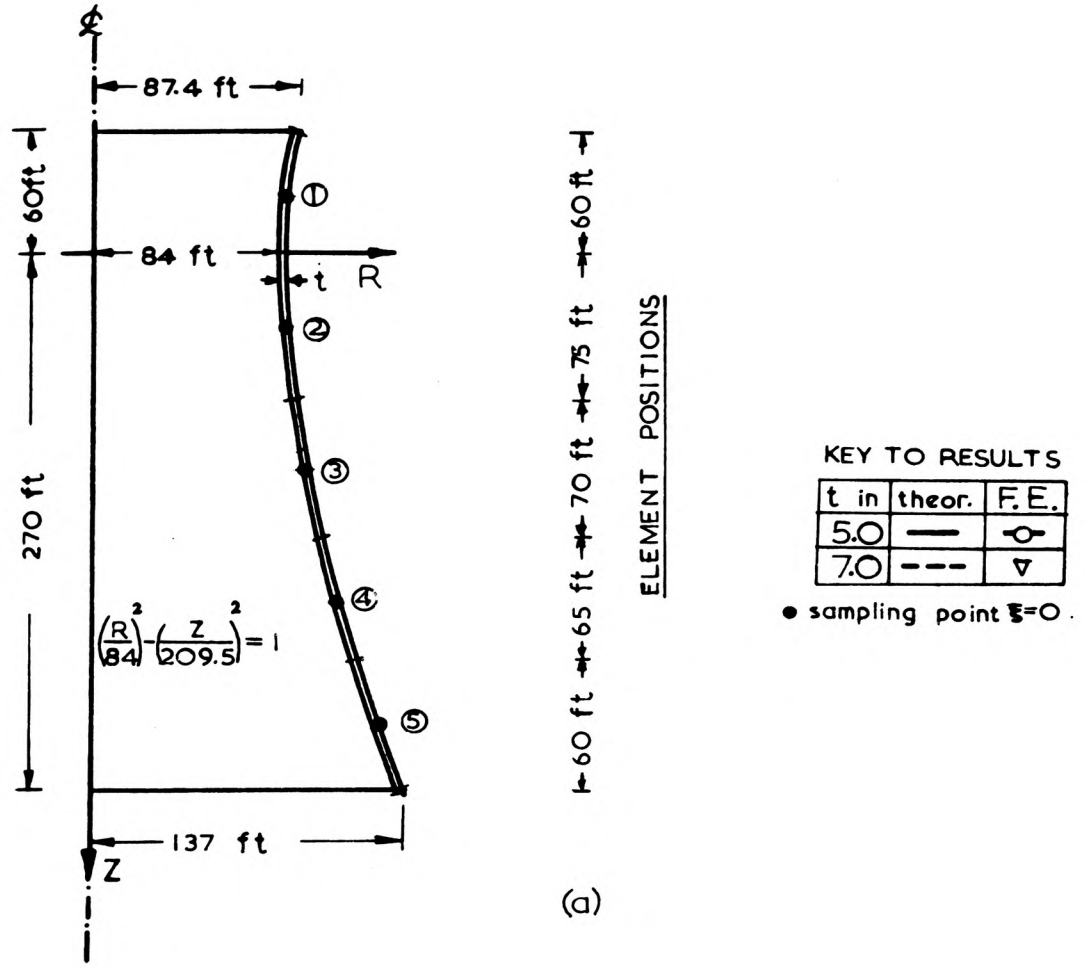
℄
87.4 ft
60ft
84 ft
t
R
270 ft
$\left(\frac{R}{84}\right)^2-\left(\frac{Z}{209.5}\right)^2=1$
137 ft
Z
60 ft
65 ft
70 ft
75 ft
60 ft
ELEMENT POSITIONS
KEY TO RESULTS
t in
theor.
F.E.
5.0
7.0
● sampling point ξ=0.
(a)

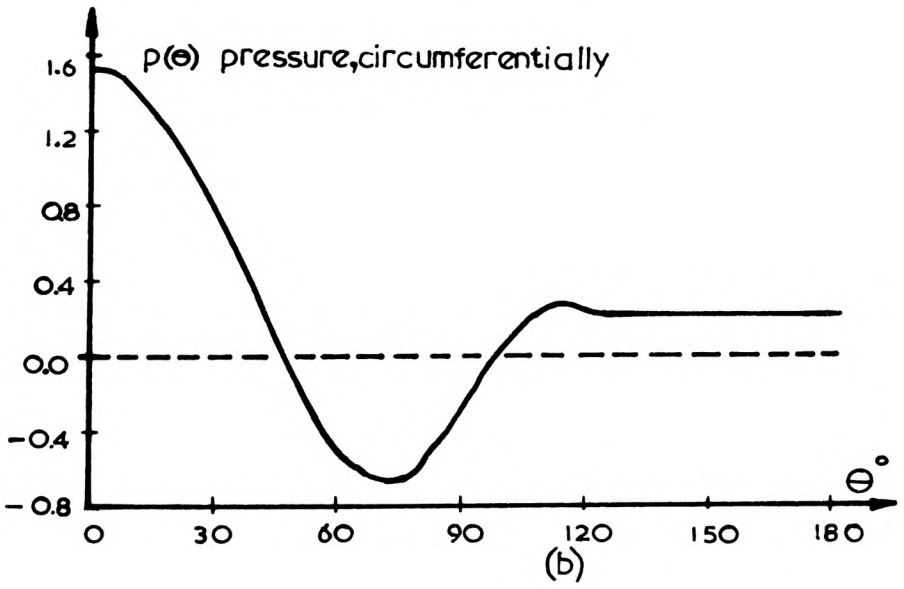
p(θ) pressure, circumferentially
1.6
1.2
0.8
0.4
0.0
-0.4
-0.8
θ°
0
30
60
90
120
150
180
(b)

FIGURE 4.16

DISPLACEMENTS CIRCUMFERENTIALLY

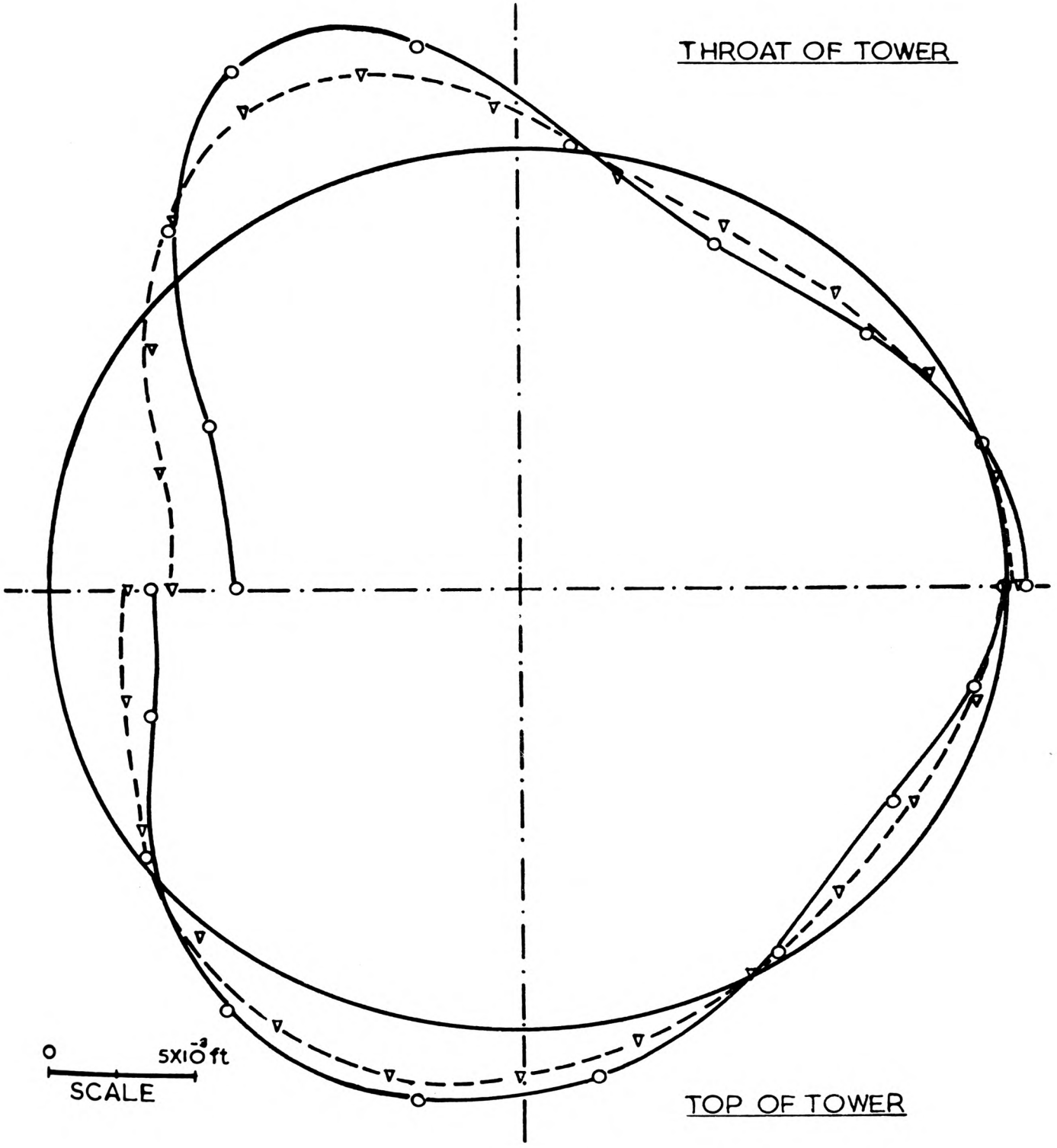

(c)

FIGURE 4.16

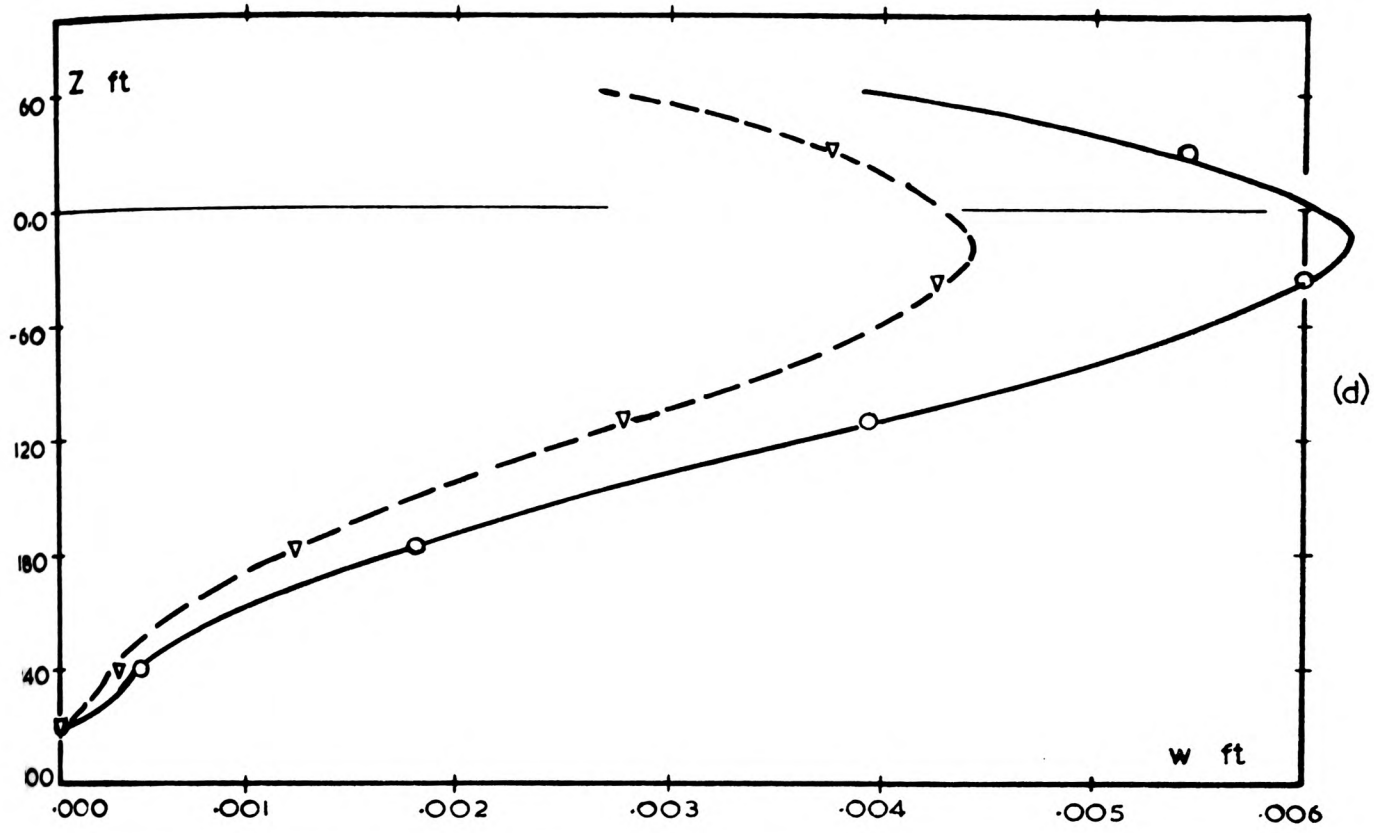
Z ft
60
0.0
-60
120
180
240
300
·000
·001
·002
·003
·004
·005
·006
w ft
(d)

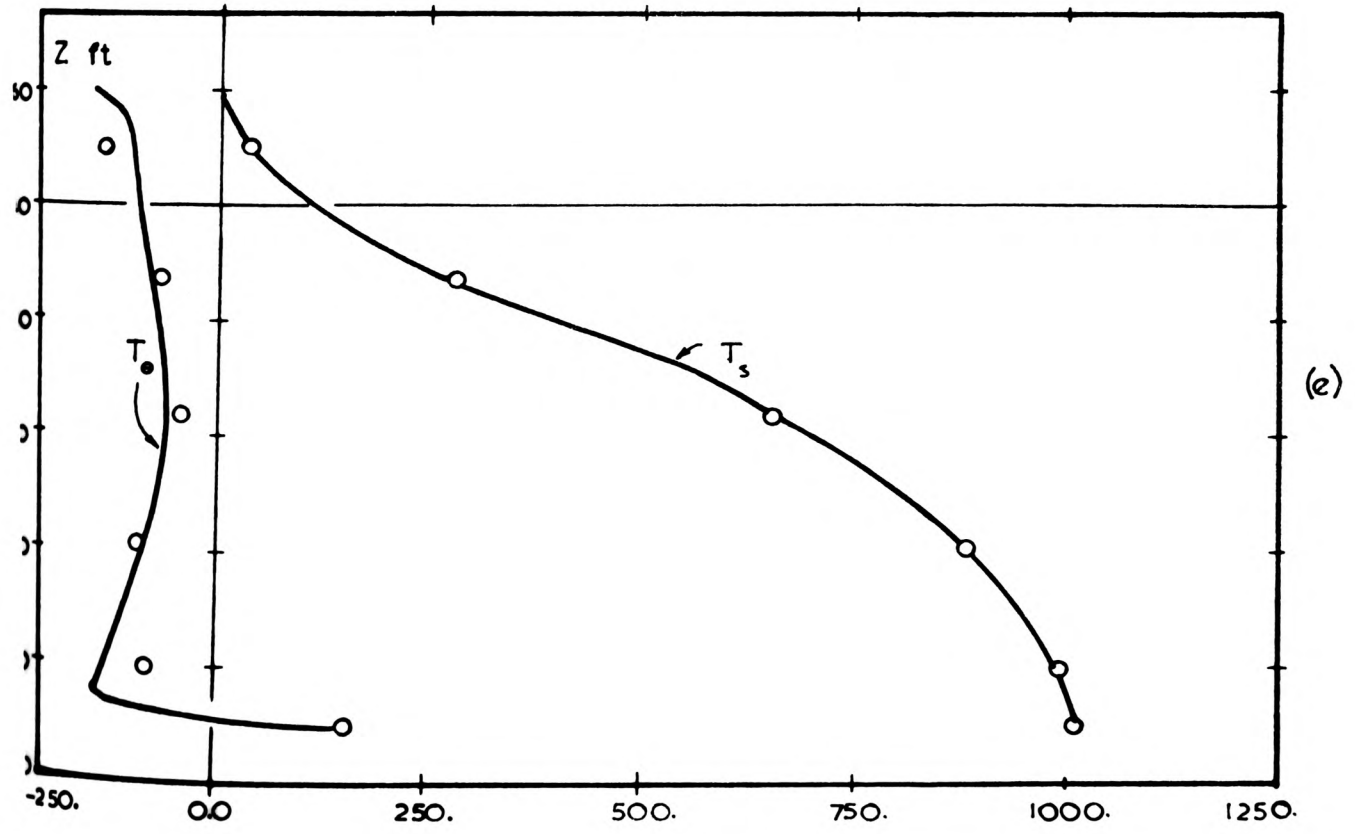
Z ft
50
0
0
0
0
0
-250.
0.0
250.
500.
750.
1000.
1250.
$T_\bullet$
T_s
(e)

FIGURE 4·16

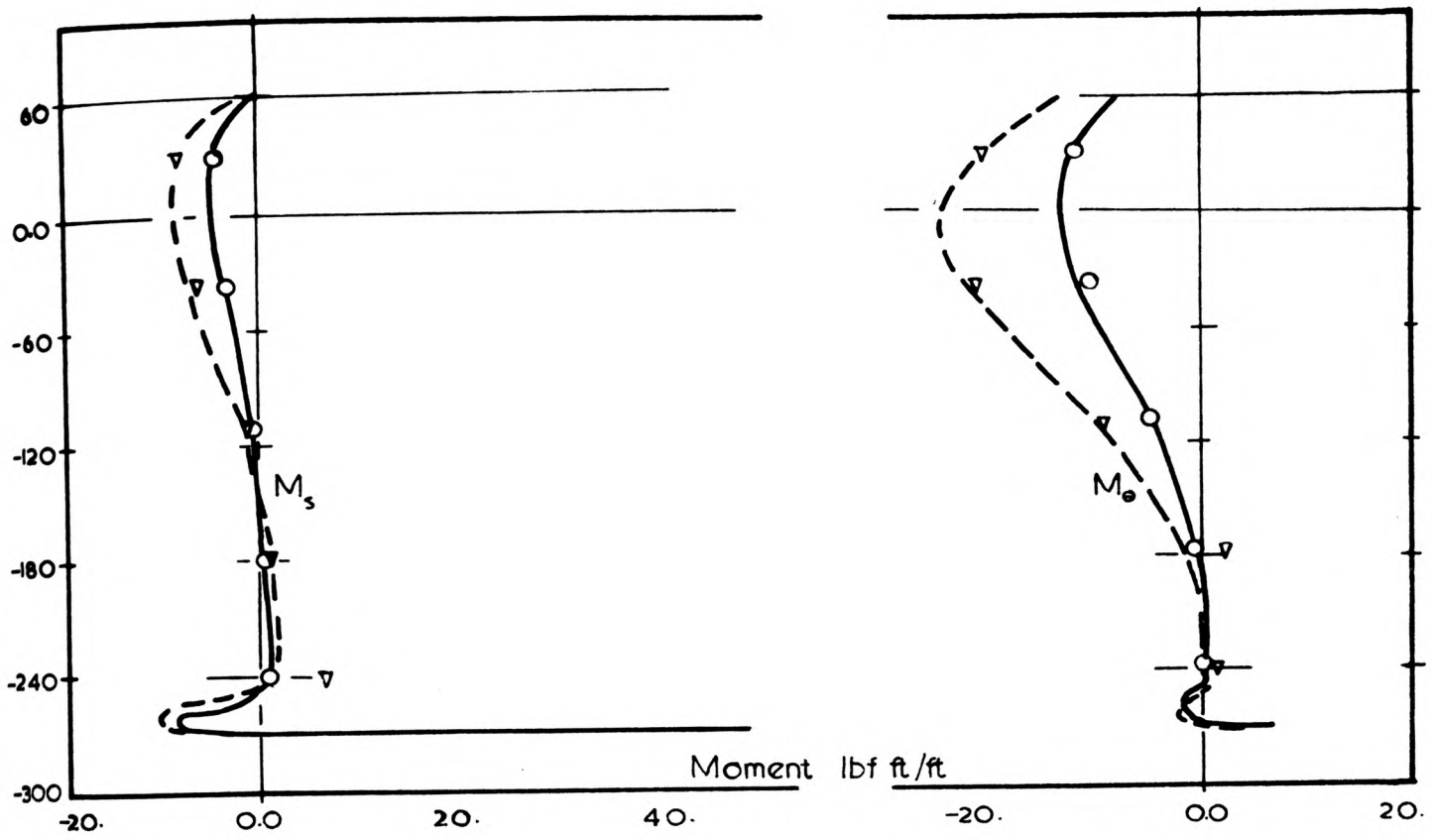

(f)

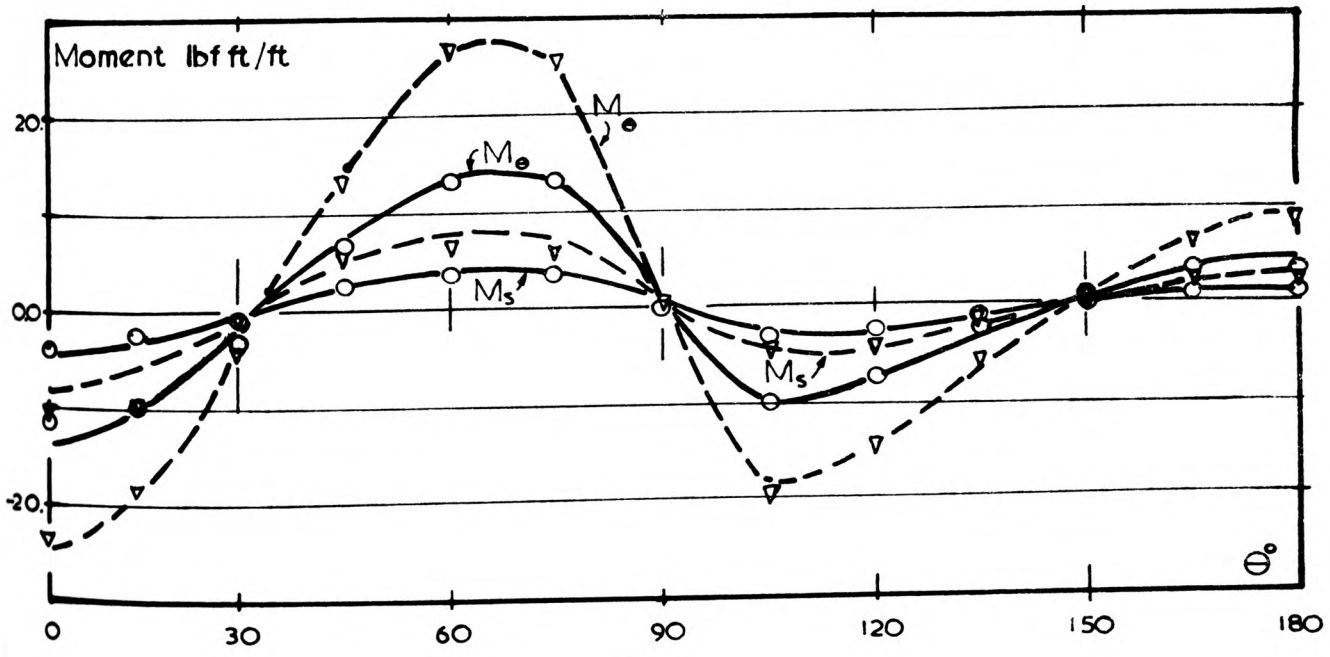

(g)

FIGURE 4.16

HEMISPHERE LOADED WITH CONCENTRATED DIAMETRAL MOMENT

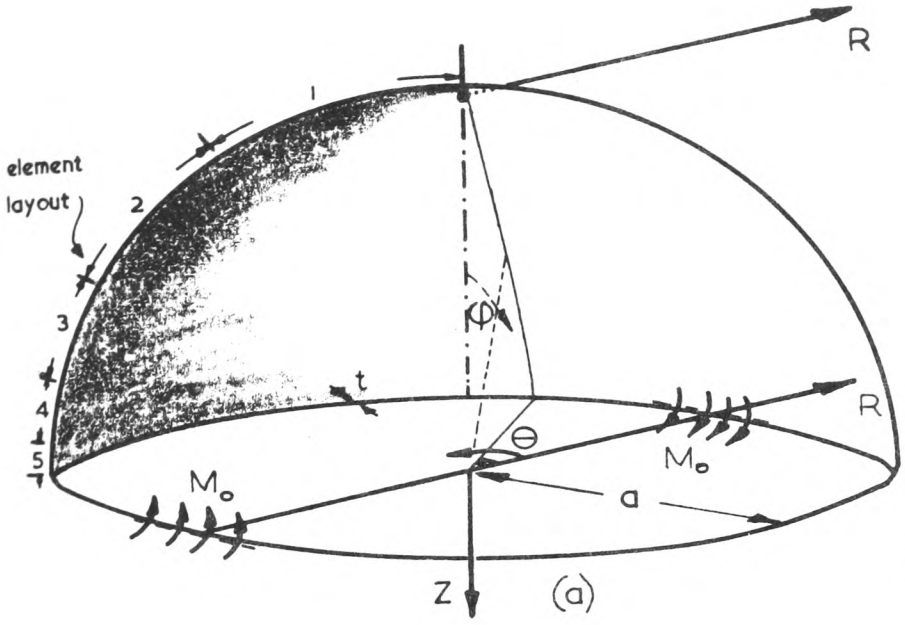

a = 6.0 in
t = 0.095 in
$E = 30 \times 10^6$ lb/in^2
$\nu = 0.3$

n-th harmonic of moment M_n is given by:

$$M_n = \frac{M_o}{\pi a}\left[1 + 2\sum_{n=1}^{\infty}\cos 2n\theta\right]$$

elm.	1	2	3	4	5
size	35°	25°	15°	10°	5°

Stresses sampled at nodes and element mid-points* namely, 0, 2.5*, 5, 10*, 15, 22.5*, 30, 42.5*, 55, 72.5* and 90 degrees from equater.

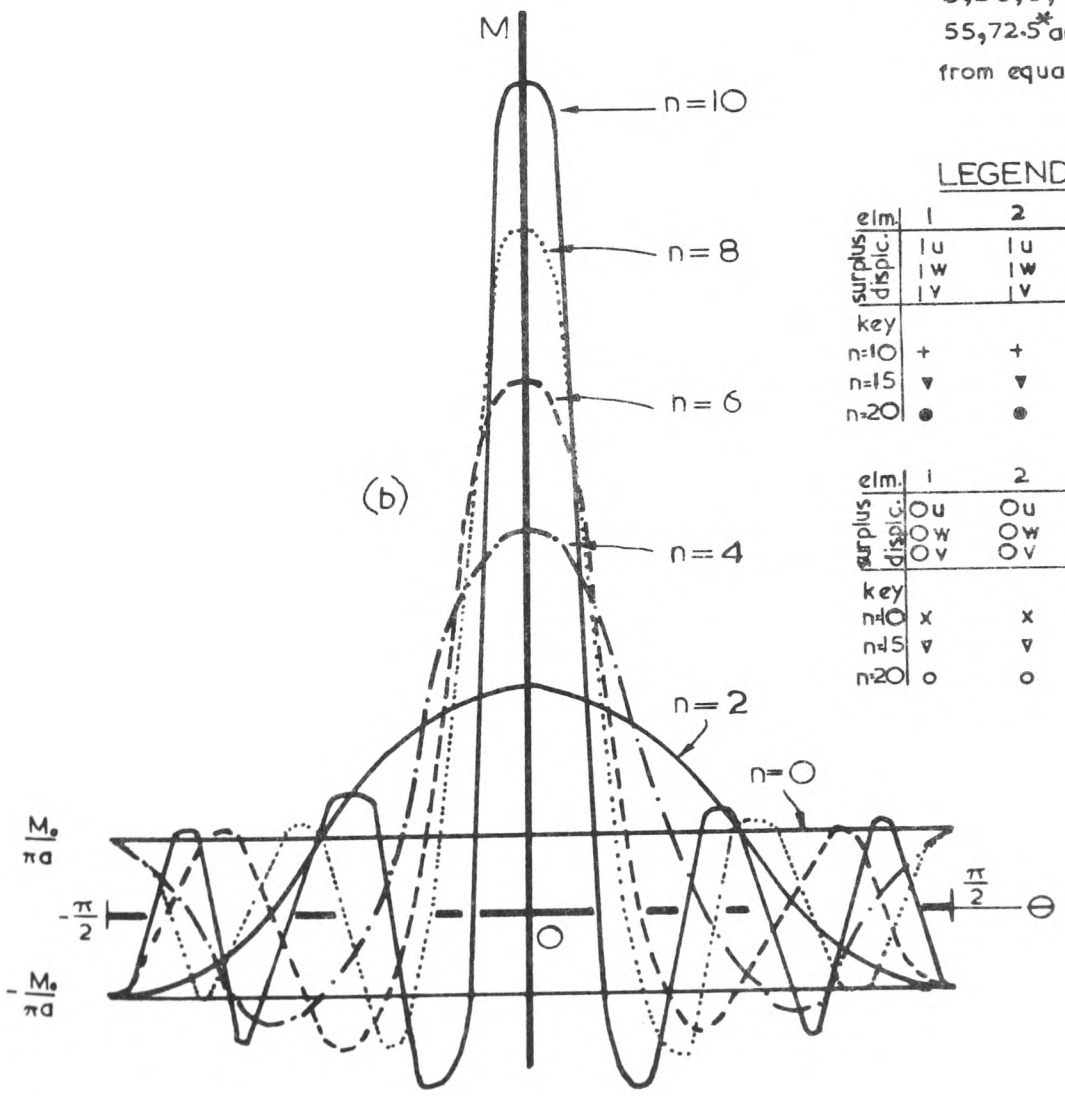

LEGEND:

elm.	1	2	3	4	5
surplus displc.	1u	1u	1u	1u	1u
	1w	1w	1w	1w	1w
	1v	1v	1v	1v	1v
key					
n=10	+	+	+	+	+
n=15	▼	▼	▼	▼	▼
n=20	●	●	●	●	●

elm.	1	2	3	4	5
surplus displc.	0u	0u	1u	2u	2u
	0w	0w	1w	2w	2w
	0v	0v	1v	2v	2v
key					
n=10	x	x	x	x	x
n=15	▽	▽	▽	▽	▽
n=20	o	o	o	o	o

FIGURE 4.17

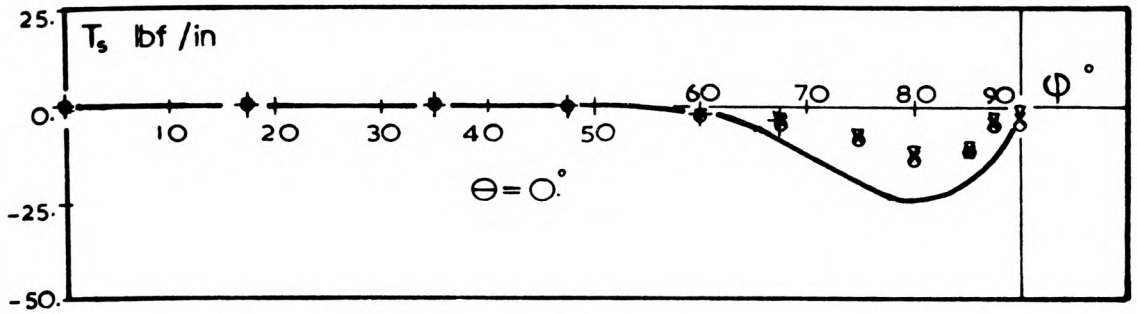

(c)

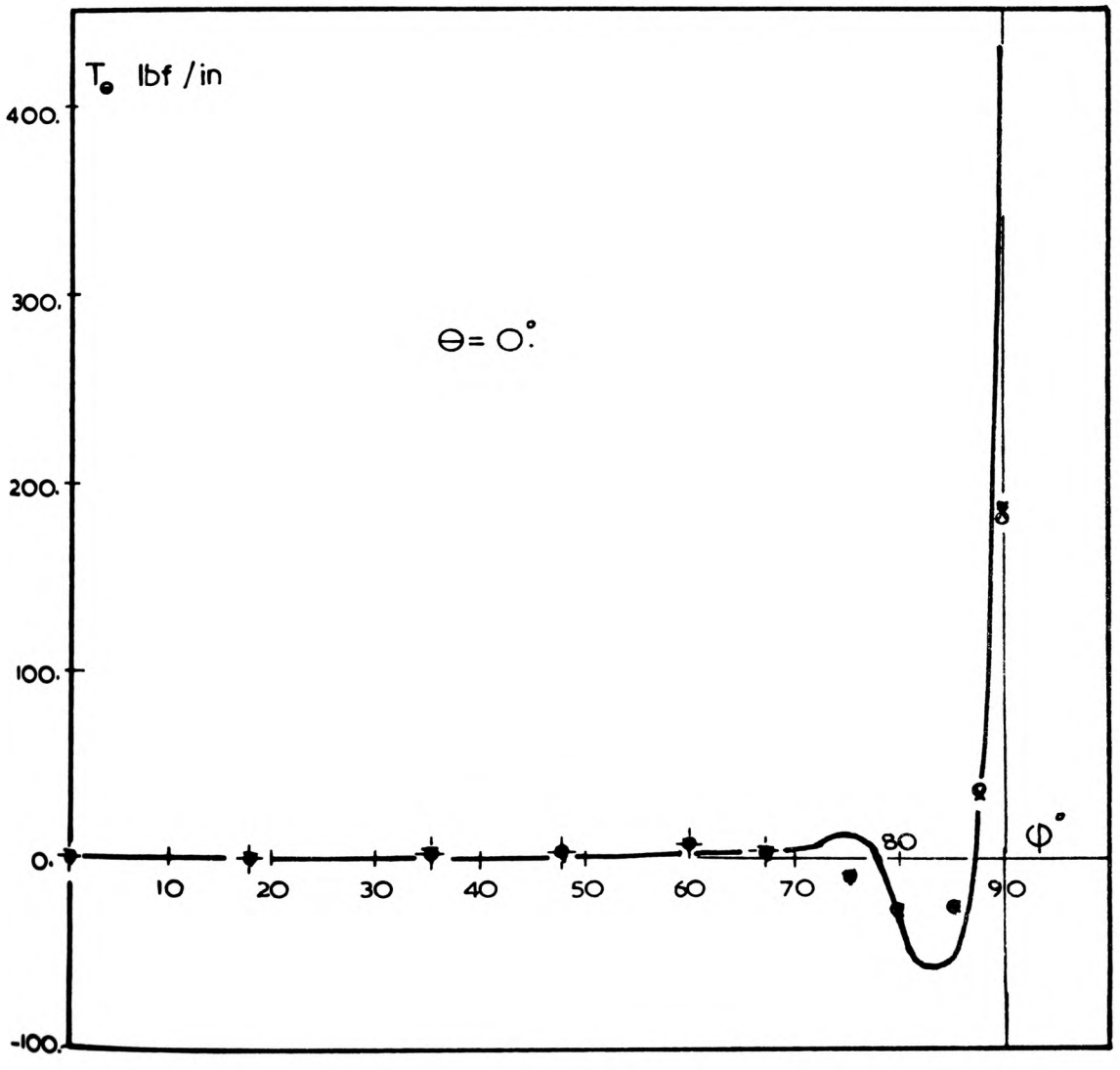

(d)

FIGURE 4.17

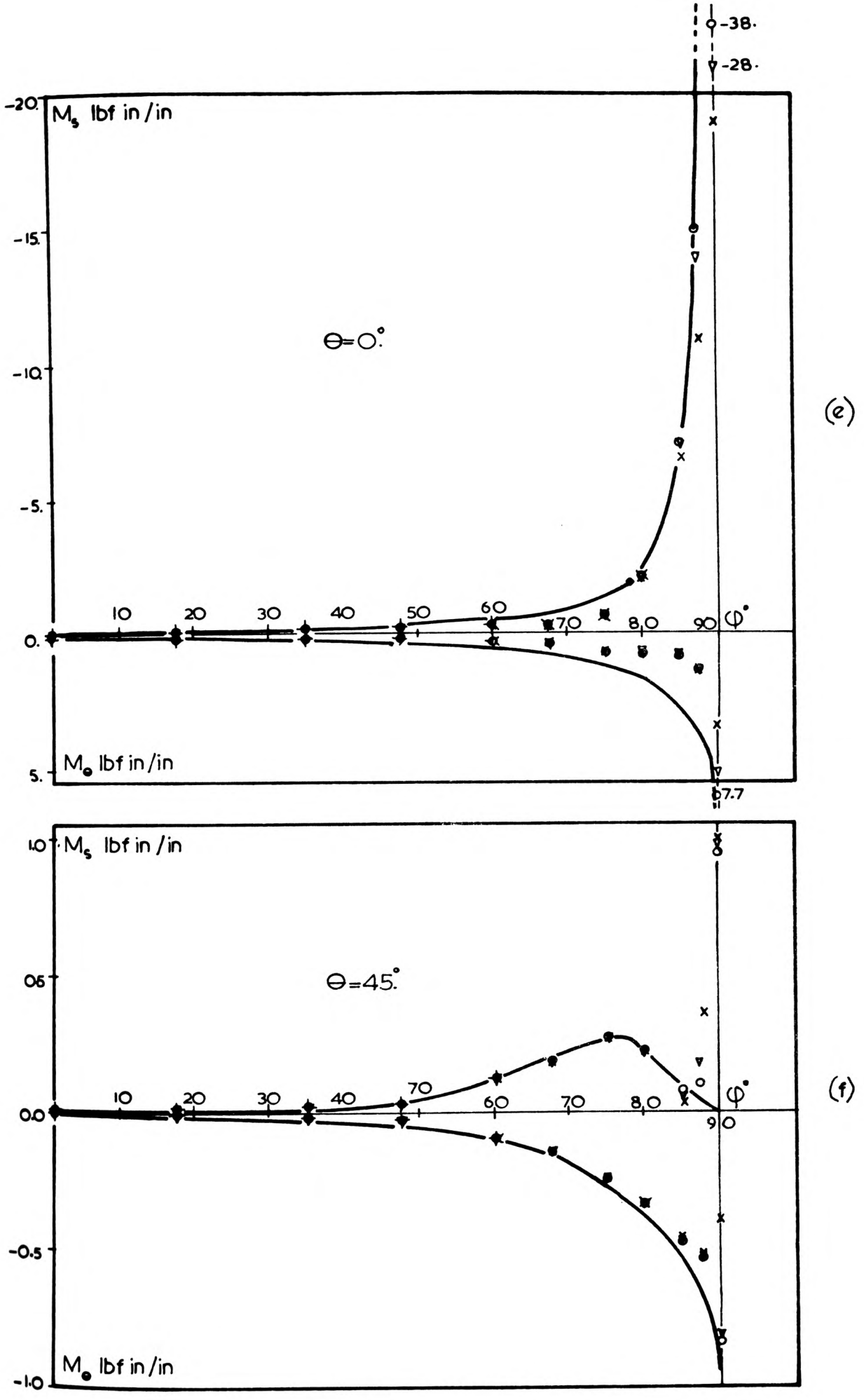
-38.
-28.
-20.
M_s lbf in/in
-15.
-10.
-5.
$\Theta=0^\circ$
10
20
30
40
50
60
70
80
90
Φ°
0.
5.
M_Θ lbf in/in
67.7
(e)
1.0
M_s lbf in/in
0.5
$\Theta=45^\circ$
10
20
30
40
70
60
70
80
Φ°
90
0.0
-0.5
M_Θ lbf in/in
-1.0
(f)

FIGURE 4.17

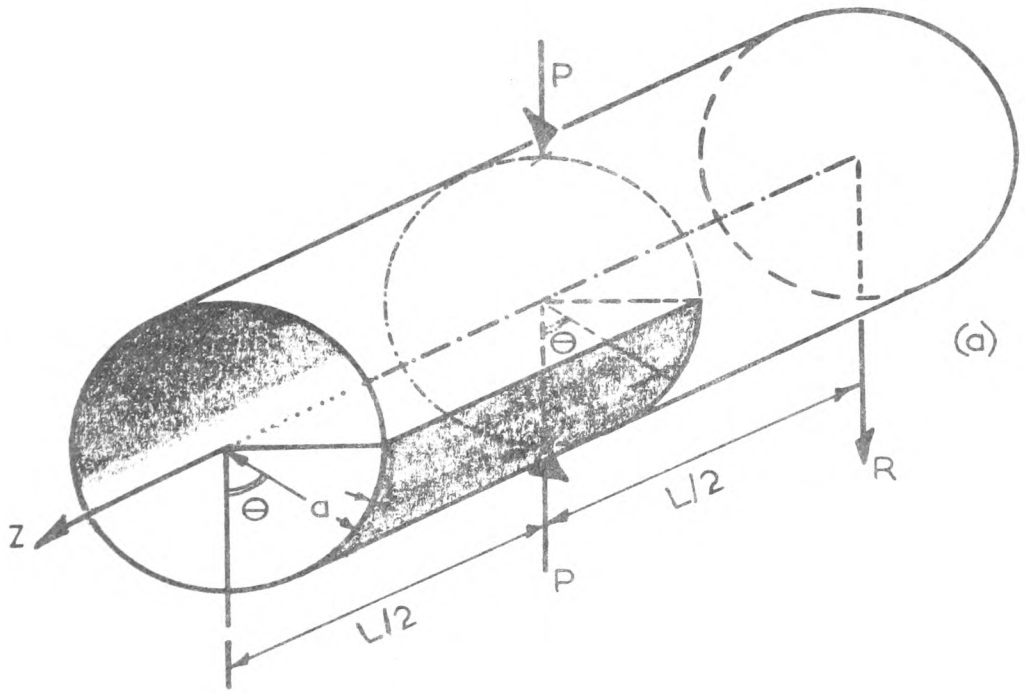

"w" = radial displacement under load P
"n" = number of harmonics used
1 element , surplus 2u, 2w, 2v.

Case (a)

L=10.35 in E=10.5 x10^6 lbf/in^2
a=4.953 in ν=0.3125
t_1=0.094 in G=4.0x10^6 lbf/in^2
t_2=0.01548 in

Case (b)

L= 2.0 in E=10.4x10^6 lbf/in^2
a=1.0 in ν=0.3
t=0.01 in G=4.0x10^6 lbf/in^2

n	$(w)_{theo}$=0.1138		$(w)_{theo}$=.2540	
	$(w)_a$ t_1=.094	error %	$(w)_a$ t_2=.01548	error %
5	0.1120	1.66	0.2431	4.28
10	0.1130	0.82	0.2445	3.67
15	0.1131	0.72	0.2447	3.63
20	0.1131	0.70	0.2448	3.60

(i)

n	$(w)_{theo}$=0.040989			
	$(w)_b$ 1 elem.	error %	$(w)_b$ 4 elem.	error %
5	.03964	3.28	.03973	3.05
10	.03995	2.53	.04008	2.20
15	.03999	2.42	.04015	2.04
20	.04000	2.37	.04017	1.99

(ii)

FIGURE 4.18

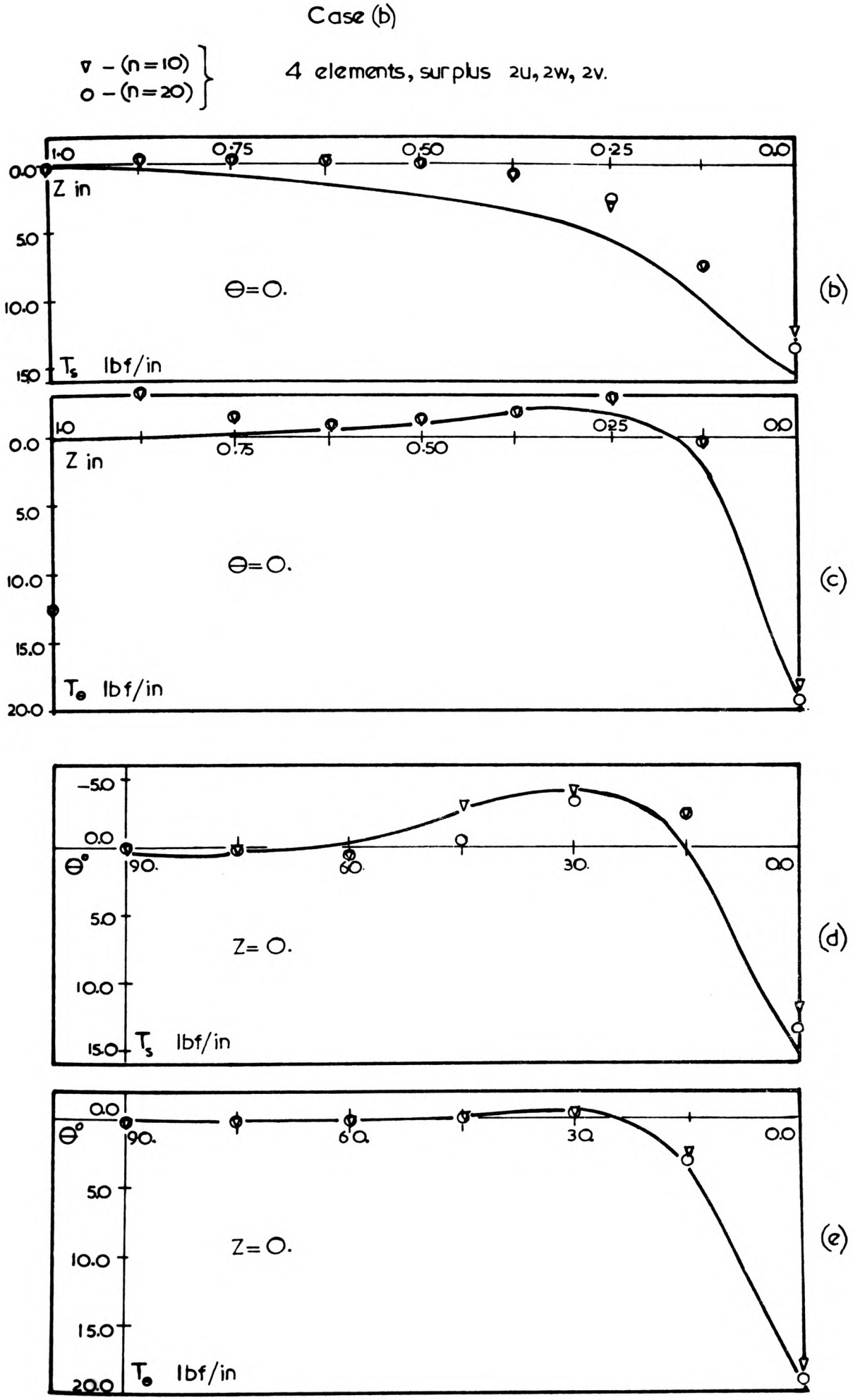
Case (b)
▽ – (n=10)
o – (n=20)
4 elements, surplus 2u, 2w, 2v.
1.0
0.75
0.50
0.25
0.0
Z in
Θ=0.
Ts lbf/in
(b)
Z in
Θ=0.
Te lbf/in
(c)
90.
60.
30.
0.0
Θ°
Z=0.
Ts lbf/in
(d)
Z=0.
Te lbf/in
(e)

FIGURE 4.18

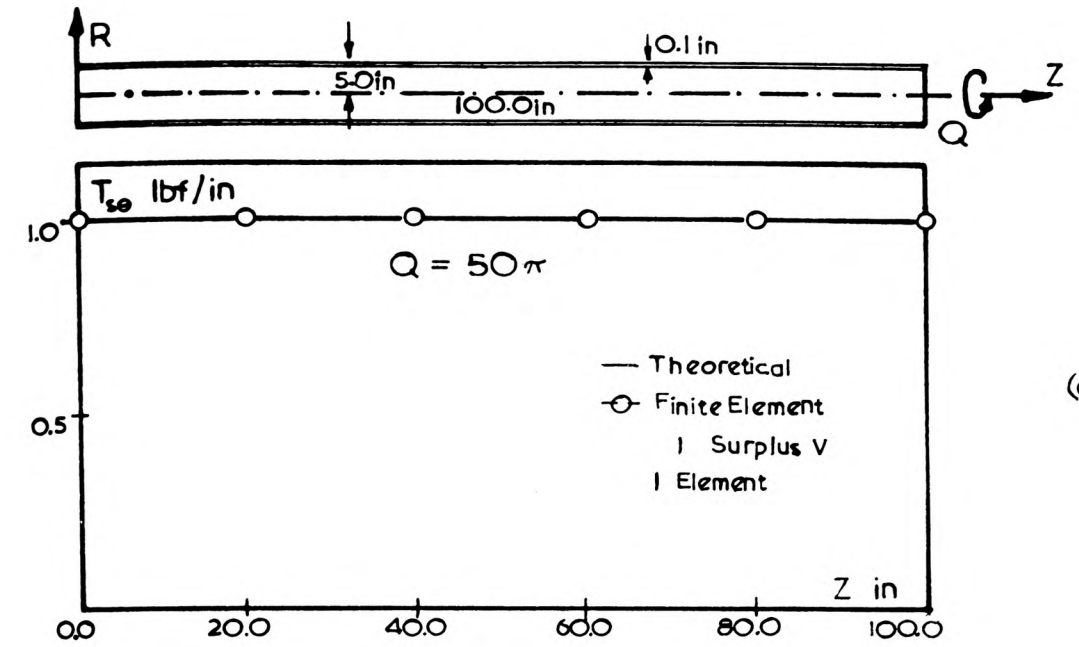

(a)

$G = 4 \times 10^6$
$\nu = 0.25$

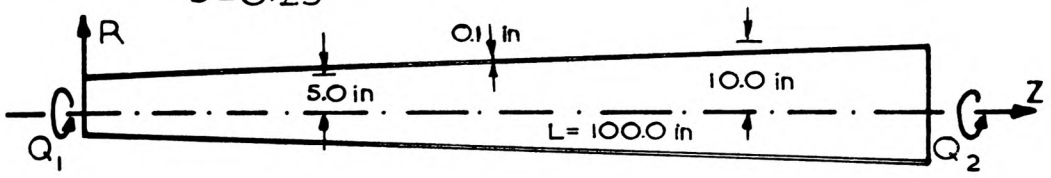

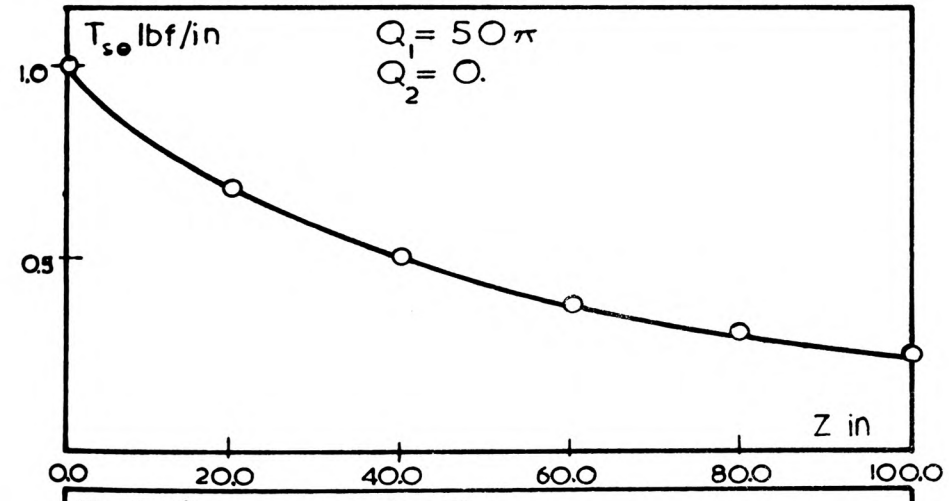

(b)

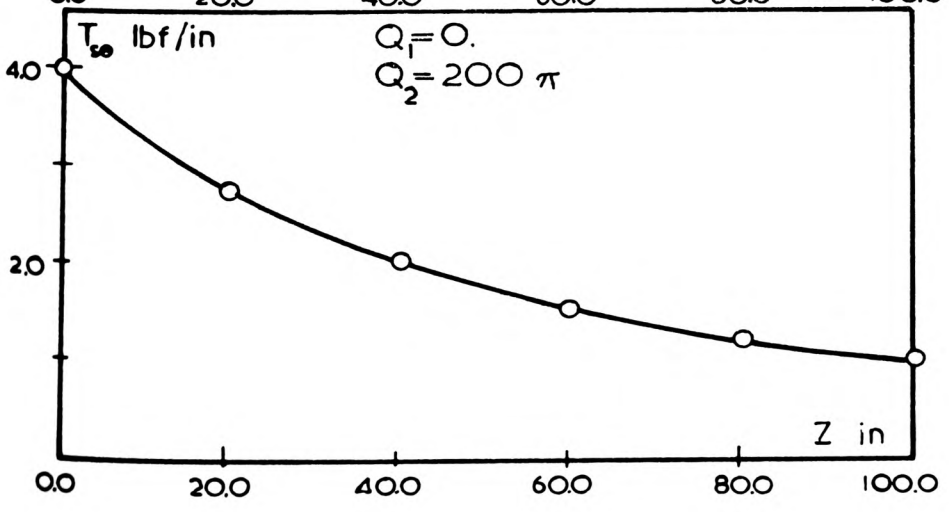

(c)

FIGURE 4.19

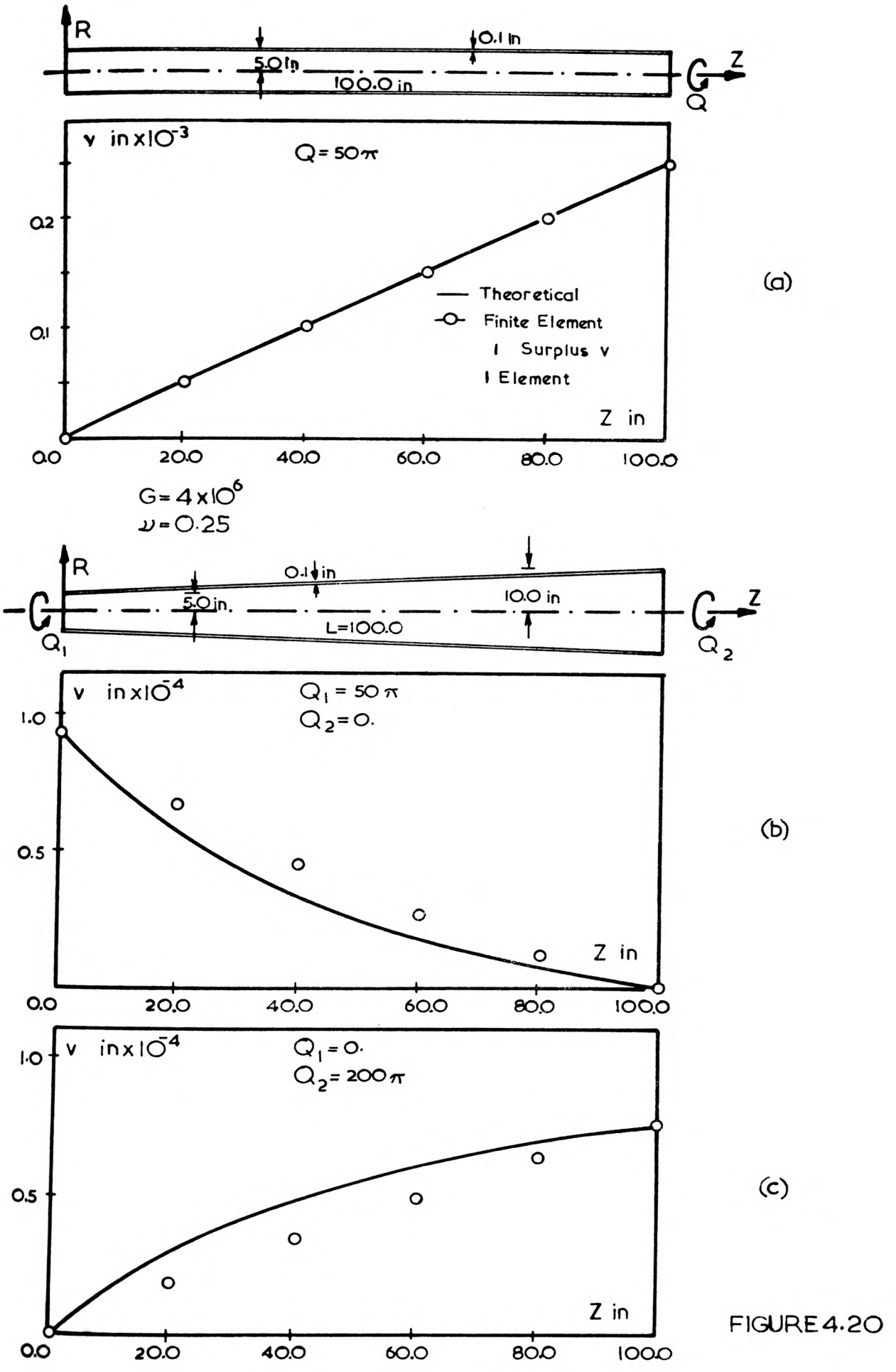
R
0.1 in
5.0 in
100.0 in
Z
Q
v in x10⁻³
Q = 50π
0.2
0.1
Theoretical
Finite Element
1 Surplus v
1 Element
Z in
0.0
20.0
40.0
60.0
80.0
100.0
(a)
G = 4 x 10⁶
ν = 0.25
R
0.1 in
5.0 in.
10.0 in
L=100.0
Z
Q1
Q2
v in x10⁻⁴
Q1 = 50 π
Q2 = 0.
1.0
0.5
Z in
0.0
20.0
40.0
60.0
80.0
100.0
(b)
v in x10⁻⁴
Q1 = 0.
Q2 = 200 π
1.0
0.5
Z in
0.0
20.0
40.0
60.0
80.0
100.0
(c)

FIGURE 4.20

TRUNCATED HEMISPHER SUBJECTED TO TORQUE

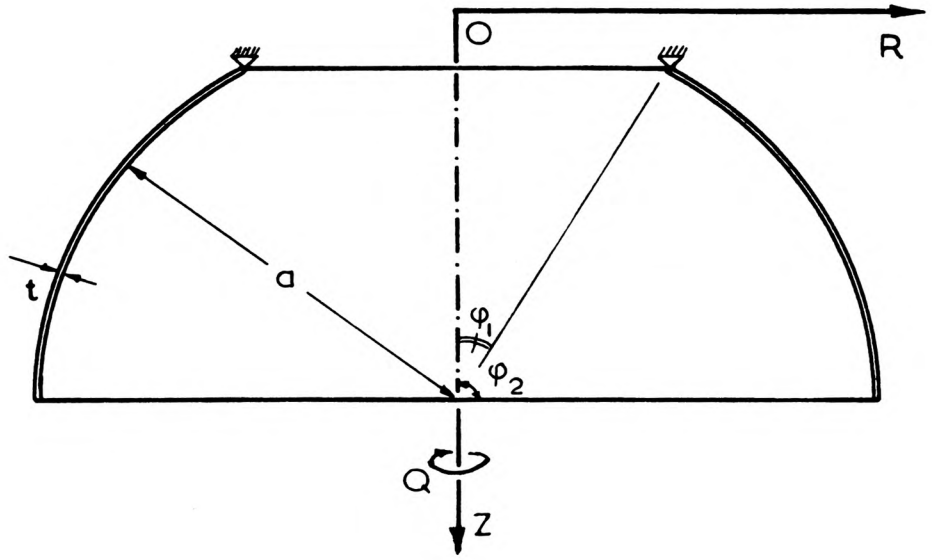

a= 10
t = 0.1
φ_1=30°
φ_2=90°
$Q = 2\pi R^2 T$

E = 2.5
G = 1.0
ν = 0.25

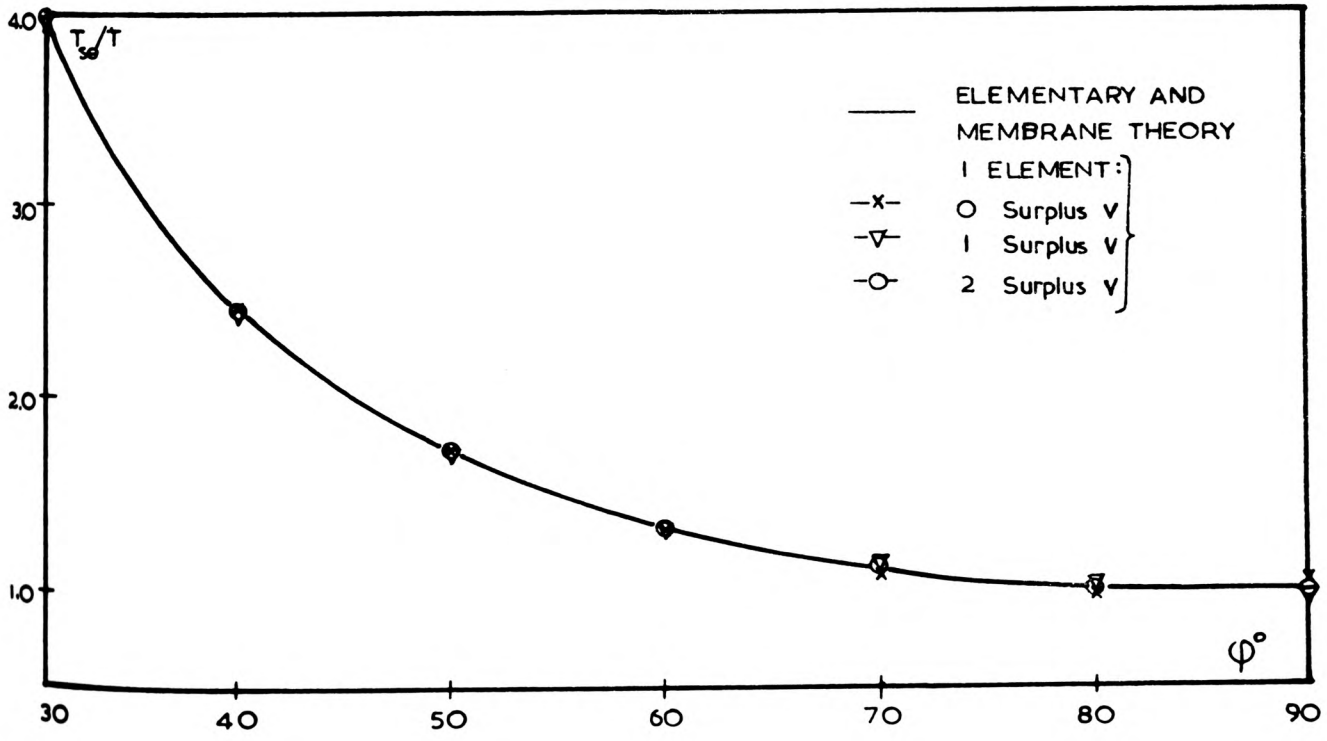

FIGURE 4.21

PART II

DYNAMIC AND BUCKLING ANALYSIS

CHAPTER 5

DETERMINATION OF NATURAL FREQUENCIES OF UNFORCED AND UNDAMPED ROTATIONAL SHELLS

5.1 INTRODUCTION

After the various major disasters in Civil Engineering structures, more importance is now being attached to the dynamic aspect of analysis of such structures. The complete analysis might depend on a full solution of the response problem using time increments the choice of which in turn will depend on the type of the structure, the number of time (or loading) increments, the combination of loading systems and finally a considerable amount of careful codification. This, at the moment appears to be a costly process. A reasonable idea of the dynamic behaviour of the structure could also be formed by determining the unforced and the undamped natural frequencies. This enables one to assess the frequency of the design loads likely to cause an excitation which could then result in a possible damage to the structure. The latter approach is a fairly cheap approximation.

Much work has been done to determine the natural frequencies for thin elastic, axisymmetric shells. Again the determination appears to fall within the two categories of mathematical analysis[1],[2],[3] and semi-analytical/numerical work[4],[5],[6].

In mathematical analyses, normally the methods of approach are along the following lines.

(a) A typical infinitesimal element of the oscillating structure is isolated. An expression is then written which relates the external, the internal and the inertia forces acting on the element. This expression is then reduced to the differential

equation of motion, the solution and the satisfaction of the boundary conditions of which could yield the natural frequencies.

(b) The alternative approach is to estimate the individual components[+] of the elemental energies involved which in this case are Kinetic and Strain Energies. Then suitable substitutions and adjustments are made to reduce the energy equation to the differential equation of motion. The manner of solution of the latter would then be similar to the method outlined in (a).

In numerical work, the approach made is almost entirely based on either the Energy method or the Virtual Work principle.

The determination of the axisymmetric modes and the corresponding frequencies based on the finite element method, were the original work of the candidate submitted for an earlier examination[8]. Some axisymmetric examples had been attempted previously the accuracy of which appeared to be satisfactory. The extended program which could enumerate the asymetrical and the torsional modes was developed from the axisymmetric program.

5.2 FINITE ELEMENT FORMULATION

The actual derivation of the finite element formulation has been covered adequately in a number of publications. No attempt will be made here to rederive the relevant equations at any stage of their development. The formulation adopted in the present work from reference (7) which is due to Zienkiewicz. The equation governing the undamped natural

---

+ By the term component, is meant algebraic addition of energy terms, since energy is a scalar quantity by definition.

frequencies for an elastic structure is given by

$$([K] - \omega^2[M])\{\delta_0\} = 0., \qquad \text{..... eqn. 5.1}$$

The stiffness matrix $[K]$ has been defined at some length in Chapters 1, 3 and 4. The matrix $[M]$ is known as the mass matrix the (p,q)-th term of which is defined as

$$[M_{pq}] = \int_V [N_p]^T [\rho] [N_q] d(vol) \qquad \text{..... eqn. 5.2}$$

where $[N]$, in its familiar form, provides the shape functions and $[\rho]$ is a diagonal matrix which entails the density and could include the rotary inertia if so required. The details of the program generating the mass matrix and a step-by-step account of the calculations involved, are presented in sections 5.4 and 5.5. An attempt is also made to attach physical significance to each term the description of which is hoped not to be regarded as a rederivation of expression 5.2

In order to determine the natural frequencies, the relationships 5.1 is re-written in a more workable form, namely,

$$[K]\{\delta_0\} = \omega^2[M]\{\delta_0\}$$

or

$$\left(\frac{1}{\omega^2}\right)\{\delta_0\} = [K]^{-1}[M]\{\delta\}$$

The product $[K]^{-1}[M]$ is only a symbolic representation since in actual practice the stiffness matrix $[K]$ is replaced by the product $[L].[L]^T$ obtained from a Choleski reduction. The mass matrix is then multiplied by $[L]^{-1}$ and $[L]^{-1T}$ respectively resulting in $[L]^{-1}[M][L]^{-1T}$ which finally is equivalent to the product $[K]^{-1}[M]$. The full mathematical development of this and other relevant details could be found in reference (7).

5.3 DISPLACEMENTS AND VELOCITIES

The displacements used here are similar to those given in Chapter 4 with a further difference that the time factor has to be included. This is achieved by multiplying the displacements of eqn. 4.3(a) and (b) by $e^{i\omega t}$ resulting in,

$$\{\delta\} = \begin{Bmatrix} u \cos j\theta \\ w \cos j\theta \\ v \sin j\theta \end{Bmatrix} e^{i\omega t} \quad , \qquad \ldots\ldots \text{ eqn. 5.3(a)}$$

or

$$\{\delta\} = \begin{Bmatrix} u \sin j\theta \\ w \sin j\theta \\ v \cos j\theta \end{Bmatrix} e^{i\omega t} \quad . \qquad \ldots\ldots \text{ eqn. 5.3(b)}$$

Again for non-zero values of j, general modes containing possible nodal circles and diameters are obtained. On the other hand for j=0, eqn. 5.3(a) results in solving the axisymmetric problems, while eqn. 5.3(b) for the same value of j=0 would yield the frequencies for torsional vibrations.

The general interaction of the modes of displacements will be clarified in the light of the following developments. From eqn. 5.2 the mass matrix is given by,

$$[m_{ij}] = \int [N_i]^T [\rho] [N_j] \, d(\text{vol}) .$$

In a similar way to the developments of section 4.2, the shape function $[N_j]$ operating on nodal variables would result in typical terms such as

$$[N_j] = [N_{j1} \cos j\theta + N_{j2} \sin j\theta] ,$$

The element $[m_{ij}]$ of the mass matrix would consist of such terms as,

$$[m_{ij}] = \int [N_{i1} \cos i\theta + N_{i2} \sin i\theta]_k^T [\rho_{k\ell}] [N_{j1} \cos j\theta + N_{j2} \sin j\theta]_\ell t_\xi \, dA \quad \ldots \text{ eqn. 5.4}$$

which, following the pattern of eqn. 4.7, would result in the complete consistent mass matrix $[M]^e_{0:n}$ corresponding to element e, containing harmonics from 0 to n given by,

$$[M]^e_{0:n} = \begin{bmatrix} M_{00} & M_{01}=0 & \cdots & M_{0n}=0 \\ M_{10}=0 & M_{11} & \cdots & \\ \vdots & \vdots & \ddots & \vdots \\ M_{n0}=0 & & \cdots & M_{nn} \end{bmatrix}$$

This matrix being diagonal indicates the uncoupling of the cross-terms and also helps in computing each mass matrix $[M_{jj}]$ independently using like terms corresponding to the j-th harmonic only.

The velocity components are $i\omega$ times the displacements which are obtained by operating the shape functions on the nodal variables in the usual manner. The velocities considered are only translational; it was thought that the rotational velocities would contribute negligible Kinetic Energy. The choice of local or global coordinates for u and w displacements is immaterial since eventually a Pythagoras-type displacement is obtained. The velocities corresponding to the j-th harmonic of displacements 5.3(a) would then appear as,

$$\begin{Bmatrix} vel(u) \\ vel(w) \\ vel(v) \end{Bmatrix} = i\omega \begin{bmatrix} \cos j\theta & & \\ & \cos j\theta & \\ & & \sin j\theta \end{bmatrix} \begin{Bmatrix} u_0 \\ w_0 \\ v_0 \end{Bmatrix} e^{i\omega t} \quad \ldots\ldots \text{ eqn. 5.5}$$

Also similar representations could be made for eqn. 5.3(b) which is used for torsional oscillations by setting j=0.

All remarks regarding the retention or rejection of Basic or Surplus displacements as discussed in Chapter 4 are valid here and the same also applies for normalisation of Basic displacements B2 and B4 of Fig. 3.21.

5.4 CALCULATION OF DENSITY MATRIX AND OTHER FACTORS

The opportunity is taken at this point to make the proper adjustments necessary for numerical integration discussed in section 4.6. Assuming homogeneous material properties,

$$(\text{infinitesimal mass } [dm]) = [\text{density } \rho].(\text{infinitesimal volume } d(\text{vol}))$$

It can be seen that the above expression results in a volume integral of the type given in eqn. 4.7 which further reduces to

$$\begin{aligned} [dm] &= [\rho]\ d(\text{vol}) \\ &= [\rho]\ t_\xi dA \\ \therefore [dm] &= [\rho] t_\xi (Rd\theta)(\frac{ds}{d\xi}d\xi). \end{aligned}$$

The rotational density $\frac{\rho t^2}{12}$ which was used in candidate's previous scheme of work was abandoned here. The infinitesimal mass at the point ξ is presented similar to that of the elastic matrix $[D]$ in section 3.4.9,

$$[dm] = \gamma . R_k (\frac{ds}{d\xi})_k W_k (t_\xi)_k [\rho]_k \quad ,$$

$$[dm] = (\gamma R_k)(\frac{ds}{d\xi})_k (\frac{ds}{d\xi})_k W_k\ (t_\xi)_k \begin{bmatrix} \rho & 0 & 0 \\ 0 & \rho & 0 \\ 0 & 0 & \rho \end{bmatrix} \qquad \ldots\ldots \text{ eqn. 5.6}$$

where k is the dummy index for Gaussian Quadrature and γ assumes values of 2π or π depending whether n=0 or n≥1 respectively.

5.5 FORMATION OF MOMENTUM AND MASS MATRICES

The approach to generate the mass matrix could be made by considering either the energy method or the virtual work principle since in either case there is a double implied multiplication of $(i\omega)$ with the infinitesimal mass (namely, velocity$(i\omega)$ x momentum$(i\omega)$ - or - displacement x mass x acceleration$(i\omega)^2$). For the convenience of forming a visual impression of the process of generating the mass matrix, the energy terminology is pursued. The change of momenta $d\{\mu\}$ are obtained

using the product of expression obtained from eqn. 5.5 and eqn. 5.6, namely,

$$d\{\mu\} = (\lceil\rho\rceil t_\xi dA).(i\omega\lceil N\rceil\{\delta^e\}e^{i\omega t}),$$

the total contribution of which to the Kinetic Energy of the element will be $\int\frac{1}{2}\{vel\}^T d\{\mu\}$. The mass matrix is ultimately obtained from the energy terms such as the expression given by the above integral, i.e.

$$\text{Kinetic Energy} = \int\frac{1}{2}\{vel\}^T d\{\mu\}$$

$$= (i\omega)^2\{\delta\}^T(\int\lceil N\rceil^T\lceil dm\rceil\lceil N\rceil)\{\delta\}$$

$$\therefore \quad \lceil M\rceil = \int\lceil N\rceil^T\lceil\rho\rceil\lceil N\rceil t_\xi dA.$$

Substituting from eqn. 5.6 for $\lceil dm\rceil = \lceil\rho\rceil t_\xi dA$,

$$\lceil M\rceil = \sum_{k=1}^{n}\lceil N\rceil_k^T\lceil\rho\rceil\lceil N\rceil_k(t_\xi)_k.(\gamma R_k(\frac{ds}{d\xi})_k W_k) \qquad \ldots\ldots \text{ eqn. 5.7}$$

where γ and W_k are defined as before.

There are two points of practical interest which are as follows.

i) In order to reduce computer time the product $\lceil N\rceil^T(t_\xi\lceil\rho\rceil\lceil N\rceil)dA$ could be reduced by the application of Choleski (the order of multiplication being implied using the parenthesis), thus,

$$(\gamma R_k(\frac{ds}{d\xi})_k(t_\xi)_k W_k)\begin{bmatrix}\rho & 0 & 0\\ 0 & \rho & 0\\ 0 & 0 & \rho\end{bmatrix} = \begin{bmatrix}\ddots & 0\\ Q & \ddots\end{bmatrix}\begin{bmatrix}\ddots & Q\\ 0 & \ddots\end{bmatrix}.$$

This is readily achieved since the density matrix is really an identity matrix times a positive constant, thus involving the square-root of the diagonal terms only and could be stored as a vector or even as a single constant. A pseudo-momentum quantity is then resulted from the product,

$$\lceil\psi\rceil = \begin{bmatrix}\ddots & Q\\ 0 & \ddots\end{bmatrix}\lceil N_k\rceil,$$

which will instantly yield the mass matrix in the form,

$$[M] = \sum_{k=1}^{n} [\psi]^T [\psi]. \qquad \text{..... eqn. 5.8}$$

It is also apparent that the necessity for reserving two $[NT,3]$ matrices for $[vel]$ and $[\mu]$ is now reduced to storage of a single $[NT,3]$ matrix for $[\psi]$. This method could lead to confusing results if applied to form the stiffness matrix and thus the stresses.

ii) The device of section 4.6, which overcame the difficulty of forming the difference of two numerically equal quantities (only for the first harmonic) is not essential here, so there is no additional adjustment required to w and v terms in the displacements nor the shape functions.

5.6 EXAMPLES

In order to form some impression of the function of the program, a few numerical examples were prepared. The order of presentation of the examples was chosen so that it generally corresponded with the developments given in most relevant text books, namely commencing with simple shapes such as rings, plates and cylinders in simple and familiar modes. The theory was then extended to embrance the θ-dependent modes for the above geometries where possible; this was achieved by a suitable choice of the nodal and the surplus displacements through an implied use of equation 5.3(a). The torsional modes were attempted by interchanging the system of displacements in equation 5.3(b) and setting $j=0$. Finally some other interesting cases which indicated the contribution of the strain energy in extensional/flexural modes were presented which also served the candidate in its educational capacity. Almost all the examples were processed with no more than 26 degrees of freedom available on the Polytechnic computer. The results were thought to be satisfactory.

5.6.1 The Ring and the Skew Washer

This example was of the simplest geometry chosen to form a quick check on the formation of the stiffness and mass matrices, during the candidate's[8] previous scheme of work. The modes and the corresponding frequencies are given in Fig. 5.1 together with the respective theoretical value. As indicated 1 element was used with 6 surplus displacements, 1u and 5w.

5.6.2 The Circular Plate

This geometry is ideal to test the frequencies obtained against the correct functioning of the boundary condition specification. The equations used for a plate clamped round its circumference were from reference (9), giving the angular frequencies for different circular modes, see Fig. 5.4. A corresponding table also indicates the convergence of the frequency with variation in the number of elements and the surplus displacements. The density used was 0.289 lbf/in^3 and the value of g was assumed to be unity.

Figure 5.3 indicates the change in frequency for a change in the support condition, namely releasing the edge clamp but fixing the centre. Errors of the same order were obtained when both considering the various modes in an attempt to vary the number of elements and in changing the boundary conditions.

The third boundary condition involving just a lateral support at the edge, presented some difficulty since no reference to theoretical value could be found. As a quick check a very simple set of calculations based on Rayleigh-Ritz method were devised which had to be solved by a very approximate numerical integration technique. The agreement found was satisfactory. No attempt was made to estimate other axisymmetric modes, see Fig. 5.4.

Since the coverage given to various coefficients in the Handbook of Plant Engineering was found to be more comprehensive than reference (9), more examples based on the Handbook with certain information built into the formulae were tried. The frequencies therefore might appear different from the frequencies corresponding to the previous set. This time four modes (0 to 3 nodal circles) were tabulated against four different harmonic numbers (n=0,1,2 and 3). It was again found difficult to have access to all the theoretical values. The results are tabulated in Figure 5.5.

5.6.3 The Long Cylinder

This example was chosen to examine the response of a long cylinder which in effect is an elastic prismatic bar to its fundamental frequencies. Only one element with no more than a total of six surplus functions was used for this case. The worst errors were encountered when considering flexure. The membrane results appear fairly satisfactory as can be seen from Fig. 5.6. The formulae from which these examples were calculated are listed in most standard text books in this field*.

5.6.4 Spherical Shells

In this case an attempt was made to compare the theoretical and the numerical angular frequencies obtained from (a) membrane considerations alone and (b) membrane and bending together with the predominance of the latter.

---

* For example Reference (9) provides an excellent coverage for these formulae.

(a) One of the simplest cases for the membrane mode is that of a sphere with radial (hoop) displacements. Symmetry with the constraint in the slopes of the lateral displacements were used in order to "force" the above mode. The decrease in the observed error of the angular frequencies is tabulated against the increase in the number of elements used, see Fig. 5.7(a).

(b) A spherical cap was chosen for the flexural mode of oscillations. The equations used for the analysis are those developed by Reissner[10]. Again the convergence to the correct frequency is tested against the usual factors, namely degrees of surplus displacement and the number of elements used , this is shown in Fig. 5.7(b).

5.6.5 Torsional Vibrations

For this mode of vibration two examples were chosen[11]. The first case was a truncated cone simply supported along both circular edges. The value of unity was used for most geometrical and material parameters. A single element represented the shell with a range of surplus degrees of freedom. The convergence of the calculated frequencies and the errors involved is given in Fig. 5.8. The second example is in the shape of a thin hemisphere, simply supported at the pole and the equator, shown in Fig. 5.9. There were a number of common factors in both examples which can readily be identified upon comparison of Figures 5.8 and 5.9. Owing to the curvature present for a single element representation (namely the tangent at end 2 being at 90^{o} to the tangent at end 1), the same shell was attempted using 2 and 3 elements with considerable improvement in the frequencies. This is shown in the table of Fig. 5.9 in which for the sake of brevity the variation of the percentage error is recorded only.

5.6.6 Short Cylinder clamped at both extremities

The candidate had come in contact with a certain class of vibration examples which unlike the plate problem, the strain energy of the former class did not entirely depend on flexure. The first of these examples was initially discussed in reference (12) is the cylinder shown in Fig. 5.10. The lowest resonance frequency of this cylinder coincides with n=6 (the number of nodal diameters) whereas the corresponding frequency for the second mode occurs at n=9. The difference in frequencies between the first mode and the second mode appears to reduce as the value of n is progressively increased. One element was used for this analysis with a total of six surplus degrees of freedom 2u, 2w and 2v. The experimental data published by Koval and Cranch[13] is a refreshing encouragement for the theoretical results both analytical and numerical.

Comparable experimental curves, using a cylinder with different geometrical parameters and support conditions were also obtained later by Weingarten[14]. The latter example is included for comparison elsewhere[15].

5.6.7 General Vibrations of a Thin Conical Frustum

Figure 5.11 depicts another shell geometry where the lowest frequencly is not necessarily at the lowest harmonic number. The experimental data chosen for this case is due to Weingarten[14]. A finite element analysis had appeared by Sen and Gould[15] only recently who use a conical shell element with a very marginal departure in geometry from that given originally by Weingarten (an error of about 0.1% increase in the length of the cone is likely to make the shell fractionally more flexible). The finite element calculations here were based on the data used by the latter to provide a basis for theoretical (numerical) comparison. The lowest frequency in this case

corresponds to the first mode of the 4-th harmonic but the error between the experimental result and the corresponding finite element frequencies appear to be somewhat higher than the error involved in the comparative frequencies of the other harmonics. The theoretically predicted values of Strutt quoted in reference (16) which are based on purely inextensional terms seem to be inadequate. The total number of degrees of freedom used here were 14 and 24 which resulted from using 1 and 2 elements respectively. It is estimated that the degrees of freedom in reference (15) were 32 after the reduction of the size by the use of Kinematic condensation. The errors between the numerical results obtained from using 2 elements and the results from the above reference are negligible.

5.6.8 Fixed Hemispherical Cap

In this example a thin shallow spherical cap was chosen which was rigidly fixed at its base corresponding to the azimuth angle of $\phi_0=30^0$. The geometrical and the material details are given in Fig. 5.12. The theoretical frequencies are extracted from reference (17) against which the finite element results are compared. For the actual plot a normalised value of $\frac{\omega}{\omega_0}$ is used instead of the numerical value of the frequency where $\omega_0 = \frac{1}{a}\sqrt{\frac{E}{\rho(1-\nu^2)}}$, each symbol having its usual meaning. It is interesting to note that the displacement of the pole for $n \geq 2$ is zero, this follows from the geometry of the displacement field. It can be seen that the differences involved are in the order of 8% compared with the theoretical values which is generally true for the first three modes. For the fourth mode the disagreement becomes more pronounced when the axisymmetric case is considered. It seems as if the finite element values for the fourth mode attempt to follow the trough-shaped variation of the third mode. This is somehow puzzling in view of the reasonable parity of all the lower modes. A hint of the

reduction in the normalised frequency value corresponding to n=1 also exists in an article by Zarghamee and Robinson[18]. Unfortunately the values published only contain the first mode, hence the findings of other workers in this field are welcome. The other interesting point is that the increase in the number of elements does not necessarily cause a reduction in the strain energy. In fact for an identical number of degrees of freedom, the lowest frequency would correspond to the highest order of the surplus displacements and not to the number of elements used to represent the mathematical model. It is evident from this example that the eigenvalues for the 2-element representation is lower than the corresponding results for the 3-element representation. This was owing to the fact that the surplus functions used for each of the two elements were $u(Q_0)$, $w(Q_0)$, $v(Q_0)$, $u(Q_1)$, $w(Q_1)$ and $v(Q_1)$, whereas the 3-element representation involved the first three of the above terms only (see Fig. 3.12 and Fig. 4.17). This statement is thought to be due to Melosh and has been extended later by Irons*. Where a division of the generator into two or three elements has become necessary, elements subtending equal azimuth angles have been used.

5.6.9 Natural Frequency of Cooling Towers

The last example here is the cooling tower which was stressed by Albasiny and Martin and has since become a classical example for both static and dynamic analysis (see Section 4.8.4). This is the 330 ft. high concrete tower with the throat radius and the top radius of 84 ft. and 87.4 ft. respectively for which a uniform shell thickness of 5.0 inches is assumed. Figure 5.13 lists the relevant details pertaining the shape and the constituent material of the shell. The existing methods of solution are as listed below,

---

* This point was made to the candidate on a number of occasions during private discussions with Professor Irons.

(a) numerical integration method developed by Carter, Robinson and Schnobrich[19],

(b) the finite difference method used by Hashish and Abu-Sitta[20],

(c) the finite element method applied recently by Sen and Gould[15].

The lowest calculated frequencly from all three methods coincides with the harmonic n=5. The agreement on all three methods is most favourable as can be seen from Fig. 5.13. In the last reference it was reported that for shell representation, a variable number of elements had to be used which increased with the increase in the number of diametral nodes. This appeared to necessitate more than a 100 per cent increase in the number of elements i.e. from 6 to 13. The latter is thought to correspond to 52 degrees of freedom. In the present work two geometrical representations of 3 and 5 unequal elements were used. The details of the element division in the latter case is already given in Fig. 4.16(a). The particulars of the position of the elements in the 3-element subdivision is indicated in Fig. 5.13. The Polytechnic IBM 1130 (16K) machine could only process the 3 element representation, since the present codification allowed a total of 28 degrees of freedom to be handled at any time. With the support conditions taken into account (u, w, v and $\frac{\partial w}{\partial s} = 0$ at the base) only two surplus displacements of $w(Q_0)$ and $v(Q_0)$ were allocated to the element positioned at the top of the tower. The 5-element representation was made to contain 3 surplus functions of $u(Q_0)$, $w(Q_0)$ and $v(Q_0)$ per element. This amounted to a total of 55 degrees of freedom which had to be referred elsewhere for processing*. The results obtained from both subdivisions are plotted for comparison against the above existing solutions. The need to increase the number of elements with the increase in harmonic was not felt here.

---

* The cooperation of the computer staff of the Mid-Glamorgan C.C. at Treasurer's Department is gratefully acknowledged.

Finally the results obtained for the first mode using just one element to represent the entire structure, is included for general interest (surplus displacements 2u, 2w and 2v, a total of 14 d.o.f.).

REFERENCES

1. A.E.H. LOVE
   "A Treatise on The Mathematical Theory of Elasticity", Dover Pub., New York, 1944, Chapter XII.
2. S.P. TIMOSHENKO AND D.H. YOUNG
   "Vibration Problems in Engineering", Van Nostrand, 3rd Edn. 1964.
3. G. NADEAU
   "Introduction to Elasticity", Holt, Rinehart and Winston Inc., New York, Chapter 10.
4. W. FLÜGGE
   "Handbook of Engineering Mechanics", McGraw-Hill, New York, 1962, Chapter 61.
5. G.B. WARBURTON
   "The Dynamical Behaviour of Structures", Pergamon Press, Oxford 1964, Chapter 6.
6. H. KRAUS
   "Thin Elastic Shells", J. Wiley and Sons Inc., New York 1967, Chapter 8.
7. O.C. ZIENKIEWICZ
   "The Finite Element Method in Engineering Science", McGraw-Hill Pub. Co. Ltd., England, 1971, Chapters 16 and 17.
8. R. DELPAK
   "Axisymmetric Vibrations of the Shells of Revolution by the Finite Element Method", University of Wales M.Sc. Thesis, 1968.
9. S.P. TIMOSHENKO AND D.H. YOUNG
   "Vibration Problems in Engineering", Van Nostrand, 3rd Edn. 1964.
10. E. REISSNER
    "On Transverse Vibrations of Thin Shallow Elastic Shells", Quarterly of Applied Maths, 13, 1955, 169-176.

11. H. GARNET, M.A. GOLDBERG AND V.L. SALERNO
"Torsional Vibration of a Shell of Revolution", Journal of Applied Mechanics, 28, 1961, 571-573.

12. R.N. ARNOLD AND G.B. WARBURTON
"Flexural Vibrations of the Walls of Thin Cylindrical Shells Having Freely Supported Ends", Proc. of Royal Soc. of Lond., 197, 1949, 238-256.

13. L.R. KOVAL AND E.T. CRANCH
"On the Free Vibrations of Thin Cylindrical Shells Subjected to an Initial Static Torque", Proceedings of the Fourth U.S. National Congress of Applied Mechanics, 1962, 107-117.

14. V.I. WEINGARTEN
"Free Vibrations of Thin Cylindrical Shells", Jour. of American Inst. of Aero. and Astro., Vol. 2, No. 4, 1964, 717-722.

15. S.K. SEN AND P.L. GOULD
"Free Vibrations of Shells of Revolution Using FEM", Journal of the Eng. Mech. Div., ASCE, 1974, 283-303.

16. V.I. WEINGARTEN
"Free Vibrations of Conical Shells", Jour. of the Eng. Mech. Div., ASCE, 1965, 69-87.

17. H. KRAUS
"Thin Elastic Shells", J. Wiley and Son Inc., New York, 1967, 237-331.

18. M.S. ZARGHAMEE AND A.R. ROBINSON
"A Numerical Method for Analysis of Free Vibration of Spherical Shells", Jour. Am. Inst. Aero and Astro, Vol. 5, No. 7, 1967, 1256-1261.

19. R.L. CARTER, A.R. ROBINSON AND W.C. SCHNOBRICH
"Free and Forced Vibrations of Hyperbolical Shells of Revolution", Structural Research Series No. 334, Civil Eng. Studies, Univ. Illinois, Urbana I 11. 1968.

20. M.G. HASHISH AND S.H. ABU-SITTA
"Free Vibrations of Hyperbolic Cooling Towers", Jour. Eng. Mech. Div., ASCE, 1971, 253-269.

"EIGEN-VALUE" ROUTINE, TEST:

Mode	Type	Exact ω	Finit.Elm ω	Error
1	Twist	920.08	920.08	.0001%
2	Hoop	1028.68	1028.68	.0006%
3	Longitudinal	807929	846947	4.83%

1 Element, Surplus 1u, 5w

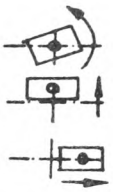

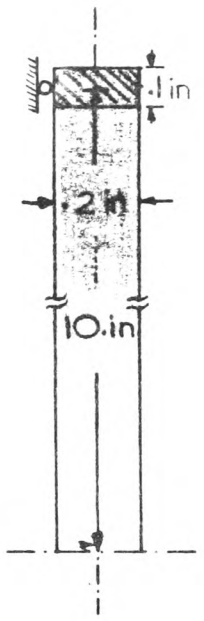

RING-BEAM, MODES OF VIBRATION

SKEW WASHER

Mode	Type	Exact ω	Finit.Elm. ω	Error
1	Twist	1212.32	1212.34	.0016%

1 Element, Surplus 1u, 5w

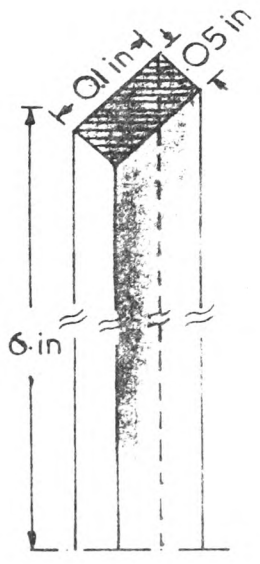

FIGURE 5.1

CIRCULAR PLATE

SIMPLY SUPPORTED

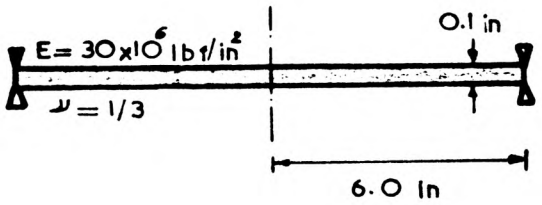

		Surplus no. of w displacement		
		1 w	2 w	3 w
1 element	ω	23.221	23.217	23.217
	error	—	—	—
2 elements	ω	23.217	23.217	23.217
	error	—	—	—

OTHER MODES

c = Number of nodal circles

Mode	Deflection pattern	ω Theoretical	ω Finite Elem. 2elem., 5w	error
c=0	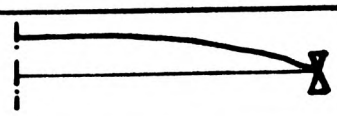	23.41 estimated	23.217	un-reliable
c=1		—	138.628	—
c=2	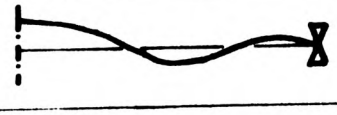	—	345.623	—
c=3		—	644.518	—

FIGURE 5.2

CIRCULAR PLATE
CENTRE CLAMPED

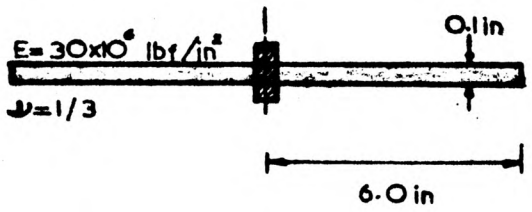

		Surplus no. of w-displacement		
		1 w	2 w	3 w
1 element	ω	32.744	32.564	32.470
	error	.90%	.40%	.10%
2 elements	ω	32.526	32.473	32.446
	error	.30%	.10%	.06%

OTHER MODES

c = Number of nodal circles

Mode	Deflection pattern	ω Theoretical	ω Finite elem. 2 elem., 5w	error
c=0	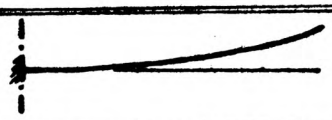	32.427	32.446	.06%
c=1	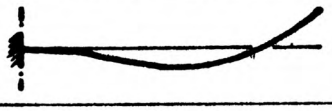	180.811	180.811	.003%
c=2	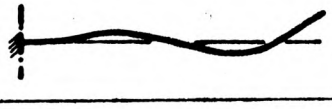	524.706	524.362	.06 %
c=3		1035.053	1035.525	.05 %

FIGURE 5·3

CIRCULAR PLATE
EDGE CLAMPED

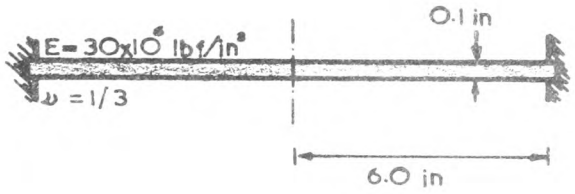

		Surplus no. of w-displacement		
		1 w	2 w	3 w
1 element	ω	88.455	88.331	88.330
	error	.17 %	.03 %	.03 %
2 elements	ω	88.331	88.330	88.330
	error	.03 %	.03 %	.03 %

OTHER MODES
c=Number of nodal circles

Mode	Deflection pattern	ω Theoret.	ω Finite elem. 2elem.,5w	error
c=0		88.306	88.330	.03 %
c=1		343.981	343.772	.06 %
c=2		768.772	769.783	.14 %
c=3		N.A.	1365.53	—

FIGURE 5-4

THIN CIRCULAR PLATE
SUMMARY OF HARMONICS AND MODES

nodal circle C	n=0		n=1		n=2		n=3	
	Th.	F.E.	Th.	F.E.	Th.	F.E.	Th.	F.E.
0	17.30	17.13	35.60	35.65	58.50	58.49	—	85.59
1	66.67	66.71	102.10	102.06	148.50	141.95	—	188.41
2	149.00	149.57	202.00	204.30	265.00	277.83	—	345.31
3	—	289.49	—	270.00	—	465.85	—	746.25

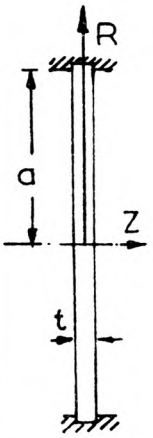

nodal circle C	n=0		n=1		n=2		n=3	
	Th.	F.E.	Th.	F.E.	Th.	F.E.	Th.	F.E.
0	6.295	6.333	—	3.402	8.80	8.81	20.50	20.496
1	35.09	35.32	34.40	37.90	50.10	59.10	88.60	88.73
2	112.00	102.29	100.22	107.24	—	141.61	—	190.55
3	200.00	202.88	—	210.66	—	279.88	—	350.72

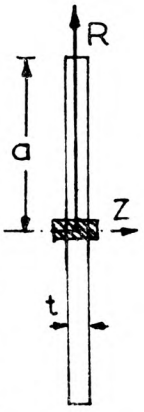

nodal circle C	n=0		n=1		n=2		n=3	
	Th.	F.E.	Th.	F.E.	Th.	F.E.	Th.	F.E.
0	8.4 *	8.358	—	23.37	—	43.02	—	67.07
1	—	49.91	—	81.36	—	117.73	—	159.91
2	—	124.52	—	174.40	—	233.54	—	289.66
3	—	242.54	—	270.02	—	413.09	—	468.63

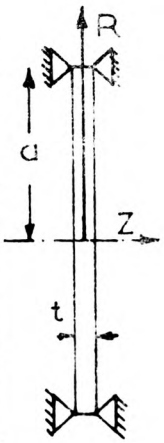

* — See text
— Not available

$a = 6.0$ $E = 30 \times 10^6$
$t = 0.1$ $\nu = 1/3$
$\rho = 1.0$

FIGURE 5.5

GENERAL VIBRATIONS OF A LONG CYLINDER

L=100. E=10x10^6
a=5.0 ν=0.25
T=0.1 ρ=1.0

$\omega_m = \frac{(2m-1)\pi}{2L}\sqrt{\frac{E}{\rho}}$ Longitudinal

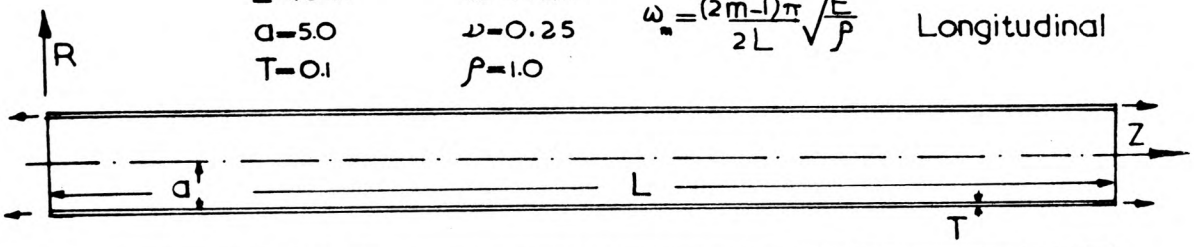

mode	1			2			3			4		
	Th.	F.E.	ε%	Th.	F.E.	ε%	Th.	F.E.	ε%	Th.	F.E.	ε%
	49.67	49.66	.02	149.02	148.74	0.2	248.36	247.33	0.4	347.71	351.77	1.2

L=100. G=4x10^6
a=5.0 ν=0.25
T=0.1 ρ=1.0

$\omega_m = \frac{(2m-1)\pi}{2L}\sqrt{\frac{G}{\rho}}$ Torsional

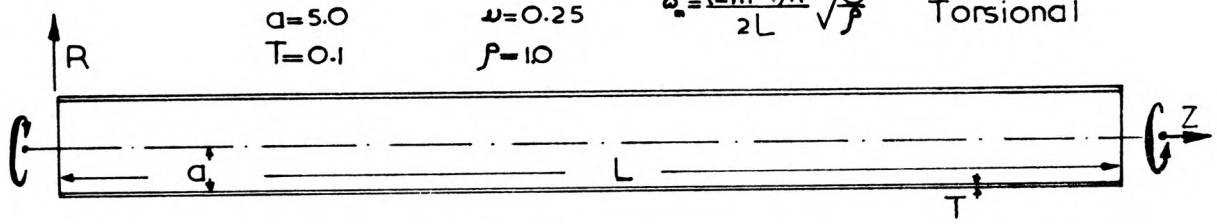

mode	1			2			3			4		
	Th.	F.E.	ε%	Th.	F.E.	ε%	Th.	F.E.	ε%	Th.	F.E.	ε%
	31.415	31.418	—	94.24	94.25	—	157.07	157.09	—	219.911	220.10	0.1

L=100. E=10x10^6
a=5.0 ν=0.25
T=0.1 ρ=1.0

$\omega_m = \left(\frac{m\pi}{L}\right)^2\sqrt{\frac{EI}{\rho A}}$ Flexural

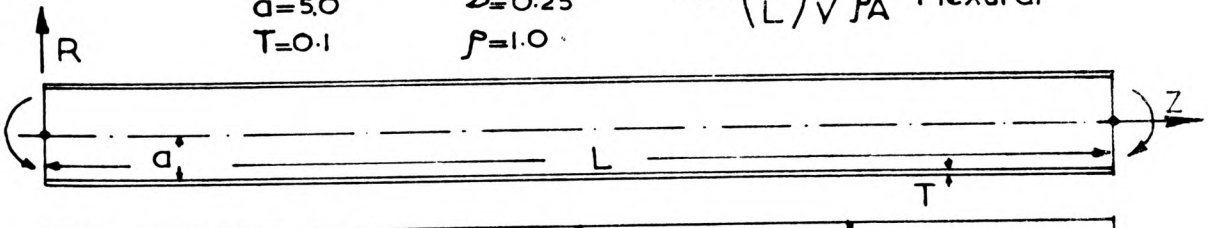

mode	1			2			3			4		
	Th.	F.E.	ε%	Th.	F.E.	ε%	Th.	F.E.	ε%	Th.	F.E.	ε%
	11.03	10.68	3.0	44.13	39.48	10.5	99.31	91.66	7.7	176.55	175.25	0.7

FIGURE 5.6

VIBRATING HEMISPHERE (ROLLERS SUPPORTED)

MODE=1

TYPE : HOOP(RADIAL)

ω_{exact}=2898.003

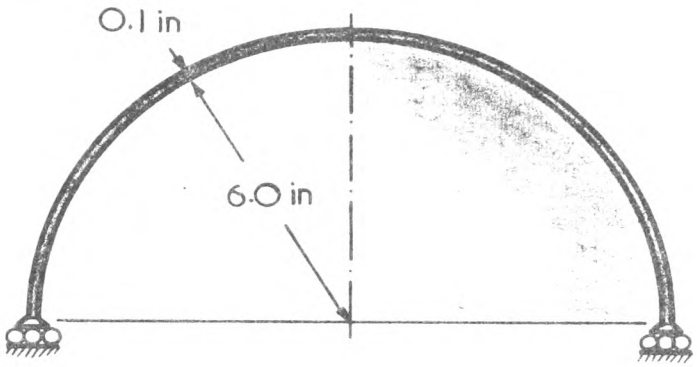

All,5 Surplus w

Elm.No.	ω Finite Elem.	Error
1	2938.039	1.38 %
2	2896.287	.059 %
3	2897.301	.024%

SPHERICAL CAP (EDGE CLAMPED)

ω_{exact} = 495.510 rad/sec
(FROM REISSNER)

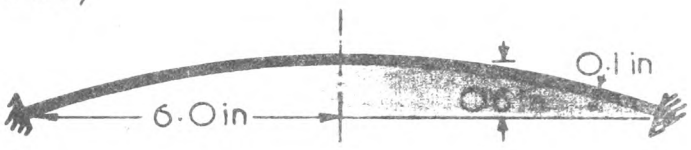

		Surplus No. Of Degrees Of Freedom				
w-Displace.		1	2	3	4	5
1 Elem.	ω	467.15	443.77	443.37	443.32	443.29
	%Error	7.35	2.25	2.20	2.15	2.15
2 Elem.	ω	432.01	431.38	431.37	431.37	431.37
	%Error	-0.62	-0.77	-0.77	-0.77	-0.77

Mode=1

Type: Bending

FIGURE 5.7

TRUNCATED CONE

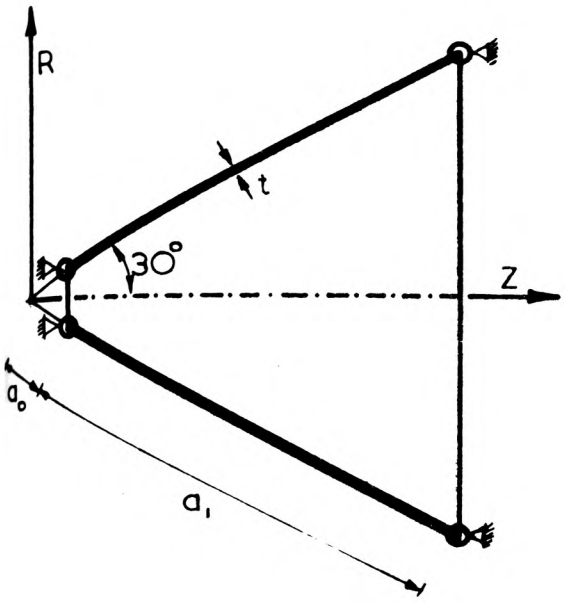

$a_0 = 1$
$a_1 = 10$
$t = 0.01$
$\eta = \frac{a_1}{a_0} = 10$
$\rho = 1$
$G = 1$
$\nu = 0.25$
$\lambda = \sqrt{\rho/G} = 1$

$\psi \rightarrow$ from tables

$\omega = \psi/(a_0 \lambda)$

$\omega = \frac{\psi}{a_0}\sqrt{\frac{G}{\rho}}$

1 ELEMENT

	Exact	SURPLUS DEGREES OF FREEDOM						
		—	1 v	2 v	3 v	4 v	5 v	
Mode 1	0.39409	0.39462	0.39426	0.39419	0.39412	0.39410	0.39409	ω Htz.
	error %	0.1346	0.0432	0.0252	0.0077	0.0026	0.0000	
Mode 2	0.73306	0.76176	0.74172	0.73342	0.73336	0.73308	0.73305	
	error %	3.9151	1.1814	0.0491	0.0410	0.0028	-0.0014	
Mode 3	1.07483	*	1.15667	1.11281	1.07765	1.07625	1.07489	
	error %	—	7.6143	3.5336	0.2624	0.1322	0.0056	
Mode 4	1.41886	*	*	1.60034	1.52036	1.42996	1.42449	
	error %	—	—	12.7906	7.1537	0.7842	0.3968	

* - choice of displacements not compatible with the mode

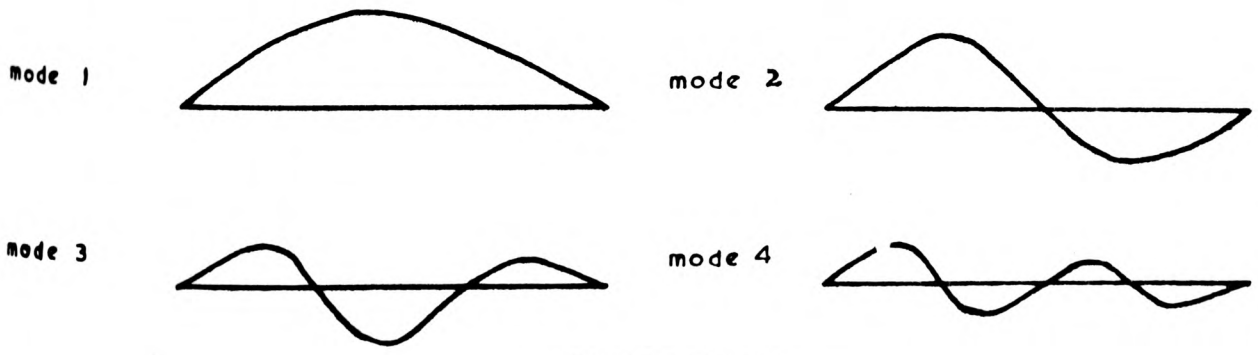

FIGURE 5.8

HEMISPHERE IN TORSION

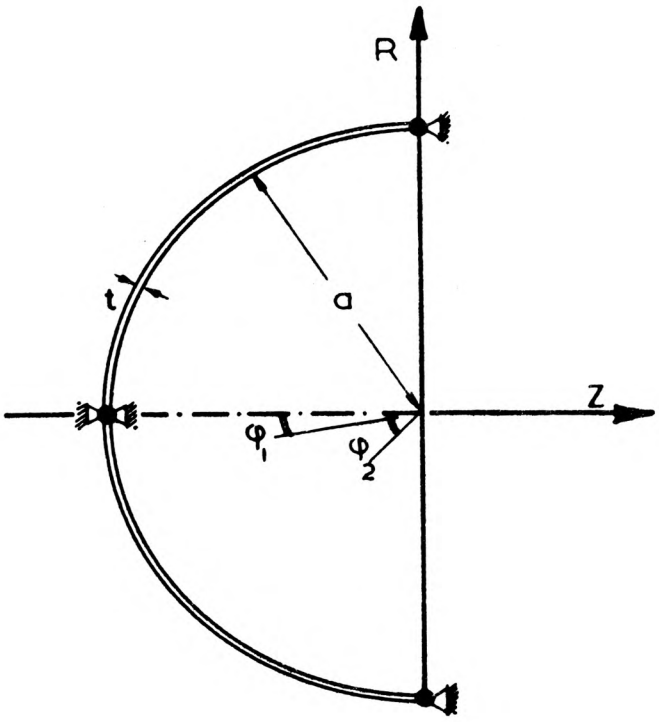

$a = 10.$
$t = 0.1$
$\rho = 1.$
$G = 1.$

GENERAL FORMULA:

$$\omega = \frac{2i}{(\varphi_2 - \varphi_1)R}\sqrt{\frac{G}{\rho}}$$

$\omega = 0.2$ Htz
$\omega_1 = 0.4$ "
$\omega_2 = 0.6$ "
$\omega_4 = 0.8$ "

% error

	MODE	SURPLUS D.O.F.					
		0v	1v	2v	3v	4v	5v
1 elemt. 90°	1	2.25	1.75	1.75	1.75	1.75	1.75
	2	9.75	9.35	6.84	6.83	6.80	6.80
	3	*	12.93	12.03	6.37	6.35	6.16
	4	*	*	17.24	15.75	6.01	5.90
2 elemt. 45° each	1	0.050	0.015	0.015	0.015	0.015	0.015
	2	6.79	6.18	6.18	6.18	6.18	6.18
	3	7.73	5.72	5.49	5.49	5.49	5.49
	4	7.90	7.57	4.66	4.66	4.63	4.63
3 elemt. 30° each	1	0.006	0.005	0.005	0.005	0.005	0.005
	2	6.11	6.08	6.08	6.08	6.08	6.08
	3	6.07	5.43	5.43	5.43	5.43	5.43
	4	5.87	4.72	4.59	4.59	4.59	4.59

*- choice of displacements not compatible with mode

FIGURE 5.9

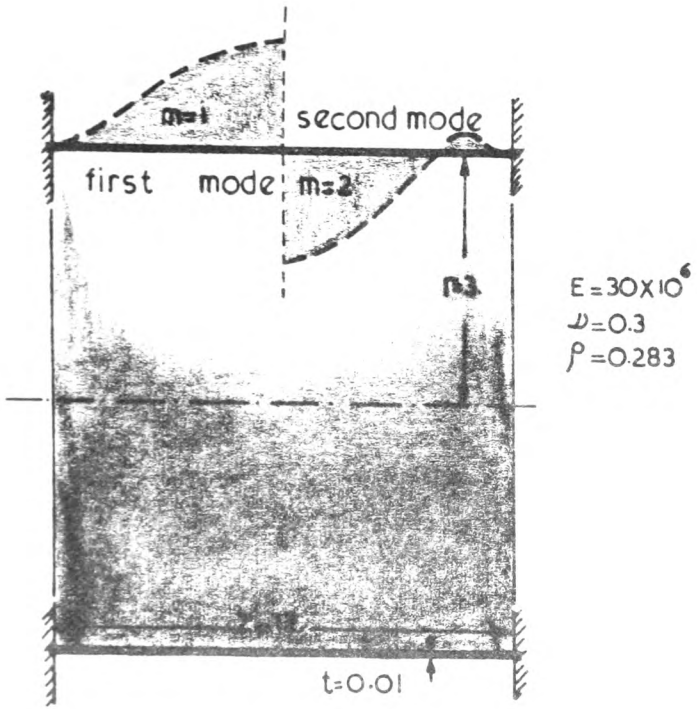

$E = 30 \times 10^6$
$\nu = 0.3$
$\rho = 0.283$

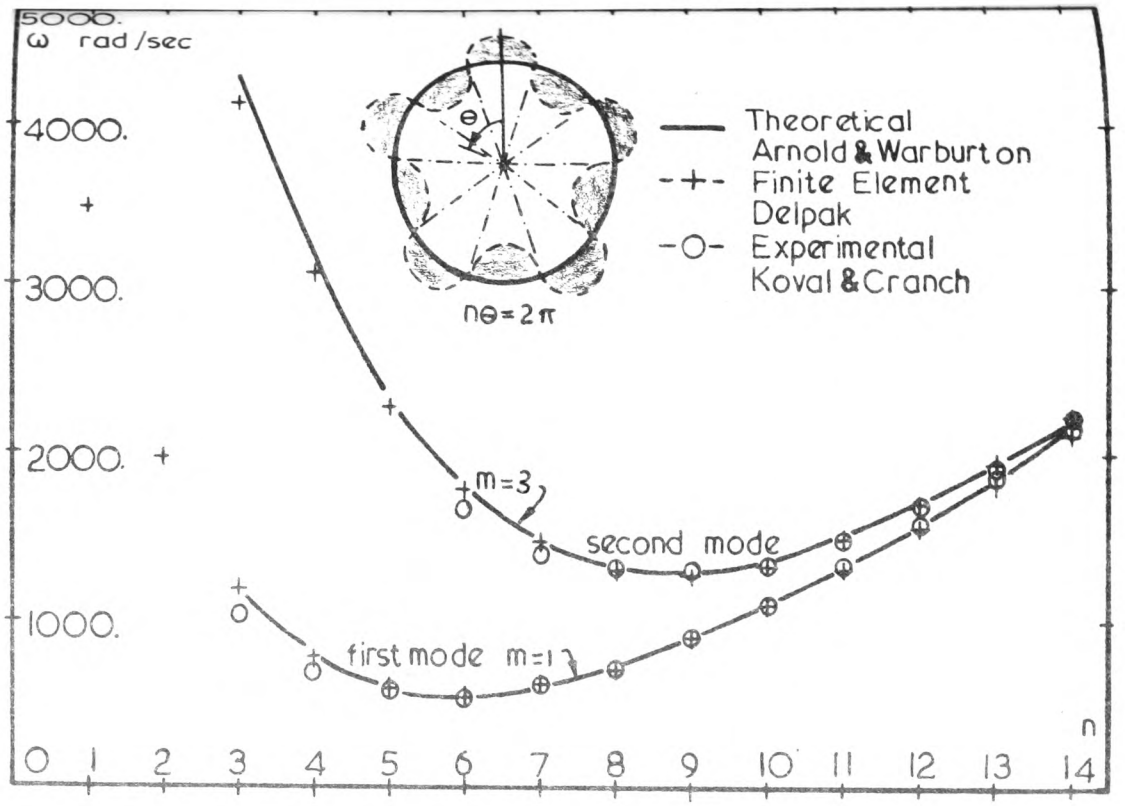

Angular Velocity ω rad/sec

n		0	1	2	3	4	5	6	7	8	9	10	11	12	13	14
m=1	Th.	—	—	—	1176.	783.	597.	552.	611	736.	902.	1100.	1321.	1568.	1837.	2128.
	F.E.	10510.	3467.	1964.	1186.	782.	587.	538.	595.	720.	886.	1084.	1307.	1554.	1823.	2115.
m=2	Th.	—	—	—	4350.	3139.	2342.	1823.	1503.	1338.	1302.	1369.	1512.	1710.	1950.	2224.
	F.E.	10677.	8571.	5944.	4160.	3009.	2254.	1762.	1458.	1303.	1274.	1345.	1491.	1690.	1932.	2206

FIGURE 5.10

THIN CONICAL FRUSTUM

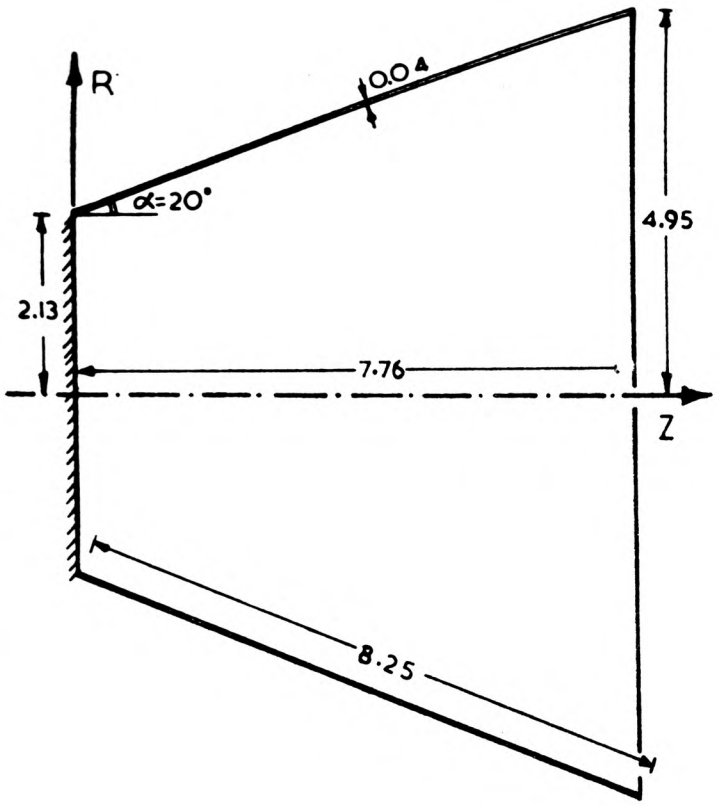

$E = 30 \times 10^6$ lbf/in^2

$\nu = 0.3$

$\frac{\rho}{g} = 0.0206$ lbf·sec^2/in^4

All measurments are in inches.

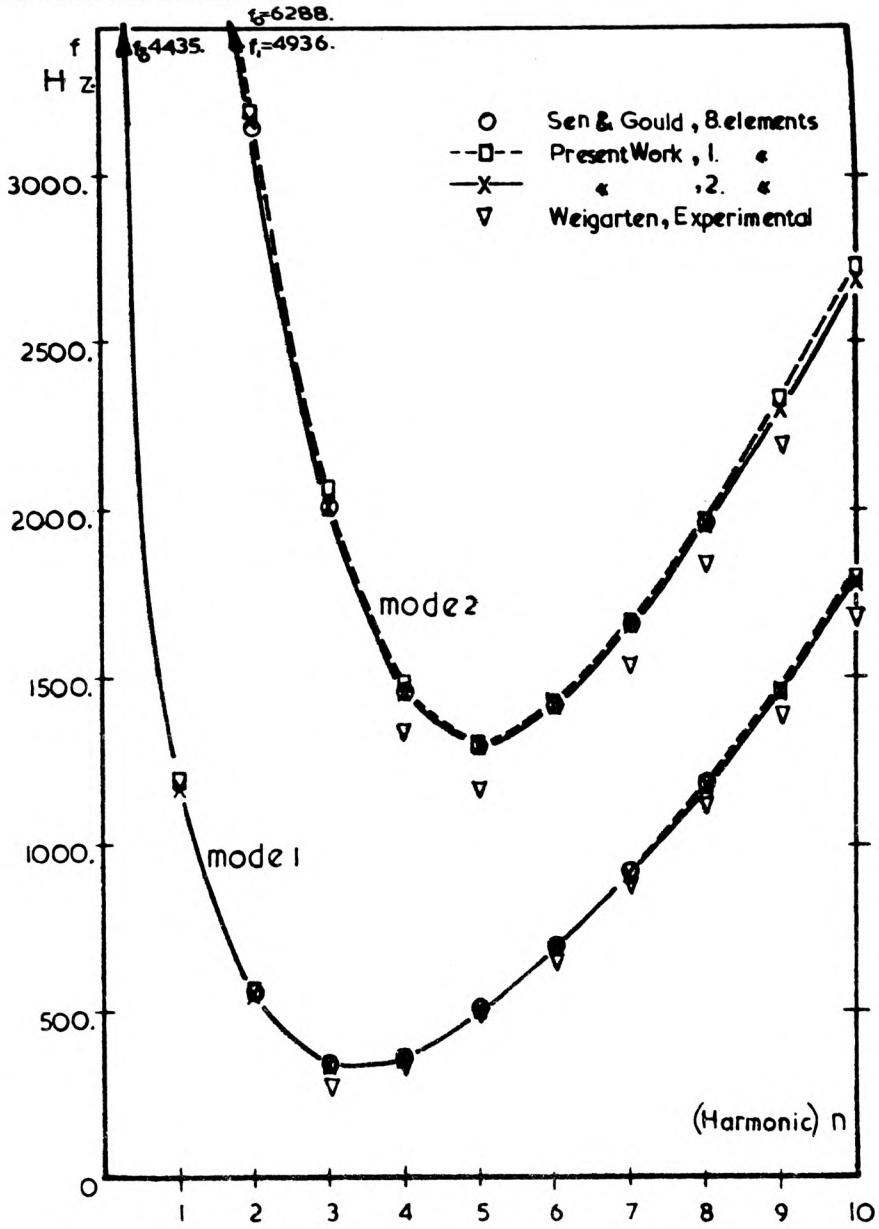

FIGURE 5.11

VIBRATIONS OF A SPHERICAL CAP

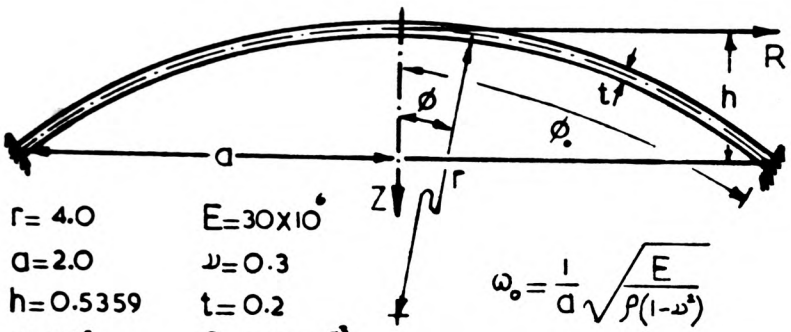

r = 4.0 E = 30×10⁶
a = 2.0 ν = 0.3
h = 0.5359 t = 0.2
ø. = 30° ρ = 0.763×10⁻³

$$\omega_0 = \frac{1}{a}\sqrt{\frac{E}{\rho(1-\nu^2)}}$$

	no. F.E.	d.o.f.	n = 0	n = 1	n = 2	n = 3	n = 4
mode 1	—	Th.	0.7515	0.8195	1.1680	1.6220	—
	1	14	0.7299	0.6653	1.0880	1.5070	1.9453
	2	26	0.7540	0.7620	1.0790	1.4910	1.9091
	3	26	0.7438	0.7586	1.0790	1.4960	1.9189
mode 2	—	Th.	1.331	1.852	2.589	3.383	—
	1	14	1.224	1.602	2.445	3.977	4.629
	2	26	1.206	1.693	2.367	3.098	3.743
	3	26	1.224	1.704	2.390	3.196	3.943
mode 3	—	Th.	2.376	2.151	3.230	4.173	—
	1	14	2.491	2.109	3.107	4.141	5.863
	2	26	2.494	2.013	3.056	3.980	4.596
	3	26	2.489	2.034	3.096	4.012	4.610
mode 4	—	Th.	2.737	3.334	4.288	5.273	—
	1	14	3.858	3.122	4.111	5.097	6.498
	2	26	3.779	3.217	4.106	5.084	5.795
	3	26	3.849	3.165	4.108	5.088	5.804

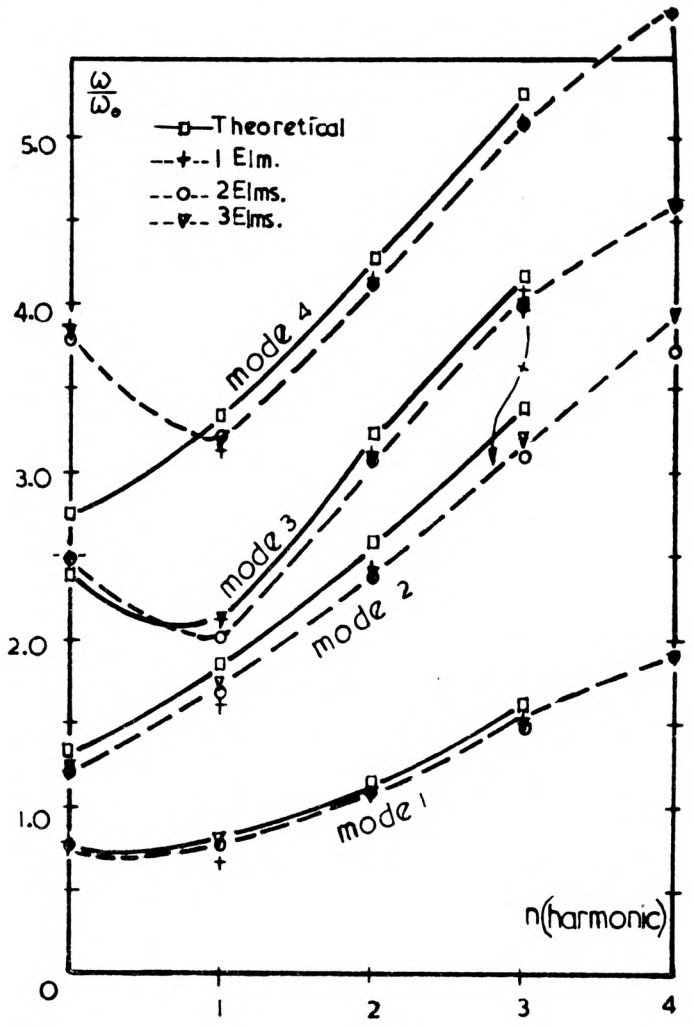

FIGURE 5.12

NATURAL FREQUENCY OF COOLING TOWERS

$t = 0.41667$ ft

$E = 432 \times 10^6$ lbf/ft^2

$\nu = 0.15$

$\rho = \frac{\gamma}{g} = 12.44$ lbf.sec^2/ft^4

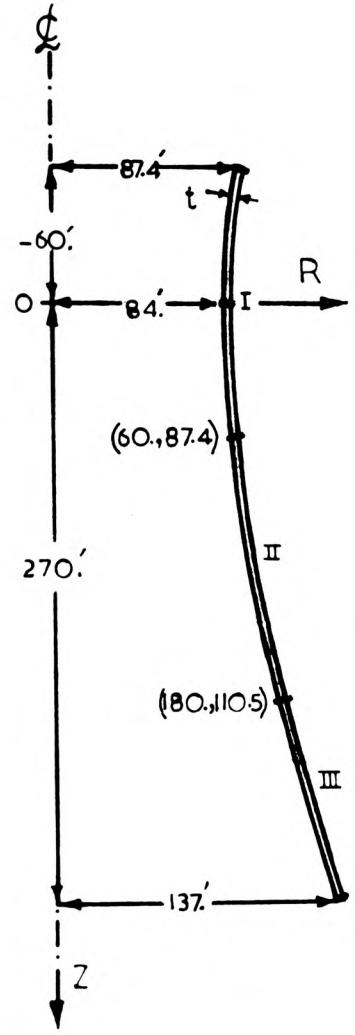

Frequency Htz.

harmonic n		mode 1	mode 2	mode 3
0	A	8·1500	11·3799	11·8257
	C	7·7494	11·4166	11·9022
	D 3	7·2066	11·5660	12·2697
	D 5	7·6599	11·5236	12·1138
	G	7·7583	11·4817	12·0747
1	A	3·3345	6·8816	10·5316
	C	3·2884	6·7405	10·5207
	D 3	3·3102	6·8143	10·7552
	D 5	3·3040	6·8130	10·5540
	G	3·2910	6·8176	10·6666
2	A	1·7848	3·7234	6·9553
	C	1·7654	3·6931	6·9562
	D 3	1·7854	3·7930	6·9936
	D 5	1·7750	3·7340	7·0440
	G	1·7662	3·6960	7·0058
3	A	1·3929	2·0150	4·3353
	C	1·3749	1·9904	4·3254
	D 3	1·3658	2·1160	4·4242
	D 5	1·3791	2·0608	4·4677
	G	—	—	—
4	A	1·2003	1·4597	2·7762
	C	1·1808	1·4475	2·7777
	D 3	1·2949	1·4208	2·8959
	D 5	1·2761	1·4583	2·9481
	G	1·1820	1·4491	2·7866
5	A	1·0441	1·4417	2·0555
	C	1·0348	1·4293	2·0558
	D 3	1·0919	1·5482	2·0230
	D 5	1·1983	1·5310	2·2155
	G	1·0354	1·4345	2·0640
6	A	1·1544	1·3335	2·0152
	C	1·1467	1·3231	2·0141
	D 3	1·1391	1·5838	1·8068
	D 5	1·3865	1·6394	2·1347
	G	—	—	—
7	A	1·3055	1·5189	1·9200
	C	1·3014	1·5133	1·9217
	D 3	1·3243	1·5180	2·0605
	D 5	1·6236	1·9261	2·3040
	G	—	—	—
8	A	—	—	—
	C	—	—	—
	D 3	1·4952	1·7721	2·1771
	D 5	1·8582	2·3529	2·6155
	G	—	—	—

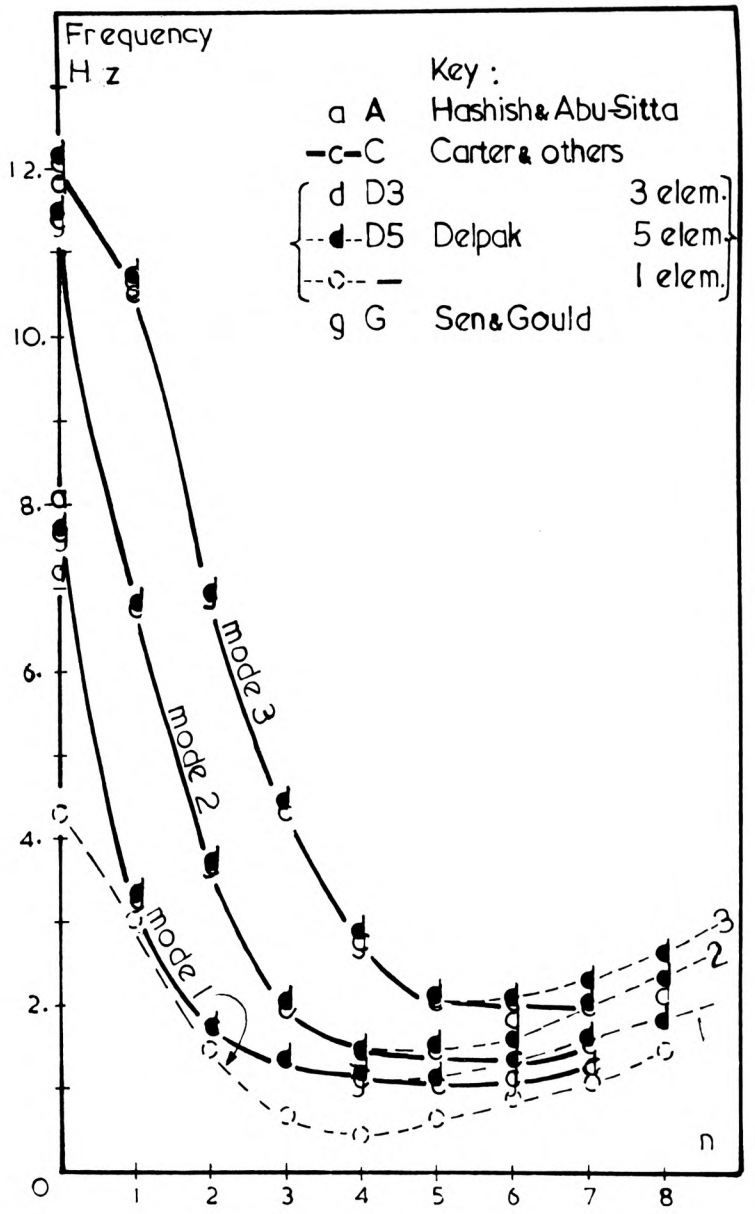

FIGURE 5·13

CHAPTER 6

BUCKLING OF THIN ELASTIC SHELLS OF REVOLUTION

6.1 INTRODUCTION

The problem of structural failure owing to excessive geometrical changes under load has been observed over a long period of engineering history. Euler and others have contributed a great deal to the estimation of the failure load in certain idealised cases. With the recent increase in the use of light weight and aesthetically pleasing structures more complicated geometries are used which are not particularly conducive to simple analytical methods.

6.2 METHODS OF ANALYSIS

There are two major non-experimental methods of estimating the buckling load.

6.2.1 Exact Method

This method consists of forming the differential equation of equilibrium for an infinitesimal element in which the external pressures on the deformed element are related to internal stresses arising from total strains. Eliminations and simplifications are made where possible by neglecting insignificant terms. Normally change of variables are made to reduce the differential equation to a familiar or a standard form which often results in a non-dimensional argument. The above equation could have a solution in the form of infinite series (with possible complex terms) or be in the form of transcendental functions resulting in iterative or graphical solutions. Prior to determining the actual roots, boundary conditions must be satisfied. It is customary to prepare charts or tables to allow for differing geometrical

and elastic parameters. The magnitude of the factors causing buckling are then calculated or read-off from the above facilities. Ample examples of these facilities can be found in Ref. (1) and (2) the preparation of which have no doubt involved arduous calculations.

6.2.2 Numerical Method

The derivation of the equations leading to the final relationships used in calculating the buckling loads can be obtained independently using either the energy method or the virtual work principle. In both cases the outcome is identical. In this scheme of research the virtual work interpretation will be adopted where required.

All relevant relationships have been derived in reference (3) and therefore only the nomenclature of the items involved with their specialised application to thin shells of revolution will be outlined. Let the displacements and strains be defined in the manner indicated in Chapters 1 and 3 by,

$$\{u\} = [N]\{\delta\}$$

and

$$\{\varepsilon\} = [B]\{\delta\}$$

respectively. Let $[G]$ define an operator so that,

$$\{\Theta\} = [G]\{\delta\},$$

where $\{\Theta\}^T$ is the listing of all such terms as $\{\frac{\partial u}{\partial s}, \frac{\partial u}{R\partial\theta}, \ldots.\}$. The stiffness and mass matrices have also been given in Chapters 1, 3 and 5 as

$$[K] = \int_V [B]^T[D][B]\,d(vol) \text{ and } [M] = \int_V [N]^T[\rho][N]\,d(vol),$$

where all the symbols have been previously defined. The geometric matrix

$[K_\sigma]$ is similarly defined by the following integral,

$$[K_\sigma] = \int_A [G]^T [T] [G] dA, \qquad \ldots\ldots \text{ eqn. 6.1}$$

The matrix $[T]$ is a square symmetrical matrix containing the in-plane stresses T_s, T_θ and $T_{s\theta}$. The actual appearance of this matrix will be given later in the text. The elements of the geometric matrix $[K_\sigma]$, being proportional to the initial stress system $[T]$, are variables, thus the magnitude λ of the load system whose inplane stresses $[T]$ cause structural buckling is given by,

$$\left([K] + \lambda[K_\sigma]\right)\{\delta\} = 0. \qquad \ldots\ldots \text{ eqn. 6.2}$$

This clearly is an eigen-value problem the approach to and the solution of which is similar to that shown in Chapter 5 (Section 5.2).

6.3 DERIVATION OF [G] MATRIX

It is shown in Reference[3] that the strains involved in an analysis of this kind consist of linear and second order terms. An example of the cartesian representation of two such components of strain was given in the above reference. Other expressions for second order strains may contain certain simplifications or modifications suited for the use of different researchers. It was thus thought appropriate to turn to the original expressions given by Love[4] in order to avoid any possible loss of relevant terms. The strains will then be expressed in cylindrical coordinates and the accuracy of the retained terms will be consistent with the general algorithm adopted in the text.

6.3.1 General Derivation

The total strains are given in page 520 of reference (4) as,

$$\left.\begin{aligned} 1 + 2\varepsilon_1 &= \frac{1}{A^2}\left\{\left(\frac{\partial X}{\partial \alpha}\right)^2 + \left(\frac{\partial Y}{\partial \alpha}\right)^2 + \left(\frac{\partial Z}{\partial \alpha}\right)^2\right\} \\ 1 + 2\varepsilon_2 &= \frac{1}{B^2}\left\{\left(\frac{\partial X}{\partial \beta}\right)^2 + \left(\frac{\partial Y}{\partial \beta}\right)^2 + \left(\frac{\partial Z}{\partial \beta}\right)^2\right\} \\ \varepsilon_{12} &= \frac{1}{AB}\left\{\frac{\partial X}{\partial \alpha}\cdot\frac{\partial X}{\partial \beta} + \frac{\partial Y}{\partial \alpha}\cdot\frac{\partial Y}{\partial \beta} + \frac{\partial Z}{\partial \alpha}\cdot\frac{\partial Z}{\partial \beta}\right\} \end{aligned}\right\} \quad \ldots\ldots \text{ eqn. 6.3}$$

where

$$\left.\begin{aligned} &\frac{\partial X}{\partial \alpha} = A + \frac{\partial u}{\partial \alpha} + \frac{v}{B}\frac{\partial A}{\partial \beta} + \frac{Aw}{R_1}, \quad \frac{\partial Y}{\partial \alpha} = \frac{\partial v}{\partial \alpha} - \frac{u}{B}\frac{\partial A}{\partial \beta}, \quad \frac{\partial Z}{\partial \alpha} = -\frac{\partial w}{\partial \alpha} + \frac{Au}{R_1}, \\ &\frac{\partial X}{\partial \beta} = \frac{\partial u}{\partial \beta} - \frac{v}{A}\frac{\partial \beta}{\partial \alpha}, \quad \frac{\partial Y}{\partial \beta} = B + \frac{\partial v}{\partial \beta} + \frac{u}{A}\frac{\partial B}{\partial \alpha} + \frac{Bw}{R_2}, \quad \frac{\partial Z}{\partial \beta} = -\frac{\partial w}{\partial \alpha} + \frac{Bv}{R_2} \end{aligned}\right\} \quad \ldots\ldots \text{ eqn. 6.4}$$

Parameters α and β are fictitious lines scribed on the original surface and X,Y,Z could be regarded as the new coordinates of a given point on the shell after the load is applied. If relevant expressions of equation 6.4 were to be substituted in one of the relationships of eqn. 6.3 e.g. the first, the total strain would appear as,

$$\varepsilon_1 = \frac{1}{A}\frac{\partial u}{\partial \alpha} + \frac{v}{AB}\frac{\partial A}{\partial \beta} + \frac{w}{R_1} + \frac{1}{2A^2}\left\{\left(\frac{\partial u}{\partial \alpha} + \frac{v}{B}\frac{\partial A}{\partial \beta} + \frac{Aw}{R_1}\right)^2 + \left(\frac{\partial Y}{\partial \alpha}\right)^2 + \left(\frac{\partial Z}{\partial \alpha}\right)^2\right\}$$

$\ldots\ldots$ eqn. 6.5

It is clear that eqn. 6.5 is the general expression for linear and second order strains offering an obvious separation of terms. It is now proposed to examine a new "primed" (dashed) system in order to obtain the second order strains directly without undue expansion and partition of the terms of different order, thus,

$$\left.\begin{aligned} \frac{\partial X'}{\partial s} &= \frac{\partial X}{\partial s} - 1 \;, \quad \frac{\partial Y'}{\partial s} = \frac{\partial Y}{\partial s} \;, \quad \frac{\partial Z'}{\partial s} = \frac{\partial Z}{\partial s} \;, \\ \frac{\partial X'}{R\partial\theta} &= \frac{\partial X}{R\partial\theta} \;, \quad \frac{\partial Y'}{R\partial\theta} = \frac{\partial Y}{R\partial\theta} - 1 \;, \quad \frac{\partial Z'}{R\partial\theta} = \frac{\partial Z}{R\partial\theta} \;, \end{aligned}\right\} \quad \ldots\ldots \text{ eqn. 6.6}$$

where variables s, R and θ replace the curvilinear parameters α and β in accordance with the rules discussed in Chapter 2.

Using the primed system, the pure second order strains could then be expressed in a scalar product form. For example ε_1 quoted above would appear as,

$$(\varepsilon_1) \equiv (\varepsilon_s) = \frac{1}{2}\left[\frac{\partial X'}{\partial s} \quad \frac{\partial Y'}{\partial s} \quad \frac{\partial Z'}{\partial s}\right] \begin{Bmatrix} \frac{\partial X'}{\partial s} \\ \frac{\partial Y'}{\partial s} \\ \frac{\partial Z'}{\partial s} \end{Bmatrix} .$$

Upon comparison of the above expression and eqn. 19.36 of reference (3) it can be seen that,

$$\{\Theta_s\}^T = \left[\frac{\partial X'}{\partial s} \quad \frac{\partial Y'}{\partial s} \quad \frac{\partial Z'}{\partial s}\right] ,$$

and similarly,

$$\{\Theta_\theta\}^T = \left[\frac{\partial X'}{R\partial\theta} \quad \frac{\partial Y'}{R\partial\theta} \quad \frac{\partial Z'}{R\partial\theta}\right] ,$$

therefore quite generally,

$$\{\Theta\}^T = \left[\frac{\partial X'}{\partial s} \;, \frac{\partial Y'}{\partial s} \;, \ldots\ldots \frac{\partial Z'}{R\partial\theta}\right]. \quad \ldots\ldots \text{ eqn. 6.7}$$

6.3.2 Simplification for Axisymmetric Shells

It is important to re-establish the convention of Chapter 2 briefly in view of the apparently small change in notation between Love[4] and Novozhilov (Section 2.2), i.e.,

$$\alpha = \alpha_1, \quad \beta = \alpha_2 \;, \quad A = A_1 \text{ and } B = A_2,$$

there is also a reversed sign convention for w-displacements. Without further justifications the following substitutions are made,

$$\left.\begin{aligned} &\frac{1}{A}\frac{\partial}{\partial\alpha}(\ldots) = \frac{\partial}{\partial s}(\ldots),\ \frac{1}{B}\frac{\partial}{\partial\beta}(\ldots) = \frac{1}{R}\frac{\partial}{\partial\theta}(\ldots), \\ &\frac{1}{B}\frac{\partial A}{\partial\beta} = \frac{1}{R}\frac{\partial R_1}{\partial\theta} = 0,\ \frac{1}{A}\frac{\partial B}{\partial\alpha} = \frac{\partial R}{\partial s} = \cos\alpha \quad \text{and} \quad \frac{B}{R_2} = \sin\alpha\ . \end{aligned}\right\} \quad \ldots\ldots \text{ eqn. 6.8}$$

Again if the shell were to have no abrupt change in geometry, namely $\frac{1}{R_1}$ was quite small, then all products of $\frac{1}{R_1}$ could be neglected.

Substituting the terms of eqn. 6.4 into the primed system of eqn. 6.6 and the modifications of relationship shown in eqn. 6.8, the following expressions are obtained,

$$\left.\begin{aligned} &\frac{\partial X'}{\partial s} = \frac{\partial u}{\partial s}\ , \\ &\frac{\partial X'}{R\partial\theta} = \frac{\partial u}{R\partial\theta} - \frac{\sin\alpha}{R}\,v, \\ &\frac{\partial Y'}{\partial s} = \frac{\partial v}{\partial s}\ , \\ &\frac{\partial Y'}{R\partial\theta} = \frac{\partial v}{R\partial\theta} + \frac{\sin\alpha}{R}\,.\,w + \frac{\cos\alpha}{R}\,u, \\ &\frac{\partial Z'}{\partial s} = -\frac{\partial w}{\partial s}\ , \\ &\frac{\partial Z'}{R\partial\theta} = \frac{\cos\alpha}{R}\,v - \frac{\partial w}{R\partial\theta}\ . \end{aligned}\right\} \quad \ldots\ldots \text{ eqn. 6.9}$$

It is desirable that the displacement processed should be in the global coordinates given in Sections 2.5 and 3.5.4. Incorporating the rotation of axes with the set of displacements given by eqn. 4.3, the matrix $[G]$ will then be given in its final form as,

$$[G]\{\delta\} = \begin{bmatrix} (\cos\alpha\frac{\partial}{\partial s} & \sin\alpha\frac{\partial}{\partial\alpha} & 0 &) \cos n\theta \\ (-\frac{n\cos\alpha}{R} & -\frac{nw}{R}\sin\alpha & -\frac{\sin\alpha}{R} &) \sin n\theta \\ (0 & 0 & \frac{\partial}{\partial s} &) \sin n\theta \\ (0 & \frac{1}{R} & \frac{n}{R} &) \cos n\theta \\ (\sin\alpha\frac{\partial}{\partial s} & -\cos\alpha\frac{\partial}{\partial s} & 0 &) \cos n\theta \\ (-\frac{n\sin\alpha}{R} & \frac{n\cos\alpha}{R} & \frac{\cos\alpha}{R} &) \sin n\theta \end{bmatrix} \begin{Bmatrix} u \\ w \\ v \end{Bmatrix}_{global} \quad \ldots\ldots \text{ eqn. 6.10}$$

The factors $\cos n\theta$ and $\sin n\theta$ displayed above belong to displacements of θ-symmetric set (eqn. 4.3(a)). If the asymmetric displacements were required, then factors $\cos n\theta$ and $\sin n\theta$ could be considered as being interchanged but an appropriate change must also be made in the sign of "n" the harmonic integer. This arises from the operator $(\frac{\partial}{\partial\theta})$ in the kinematic equations.

6.4 INPLANE STRESS RESULTANT [T]

As can be seen from eqn. 6.1, the matrix [T] fulfils the same role as the matrices [D] and [ρ] in the formation of the appropriate integrals. The manipulation of matrix [T] is normally fairly simple but a case could arise where a more complicated analysis would be needed. In practice there are restrictions in the use of the scalar,

$$\{\delta\}^T[G]^T[T][G]\{\delta\} \quad ,$$

which involves a detailed study of trignometric terms associated which in turn is a peculiarity of the Geometric Matrix only. The elastic matrix [D] and the density matrix [ρ] were dependent on physical isotropy and homogeneity of the constituent material of the shell which is independent of any external factors and therefore free of any artificial set of coordinates. On the other hand the stress matrix [T] depends

on the manner of loading and is therefore "orientation" conscious and in reality should appear either as

$$\begin{bmatrix} T_s \cos n\theta & T_{s\theta} \sin n\theta \\ T_{s\theta} \sin n\theta & T_\theta \cos n\theta \end{bmatrix}$$

or

$$\begin{bmatrix} T_s \sin n\theta & T_{s\theta} \cos n\theta \\ T_{s\theta} \cos n\theta & T_\theta \sin n\theta \end{bmatrix},$$

which has the obvious implied simplifications when n=0. Thus upon integrating the (i,j)-th element of the geometric matrix from the terms

$$\begin{aligned} [G_i] &= [G_{i1} \cos i\theta + G_{i2} \sin i\theta] \\ [G_j] &= [G_{j1} \cos j\theta + G_{j2} \sin j\theta] \end{aligned}$$

the following equation results

$$[K_\sigma]_{ij} = \int [G_{i1}\cos i\theta + G_{i2}\sin i\theta]_k^T [T]_{k\ell} [G_{j1}\cos j\theta + G_{j2}\sin j\theta]_\ell \, dA.$$

Carrying out the multiplication to the full, the following products are obtained.

cosiθ cosnθ cosjθ , siniθ sinnθ cosjθ

siniθ cosnθ sinjθ , cosiθ sinnθ sinjθ

siniθ cosnθ sinjθ , cosiθ sinnθ sinjθ

siniθ sinnθ cosjθ , cosiθ cosnθ cosjθ

cosiθ cosnθ cosjθ , siniθ sinnθ cosjθ

siniθ cosnθ sinjθ , cosiθ sinnθ sinjθ

which basically are the products of the following,

* 3 cosines,

\+ 3 sines,

\+ 2 cosines x 1 sine,

* 1 cosine x 2 sines.

Using simple rules of trigonometry these could be reduced to a simple product such as,

* cosine (sum or difference) x cosine,

\+ cosine (sum or difference) x sine,

\+ sine (sum or difference) x cosine,

* sine (sum or difference) x sine,

which in tern would result in either of the following terms,

\+ sin (sum or difference)

* cosine (sum or difference).

Both integrals would vanish identically when integrated from 0, 2π except for the latter term (i.e. *) when (sum or difference) = 0. In practice the following cases arise,

$$\left.\begin{array}{llll} n=0 \ , & i=j=0 \ , & \text{integral} = 2\pi \ , & (a) \\ n=0 \ , & i=j\neq 0 \ , & \text{integral} = \pi \ , & (b) \\ n\neq 0 \ , & 2i=2j(=n) \ , & \text{integral} = \frac{\pi}{2} \ . & (c) \end{array}\right\} \quad \ldots\ldots \text{ eqn. 6.11}$$

These three conditions are applied in the following cases,

a) axisymmetric in-plane forces causing axisymmetric buckling,

b) axisymmetric in-plane forces causing asymmetric buckling,

c) asymmetric in-plane forces causing asymmetric buckling in which case the in-plane harmonic is twice the displacement harmonic.

It is now possible to process the $[T]$ matrix ready for integration. The procedure is similar to the method discussed in Chapters 3, 4 and 5 which is multiplying the elements of $[T]$ by the weighting factor at the Gauss-point, thus

$$[T]\, dA = \gamma\, R_k \left(\frac{ds}{d\xi}\right) W_k \left[T_{ij}\right]_k \quad \ldots\ldots \text{ eqn. 6.12}$$

where γ assumes the values of 2π and π depending on the nature of the problem. If the case (c) above is encountered rather than making excessive coding, it is sufficient to adjust $[T]' = \frac{1}{2}[T]$ to accommodate the factor of $\frac{1}{2}$ in the integration constant $\frac{\pi}{2}$.

6.5 THE FORMATION OF THE GEOMETRIC MATRIX $[K_\sigma]$

In forming the stiffness and the mass matrices, step-by-step procedures were used to explain the manner of codification. In both cases Energy Methods were used for clarification. Special emphasis was placed on interpreting terms such as $[D]\{\varepsilon\}$ and $[\rho]\{v\}$. It was thought that the Virtual Work method would result in a more favourable manner of explaining the formation of the Geometrical Matrix along the lines given by Chan and Firmin[5]. It was shown in reference (5) that owing to rotations $\frac{\partial w}{\partial s}$ and $\frac{\partial w}{R\partial\theta}$ the in-plane stress resultants $[T]$ will have transverse components giving rise to moments shown below,

$$(T_s R d\theta)\left(\frac{\partial w}{\partial s} ds\right) \quad , \quad (T_\theta . ds)\left(\frac{\partial w}{R\partial\theta} R d\theta\right),$$

bearing in mind that $Rd\theta ds = dA$. One can now substitute for dA from eqn. 6.12 namely,

$$(T_s)_k \cdot \left[\gamma R_k \left(\frac{ds}{d\xi}\right)_k \cdot W_k\right] \cdot \left(\frac{\partial w}{\partial s}\right)_k \quad , \quad (T_\theta)_k \left[\gamma R_k \left(\frac{ds}{d\xi}\right)_k W_k\right] \cdot \left(\frac{\partial w}{R\partial\theta}\right)_k .$$

It is worthwhile to note that k is the dummy-index when evaluating various quantities at the point ξ_k for numerical integration. The two terms can be represented by a single matrix notation,

$$(\text{Force})_{\text{transverse}} = [T]_k \cdot [G]_k \{\delta\} \cdot \left(\gamma R_k \left(\frac{ds}{d\xi}\right)_k W_k\right), \qquad \ldots\ldots \text{ eqn. 6.13}$$

terms relating to T_s and T_θ indicate moments about θ and s respectively. The Virtual Work done is now a simple scalar product of $(\text{rotation})^{\text{Vir}}$ x $(\text{moment})^{\text{real}}$,

$$(\text{elemental Virtual Work done}) = \{\overset{*}{\delta}\}[G]_k^T \cdot [T]_k [G]_k \cdot \left(\gamma R_k \left(\frac{ds}{d\xi}\right)_k W_k\right).$$

Thus upon integration, the (i,j)-th element of the Geometric Matrix would appear as,

$$\left[K_{ij}\right]_{\sigma} = \sum_{k=1}^{n} \left[G_{i\ell}\right]_k^T \left[T_{\ell m}\right]_k \left[G_{mj}\right]_k . (\gamma R_k (\frac{ds}{d\xi})_k W_k) . \qquad \ldots\ldots \text{ eqn. 6.14}$$

It must not be forgotten that the slope normalisation process described in Chapter 3 also applied here in contrast to Chapter 5 where no slope terms were needed since the slope functions B1 to B4 and $S_0, \ldots, S_N$ were used purely to provide velocities (see last paragraph of 5.3). A further adjustment to the Geometric Stiffness matrix could be made which entails the inclusion of terms resulting from external agencies on the deformed geometry of the shell in reference(6).

6.6 EXAMPLES

Some difficulty was experienced in choosing suitable theoretical examples for the purposes of comparison with the finite element results. It was found that plate structures and cylindrical shells had constituted a significant proportion of the published numerical examples. In some cases reference had to be made to the original articles, some of which were not published in English.

6.6.1 Buckling of thin uniform discs

The problem of axisymmetric buckling of circular plates has been studied theoretically and for simple cases there are formulae to provide the theoretical buckling loads. The plate which is rigidly fixed round its perimeter is the simplest case since certain boundary conditions are easily satisfied. The theoretical buckling load is given[7] by the expression,

$$P_{cr} = k \frac{D}{a^2} , \qquad \ldots\ldots \text{ eqn. 6.15}$$

where k is a factor proportional to the first non-trivial root of the first order Bessel function. Other values of k corresponding to higher roots are of no physical importance but numerically they provide a basis for comparison of other roots "zooed" from an eigenvalue routine. The theoretical roots were obtained by referring to mathematical tables. Equation 6.15 can be used to determine the buckling loads for other boundary conditions but satisfying the boundary conditions become more complicated. The candidate used a very approximate plot to determine the second and third roots. It is interesting to note that the buckled shape of two circular discs, one simply supported and the other centrally supported is identical and thus the axisymmetric buckling loads are also identical. This argument could not be used in the case of natural vibrations of circular plates, since the effective mass vibrating alters with the change in position and the manner of support. The buckling loads for asymmetrical modes were calculated by Galerkin[8] for the case of a rigidly fixed plate. The governing equation involved the Bessel functions of differing parametric order which is simplified to the form below,

$$2nJ_n(\gamma r) - (\gamma r).J_{n-1}(\gamma r) = 0. \qquad \ldots\ldots \text{ eqn. 6.16}$$

where r is the radius in polar coordinates and $\gamma^2 = \frac{P}{D}$. The buckling load P_{cr} could still be estimated through eqn. 6.15.

The determination of buckling loads for simply supported discs is more involved. In the absence of any theoretical values the following semi-analytical method was used. It was thought that the higher buckling modes adopt such deformations along any non-nodal radius which would allow the introduction of knife-edge supports along a nodal circle without any alteration in the value of the buckling load. Assume that a buckling load of $(P_{cr})_2$ corresponding to the second mode (i.e. one nodal circle) of an edge-clamped disc were to be estimated by the following formula,

$$(P_{cr})_2 = k_2 \cdot \frac{D}{a^2}.$$

This buckling load is also common to a smaller simply supported disc, of radius $r=\alpha$ corresponding to the radius of the nodal circle of the original plate. The buckling load is then given by

$$(P_{cr})_{s.s.} = (k)_{s.s.} \cdot \frac{D}{\alpha^2} = (P_{cr})_2 ,$$

$$(k)_{s.s.} = k_2 \cdot \frac{\alpha^2}{a^2} .$$

It must be emphasised that k_2 should be based on an appropriate root of eqn. 6.16 which corresponds to second or a higher buckling mode. It was found that the current tables of mathematical functions common to most colleges were devoid of the roots required. Use was then made of the standard package provided by the computer manufacturer. Firstly the individual values of $J_n(\beta)$ and $J_{n-1}(\beta)$ were generated and stored for increasing values of the argument β. Then an auxiliary function ϕ was defined and stored as follows,

$$\phi(\beta) = 2nJ_n(\beta) - \beta . J_{n.}(\beta).$$

The values of β_i corresponding to $\phi(\beta_i) = 0.$ were then recorded as the successive roots of eqn. 6.16. Only the first buckling modes of a simply supported plate based on this method were calculated for n=1,2 and 3. No attempt was made to estimate the corresponding buckling loads for the centre supported disc. The results of the variation in the buckling load for differing support conditions and other variables is tabulated in Figure 6.1.

6.6.2 Buckling of Annular Plates

The theoretical buckling loads for a disc with central hole is given in reference (7). The results originally are due to Meissner as mentioned in the above reference. The initial stress system causing buckling is no longer uniform thus the correct stresses obtained from

a previous static analysis have to be used. The boundary conditions imposed are confined to simply supporting or clamping the outer edge only. The values of the factor k in eqn. 6.15 is plotted against the ratio of the inner radius to the outer radius for both support conditions shown in Fig. 6.2. The values of the above factor are also plotted for the incorrect values of the inplane stresses to determine the errors involved. As can be seen the deliberate error has only a marginal influence on the simply supported values whereas the clamped values are affected substantially.

Figures 6.3 and 6.4 indicate the variation of k with a change in the number of waves in the circumferential direction. Each graph contains two buckling modes for a particular value of $\frac{a}{b}$, Fig. 6.3 being for the simply supported condition whereas Fig. 6.4 represent the corresponding values when the outer edge is clamped. As can be seen no corresponding theoretical values of k could be found for comparison.

6.6.3 Buckling of Circular plates with Radially Varying Thickness

The theoretical values used here are due to Egger[9] although there were also contributions from other workers. It is assumed that the thickness is a function of the radius r so that,

$$t = t_0 r^{\beta}$$

where β could be any real number (positive or negative, integer or fractional). The plotted values of k are for a radial ratio of (inner radius/outer radius) = 0.2 and 0.25, each boundary condition is represented by a separate graph shown in Fig. 6.5. The value of β=0 corresponds to a uniform disc.

6.6.4 Shear Buckling of Annular Plates

The final plate example to be given here is buckling of annular plates as a result of applying an outside torque while keeping the inner edge rigidly fixed. The values of k given by Dean[10] are for a uniform plate which together with the finite element results are given in Figure 6.6. The results for non-uniform thickness could be found in an article by Federhofer and Egger[11]. The results in this case were not impressive with fairly large errors.

6.6.5 Buckling of Long, Thin Cylinders

The buckling of a long slender cylinder falls within the following categories,

a) Buckling due to axial compression is predicted using at least three different methods, the most elementary of which is due to Euler. Other formulae are specialised cases of the general cylinder problem and are given by Timoshenko[12] and Flügge[13].

b) The estimation of buckling loads owing to uniform shear also involves three distinct theoretical formulae which are due to Greenhill[14], Timoshenko[15] and Flügge[16]. The result of the cases (a) and (b) are presented in a tabular form in Figure 6.7.

6.6.6 General Buckling of Cylindrical Shells

The general buckling of cylindrical shells in view of its importance and relative simplicity of formulation compared with other shells of revolution, has received some considerable attention in contempory literature. The comparison made here is based on the research done

by Flügge*.

a) Cylinder with axial compression - It was decided to choose seemingly an unusual thickness of t = 0.0547722 in and a radius of 5.0 in. The reason was that the curve given in ref. (16) page 427 was calculated for a parametric value of

$k = \frac{t^2}{12a^2} = 10^{-5}$ corresponding to the above dimensions.

Isolated values of the buckling load versus the shell length were calculated and plotted as shown in Fig. 6.8. The festoon plots of Fig. 10 in the above reference were abandoned and only the minima corresponding to the different harmonics were computed. In all the calculations only 1 element was used with 2 surplus displacement for each of u, w and v-displacement. Use was made of symmetry in all instances.

b) Cylinder with radial pressure - The approach made for the buckling of the cylinder with compressive hoop stresses is similar. The same geometric and elastic data as in (a) were used. The critical hoop resultant T_θ was plotted against the length L and only three points were used to plot a certain section of the buckling curve for a given harmonic. The results are compared with the theoretical data in Fig. 6.9.

---

* There are results available from other workers in particular von Mises but according to Timoshenko the differences involved are small, ref. (15), footnote p. 479. Also see Yung-shih Wang and David P. Billington "Buckling of Cylindrical Shells by Wind Pressure", Jour. Eng. Mech. Div., EM5 Oct.74, P.1005, ASCE.

c) Cylinder under axial compression and radial pressure - In view of the complexity of the problem involved, the theoretical buckling load for only two lengths of cylinder namely $L = \pi a$ and $L = \pi a/3$ were available. In order to have a meaningful comparison between the theoretical and finite element results, the ratios of resultant $\frac{T\theta}{Ts}$ fed in the input data were carefully controlled. The results of this computation are plotted in Fig. 6.10. It is interesting to note that the cylinder with the particular parametric value of $k = 10^{-5}$ is approximately six times more sensitive to the radial stresses than it is to the axial stresses when buckling becomes the design criterion.

d) Cylinder subjected to shear - The calculation of buckling loads, with the effect of shear in mind in the above reference, is clearly separated for long and short cylinders. For the previously used value of k, there appears to be a gap in the theoretical results for values of L between 5 to 22 inches. The agreement between the theoretical and numerical results are not favourable. The minima for different values of n appears to be a different cylinder length than that predicted theoretically. In the theoretical formulation when the cylinder length was assumed to be short, a large value for n was assumed. This assumption was implemented to an extent that n was permitted to vary continuously. Naturally in any finite element input data, specific values of n must be fed and as such n=6 was the highest harmonic value prepared. The variation in the buckling loads for the cylinder length outside the theoretical range appeared smooth and there did not appear to be difficulties of any kind. The results are summarised in Fig. 6.11. Values of shear buckling with non-zero meridional resultants were also attempted; the values used were $T_s = -1550$ and $T_s = +1860$. These stresses

correspond to in-plane parameters of 0.25 and -0.30 shown in Fig. 21. P.448 of the above reference respectively which are plotted in Figures 6.12 and 6.13. One perplexing outcome was that the buckling stress with the in-plane compression was numerically larger than the corresponding value for a tensile meridional resultant. This aspect was checked a number of times with the same numerical conclusions.

6.6.7 Symmetrical Buckling of Thin Compressed Spheres

The sphere examined has its dimensions and other details given in Fig. 6.14. Three distinct element subdivisions were tried and the convergence appears to be at hand even with two elements. Upon further attempts it was found that the mode corresponding to n=1 provided even a lower numerical buckling mode (about one half of the full theoretical result). It is hoped that this will be checked by other workers. The theoretical buckling pressure given here is from ref. (15) P.157 and ref. (16) P. 377, the numerical values of the pressures in each case being identical.

6.6.8 General Buckling of Thin Shallow Spherical Caps Subjected to Uniform Pressure

The final stability example is the cap shown in Fig. 6.15, the determination of the buckling pressures for which is carried out in two stages.

a) For symmetrical analysis the following three results are quoted,

Source	G,G,P & M[17]	Tillman[18]	B[19] & H[20]
Pressure	63.10	68.28	64.00

The finite element results using 2u and 3w surplus displacements are tabulated in Fig. 6.15 and vary from 65.14 to 66.86 for 2 and 3 elements respectively.

b) The results for asymmetrical analysis are plotted and also given in the above Figure. The theoretical results used for comparison are from references (18), (19) and (20) which are extracted from an article by Tillman[18].

Both theoretical curves show a decrease in the buckling pressure with a corresponding increase in the number of nodal diameters for values of $n \geq 2$. The results given by Huang[20] indicate a clear minimum buckling pressure occurring at n=3, for the particular geometry of the cap shown in Fig. 6.15. With any further increase in the value of the harmonic n, the buckling pressure would also increase without being confined to a limiting or an asymptotic value.

It can be seen from the values of P_{cr} that a single element representation is totally inadequate. Even with a change to a two equal element geometry, the variation in the pressure due to an increase in the harmonic number n, above the value of unity, cannot be accommodated satisfactorily. Only the mathematical model represented by three equal elements, attempts to follow the theoretical curves to a limited degree of success. There is a definite minimum corresponding to n=3 above which the numerical values of the buckling pressure increase in a similar manner to the theoretical curve but to an exaggerated extent (values for $n > 3$ are not plotted). The total number of degrees of freedom used in this example was 28.

REFERENCES

1. S.P. TIMOSHENKO, J.M. GERE
"Theory of Elastic Stability", P. 512-517, McGraw-Hill, New York, 1961.

2. W. FLÜGGE
"Stresses in Shells", P. 422 Chap. 7, Springler-Verlag, Berlin 1967.

3. O.C. ZIENKIEWICZ
"The Finite Element Method in Engineering Science", Chapter 19, McGraw-Hill, London, 1971.

4. A.E.H. LOVE
"A Treatise on the Mathematical Theory of Elasticity", Chapter XXIV, fourth Edn., Dover Pub., New York, 1944.

5. A.S.L. CHAN, A. FIRMIN
"The Analysis of Cooling Towers by the Matrix Finite Element Method", Part II, P. 971, Aero. Jour., Dec. 1970.

6. A.S.L. CHAN, A. FIRMIN
"The Analysis of Cooling Towers by the Matrix Finite Element Method", Part II, P. 971, Aero. Jour., Dec. 1970.

7. S.P. TIMOSHENKO, J.M. GERE
"Theory of Elastic Stability", P. 391, McGraw-Hill, New York, 1961.

8. B. GALERKIN
"Sur la stabilite d'une plaque uniformément comprimée paralélement à sa surface, limitée par deux arcs de cercles concentrique et par deux rayons", P. 1392, Vol. 179, Compt. rent., Académie Des Science, 1924.

9. H. EGGER
"Knickung der Kreisplatte und Kreisringplatte mit veränderlicher Dicke", P. 190, Vol. 9, Ingenier - Archiv, Springler-Verlag, Germany, 1941.

10. W.R. DEAN
"The Elastic Stability of an Annular Plate", P. 268, Vol. 106, Proc. of Roy. Soc., London, 1924.

11. K. FEDERHOFER UND H. EGGER
"Knickung der auf Scherung beanspruchten Kreisringplatte mit veränder licher Dicke", P. 155, Vol. 14, Ingenier-Archiv, Springler-Verlag, Germany, 1943.

12. S.P. TIMOSHENKO, J. GERE
"Theory of Elastic Stability", P. 458, McGraw-Hill, New York, 1961.

13. W. FLÜGGE
"Stresses in Shells", P. 428, Springler-Verlag, Berlin, 1960.

14. A.G. GREENHILL
Proc. Inst. of Mech. Engrs., London, 1883.

15. S.P. TIMOSHENKO, J. GERE
"Theory of Elastic Stability", P. 503, McGraw-Hill, New York, 1961.

16. W. FLÜGGE
"Stresses in Shells", P. 438, Springler-Verlag, Berlin, 1960.

17. R.H. GALLAGHER, R.A. GELLATLY, J. PADLOG and R.H. MALLETT
"A Discrete Element Procedure for Thin-Shell Instability Analysis", AIAA Jour.,P. 138, Jan. 1967.

18. S.C. TILLMAN,
"On the Buckling Behaviour of Shallow Spherical Caps under a Uniform Pressure Load", Int. Jour. Solids and Struct. P. 37, Vol. 6, 1970.

19. B. BUDHANSKY
"Buckling of Clamped Shallow Spherical Shells", Proc. Symp. on the Theory of thin elastic Shells, P. 64, North Holland 1950.

20. N.C. HUANG
"Unsymmetrical Buckling of Thin Shallow Spherical Shells", Jour. Applied Mech. 30, 447, 1964.

BUCKLING OF THIN CIRCULAR PLATE
SUMMARY OF HARMONICS AND MODES

VALUES OF P_{cr}

nodal circle C	n=0		n=1		n=2		n=3	
	Th.	F.E.	Th.	F.E.	Th.	F.E.	Th.	F.E.
0	412.	412.93	742.26	714.78	1145.83	1145.09	1621.24	1620.40
1	1381.	1384.95	1994.40	1998.18	2681.50	2686.26	3446.52	3517.64
2	2830.	2927.07	3800.25	3883.67	4783.	5596.83	—	7376.64
3	—	5996.60	6162.6	8596.55	—	9946.84	—	15647.9

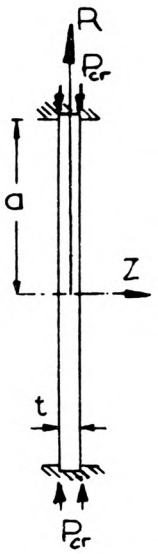

nodal circle C	n=0		n=1		n=2		n=3	
	Th.	F.E.	Th.	F.E.	Th.	F.E.	Th.	F.E.
0	118.*	120.44	—	26.270	—	70.011	—	202.15
1	825.*	818.85	—	463.45	—	703.86	—	1115.42
2	2090.*	2071.	—	1545.89	—	1957.40	—	2682.00
3	—	4127.38	—	3187.77	—	3965.54	—	4941.36

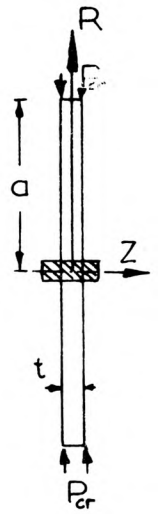

nodal circle C	n=0		n=1		n=2		n=3	
	Th	FE	Th	FE	Th	FE	Th	FE
0	118.*	120.44	350.77*	371.73	689.75*	701.26	1082.09*	1104.78
1	825.*	818.85	—	1345.90	—	1956.34	—	2641.71
2	2090.*	2071.	—	2929.41	—	3960.30	—	4894.10
3	—	4127.38	—	5271.11	—	7258.47	—	8032.69

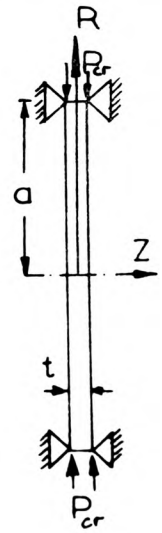

* See text
— Not available

a=10. E=30x10⁶
t=0.1 ν=1/3
T_0=T_1=1.0

FIGURE 6.1

BUCKLING OF THIN UNIFORM ANNULAR PLATES

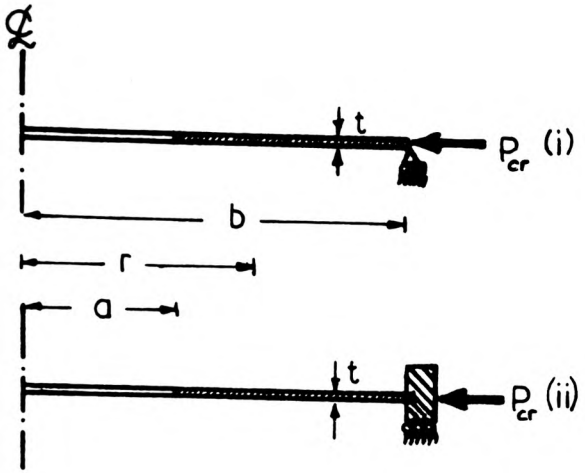

b = 10.
a = variable inner radius
t = 0.1
$E = 30 \times 10^6$, $\nu = 1/3$
$D = \frac{Et^3}{12(1-\nu^2)} = 2815.$
$P_{cr} = \frac{kD}{a^2}$

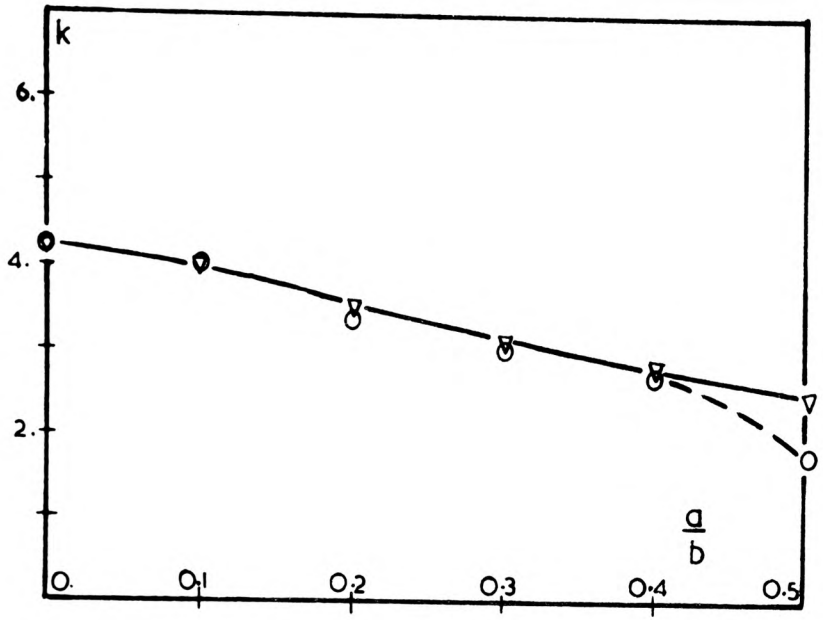

(i)

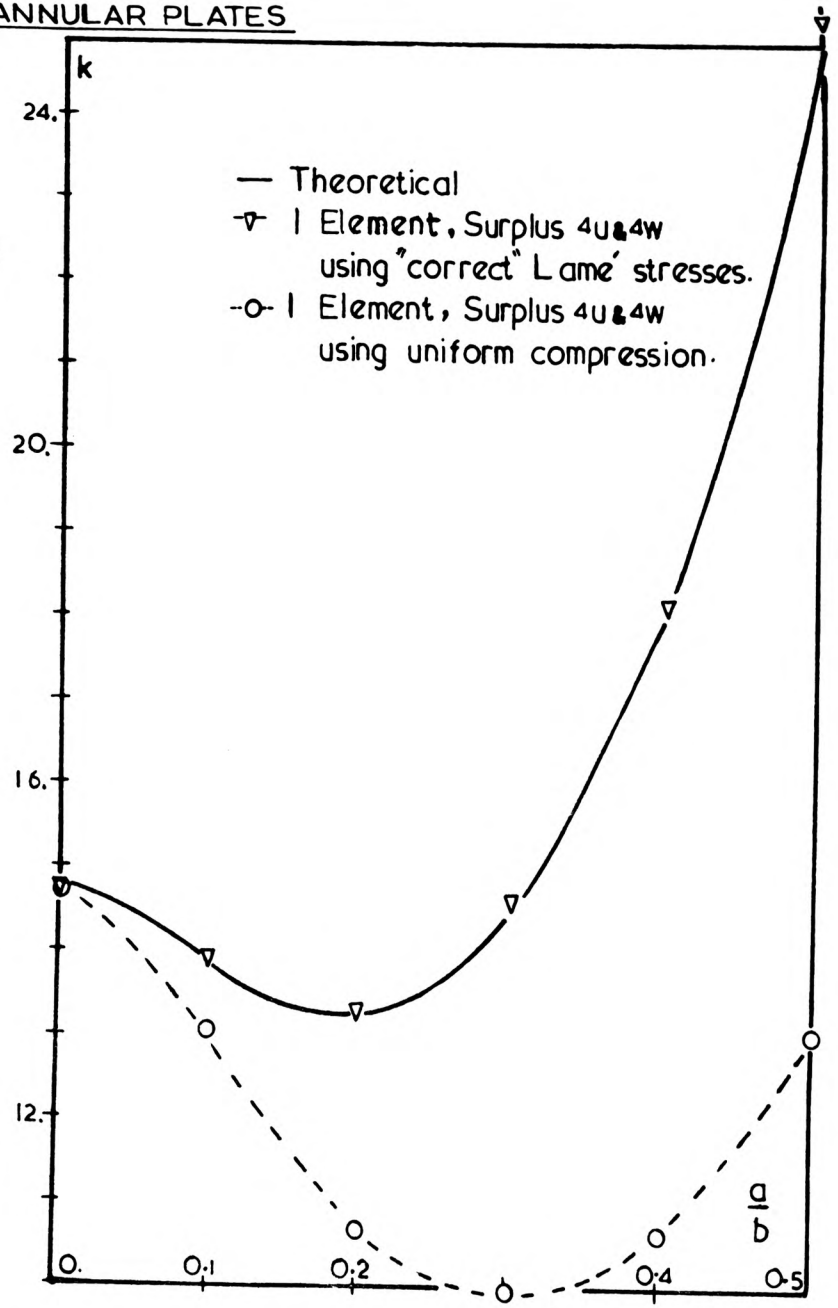

(ii)

FIGURE 6.2

UNSYMMETRICAL BUCKLING OF ANNULAR PLATES

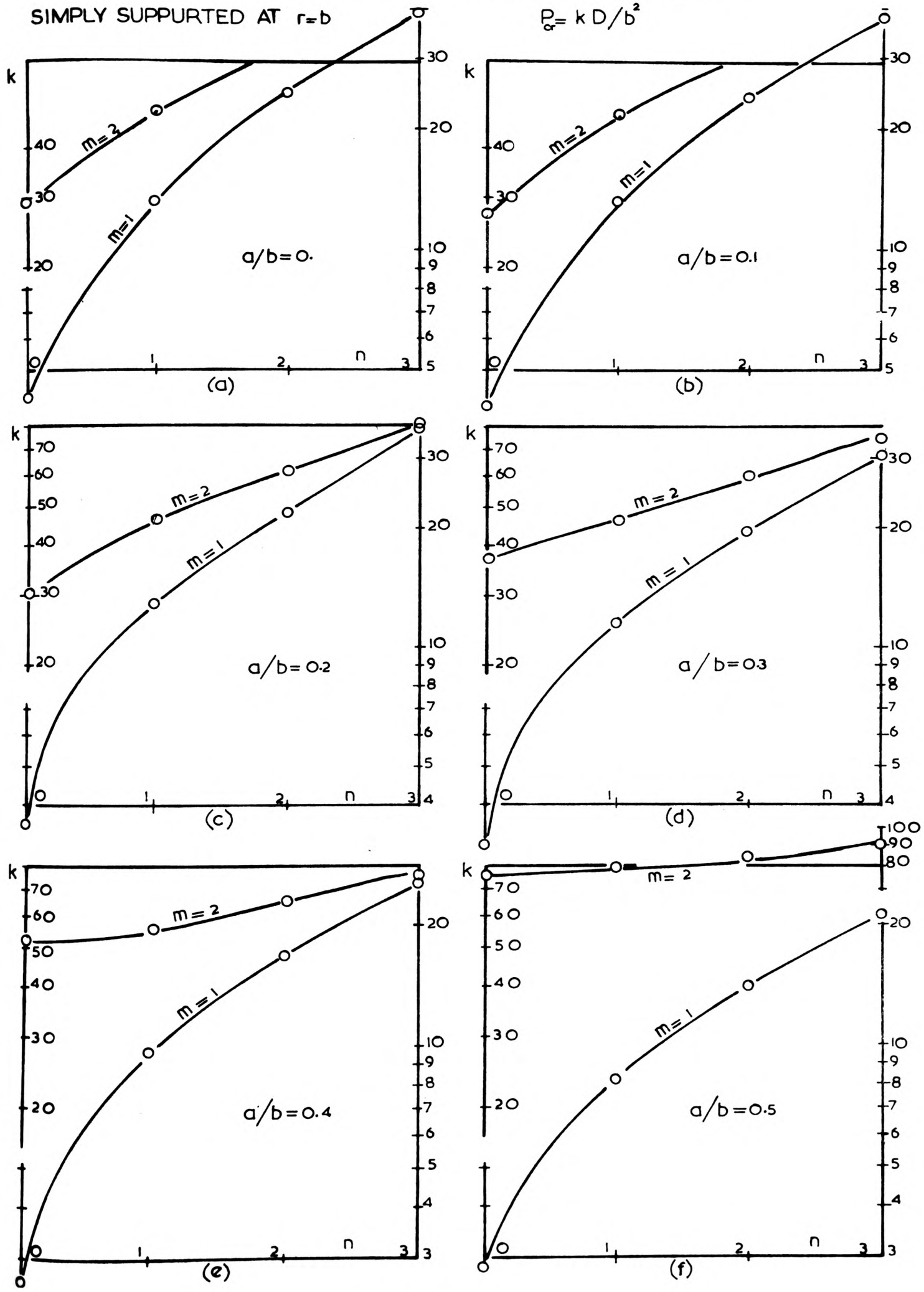

FIGURE 6·3

UNSYMMETRICAL BUCKLING OF ANNULAR PLATES

FIXED AT r=b . $P_{cr}=kD/b^2$

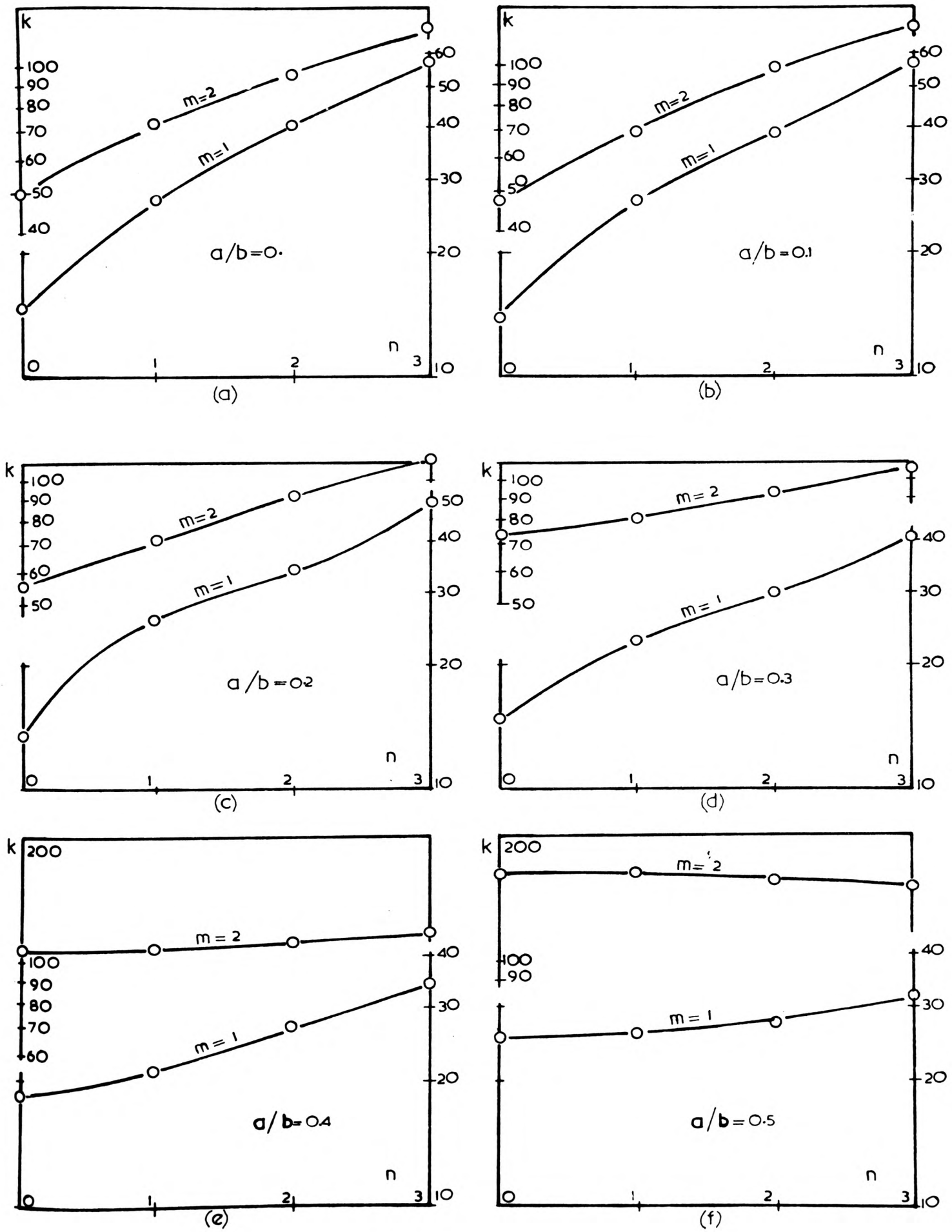

FIGURE 6.4

BUCKLING OF CIRCULAR PLATES WITH RADIALLY VARYING THICKNESS

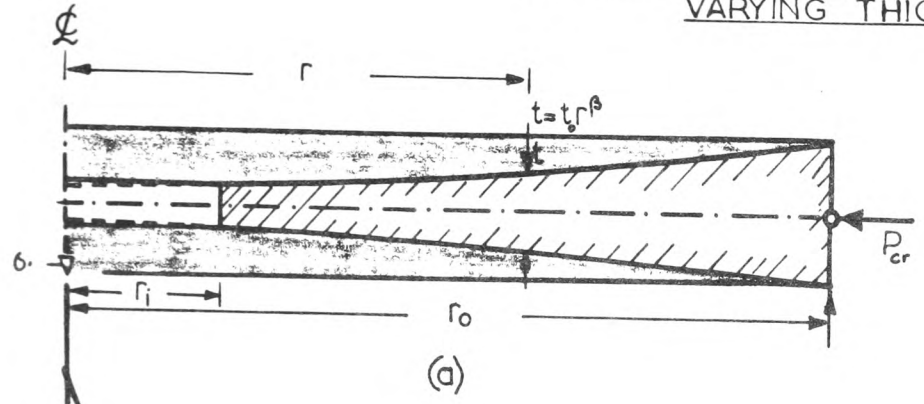

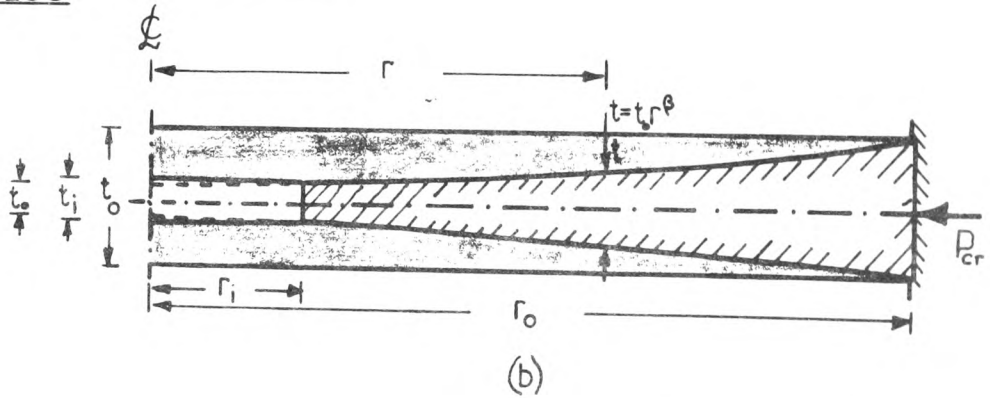

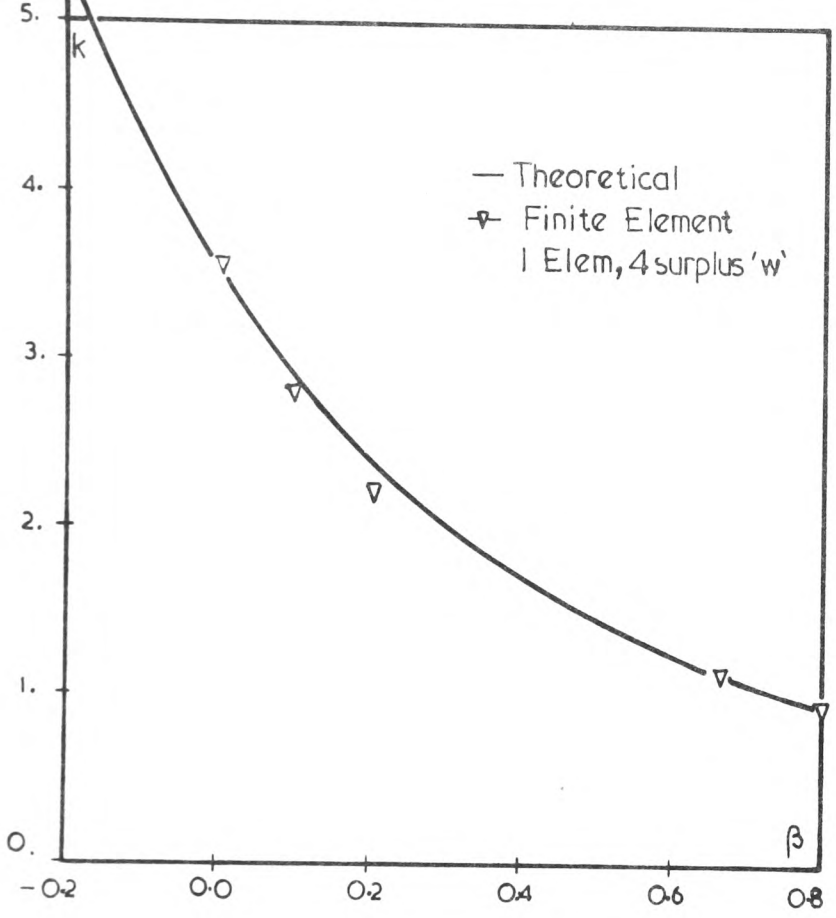

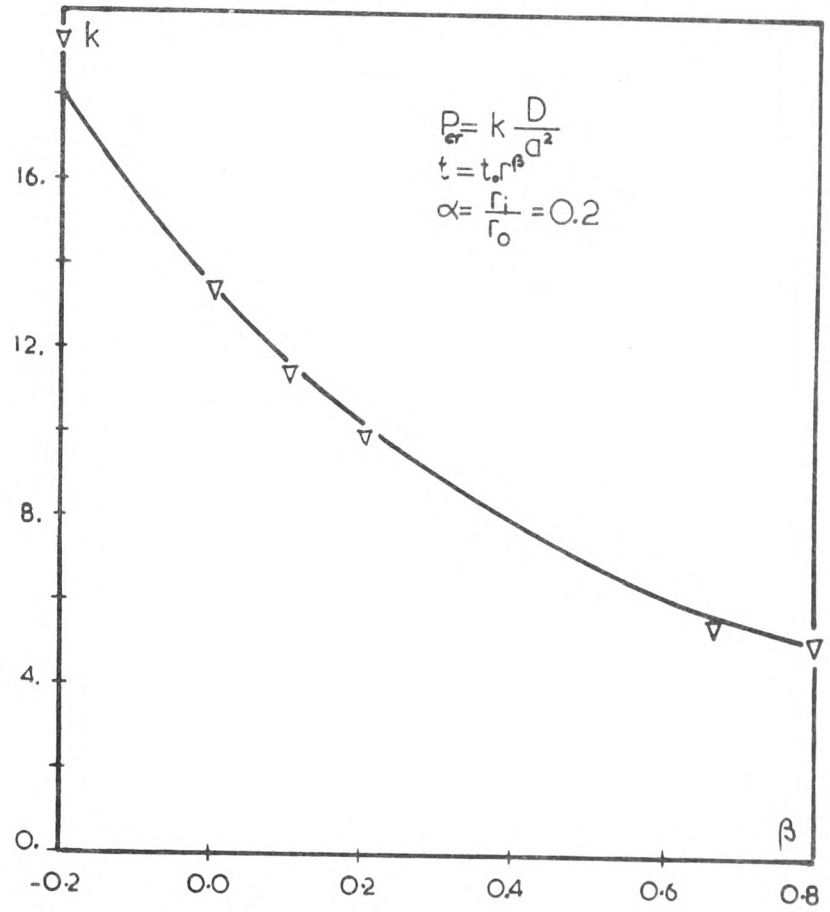

FIGURE 6·5

TORSIONAL BUCKLING OF ANNULAR PLATES

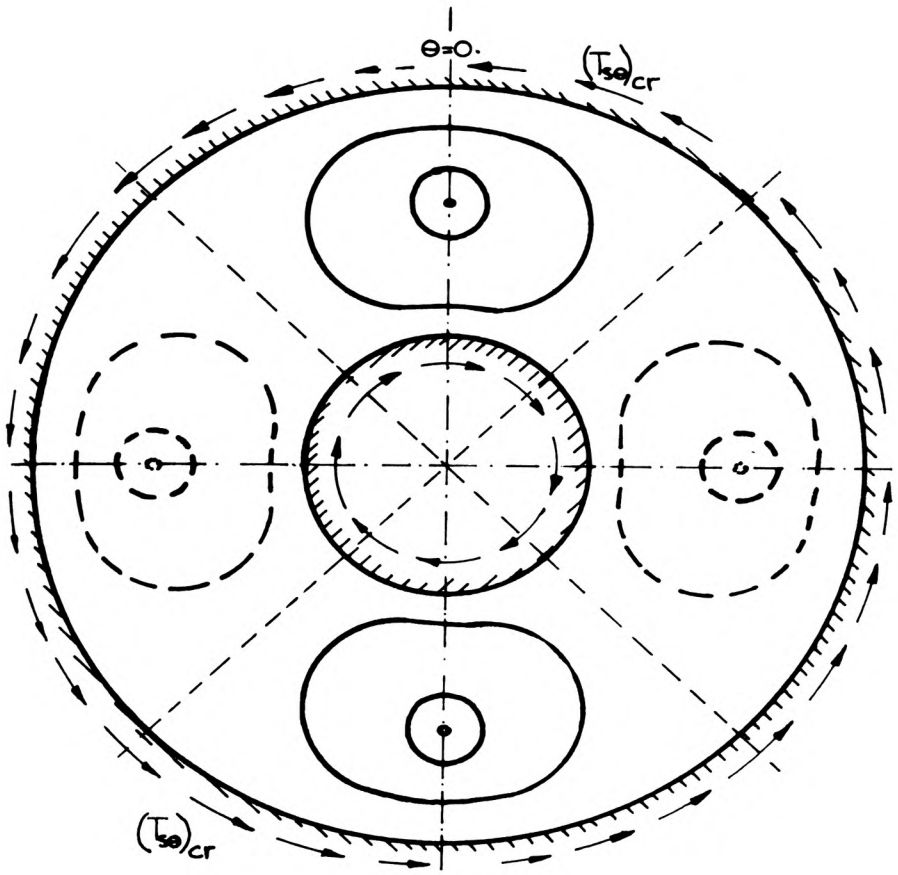

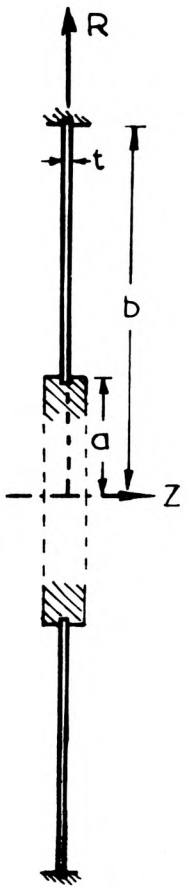

$b = 10$ in
$\alpha = b/a$
$t = 0.1$ in

$E = 30 \times 10^6$ lbf/in^2
$\nu = 1/3$

1 Finite Element used, 2 surplus u,w&v.

BUCKLING SHEAR $T_{s\theta}$

	n = 1	n = 2	n = 3	n = 4
Theo.Dean	1548.	1013.	1013.	1224.
Fin. Elem.	1394.	970.	1136.	1661.
% error	10.	4.	11.5	30.

$\alpha = \frac{a}{b} = 0.20$

	n = 1	n = 2	n = 3	n = 4
Theo.Dean	2153.	1421.	1301.	1463.
Fin. Elem.	2337.	1590.	1573.	2069.
% error	8.	11.2	18.9	34.

$\alpha = \frac{a}{b} = 0.25$

FIGURE 6.6

BUCKLING OF A LONG THIN CYLINDER

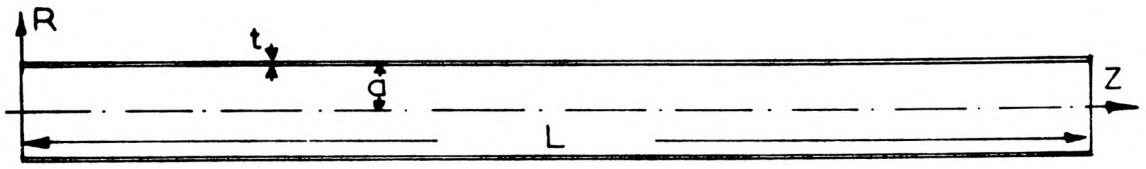

$L = 100.$
$a = 5.0$
$t = 0.1$

$E = 10 \times 10^6$
$\nu = 0.25$

(a)–Owing to axial forces T_s.

$$T_E = \frac{\pi^2 E a^2 t}{2L^2} \qquad T_T = \frac{Et^2}{a\sqrt{3(1-\nu^2)}} \qquad T_F = \frac{q_2 Et}{(1-\nu^2)}$$

$$q_2 = 10.5/10^3$$

1 Element 2 surplus.u,w,v.	Euler strut $(T_E)_s$	Timoshenko $(T_T)_s$	Flügge $(T_F)_s$
11560.	12337.	11926.	11200.

(b)–Owing to shear (torsional) stresses $T_{s\theta}$.

$$T_G = \frac{Eat}{L} \qquad T_T = \frac{Et\lambda}{2(\lambda^2+1)} \qquad T_F = \frac{E t^{5/2}}{3\sqrt{2}(1-\nu^2)^{3/4} a^{3/2}}$$

$$\lambda = \pi a/L$$

1 Element 2 surplus.u,w,v.	Greenhill $(T_G)_{s\theta}$	Timoshenko $(T_T)_{s\theta}$	Flügge $(T_F)_{s\theta}$
62347.	50000.	76649.	87466.

FIGURE 6.7

BUCKLING OF THIN CYLIDERS
DUE TO AXIAL LOADING

a = 5.0 in $E = 10 \times 10^6$ lbf/in^2
t = 0.547722 in $\nu = 0.25$
L variable

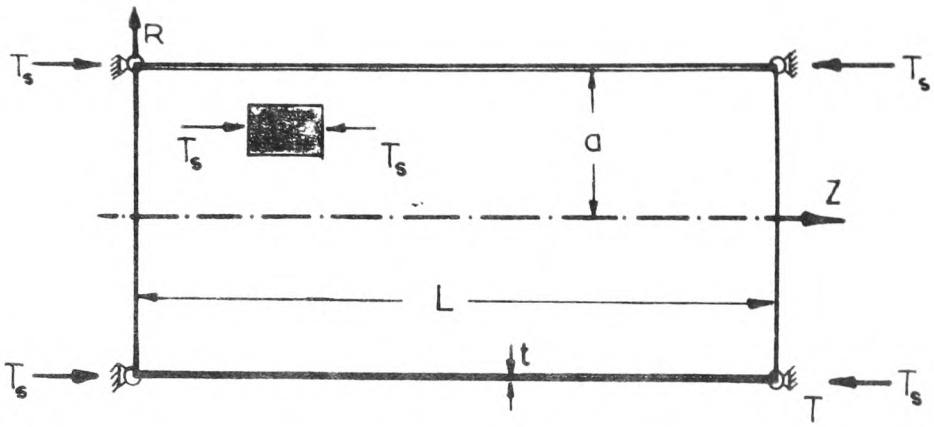

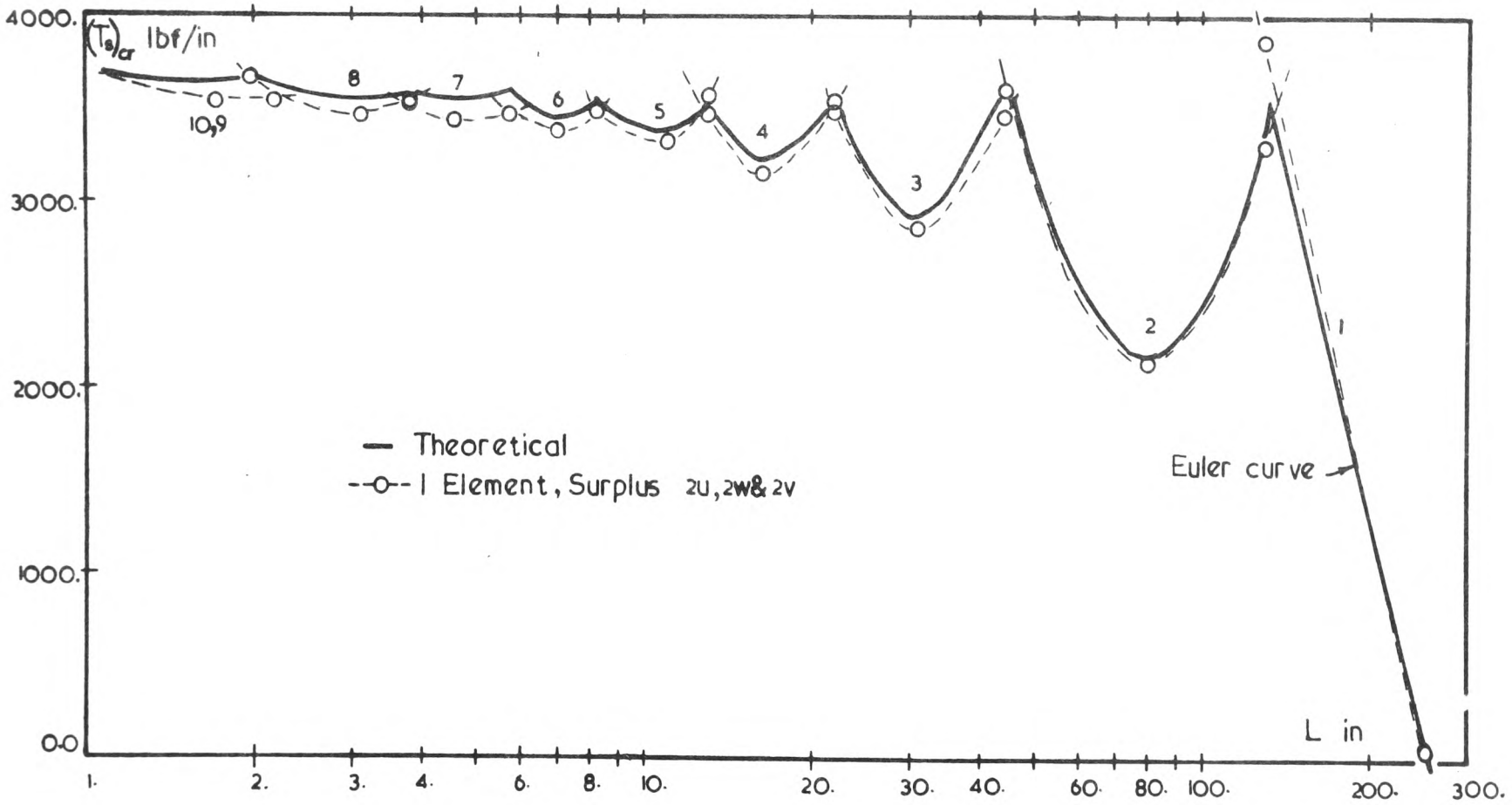

FIGURE 6.8

BUCKLING OF THIN CYLINDERS
DUE TO RADIAL PRESSURE

a = 5·0 in E = 10 x 10⁶ lbf/in²
t = 0·547722 in μ = 0·25
L variable

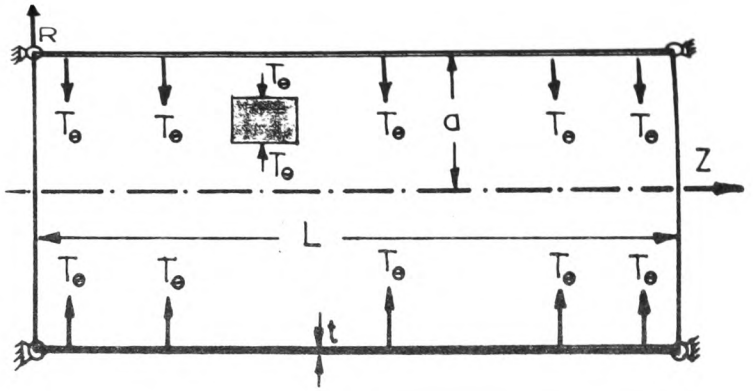

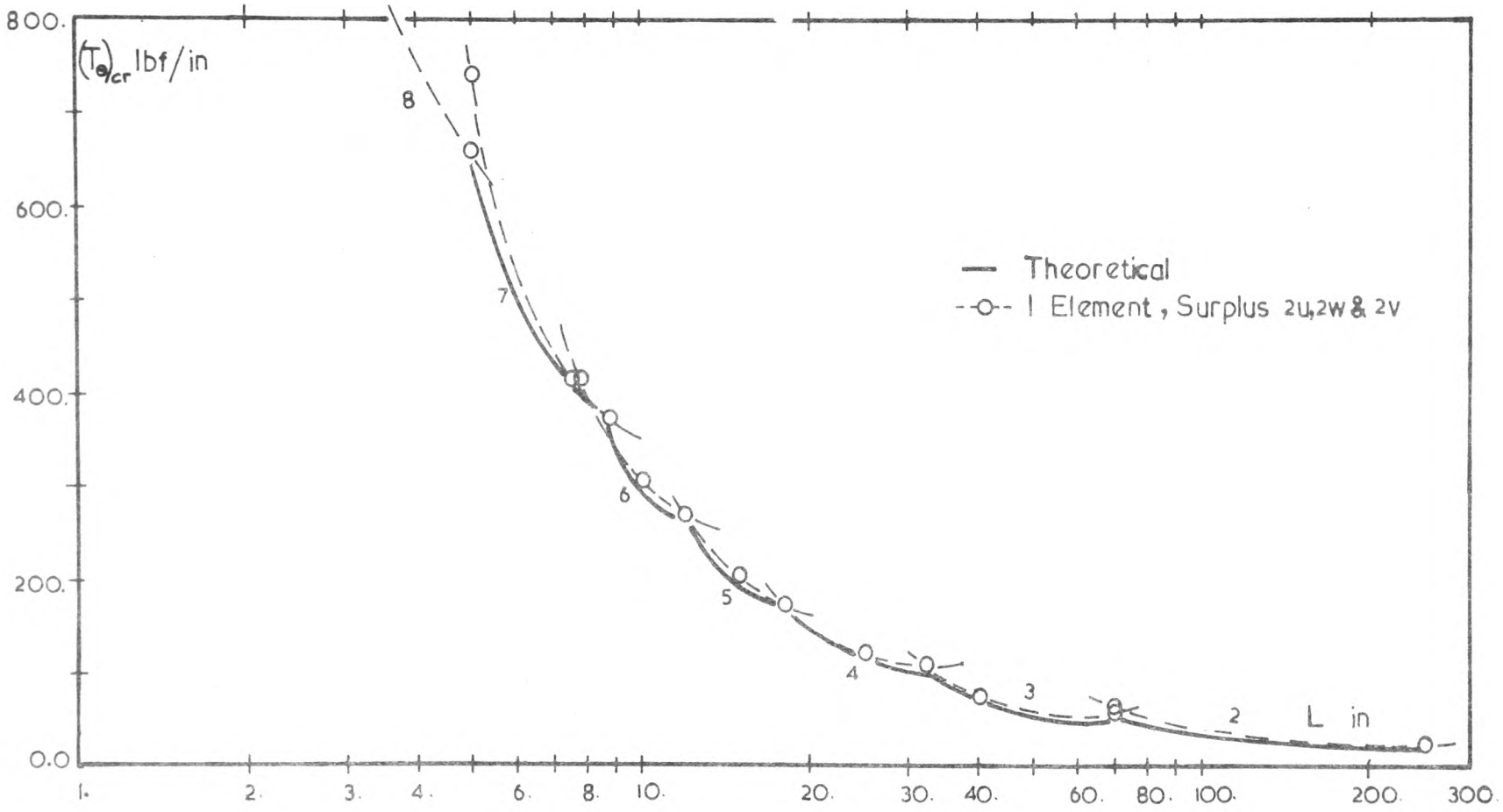

FIGURE 6.9

BUCKLING OF THIN CYLINDERS UNDER BIAXIAL STRESS SYSTEMS

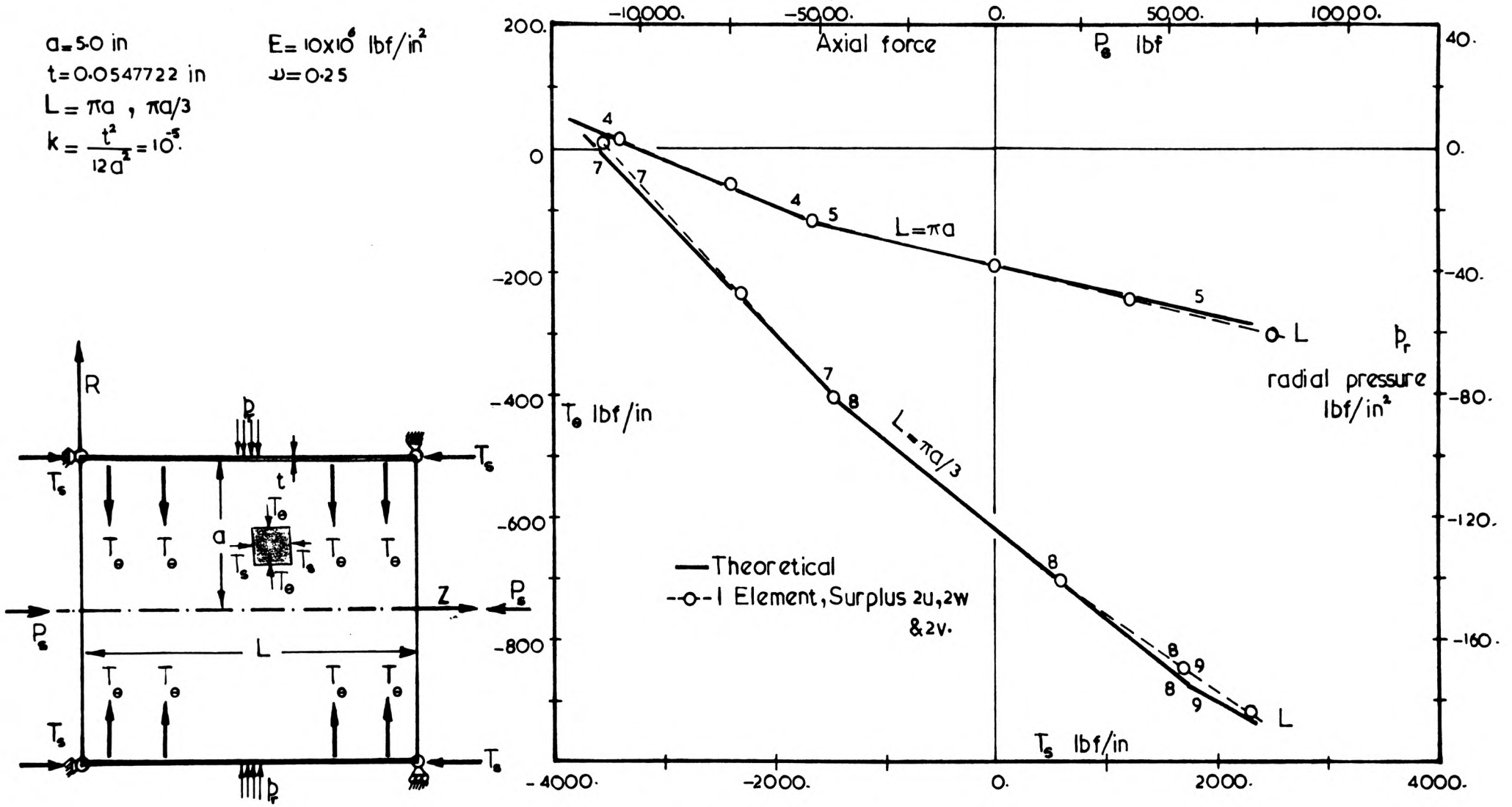

FIGURE 6·10

SHEAR BUCKLING OF
THIN CYLINDERS

$a = 5.0$ in $E = 10 \times 10^6$ lbf/in^2
$t = 0.0547722$ in $\nu = 0.25$
L variable
$k = \frac{t^2}{12a^2} = 10^{-5}$
$T_s = T_\theta = 0$.

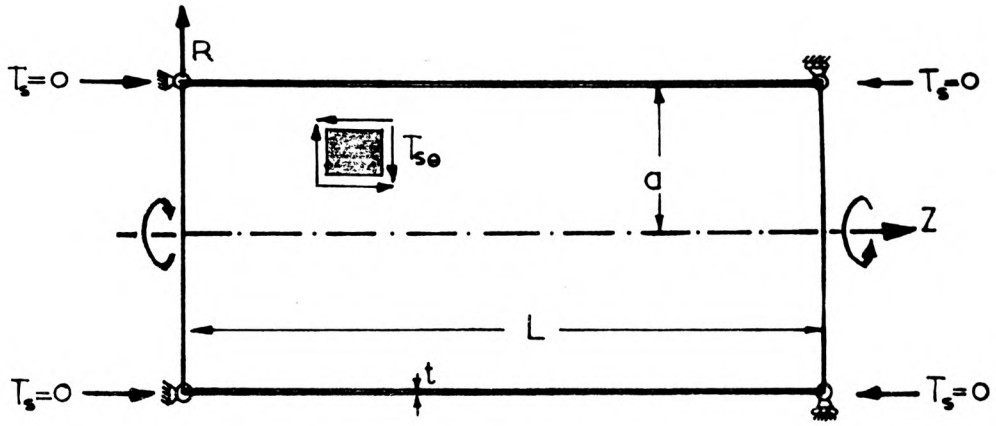

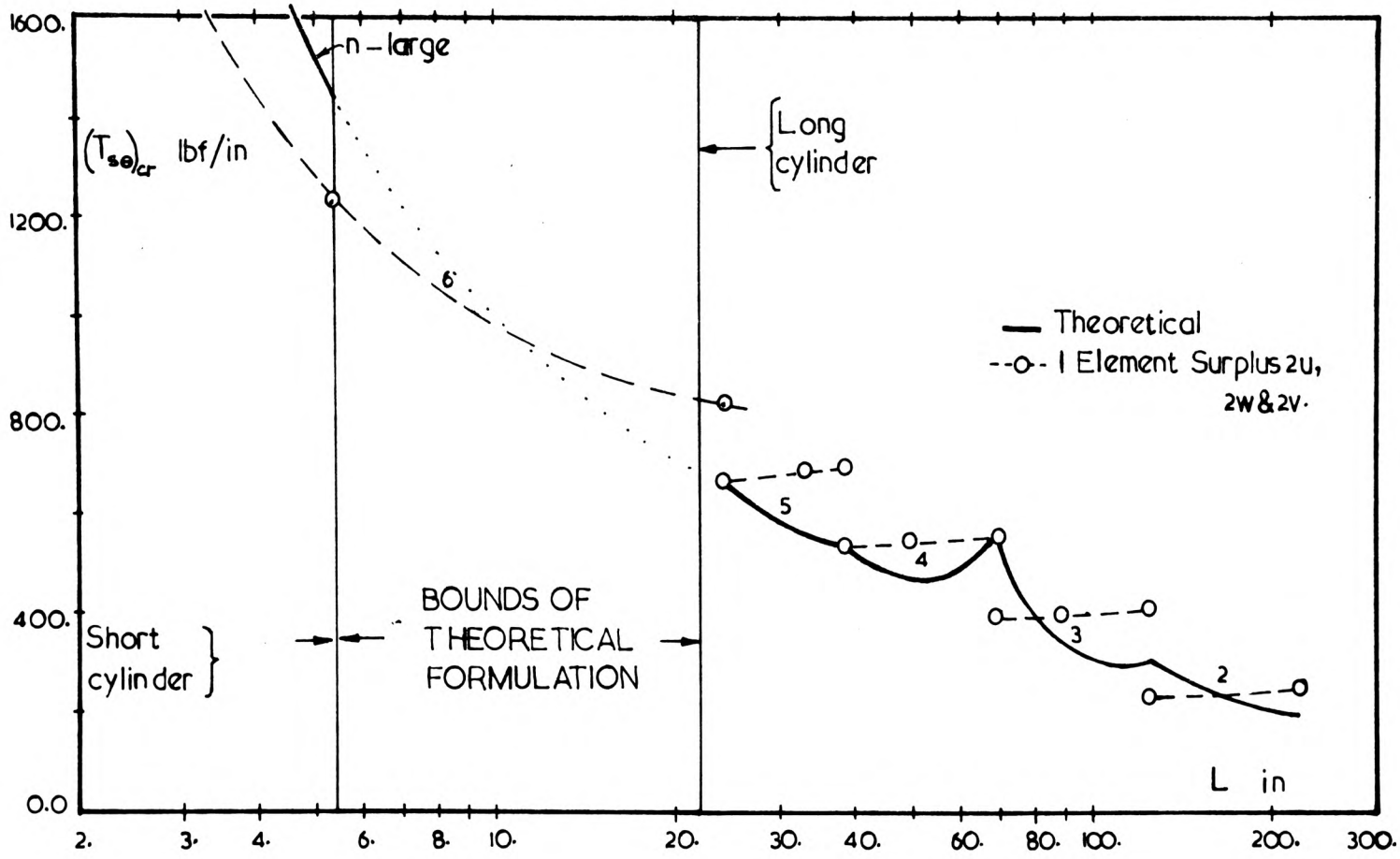

FIGURE 6.11

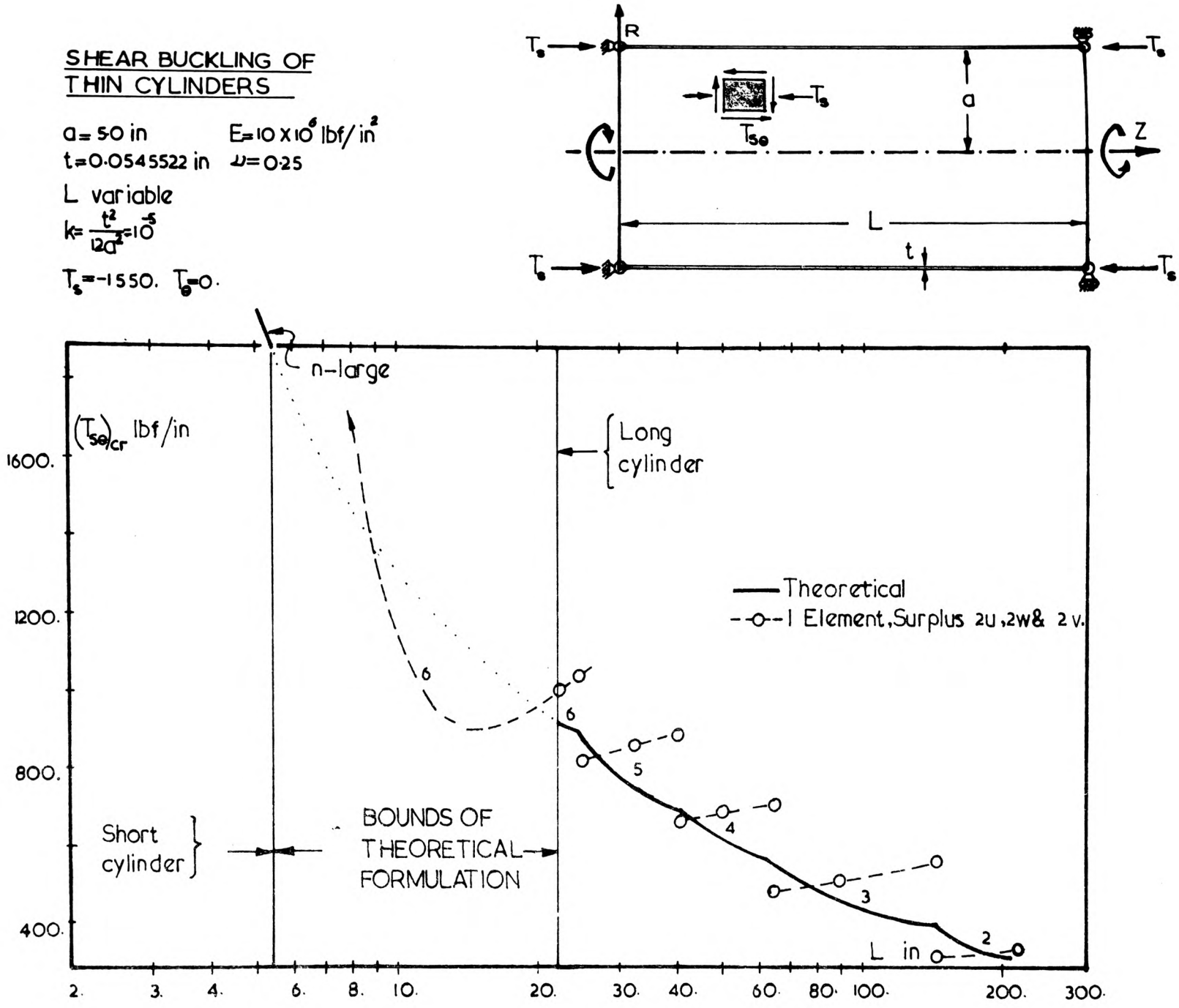
SHEAR BUCKLING OF
THIN CYLINDERS
a = 5·0 in
E = 10 x 10^6 lbf/in^2
t = 0·0545522 in
ν = 0·25
L variable
k = t^2/12a^2 = 10^-5
T_s = -1550. T_θ = 0.
R
T_s
T_θ
a
Z
L
t
n-large
(T_sθ)_cr lbf/in
1600.
1200.
800.
400.
Long
cylinder
Theoretical
1 Element, Surplus 2u, 2w & 2 v.
Short
cylinder
BOUNDS OF
THEORETICAL
FORMULATION
L in
2.
3.
4.
6.
8.
10.
20.
30.
40.
60.
80.
100.
200.
300.

FIGURE 6·12

SHEAR BUCKLING OF
THIN CYLINDERS

a = 5.0 in $E = 10 \times 10^6$ lbf/in^2

t = 0.0547722 in $\nu = 0.25$

L variable

$k = \frac{t^2}{12a^2} = 10^{-5}$

$T_s = +1860$. $T_\theta = 0$.

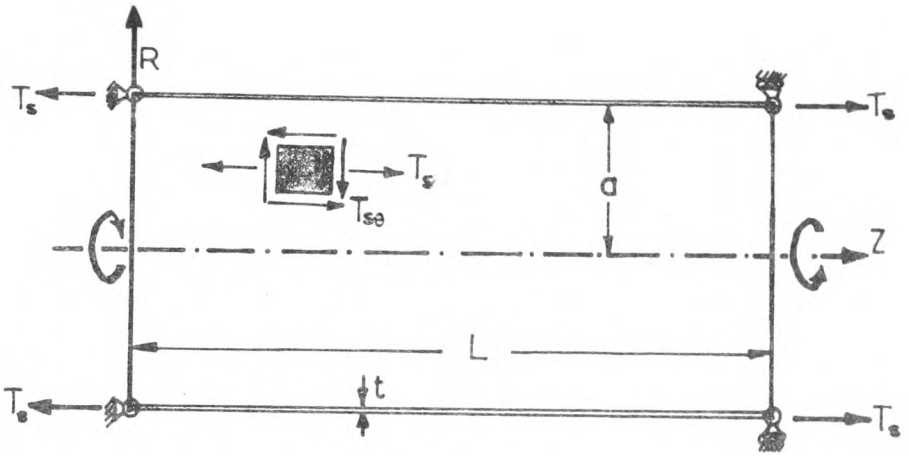

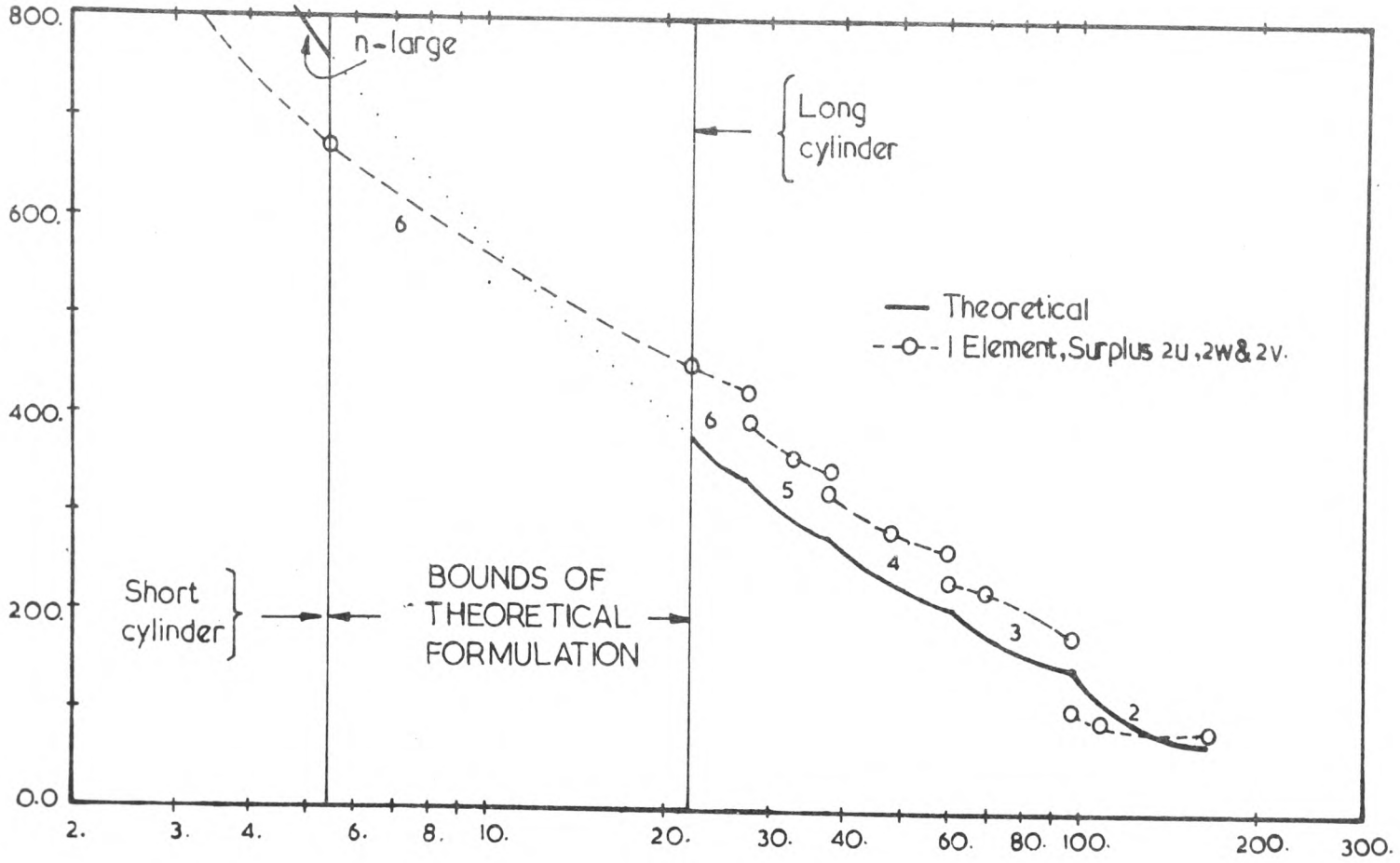

FIGURE 6.13

SYMMETRICAL BUCKLING OF A THIN COMPRESSED SPHERE

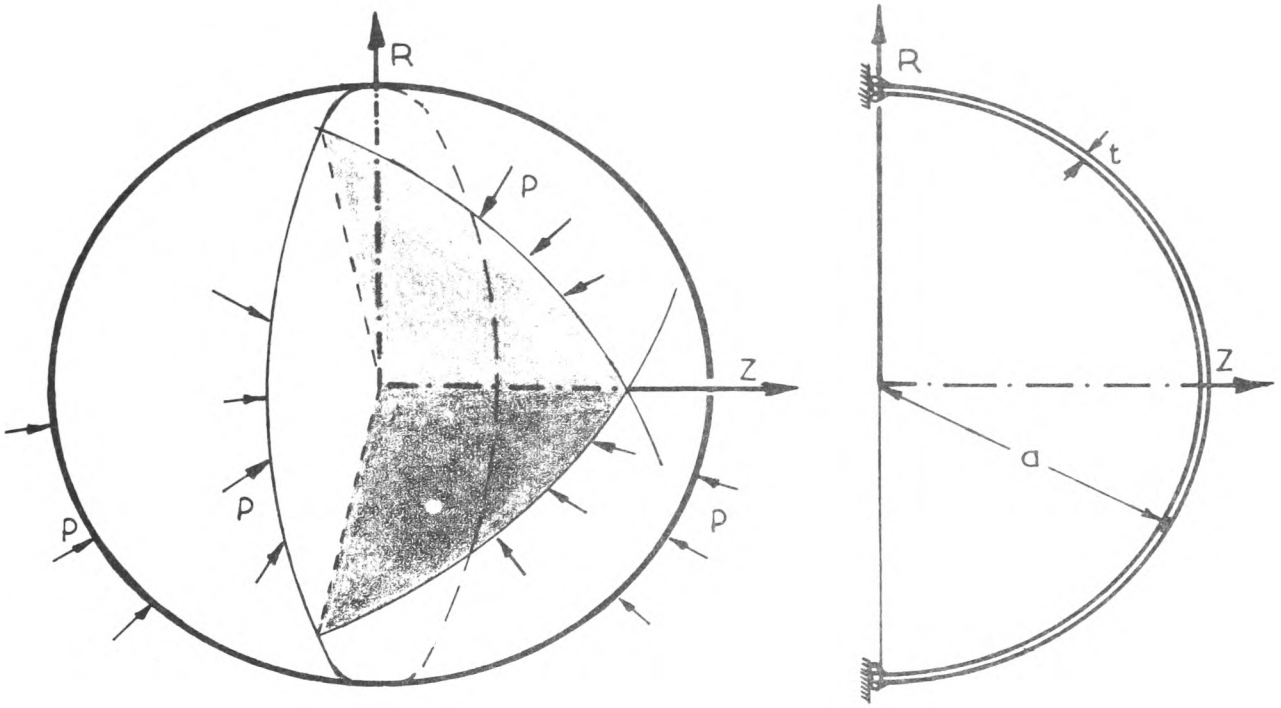

$a = 4.0$ in
$t = 0.04$ in
$T_s = T_\theta = pa/2$

$E = 30 \times 10^6$ lbf/in^2
$\nu = 0.3$
$(T)_{cr} = \dfrac{t^2 E}{\sqrt{3(1-\nu^2)} \cdot a}$

$(p)_{cr} = 3631.$
$(T)_{cr} = 7262.$

BUCKLING STRESS RESULTANT

Theoret.	1 Element 4U & 4W	2 Elements 4U & 4W	3 Elements 3U & 3W
T=7262	T=13702	T=7553	T=7374

FIGURE 6.14

BUCKLING OF THIN SPHERICAL CAPS

r = 19.577 in t = 0.0537 in
a = 4.0 in E = 6.5×10⁶ lbf/in² $\lambda = 2\left[3(1-\nu^2)\right]^{1/4}\left[\frac{H}{t}\right]^{1/2} = 7.0878$
H = 0.413 in $\nu = 0.32$

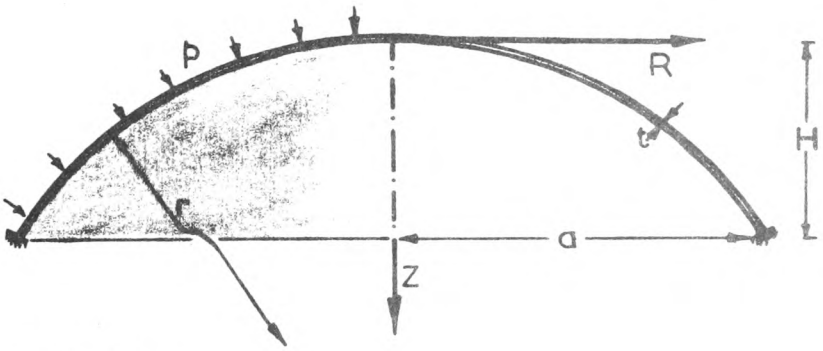

LEGEND:

Theoretical { Tillman —o— ; Budiansky & Huang —▽—

Finite Elem. { 1 Elem., Surplus 2u, 2w & 2v ···x··· ; 2 Elem., Surplus 2u, 2w & 2v --e-- ; 3 Elem., Surplus 0u, 3w & 0v —e—

Buckling pressure p_{cr} n=0	Theoret.		1 element 2U & 3W	2 elements 2U & 3W	3 elements 2U & 3W
	63.79	68.28	66.49	65.14	66.86

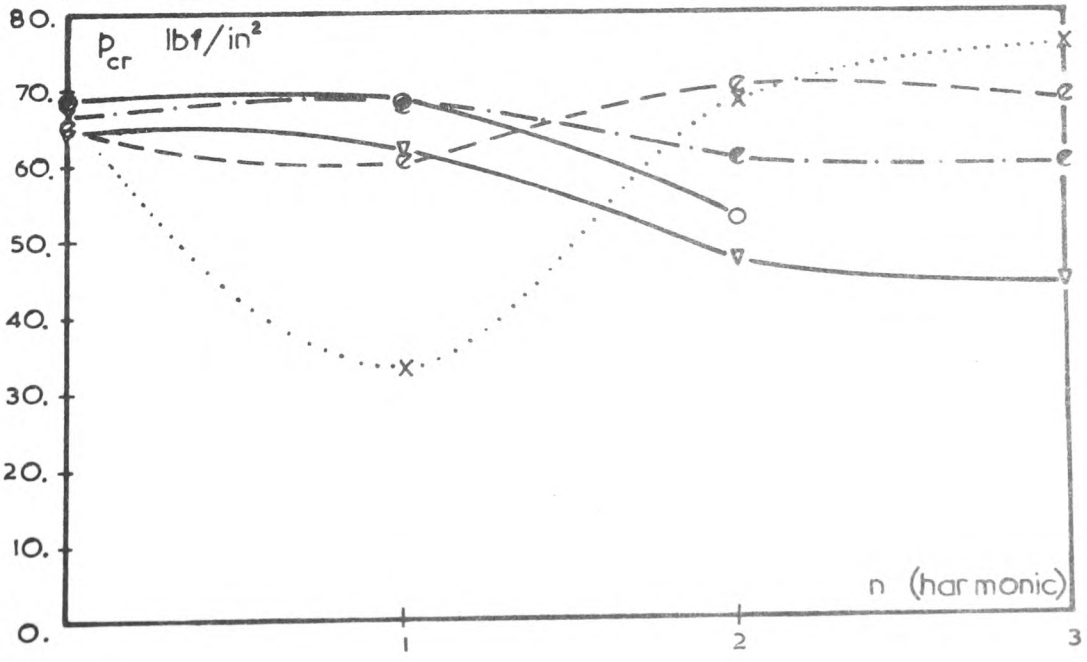

FIGURE 6.15

PART III

SOME EXPERIMENTAL VERIFICATION OF THE LINEAR SHELL THEORY

CHAPTER 7

EXPERIMENTAL STATIC STRESS ANALYSIS

7.1 PRELIMINARY REMARKS

It is an accepted practice that theoretical and experimental work should progress in parallel. Sometimes theories are sought to explain some unknown phenomenon and at other times experiments have been designed to verify theoretical predictions. In the case of the present work it was decided to devise physical experiments which could provide relevant data to enable comparison with some theoretical results. It was realised that owing to shortage of time not every numerical example could be investigated by fabricating and testing a corresponding model. The choice was confined to a single geometry which was to be a model in the shape of a cooling tower. It was decided to perform both static and dynamic tests on such a model in order to compare experimental and theoretical results. No attempt will be made to project the processed results obtained from such a model to predict the behaviour of a corresponding prototype. In fact it may be unwise to have a prototype with dimensions in some way linked to that of the model, since it was almost impossible, at the time, to control the variations of the different factors governing the geometry of the model. It was hoped that this attempt would provide the necessary confidence in the future use of the computer programs developed in this work.

7.2 MODEL FABRICATION

It is intended that only the salient points involved in producing the models in the shape of a cooling tower should be discussed. After some initial consultations it was decided to use perspex as the basic material of the model. It had been found that this material had certain desirable fabrication properties such as the possibility of thermal

forming, ease of machining at normal temperatures and successful cementing of two or more pieces with the aid of special adhesives. It was also known that, due to creep, no meaningful results could be obtained until the material had reached a steady state. Some strain hardening was also expected, the source of which will be outlined in the next chapter. In making the model, repeated reference to the appropriate ICI publications for acrylic materials was made.

Attempts were made to form the model by heating a sheet of perspex $\frac{1}{8}$ in. thick, to the correct temperature and, while the sheet remained flexible, to position it over a previously prepared mould and vacuum from it. A near vacuum was produced in a cylinder using a compressor and a set of valves. Various attachments to the pipes had to be included in the process for reasons apparently unrelated to vacuum forming. For example a gauze had to be fitted to the end of the suction tube to prevent a possible flow of 'rubbery' perspex into the pipes. Vacuum forming proved unsuccessful after a few attempts. Firstly, the leaks in the piping did not allow the build-up of a sufficient pressure difference to enable thermal formation, secondly a continuous supply of vacuum proved difficult since as soon as the vacuum was withdrawn, the sheet retracted to its almost undeformed flat position and thirdly the rush of air lowered the temperature of the heated perspex. On more than one occasion tearing of the sheet in the central region (being the loaded area), took place.

It was then decided to pressure form the model. This time by pressurising the cylinder to about 30.0 psi and by reversing the valves, the pressure difference and hence the forming force was doubled. For the reasons stated above this also proved frustrating.

Finally it was decided to mechanically form the model using a plunger attached to a circular disc activated by a lever, see the sketch in Fig. 7.1. It was first expected that a surface of revolution would be formed lacking the Venturi-type "neck" which is so common to the presently constructed cooling towers. Fortunately a slight "throat" appeared as the stretched sheet and the surrounding frame roughly kept their original temperature. Near the disc of the plunger the membrane appeared to suffer some loss in the radius of the surface of revolution which caused the formation of the slight throat mentioned above, see Fig. 7.2. The plunger also caused a progressive increase in the thickness of the shell towards the base of the model tower which was welcomed since most full-scale cooling towers are constructed to exhibit similar variations in thickness. To release the disc at the end of the plunger it was then necessary to cut the top of the tower owing to the throat formation. Six perspex models were produced using this technique. The sheet with $\frac{1}{8}$ in. thickness was found to be of ideal thickness, since the $\frac{1}{4}$ in. sheet was too strong and the sheet thinner than $\frac{1}{8}$ in. tore as it was being formed. The "softening" temperature of the sheet was also critical and was found to be in the range $155^{o}C$ to $160^{o}C$. It was observed that any drop in the temperature did not allow sufficient flexibility and any excess of the oven temperature caused undesirable blistering of the surface of the sheet. The regulation of the length of the heating interval is provided by a formula given in ICI's appropriate manuals. The average dimensions of towers made are shown in Fig. 7.3, whereas the model is presented in Plate 7.1.

7.3 LOADING FRAME AND THE RECORDING EQUIPMENT

The loading frame consisted of a platform and a three sided box 'rigidly' fixed to the platform at one end. At the opposite end facing the open side of the box, a pin was fixed on the platform projecting upwards by about 50.mm with a thread at the upper extreme. The pin

was to provide an axis of rotation for the model. The model was first screwed at the base to a solid wooden conical frustrum with a central hole which matched the diameter of the pin above. The model and the base were then eased into position with the pin at its central axis and were fixed against circumferential rotation by tightening a butterfly nut positioned on two washers on the thread. A specially prepared rubber bag made of neoprin sheets and 'sealed' to be air-tight was then adjusted into position in the box, so that it was in contact with the box, on three sides and in contact with the model on the fourth side. Plates 7.2, 7.3 and 7.4 show the individual parts and the full assembly of the testing rig.

The membrane was inflated by a foot pump through a valve. From the valve also an air-line was taken to a mercury manometer. There were initially seven positions along a given generator chosen for strain measuring purposes. Four strain-gauges were cemented at every position. The set consisted of two meridional and two circumferential gauges, one set of each for the inside and the outside of the model, with twenty-eight matching dummies cemented to a piece of perspex. All gauges were connected to standard Bruel & Kjaer recording equipment (models 1516, 1542 and 1543), shown in Plate 7.4. Figure 7.4 is a block diagram indicating the manner of connection of the individual items discussed above.

7.4 TEST PROCEDURES AND RELEVANT OBSERVATIONS

It was thought that if the model were to be loaded incrementally, then the recorded strains could be plotted against the loads (pressures) enabling the calculation of linearised strain per unit pressure for each gauge. The stresses could then be calculated from the linearised strains since the numerical value of the elastic constants had previously been

determined. By rotating the model about its axis, a corresponding set of results for a different value of the circumferential angle θ was obtained. A comparison could then be made between the theoretical and experimental results based on calculating the pressure as unity (since the stresses are obtained from the slopes of the strain/pressure graph).

There were some difficulties in conducting the experiment, in the way of recording the correct strains. Some of these points are listed below.

i) Two gauge positions became unreliable and thus the reading along five points only on the meridian could be considered.

ii) Almost half the gauges became difficult to zero, some of them with initial strains of the order of 2×10^{-3} which increased the task of measuring the variation of the strains to satisfactory accuracy.

iii) The readings on the manometer very often had to be estimated due to drop in pressure observed in iv) below.

iv) Owing to some leakage in the connections and the bag, the operator was compelled to pump constantly to maintain a satisfactory pressure head in order to take a reading. In practice a drift was noticed after a particular gauge was selected. By the time the drift had settled (about 5 to 20 seconds) the pressure had dropped by 0.1 or 0.2 inches of mercury. The uncertainty then arose whether the change in strain reading was due to electrical circuitry or to genuine mechanical reduction in pressure. The bag had to be reflated to a predetermined pressure head and the pointer on the strain recorder had to be noticed carefully.

The object was to assess the incremental direction of the change in strain, corresponding to a definite increase in applied pressure. This very often had to be done when the scale selector was on low sensitivity owing to large initial readings which made strain recording less definite and more speculative.

v) Owing to the above mentioned failure in zeroing the gauges, the scale selector had to be altered continuously, since the 'non-zero' gauges were generally in a random order.

vi) It was found that at a given pressure the entire strain reading would completely alter the anticipated direction on the strain/pressure graph and become unreliable and unpredictable. It was observed that at such pressures the physical inflation of the bag produced an unwanted component of axial compression by wrinkling over the top of the tower. This is sketched in Fig. 7.5. Naturally, the number of pressure increments became limited. It was found that the maximum range of pressure head was between 1.2 and 1.4 inches of mercury.

vii) After unloading (deflating), the readings did not return to their original unloaded values (initial readings). This was attributed to material creep and was found to generally vary between 10% to 15% of the mechanical strains corresponding to each pressure increment. However, no corrective measures were taken to compensate for the influence of creep on the results.

7.5 COMMENTS ON THE RESULTS

The task of processing these results was mammoth, since each experiment involved between 4 to 7 increments of pressure. All these experimental points had to be plotted and the slopes had to be judged and recorded. The conversion from strains to stress resultants could then be made. Finally the units had to be adjusted to convert the stress resultants from N/mm/(in Hg) to N/mm/(N/mm^2). The experiment was then repeated to enable the averaging of the final stress resultants. Only at that stage could some experimental results be retained as consistent and others be discarded. If the outcome of any test did not appear to indicate a reasonable correlation, another attempt to obtain fresh experimental results was made. The tower was loaded for different values of the circumferential angle θ, namely for $\theta = 0^o$, 45^o, 90^o and 180^o.

Prior to the above experiments, a number of tensile test-pieces had been loaded and the value of the elastic constants had been verified and compared with those given in manuals. The E and ν values were found to be $3065 N/mm^2$ and 0.35 respectively. The density which was calculated for dynamic experiments was 1.194×10^{-3} gm/mm^3.

The theoretical results were based on a particular distribution of pressure. It was assumed that a uniform pressure p_u acted on the tower for $\frac{-\pi}{2} \leq \theta \leq \frac{\pi}{2}$. This pressure was then represented in terms of Fourier components in the normal form,

$$p = p_0 + \sum_{i=1}^{\infty} p_i \cos i\theta$$

where p_i was estimated to be

$$p_i = \frac{4p_u}{i\pi} \cdot \sin\left(\frac{i\pi}{2}\right) \qquad i = 1,3,5,7,\ldots$$

and

$$p_0 = \frac{1}{2} p_u.$$

Altogether 8 components were included in the analysis, namely i=0,1,3,...,13. These coefficients and their approximate, accumulative representation of the pressures, for half of the tower are indicated in Fig. 7.6(a) and (b).

The tower was divided into 5 non-equal elements for which the variation in thickness was incorporated. Each element had only 3 surplus degrees of freedom (1u, 1w and 1v). The total degrees of freedom amounted to 55 which meant the data could be processed using the Polytechnic 16K IBM 1130. The details of the geometry used in the data is shown in Fig. 7.7.

Figures 7.9 to 7.12 show the variation of the resultants T_s and T_θ with respect to the height Z. There appeared to be something seriously in error with the results $(T_s)_{\theta=0}$ and $(T_s)_{\theta=90}$. The experimental results shown are scaled down by a factor of 10. The calculations were checked a number of times and finally the results were averaged over four individual loadings for $\theta=0^o$.

In view of this apparent lack of consistency, it was decided to fix gauges at a single point towards the base of the tower and repeat the experiment as a single point check. The results obtained from this gauge are shown by an asterisk(*) in Figures 7.9 to 7.12. It seems as if the new results are generally as inconclusive as the previous set. However, it is obvious that the value of T_s for $\theta = 0$ determined experimentally has emerged many times larger than the corresponding theoretical values.

As yet the candidate has not been able to produce a satisfactory explanation for these two oddities. As can be seen the confusion is not helped, since variation in other stress resultants appear reasonably.

The departure from the theoretically predicted curve appears to fall within the following patterns.

a) Some experimental curves appear to be shifted by a constant amount as shown in Fig. 7.11(T_θ).

b) With some curves the variation seems to be magnified or reduced about the theoretical curve, shown in Fig. 7.10(T_θ).

c) The values of some experimental curves tend to be magnified or reduced about the Z axis, see Fig. 7.12.

The observed departures were attributed partly to points (i) to (vii) given in the previous section and partly to the points listed below.

i) The generator of the tower was not a precise hyperbola. Apart from this variation in geometrical parameters, there were also small ripples in the form of rings about the main axis.

ii) The physical contact between the air-bag and the outside gauges might have been a significant contributor to some anomolies. In the first instance the effect of the direct pressure on the gauges is a suspicious factor, the extent of influence of which cannot be assessed by the author. In the second instance some confusion results in interpretation of the slope of the strain/pressure curve. Very often results of the nature of segments 1, 2 and 3 are obtained, as shown in Fig. 7.8. This is thought to be caused by frictional slips between the bag and the model. The dilemma was to decide on the correct slope of the curve. Was it alternative I which

was the correct regression curve or alternative II which was the average of the slopes of the segments 1, 2 and 3? The choice of various alternatives has often been a matter of speculative judgement rather than a strict, uniform and consistent approach.

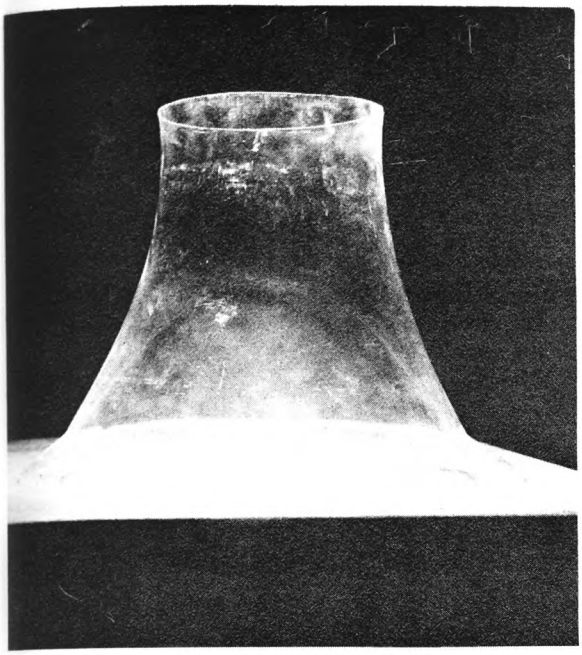

PLATE 7.1

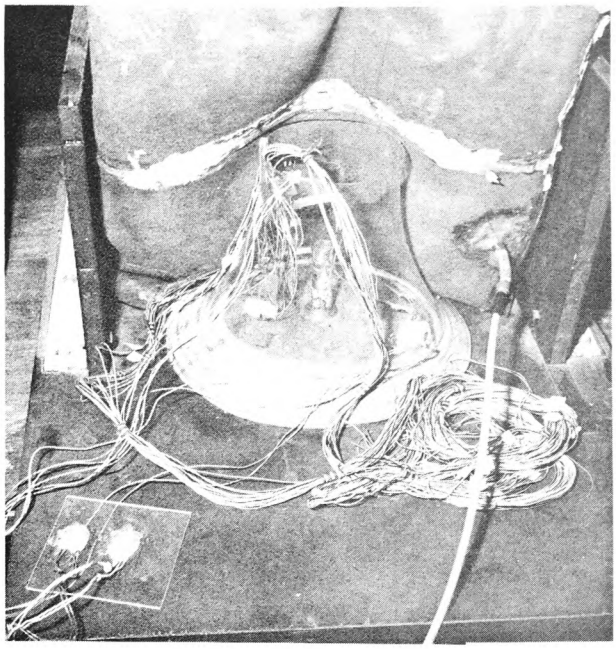

PLATE 7.2

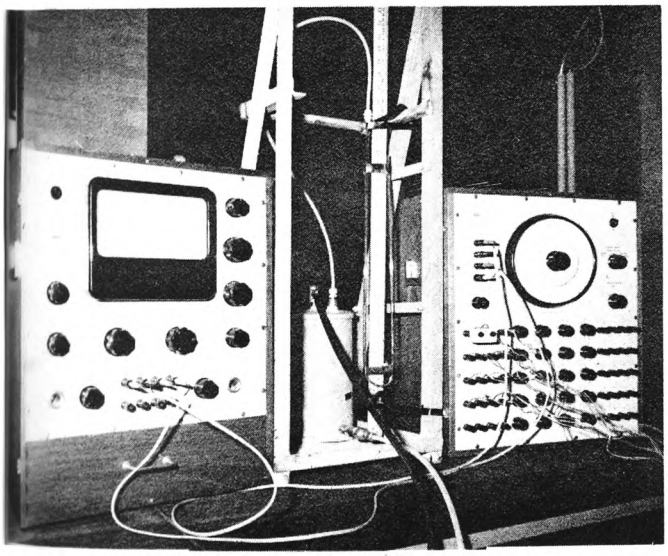

PLATE 7.3

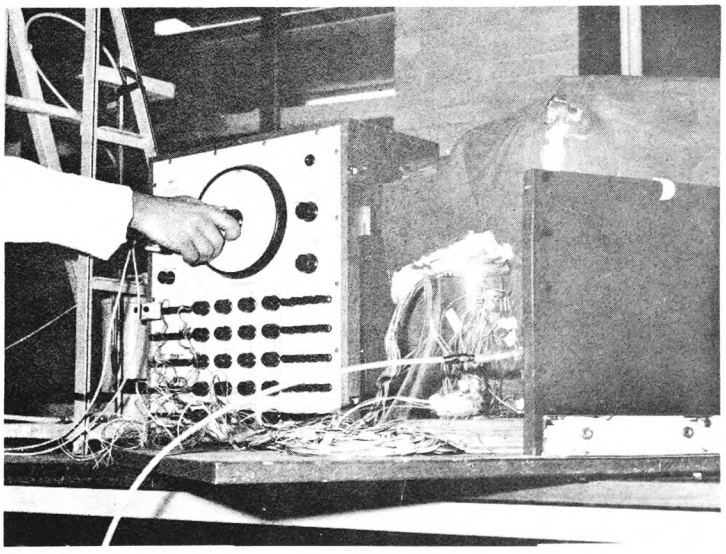

PLATE 7.4

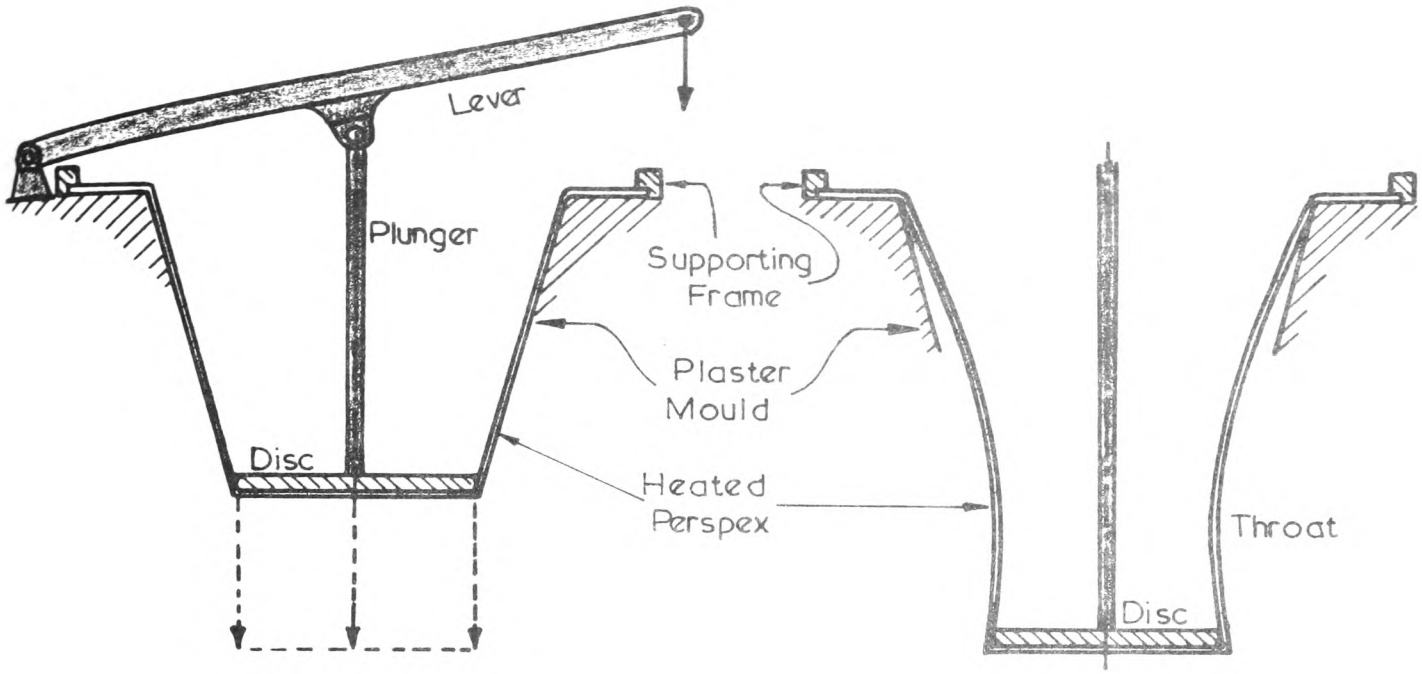

FIGURE 7.1

FIGURE 7.2

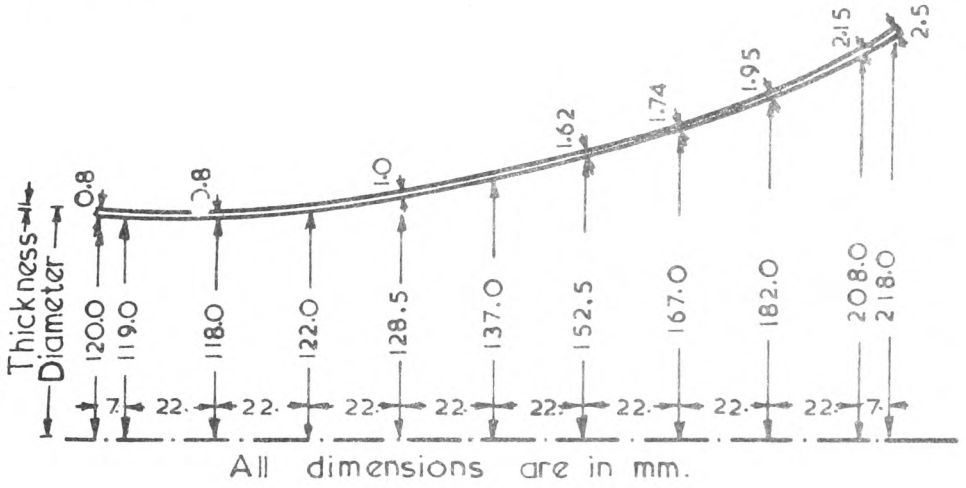

FIGURE 7.3

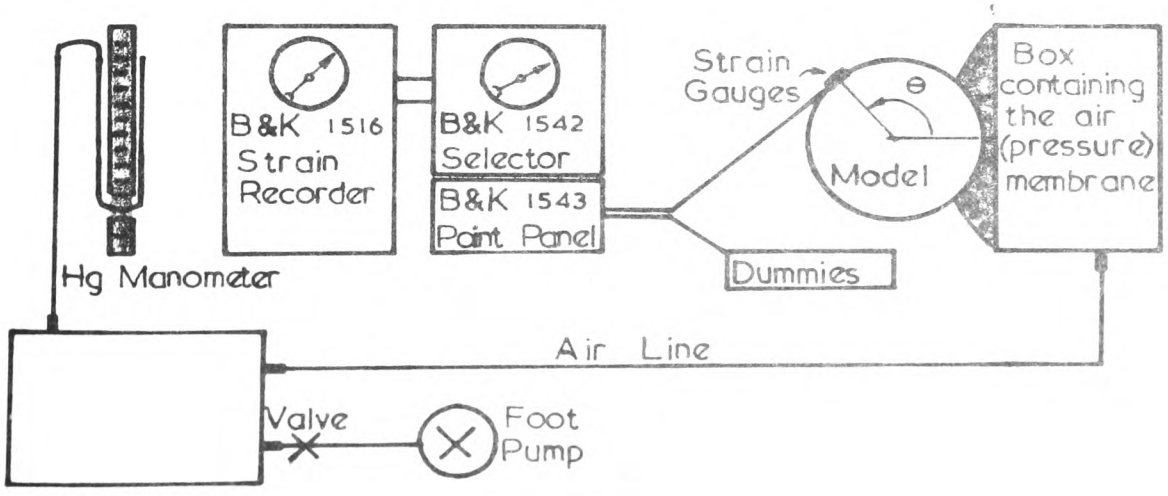

FIGURE 7.4

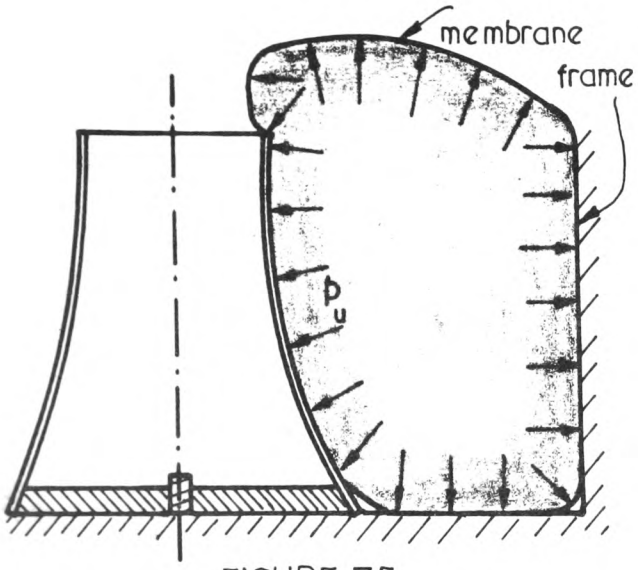

FIGURE 7.5

n	0	1	3	5
p_i	0.5	.636	-.212	.127

n	7	9	11	13
p_i	-091	.0708	-.0579	.049

(a)

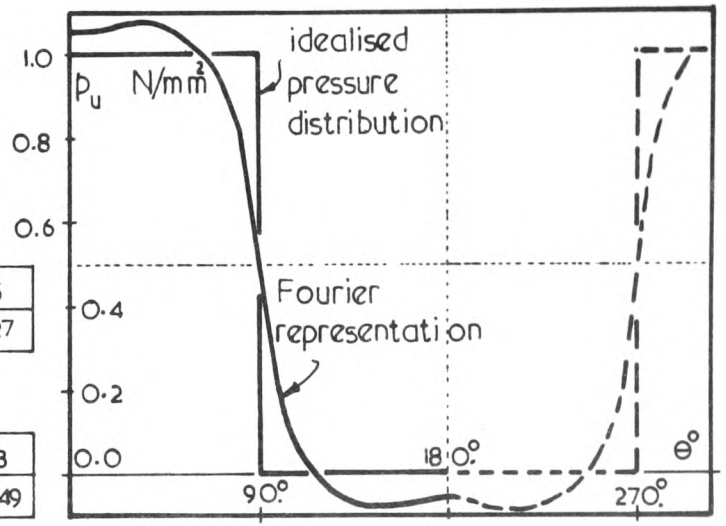

(b)

FIGURE 7.6

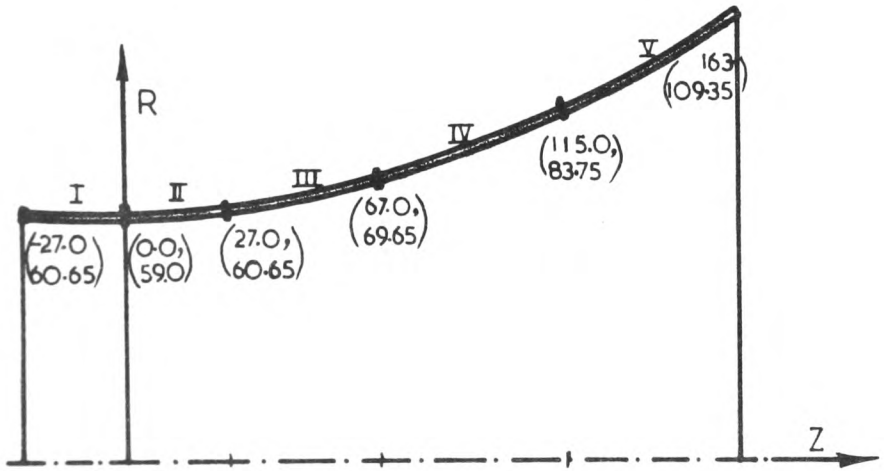

FIGURE 7.7

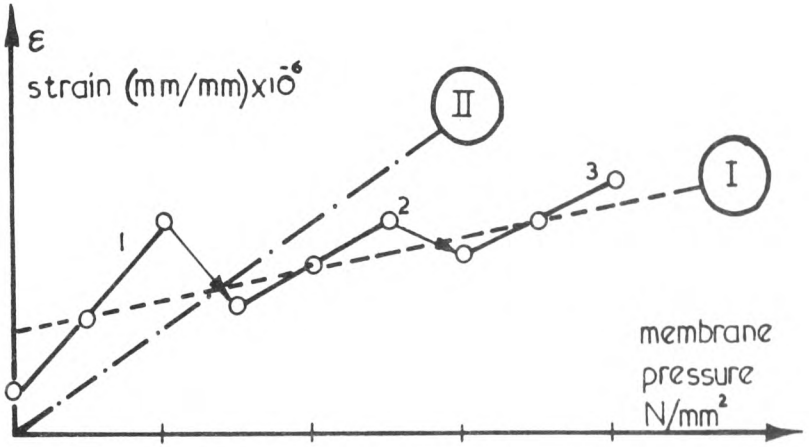

FIGURE 7.8

$\Theta = 0^{\circ}$

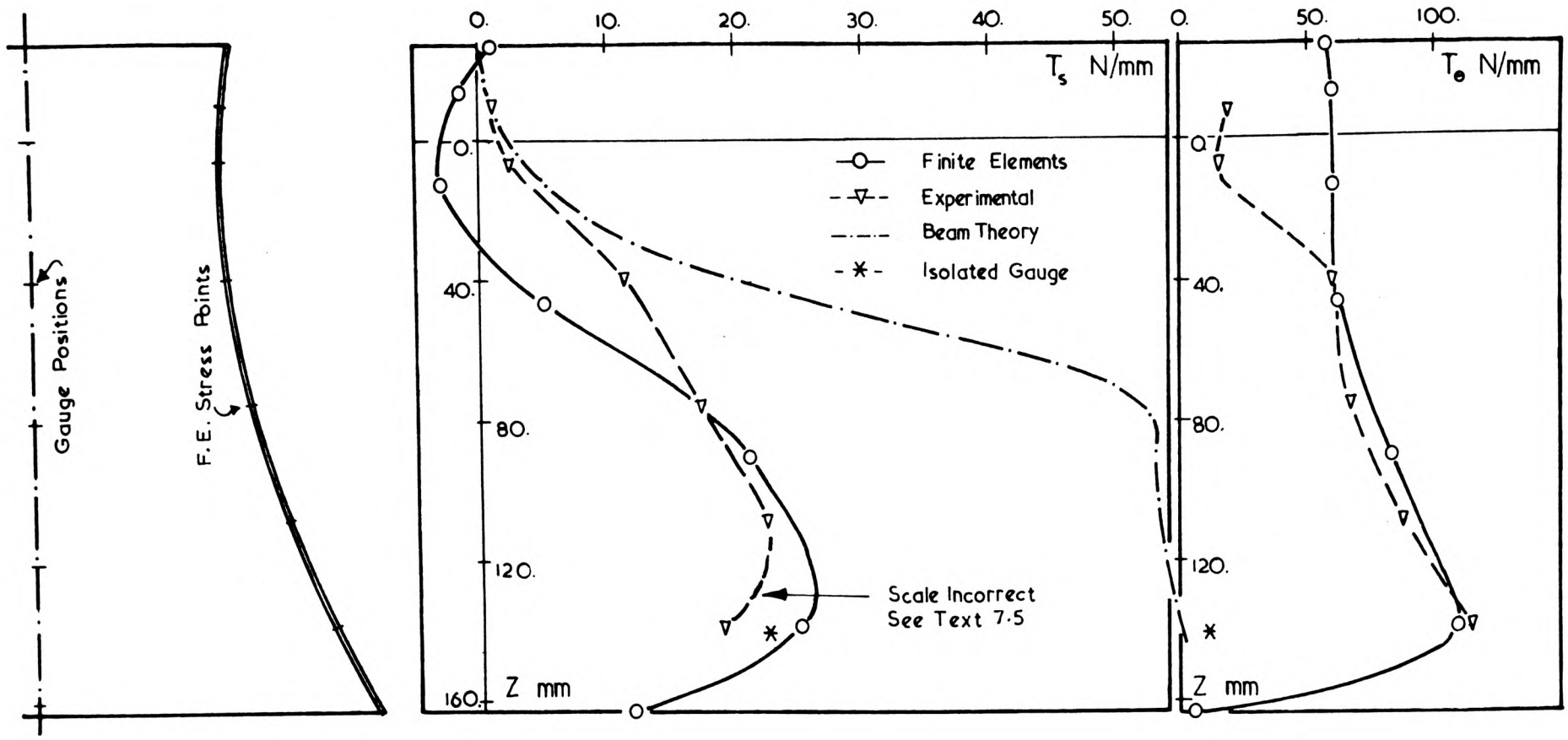

FIGURE 7.9

$\Theta = 45^\circ$

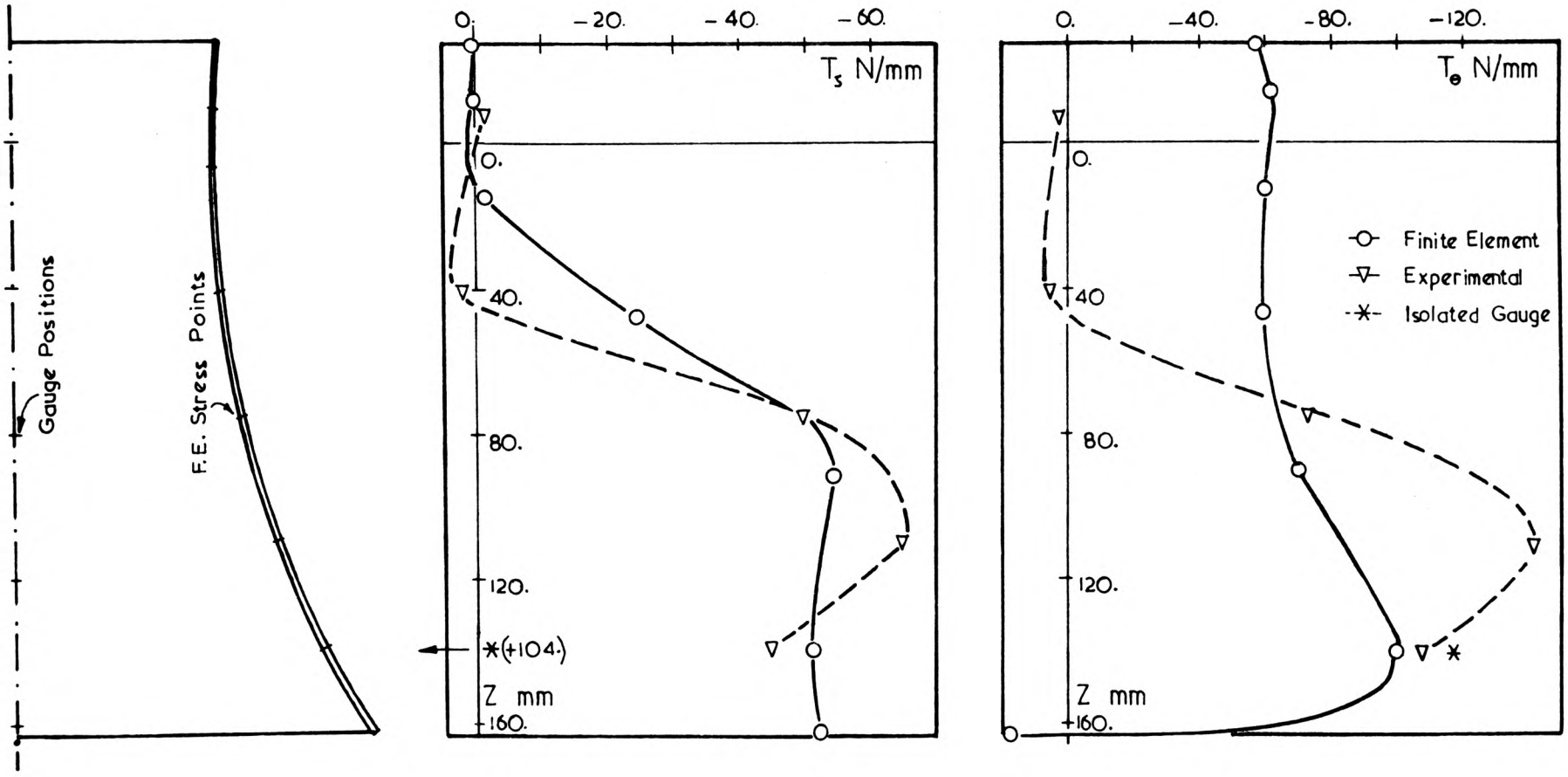

FIGURE 7.10

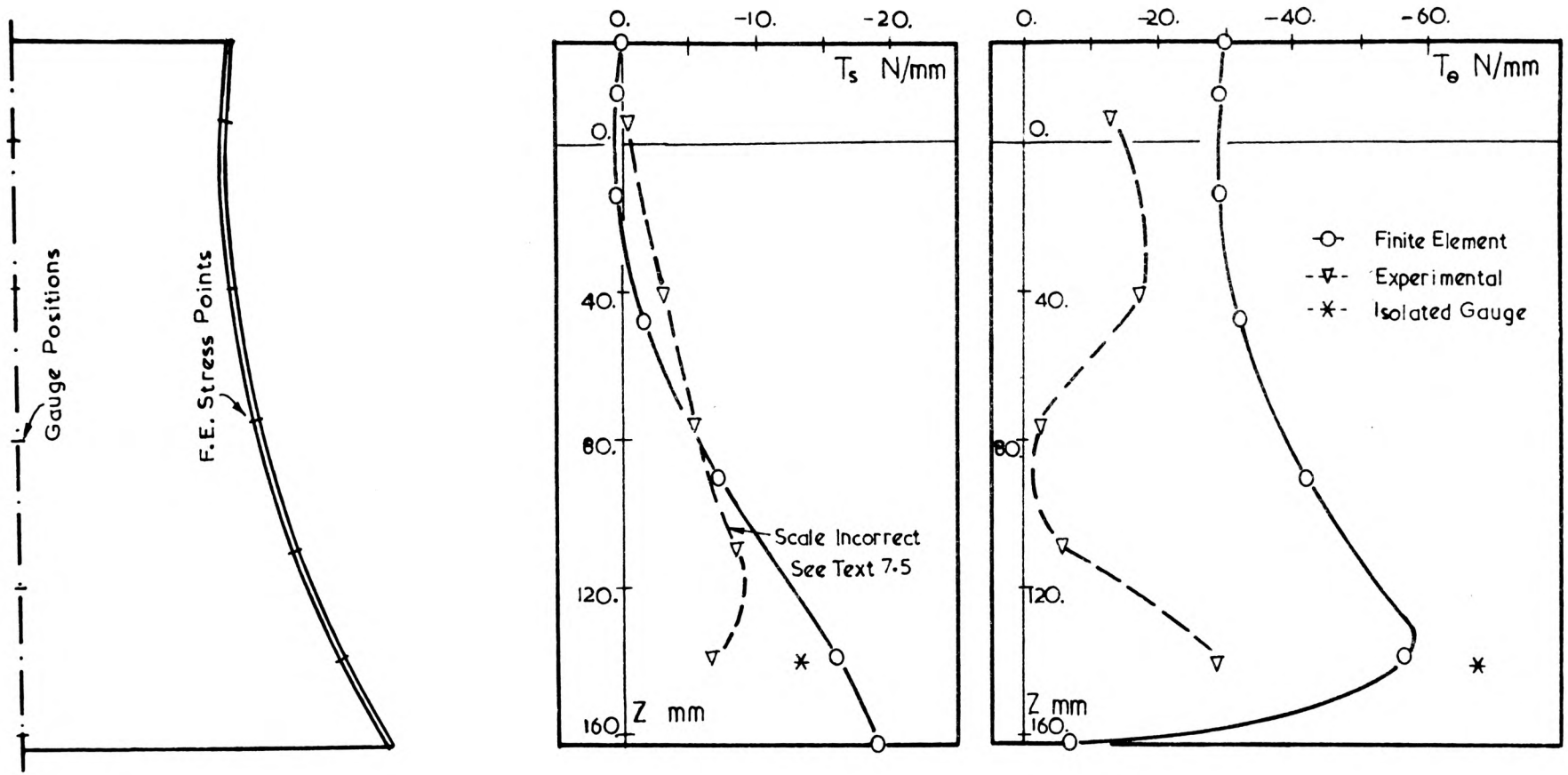
Θ=90°
Gauge Positions
F.E. Stress Points
0.
-10.
-20.
T_s N/mm
0.
40.
80.
120.
160.
Z mm
Scale Incorrect
See Text 7.5
0.
-20.
-40.
-60.
T_θ N/mm
Finite Element
Experimental
Isolated Gauge

FIGURE 7.11

$\Theta = 180^{\circ}$

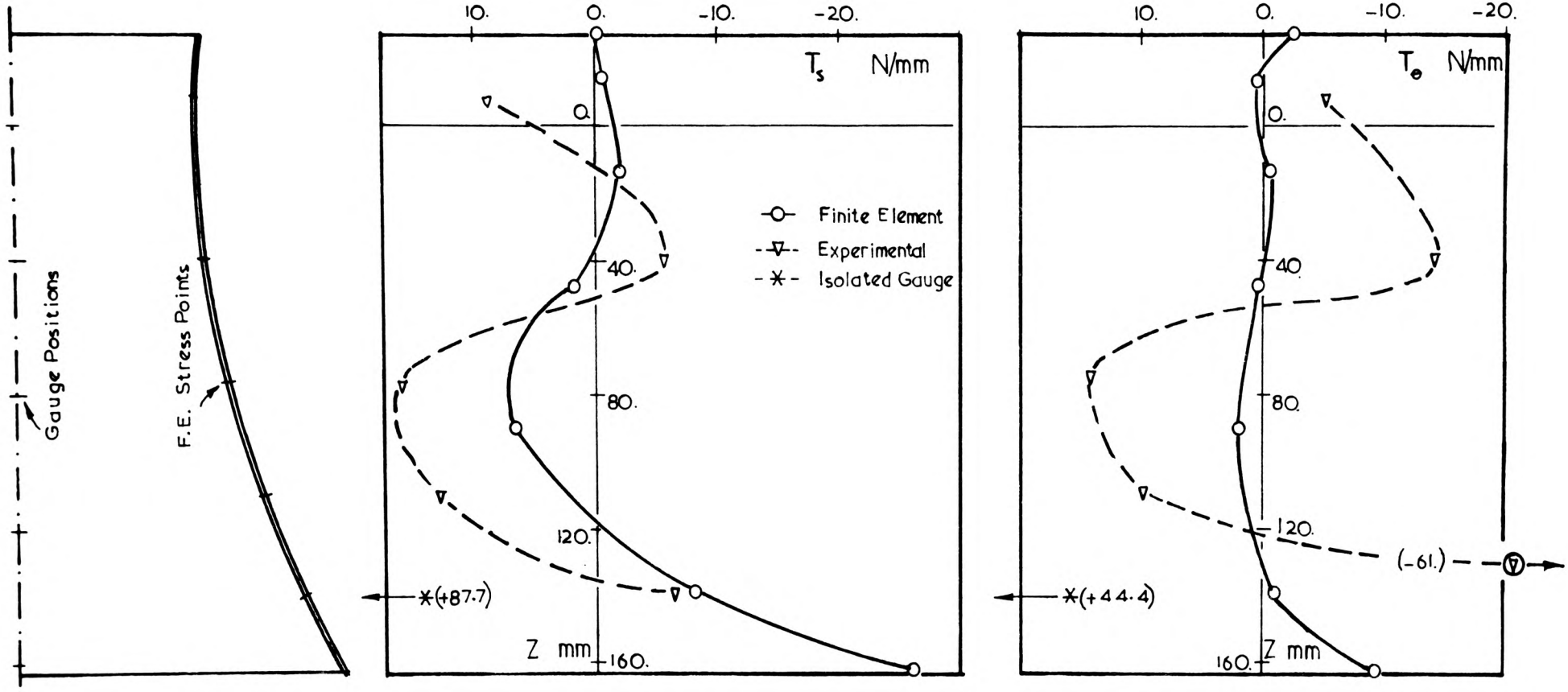

FIGURE 7.12

CHAPTER 8

EXPERIMENTAL DETERMINATION OF UNDAMPED AND UNFORCED NATURAL FREQUENCIES

8.1 INTRODUCTION

The determination of natural frequencies of an undamped and unforced model was the last aspect of the experimental investigation in this scheme of work. It was intended again that a comparison should be made between theoretical and experimental results. The details of constructing a model in the shape of a cooling tower suitable for this type of investigation were discussed in the previous chapter and no further reference will be made here.

The candidate, being trained in the field of Civil Engineering initially, benefited from collaborating with a colleague[+], with knowledge of experimental dynamics.

8.2 SETTING UP THE MODEL, INSTRUMENTATION AND OBSERVATIONS

At the early stages of the experimental investigation, the vibration program had not been fully tested and as such no serious attempt was made to predict any theoretical frequencies for the model tower. In order to commence the experimental procedures, it was decided to identify the natural frequencies between about 100.0 Hz. to 1000.0 Hz. It was not felt at the time, that any natural frequency would be encountered below 100.0 Hz. The test equipment was then chosen with the above frequency range in mind.

+ Mr. W. Hague, Department of Mechanical Engineering of the Polytechnic of Wales, formerly of Bristol Siddely Engines Ltd., Bristol.

Existing equipment was utilised in order to avoid purchase of non-standard, specialised equipment. The model was set up as shown in Plate 8.1, the set up and test procedure being listed below.

i) A set of parallel arcs was marked on the model with silver paint, to provide a partially covered metallic surface.

ii) The model was secured rigidly at its base, through a threaded axial steel rod, to a conventional Seismic Block (concrete block) which isolated the model from any possible random disturbances on the laboratory floor.

iii) The same steel rod which was slightly longer than the model had its projecting extremity also threaded. An arm positioned at 90^{o} to the rod was then sandwiched rigidly and held in position between two nuts on the threaded section. The arm became almost a radius at the top of the tower.

iv) From this arm a perspex templet, cut in the shape of a generator of the tower, was suspended so that it was in a plane very close to the axis of the tower. The position of the templet was adjusted to maintain a uniform gap between corresponding points of the tower generator and the nearside edge of the templet.

v) An adjustable probe was then mounted on the templet with an arbitrary gap of approximately 0.2 mm. between it and the shell surface. By rotating the arm about the axis and adjusting the nuts, the templet and thus the probe could be guided to almost infinite variety of circumferential and meridional positions.

vi) A shaker was attached to the top of the tower to cause radial displacements. The shaker was driven by an oscillator with

adjustable frequency and amplitude.

vii) The signal from the probe was fed through a vibration-meter capable of giving both the average gap between the probe and the model and the amplitude of oscillation. The signal was also fed to an oscilloscope.

The above arrangement, although it indicated some fundamental frequencies, was incapable of separating the minor natural frequencies. It was later realised that in order to determine a particular mode, some notion of the phase difference between the shaker and a particular point on the model was also required. There was however, some limited success in identifying the antinodes both meridionally and diameterally owing to almost uninhibited swivelling action of the probe.

It was then decided to replace the oscilloscope with a frequency analyser. The analyser was capable of generating the frequencies but the signal had to be amplified prior to connection to the shaker. The signal emerging from the probe could then be taken to the analyser via the vibration-meter and a demodulator. By an appropriate choice of the integration cycles which depended on the frequency of excitation, the amplitude of oscillation and the phase angle could be read digitally and recorded. The final assembly is indicated diagramatically in Figure 8.1. Plates 8.1 and 8.2 show the actual equipment in use. The acquaintance with various measuring equipment and their mode of use formed an edifying part of candidate's work.

8.3 RESULTS AND COMMENTS

By this time there were indications that the vibration program had proved successful when tried for a number of simple cases. In view of this it was felt that the occasion for determination of theoretical frequencies of the model was apt.

The information used was based on geometrical, elastic and physical data given in section 7.5. The finite element divisions used in the dynamic analysis were similar to the divisions considered for the static analysis discussed in Chapter 7. Only three surplus degrees of freedom (lu, lw and lv) were allocated to each element with the base of the tower assumed to be rigidly fixed which resulted in an overall size of 55 degrees of freedom. The core used varied between 32K to 34K and the time of execution lasted between 12 to 18 minutes. The execution time involved generation and assembly of 5 elemental stiffness matrices, a Choleski reducation and inversion of the lower triangle of the stiffness matrix, pre and post multiplication of the mass matrix by the resulting triangle and finally the extraction of the four lowest roots by iteration.

The data was processed commencing with n=0 harmonic. It was noticed with great disappointment that the natural frequencies fell with the increase in the number of nodal diameters contrary to popular belief[+]. A number of published articles were then noticed by the candidate quite fortuitously most of which are listed in Chapter 5. These references had provided experimental and theoretical data for shells such as cylinders, cones and hyperbolae of revolution. Each

---

+ This false impression had been created owing to the predicted frequency of the elastic continua (e.g. beams and plates) in flexure. In these cases any increase in the number of waves defining the mode of vibration would result in a corresponding increase in the frequency of oscillation. Ample examples of this have been listed in standard text books. See also Chapter 5 and examples on plates, Fig. 5.2 - Fig. 5.5.

showed that there was a frequency corresponding to a diametral mode which formed a minimum on a frequency/nodal diameter plot.

Some considerable number of hours had been spent previously in collecting the experimental data relating to natural frequencies between 100.Hz and 1000.Hz. The variation in amplitude and the change of phase of the above results were later recorded in a chart form. These data did not contribute to the present analysis directly since the finite element calculations predicted a minimum natural frequency at about 20 Hz. This meant that the above data were only comparable with the higher modes of the nodal diameters between n=0, ... 20 or the first few modes of fairly large values of n.

It was then decided to paint more metallic grids around the top part of the tower so that the modes corresponding to specific nodal diameters could be identified. The resonance sweep was also made at fairly low frequencies since some notion of the orders of frequencies was established. This presented a practical difficulty since frequencies between 10 and 20 Hz could not be maintained for long periods of time as they coincided with a resonant frequency of the shaker/mounting assembly. Another difficulty was encountered when the probe was positioned at different angles around the circumference of the top of the model. It was found that the initial amplitude of the shaker, positioned at $\theta=0^{o}$, was damped progressively as the probe approached $\theta=180^{o}$. The damping was found to be an unfavourable property of the perspex model. It was then realised why some other workers had preferred metallic models.

Frequencies were then recorded between 15 to 30 Hz in increments of 0.1 Hz. This resulted in a positive identification of the lowest five frequencies. The separation of the other modes became more difficult owing to closeness of resonant frequencies and overlapping of respective displacements. However the next two frequencies are given

with some degree of certainty. The favourable correspondence of experimental and theoretical resonance frequencies were found encouraging with theoretical resonant frequencies being fractionally higher as expected. The results of the theoretical frequencies in Hz of the tower versus the nodal diameter n is given in Figure 8.2(a) and (b). The comparison between the experimental and the corresponding theoretical frequencies of the lowest seven modes is given in Figure 8.3.

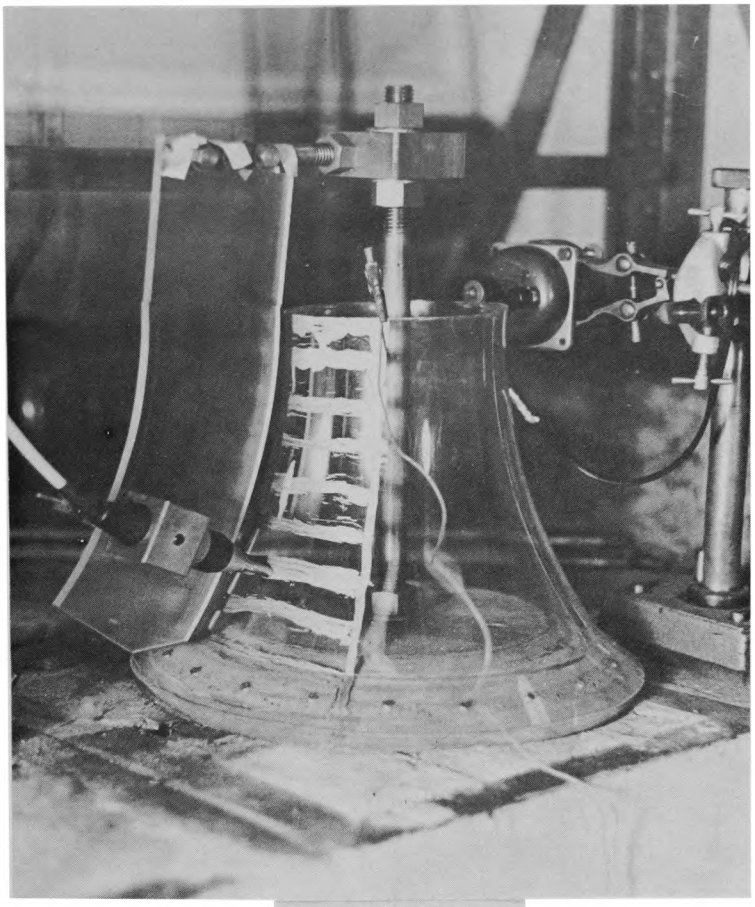

PLATE 8.1

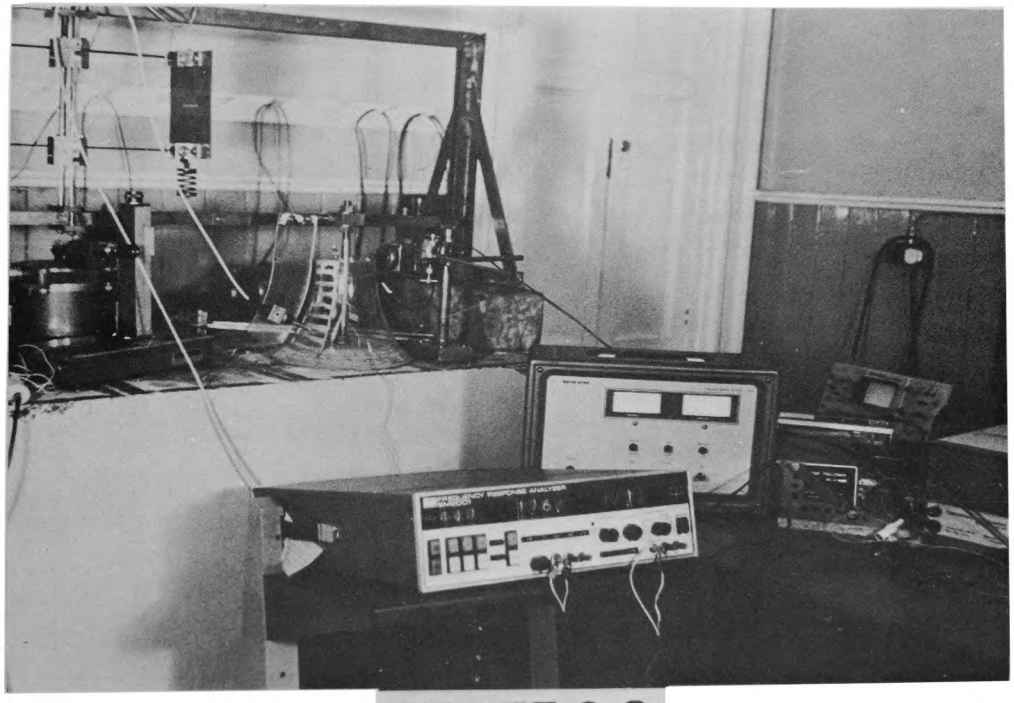

PLATE 8.2

BLOCK DIAGRAM OF MODEL AND
EQUIPMENT SETUP IN VIBRATION TESTING

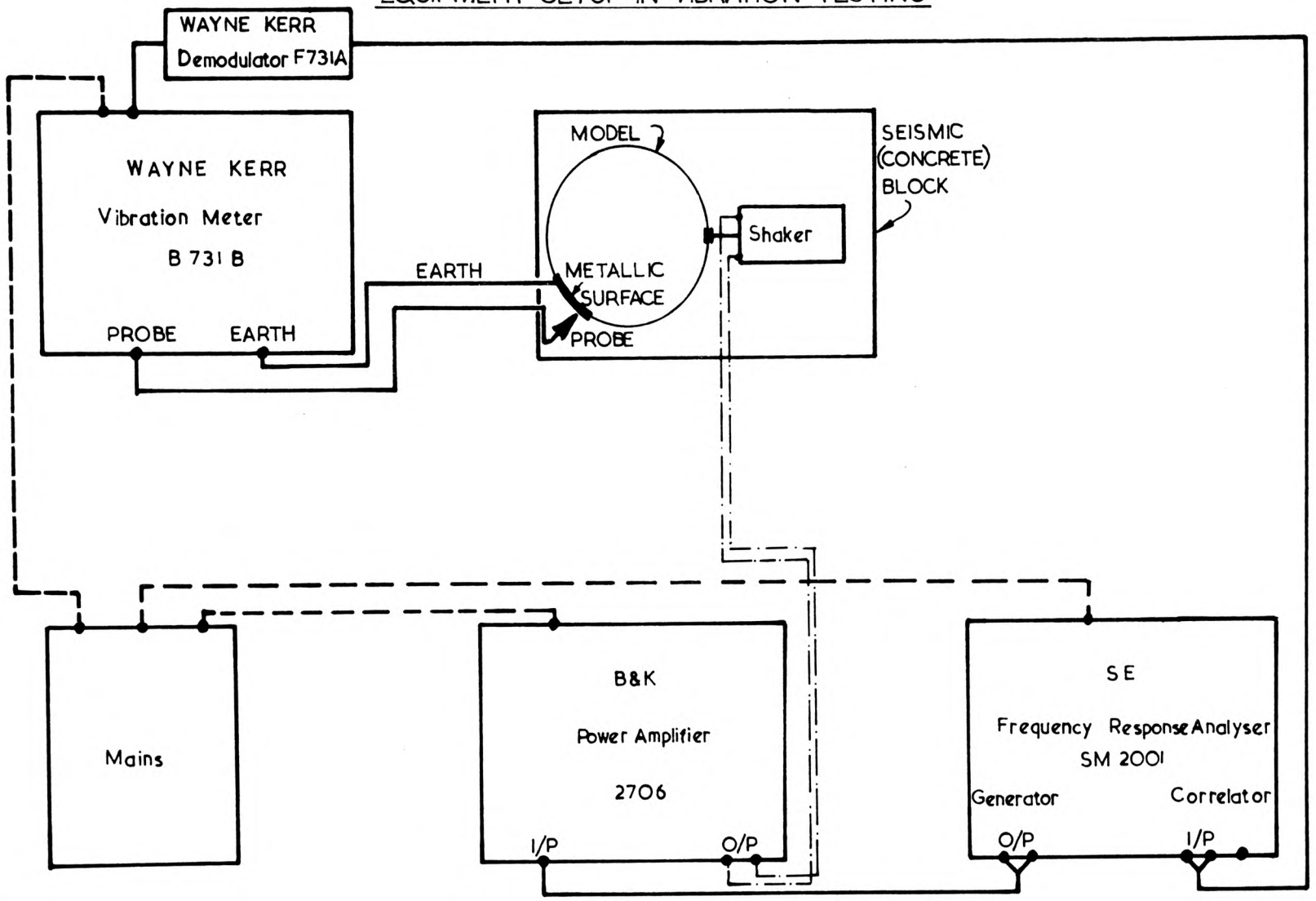

FIGURE 8.1

THEORETICAL FREQUENCIES OF MODEL PERSPEX COOLING TOWER

Frequency Hz

n	mode 1	mode 2	mode 3	mode 4
0	80·57	83·43	91·63	102·21
1	41·27	59·97	78·37	88·91
2	25·91	36·50	58·46	75·96
3	21·33	24·20	40·57	59·33
4	19·99	22·18	31·00	45·60
5	22·19	25·39	29·07	38·21
6	28·15	29·55	33·60	35·94
7	35·60	35·79	41·10	41·88
8	43·25	44·08	50·46	50·29
10	61·81	63·79	72·49	73·72
12	84·40	88·11	99·25	102·20
16	140·79	150·81	165·46	174·33
20	212·01	231·54	248·12	265·87

(a)

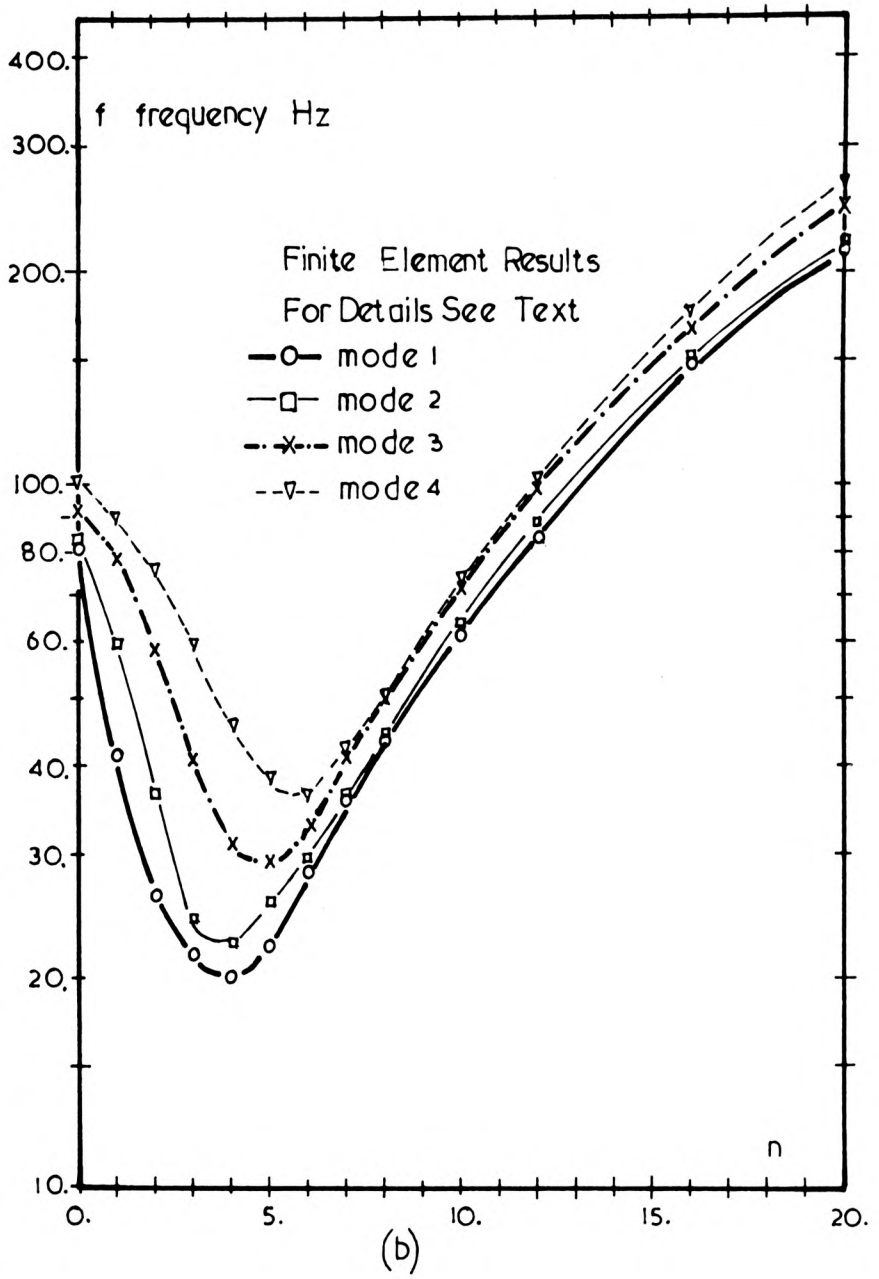

(b)

FIGURE 8.2

COMPARISON OF THEORETICAL AND EXPERIMENTAL FREQUENCIES

n harmon	m mode	order of reson.	f Hz frequency	Comments
4	1	I	19.4	Definite mode shape
3	1	II	20.9	Definite mode shape
5 4	1 2	III IV	21.5 22.0	III Dominant about 21.5 Hz IV Dominant about 22.0 Hz
3	2	V	24.0	Fairly definite mode
2 5	1 2	VI VII	24.8 26.5	Cannot really discriminate

(a)

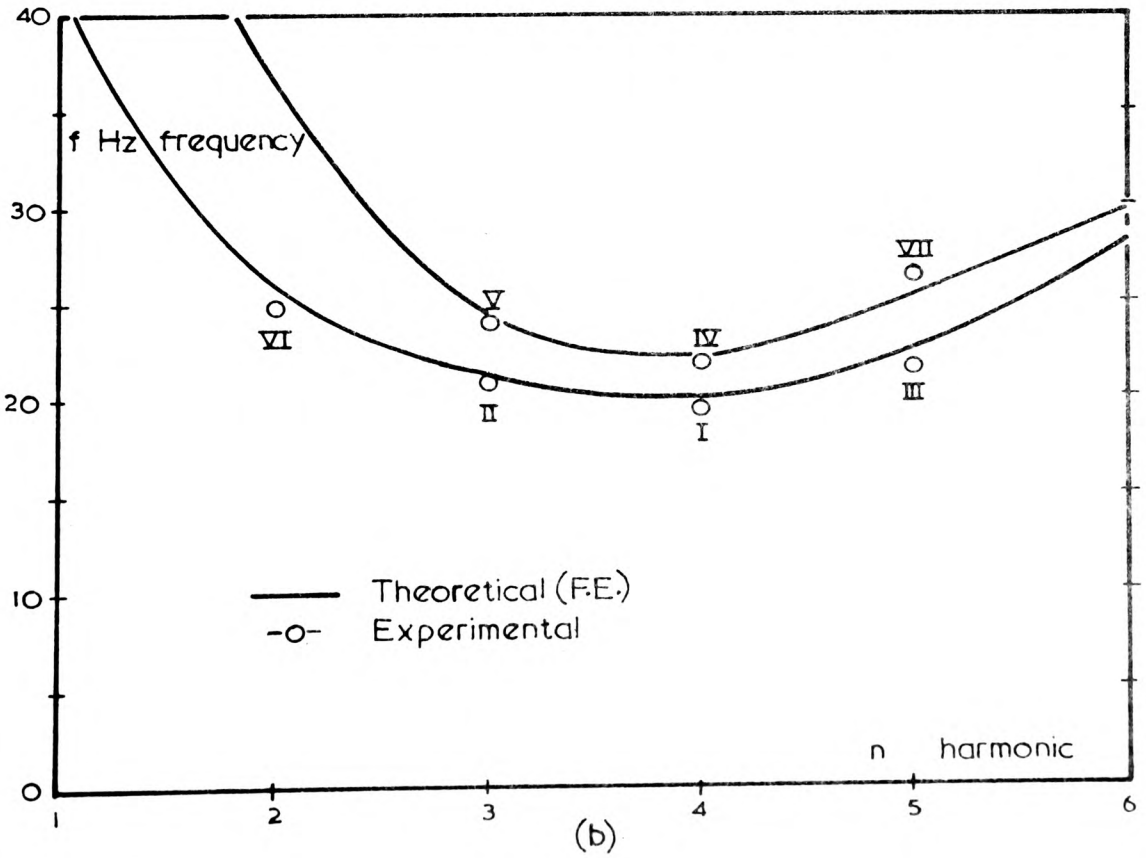

(b)

FIGURE 8.3

PART IV

THE INLUENCE OF INPLANE LOADS

CHAPTER 9

THE EFFECT OF THE TIME-INVARIANT EXTERNAL FORCES ON THE FREE VIBRATION MODES

9.1 INTRODUCTION

Determination of the natural frequency of thin elastic shells of revolution was dealt with in Chapter 5. The situation becomes more critical when the structure is loaded in a manner which results in a system of in-plane stress resultants. If these in-plane resultants were compressive, the structure would then need a closer examination.

Generally the compressive forces reduce the stiffness of the structure and since the corresponding change in mass matrix is negligible then any possible excitation at the lower part of the frequency spectrum could result in "premature" resonance. In some cases when the structure is partly in tension and partly in compression, local instability could be expected. This may result in local failure, causing an overall collapse owing to serious local change in geometry.

9.2 FINITE ELEMENT FORMULATION

The equation used here is taken from reference (1) with two trivial variations in presentation and notation. The symbols used for stiffness, geometric and mass matrices are $[K]$, $[K_\sigma]$ and $[M]$ respectively. The interaction of in-plane forces with the stiffness and mass matrices are given as

$$([K] + \lambda[K_\sigma])\{\delta\} - \omega^2[M]\{\delta\} = 0, \qquad \text{..... eqn. 9.1}$$

where λ and ω^2 are as defined in Chapters 5 and 6. The following simple observations then follow:

1) For zero value of the frequency ω, the fundamental stability relationship given in eqn. 6.2 is obtained, the roots of which give the buckling stresses.

2) For zero value of λ, the relationship simplifies to eqn. 5.1 which results in natural, unforced and undamped frequency ω_n.

3) If the external forces stiffen the structure, then λ is generally positive. The additional "hardening" raises the natural frequency ω, so that $\omega > \omega_n$.

4) If the external forces "soften" the structure, the reverse process to 3) takes place, namely $\omega < \omega_n$.

5) If $\lambda = -\lambda_c$ ($|\lambda_c|$ corresponds to a critical load), then the total stiffness disappears and the structure has no resistance to any subsequent disturbances.

The terms "hardening" and "softening" are used somewhat loosely in the above development. The meaning attached to the above terms is associated with an increase or reduction in the structural stiffness which depend on the algebraic term $([K] + \lambda[K_\sigma])$.

9.3 PRACTICAL DETAILS

The techniques of generating the matrices $[K]$, $[K_\sigma]$ and $[M]$ is symbolised by eqns. 3.18, 4.19, 5.7 and 6.14 thus no further reference will be made to their calculation. Each matrix is formed and stored individually in a common subroutine. There is an obvious saving in computer time when all three matrices are generated within the same integrating loop. The matrix $[K]$ occupies a vector in a lower triangle form whereas $[K_\sigma]$ and $[M]$ are stored in a nx(n+1) array as two triangles, namely $[K_\sigma \diagdown M]$. The change in structural behaviour due to the addition of in-plane loads can be incorporated by including a simple code in the

input data. In the absence of any such code, the natural frequencies and the buckling pressures are calculated instead.

9.4 TRAVELLING WAVES

The problem of travelling waves in rotating discs is discussed in some standard texts on vibration. For example reference (2) provides a collection of formulae and tables enabling the estimation of any increase in disc frequency due to a steady angular velocity. The extension of this work to any surface of revolution, though fundamentally easy, requires some care. Both the Virtual Work method and the Strain Energy method were used by the candidate to obtain the mass matrix $[M]$. In both cases the final equation derived was the same. Here, only the Virtual Work approach will be presented.

The correct consideration of geometrical and kinematic properties is essential at this stage of development.

Consider the shell of revolution of Fig. 9.1(a). Let the orientation of the radii involved be as shown in Fig. 9.1(b). In view of the remarks made in Chapters 2 and 6, the following relationships can be written,

$$\phi = 90-\alpha \qquad R_2 = R/\cos\alpha \qquad \psi = \theta\cos\alpha$$

The normal displacement w would be along R_2 and v along the circumference. If a hypothetical point mass were to travel circumferentially at a radius R, the traversed curve would have a radius of curvature defined by R_2 which would also act as its normal, see Fig. 9.2(a). Thus the osculating plane would contain any two adjacent radii of curvature R_2 and the portion of the curve subtending an angle ψ shown in Fig. 9.2(b). The tangent to the curve would then be along the circumferential displacement v and the tangent to the meridian can be recognised as the binormal to the curve. It is shown in reference (3) that the accelerations are in the osculating plane

as depicted in Fig. 9.2(b) above. It is therefore convenient to refer to displacements in local coordinates which are labelled with a bar. The equations given below are then considered,

$$\left.\begin{aligned} r &= R_2 + \bar{w} \\ \bar{v} &= R_2\psi \end{aligned}\right\} \quad , \qquad \ldots\ldots \text{ eqn. 9.2}$$

$$\left.\begin{aligned} (\text{vel})_r &= \dot{r} = \frac{d\bar{w}}{dt} \\ (\text{vel})\psi &= r\dot{\psi} = \frac{d\bar{v}}{dt} \end{aligned}\right\} \quad , \qquad \ldots\ldots \text{ eqn. 9.3}$$

$$\left.\begin{aligned} (\text{accn})_r &= \ddot{r} - r\dot{\psi}^2 = \frac{d^2\bar{w}}{dt^2} - \frac{\cos\alpha}{R}\left(\frac{d\bar{v}}{dt}\right)^2 \\ (\text{accn})_\psi &= r\ddot{\psi} + 2\dot{r}\dot{\psi} = \frac{d^2\bar{v}}{dt^2} + \frac{2d\bar{w}}{dt}\frac{\cos\alpha}{R}\frac{d\bar{v}}{dt} \end{aligned}\right\} \qquad \ldots\ldots \text{ eqn. 9.4}$$

It is now necessary to define the type of motion so that the above velocities and accelerations can be expressed more explicitly. Let the surface rotate with an angular velocity p and the travelling waves with a velocity of ω. The relative angular velocity is then given by $(\omega \pm p)$ and the angle covered in time t by $(\omega \pm p)t$. If the circumference now breaks into n full waves, the entire angular position could be represented as $[n\theta \pm (\omega \pm p)t]$. The exponential $e^{i\omega t}$ of Chapter 5 is now modified to,

$$e^{i[n\theta \pm (\omega \pm p)t]} = e^{in\theta} \cdot e^{\pm i(\omega \pm p)t}.$$

Thus the displacements could retain their initial form given in Chapters 4 and 5 with a slight modification given below,

$$\begin{Bmatrix} \bar{u} \\ \bar{w} \\ v \end{Bmatrix} = \begin{Bmatrix} \bar{u}_0 \cos n\theta \\ \bar{w}_0 \cos n\theta \\ \bar{v}_0 \sin n\theta \end{Bmatrix} . e^{\pm i(\omega \pm p)t} \qquad \ldots\ldots \text{ eqn. 9.5(a)}$$

or

$$\begin{Bmatrix} \bar{u} \\ \bar{w} \\ \bar{v} \end{Bmatrix} = \begin{Bmatrix} \bar{u}_0 \sin n\theta \\ \bar{w}_0 \sin n\theta \\ \bar{v}_0 \cos n\theta \end{Bmatrix} . e^{\pm i(\omega \pm p)t} \qquad \ldots\ldots \text{ eqn. 9.5(b)}$$

The above displacements (taking the first set for example) are then substituted in eqns. 9.3 and 9.4 to obtain the velocity and accelerations,

$$\begin{Bmatrix}(vel)_r\\(vel)_\psi\end{Bmatrix} = \pm i(\omega \pm p)\begin{Bmatrix}-\bar{w}_0 \sin n\theta\\ \bar{v}_0 \cos n\theta\end{Bmatrix} e^{\pm i(\omega \pm pt)} \quad \ldots\ldots \text{ eqn. 9.6}$$

$$\begin{Bmatrix}(accn)_r\\(accn)_\psi\end{Bmatrix} = \left[\pm i(\omega \pm p)\right]^2 \begin{Bmatrix}-\bar{w}_0 \cos n\theta - \frac{\cos\alpha}{R}\bar{v}_0^2 \cos^2 n\theta\\ -\bar{v}_0 \sin n\theta - \frac{2\cos\alpha}{R}\bar{v}_0\bar{w}_0 \cos n\theta \sin n\theta\end{Bmatrix} X$$

$$e^{\pm i(\omega+p)t} \quad \ldots\ldots \text{ eqn. 9.7}$$

The procedure is now systematic, namely the force vector $\{dF\}$ is obtained from multiplying the elemental mass $[dm]$ by the acceleration vector $\{a\}$. The force $\{dF\}$ is allowed to work on a compatible Virtual displacement system $\{\delta_q^*\}$ and the elemental Virtual Work done[4],[5] is written down as

$$d(\text{Virtual Work}) = \begin{Bmatrix}\bar{w}_0^* \cos q\theta\\ \bar{v}_0^* \sin q\theta\end{Bmatrix}[\rho]\, d(vol) \begin{Bmatrix}a_r\\ a_\psi\end{Bmatrix}$$

$$= \Big[\Big(-\bar{w}_0^*\bar{w}_0 \cos n\theta \cos q\theta - \frac{\cos\alpha}{R}\bar{v}_0^*\bar{v}_0^2 \cos^2 n\theta \cos q\theta\Big) +$$

$$\Big(-\bar{v}_0^*\bar{v}_0 \sin n\theta \sin q\theta - \frac{2\cos\alpha}{R}\bar{v}_0^*\bar{v}_0\bar{w}_0 \cos n\theta \sin n\theta \sin q\theta\Big)\Big] X$$

$$t\,[\rho]\, R\,d\theta\,ds\, e^{\pm i(\omega\pm p)t} \cdot \left[\pm i(\omega \pm p)\right]^2$$

The non-zero value of the elemental Virtual Work done, round the circumference, is obtained when q=n which would only leave the terms shown below,

$$d(\text{Virtual Work}) = -\gamma(\bar{w}_0^* w_0 + \bar{v}_0^* v_0) Rt[\rho]\, ds. \left[\pm i(\omega+p)\right]^2 e^{\pm i(\omega\pm p)t}$$

$$(\text{Virtual Work}) = -\gamma\left[\pm i(\omega\pm p)\right]^2 \{\delta\}^{*T} \int [N]^T [\rho] [N] tR ds. \{\delta\} e^{\pm i(\omega\pm p)t} \quad \ldots\ldots \text{ eqn. 9.8}$$

This result is almost identical with the results given in sections 5.4 and 5.5, the difference being that the term ω^2 is replaced by $(\omega\pm p)^2$ which is the relative angular velocity. It is therefore convenient to proceed with the determination of the angular frequencies ω' of the vibrating shell in the normal manner but noting that $\omega'^2 = (\omega\pm p)^2$ where p will be given initially.

9.5 EXAMPLES

Very few examples have been considered mainly due to the candidate's difficulty in identifying suitable cases. The examples attempted consisted of shells defined by simple geometries.

9.5.1 Long Cylindrical Shell

The shell of Fig. 9.3 was chosen as the first example so that the structure was compelled to behave as a uniform beam. The equation predicting the frequencies under an imposed axial load was taken from reference (6). The apparent error in frequencies corresponding to zero axial load is somewhat exaggerated due to squaring of the angular frequency ω. The graph shows that when Euler load has been reached, the frequencies vanish. Later a mode corresponding to two nodal diameters was assigned to the cylinder and again the frequencies disappeared when a critical load corresponding to two nodal diameters was reached. This is not shown in the figure.

9.5.2 Circular Plate

The circular plate of Fig. 5.5 and Fig. 6.1 was considered as a suitable parallel to the square plate example of reference (1). The plate was simply supported at its edge in the first instance and rigidly fixed at its edge subsequently. In both cases the relationship between ω^2 and the buckling load P_{crit} was linear as shown in Figs. 9.4(a) and (b) and the intercepts on ω^2 and P axes corresponded to the results given in Figures 5.5 and 6.1.

9.5.3 Turbine Disc

In this example the plate discussed in the previous section was rigidly fixed about its principal axis (Z-axis), as shown in Fig. 9.5 and was subjected to an angular velocity of p rad/sec. The velocity p was allowed to assume values of 0., 0.1, 1.0, 10., 100. and 10000. rad/sec. The inplane forces resulting from the above velocities were then incorporated in frequency calculations to provide the curves for the above figure. Owing to physical limitations of the logarithmic cycle, only the values of p for $0.1 \leqslant p \leqslant 100.$ could be plotted. The frequencies for p=0 were almost identical to those of p = 0.1. Except for the frequency disparity for symmetrical modes i.e. n=0., all the other first modes were so close that the theoretical and numerical results coincided.

It was realised later that not all modes were flexural as predicted by theory, for example the following frequencies were noticed:

n = 1 m = 1

p rad/sec.		100.		1000.			
ω	F.E.	100.754	F	551.796	E	1005.922	F
rad/sec	Theo.	100.000	F	-		1000.000	F

n = 2 m = 1

p rad/sec.		100.		1000.			
ω	F.E.	153.034	F	1328.57	E	1527.53	F
rad/sec	Theo.	153.563	F	-		1532.97	F

where the abbreviations F and E used represent Flexural and Extensional modes respectively. The formulae used for flexural frequencies were from references (2) and (7).

Regarding the estimation of frequencies of turbine discs with non-uniform thickness the contents of reference (8) were noted but no attempt was made to examine any numerical examples.

REFERENCES

1. R.G. ANDERSON, B.M. IRONS, O.C. ZIENKIEWICZ
"Vibration and Stability of Plates Using Finite Elements", P.1031, Vol.4, Int. Jour. Solids Structures, 1968.

2. S.P. TIMOSHENKO, D.H. YOUNG
"Vibration Problems in Engineering", P. 455-461, 3rd Edn., Van Nostrand Pub. Co. Inc., New York, 1964.

3. R.H. ATKIN
"Classical Dynamics", P. 51-52, W. Heinemann Pub. Co. Ltd., London, 1959.

4. L.E. GOODMAN, W.H. WARNER
"Dynamics", Chapter VIII, Wadsworth Pub. Co. Inc. Calif., 1963.

5. C.E. WEATHERBURN
"Elementary Vector Analysis", P. 167-168, G. Bell & Son Ltd., London, 1958.

6. G.B. WARBURTON
"The Dynamical Behaviour of Structures", P. 135-136, Pergamon Press, Oxford, 1964.

7. W. STANIAR
"Plant Engineering Handbook", P. 37-40, McGraw-Hill Book Co. Inc., New York, 1959.

8. J. PRESCOTT
"Applied Elasticity", P. 614-619, Longmans, Green and Co., London, 1924.

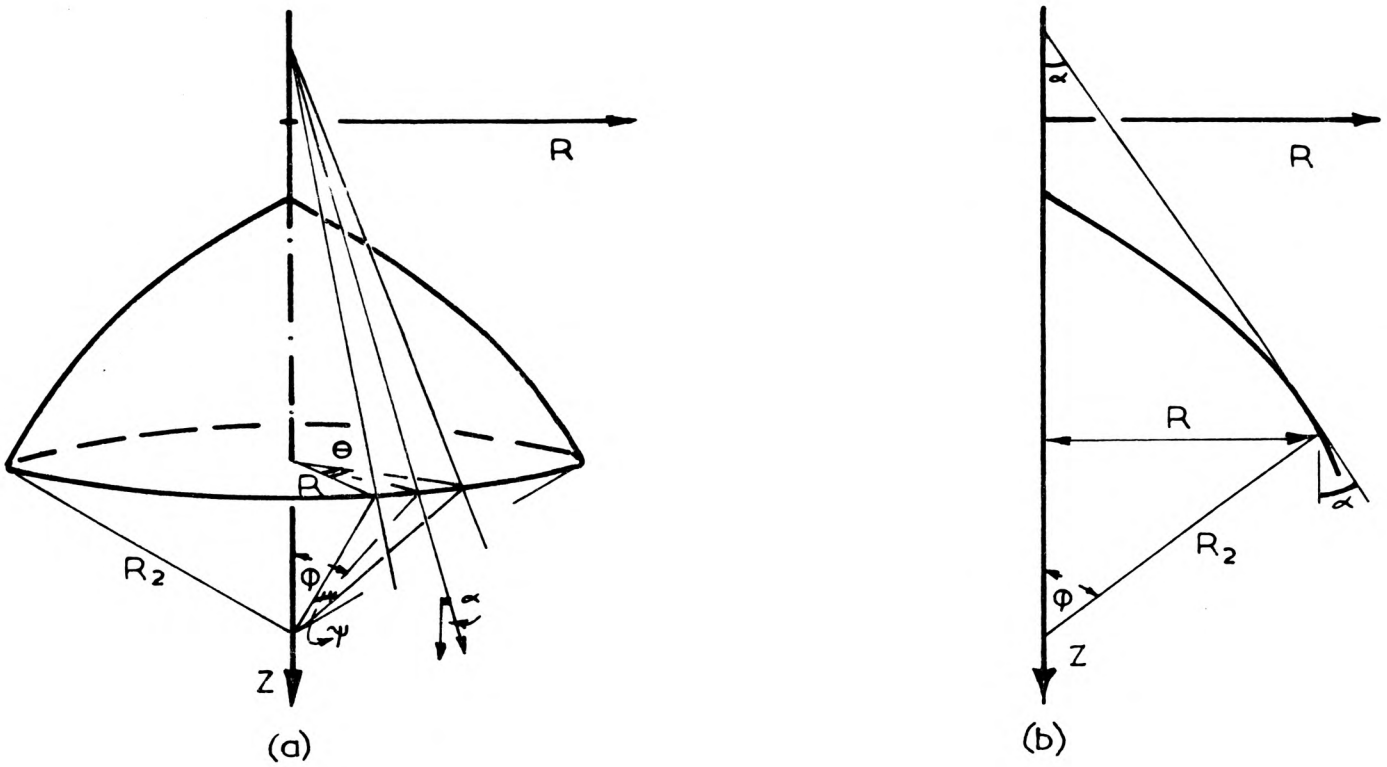

FIGURE 9.1

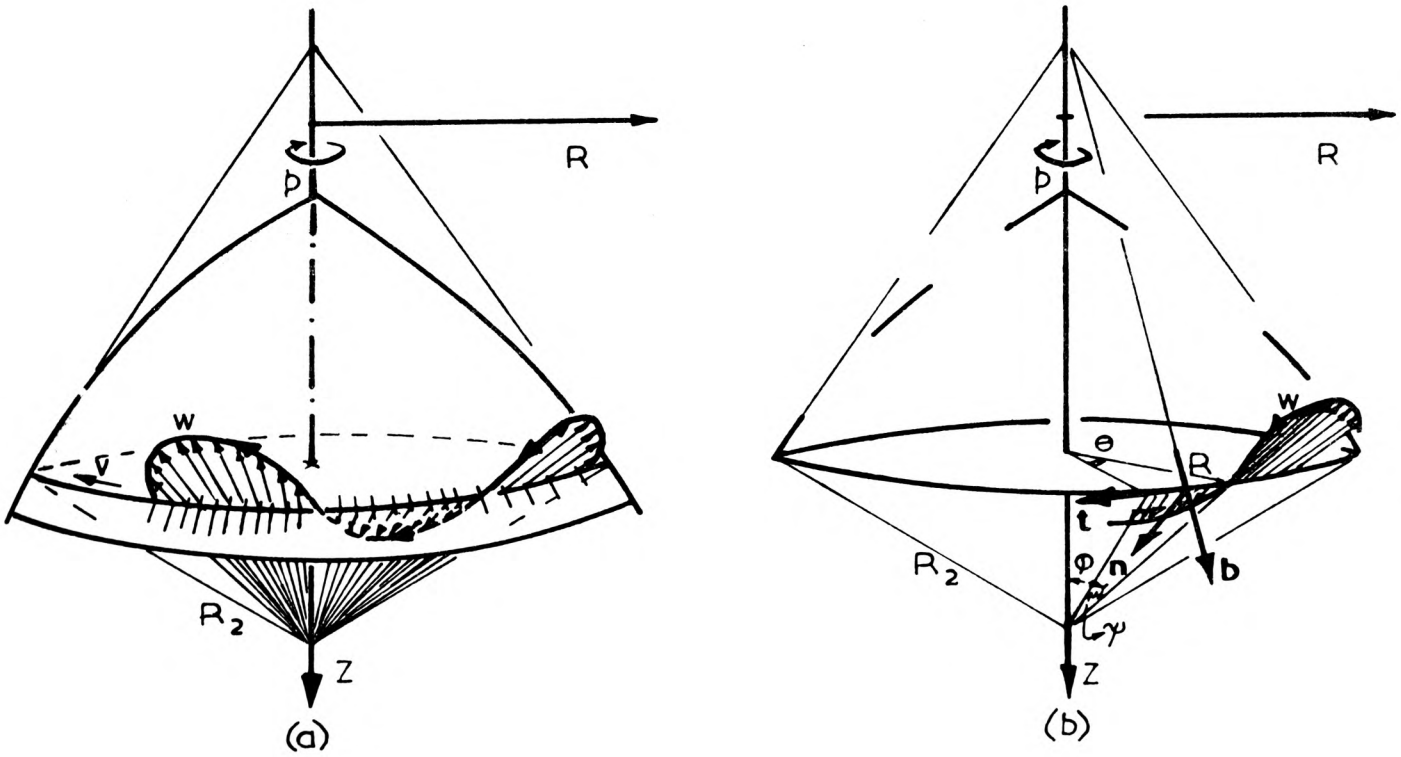

FIGURE 9.2

VIBRATION OF AN AXIALLY LOADED CYLINDRICAL SHELL

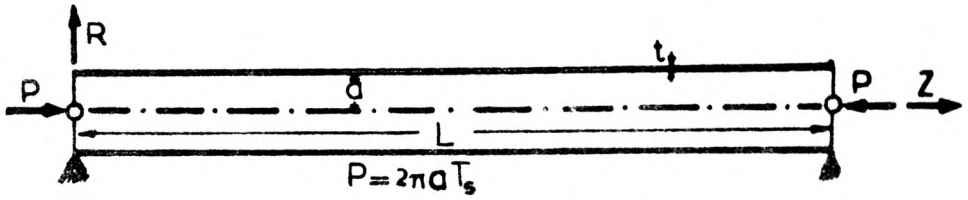

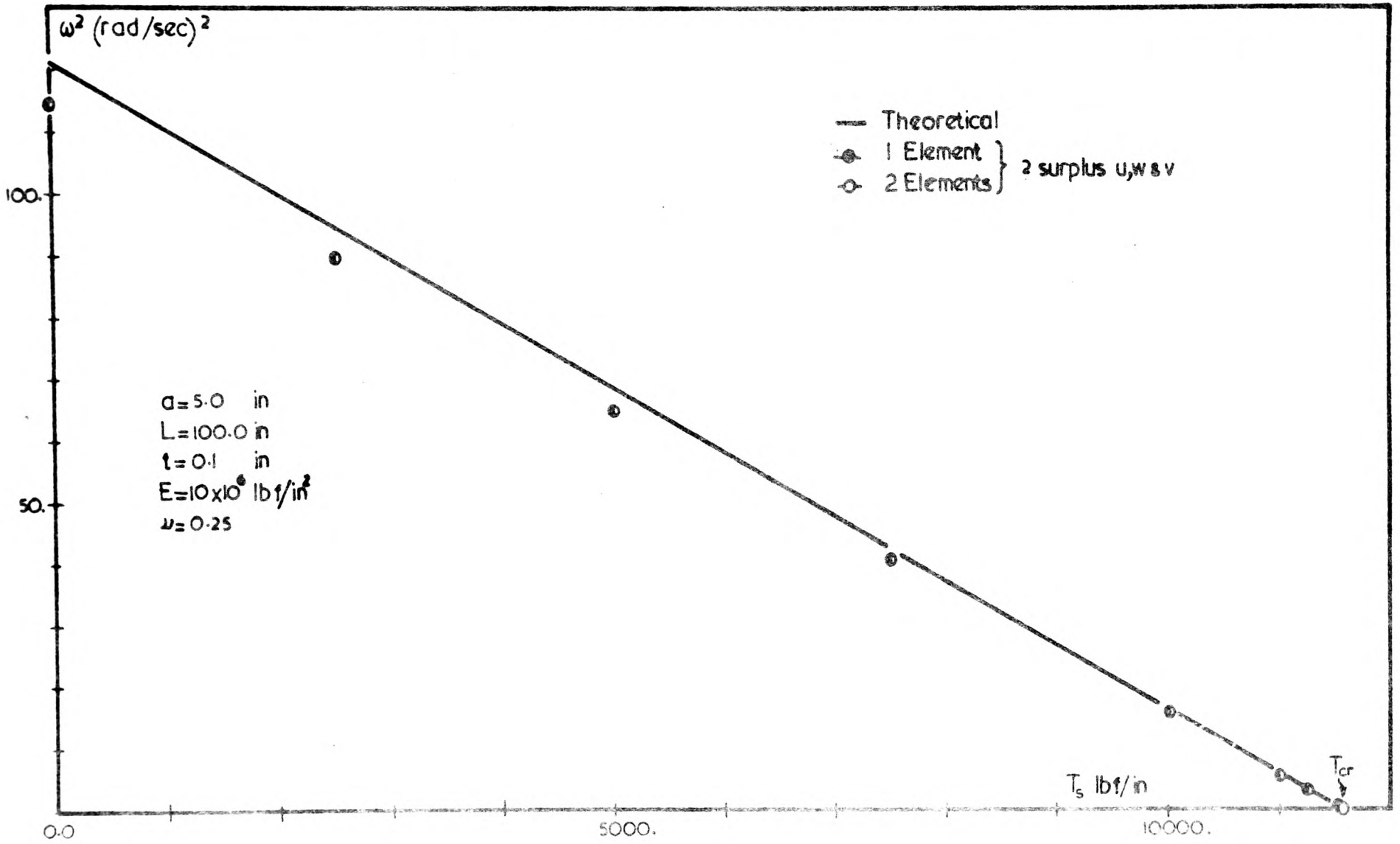

FIGURE 9.3

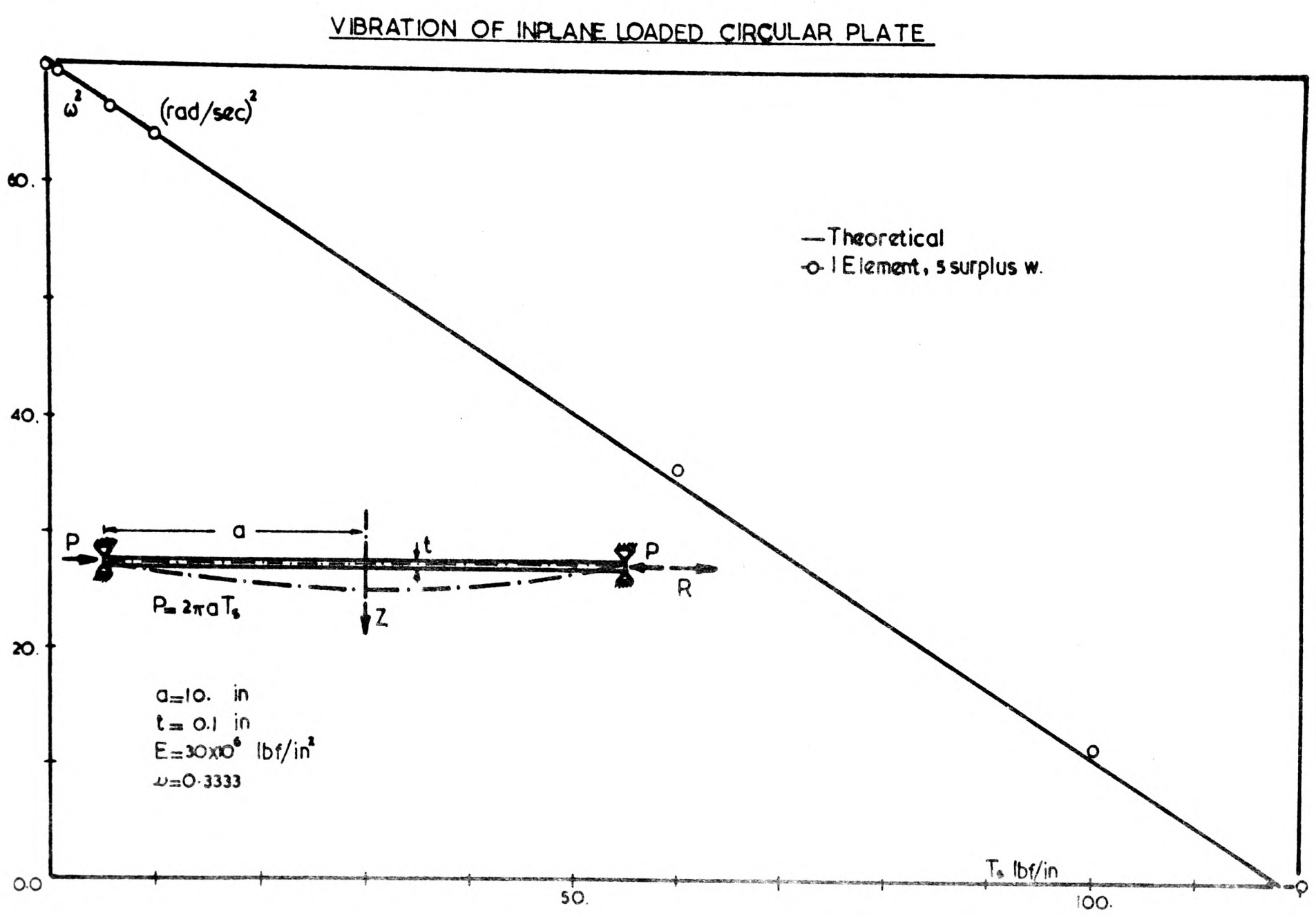
VIBRATION OF INPLANE LOADED CIRCULAR PLATE
ω²
(rad/sec)²
60.
40.
20.
0.0
50.
100.
T₀ lbf/in
—Theoretical
-o- 1 Element, 5 surplus w.
P
a
t
P
R
Z
P= 2πaT₀
a=10. in
t= 0.1 in
E=30x10⁶ lbf/in²
ν=0·3333

FIGURE 9.4(a)

VIBRATION OF INPLANE LOADED CIRCULAR PLATE

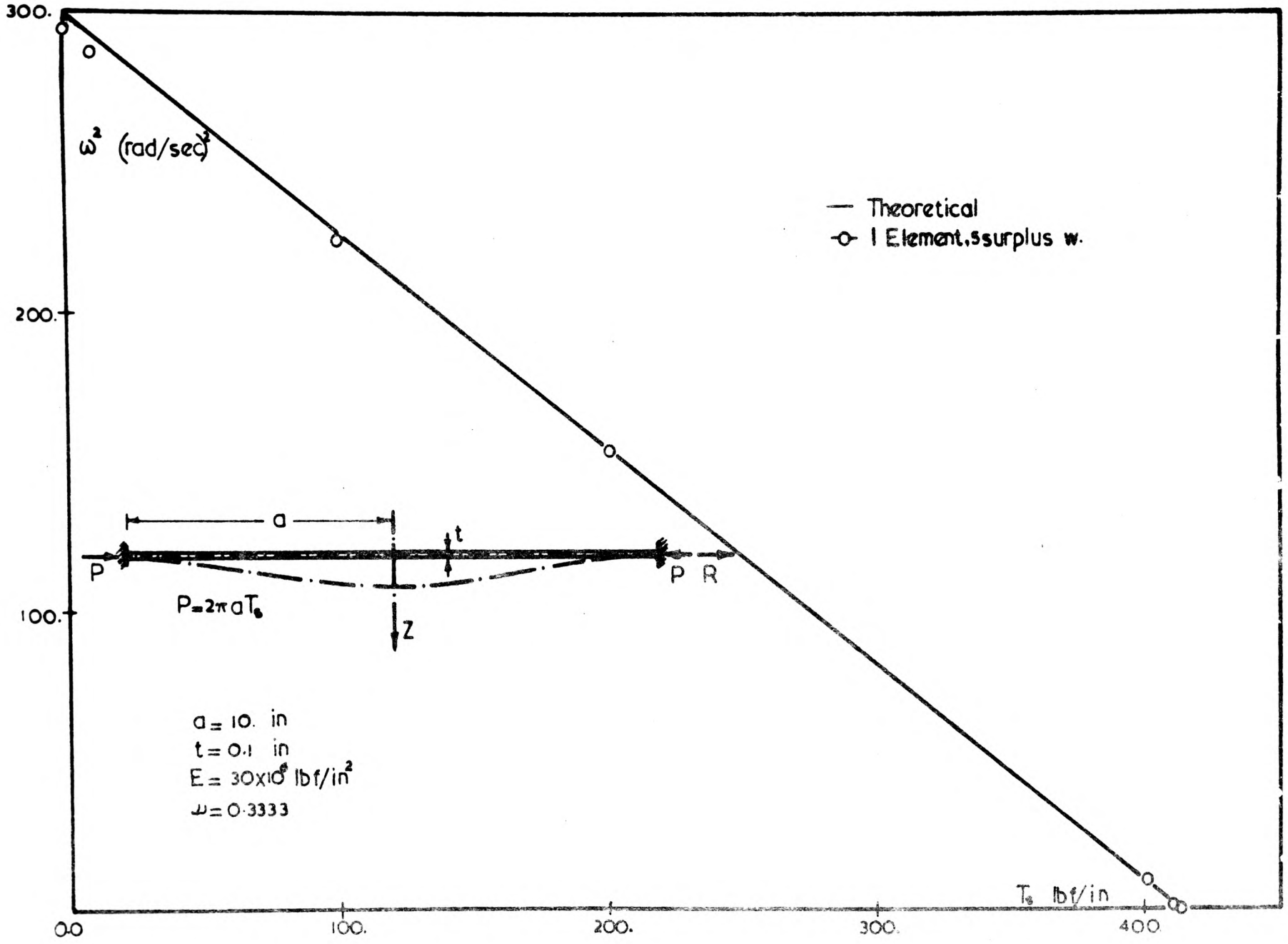

FIGURE 9.4(b)

FREQUENCIES OF A ROTATING DISC

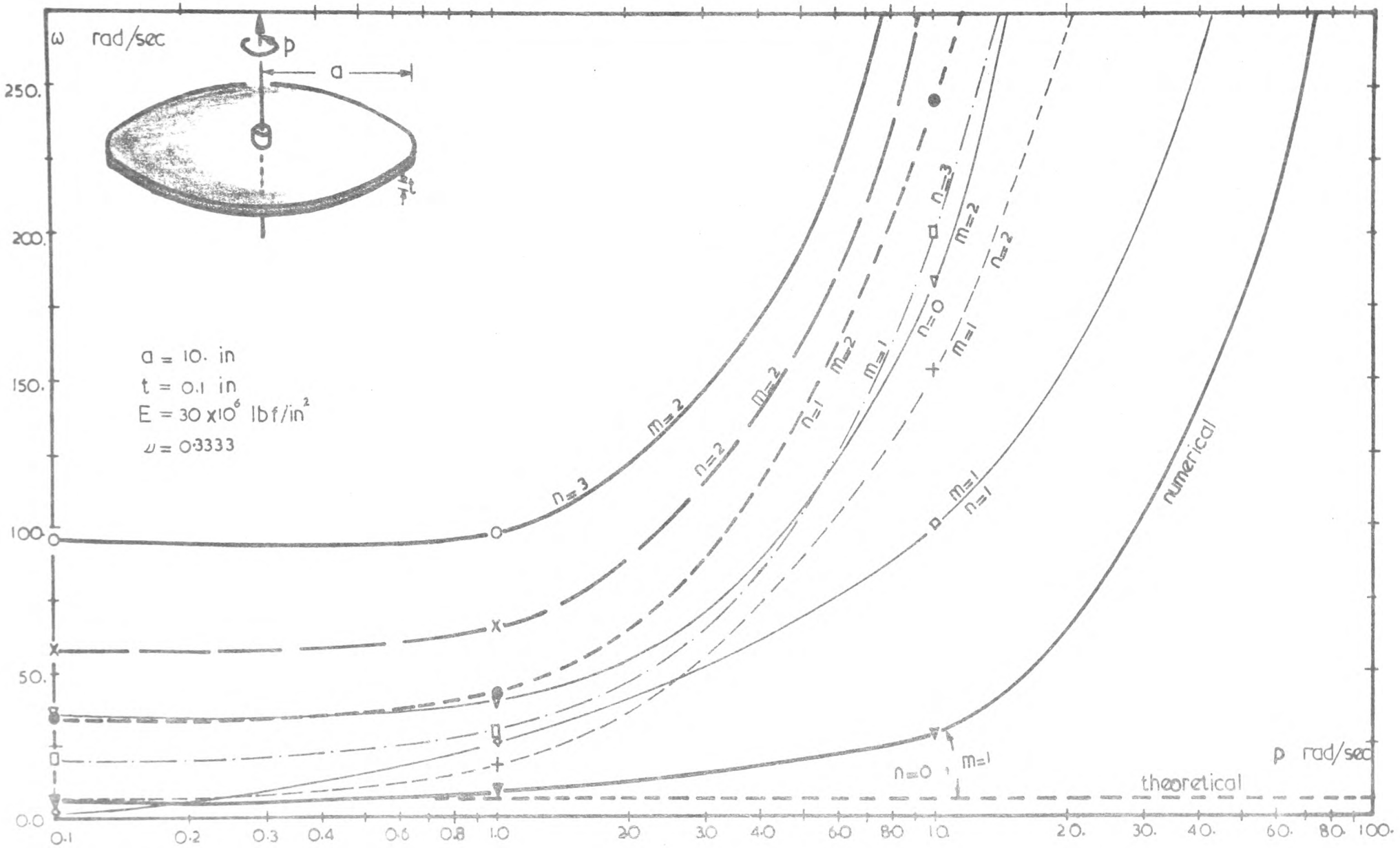

FIGURE 9.5

CHAPTER 10

CONCLUDING REMARKS

The following observations are made on the contents of the previous Chapters.

The derivations of Kinematic relationships from the original equations, made in Chapter 2, is not regarded as a notable step but the extention of representation of these equations could prove helpful. The candidate is aware of the existence of a number of strain-displacement relationships*. The purpose here is not to recommend one theory in preference to the other but is to give the engineer an opportunity of choosing one or more kinematic alternatives if he so desires. This implies that the choice of formation of strains could be made a matter of calling the appropriate subroutine at any given time. The presentation of the $[B]$ or $[G]$ matrices in a differential operator form is hoped to facilitate the codification and the implementation of the above features.

The success of some numerical examples in Chapter 3 was an encouraging factor in developing the element for further aspects of studying the behaviour of rotational shells. There were also some setbacks. For example the spherical cap was one case for which satisfaction of statical equilibrium proved difficult when a comparatively coarse mesh was used. Satisfactory edge equilibrium was achieved subsequently with the graded mesh shown in Fig. 3.35. The other point of concern for some considerable time was the toroidal shell, the details

---

* Amongst the Kinematic relationships used in current literature, the theories due to Timoshenko, Novozhilov, Flügge, Donnell and Lurè can be mentioned.

of which are given in Fig. 3.36 where the displacements and the hoop stress resultants (being inter-related) did not follow the results published by other workers. Since the change in curvature near the azimuth angle of $\phi=90^{o}$ becomes more pronounced, a graded mesh was also used to yield satisfactory agreement. It is the speculative belief of the candidate that the following factors contributed to the delayed convergence of the results. Firstly the other workers had included the contribution of lateral shear in their estimation of the stiffness matrix whereas in the present work no such provision was made. The second factor was attributed to an undefined combination of geometrical dimensions of the element. The qualitative explanation offered which has no rational basis could be stated as follows. There is an appropriate decay feature (Saint Venant effect) for shells of revolution which depends on such variables such as thickness, radius and the generator length s. For these rotational shells where the thickness is numerically a much smaller quantity than the remaining dimensions, the decay can take place over a small length of the meridian near an external node. The Surplus functions associated with the internal nodes may not be able to respond to such rapid changes in displacements, thus the oscillation of the Surplus functions could appear somewhat erratic. Theoretically this problem could be overcome by an adequate increase in the number of internal nodes for the element with a corresponding increase in the number of integrating points. In practice owing to physical limitations in programming, the candidate was compelled to increase the number of elements.

A similar situation which was a combination of points observed in the last paragraph also occurred in Chapter 4. The example was the thin cylinder of Fig. 4.11 subjected to an edge moment. The statical satisfaction of this loading condition, involved the build up of meridional stresses from zero value at any edge to its full value a short distance away. There were other examples which theoretically

involved the inclusion of an infinite number of Fourier components. The latter examples arose from the imposition of concentrated loads on a rotationally symmetrical shell. The outcome which was upheld with guarded optimism was in one case obtained by piecewise improvement of internal shape functions. The total number of degrees of freedom could not be increased owing to the size of the computer.

The agreement between theoretical and numerical values of natural frequency was generally satisfactory. There are two minor points in connection with the dynamic analysis. The first point was observed when the rotary inertia term arising from $\frac{\partial(w)\,\text{local}}{\partial s}$ was eliminated from the Kinetic Energy. It was noticed that the corresponding torsional mode (about the axis normal to the plane containing the cross-section and the z-axis) for the ring of Fig. 5.1 also ceased. The other observation was that any misrepresentation of geometry owing to an inadequate number of elements caused a reduction of the stiffness of the mathematical model leading to a general drop in frequencies. Similar behaviour to this was also observed in the static case, namely the example shown in Fig. 3.32.

The critical loads obtained from the buckling analysis compared favourably with the theoretically predicted values except for the cases where shear was the cause of instability. The candidate had always understood that the shear buckling systems, being conjugate, create a numerical difficulty because the eigenvalues are in pairs, namely $\pm(T_{s\theta})_{cr}$. Apparently when requiring the critical shear resultants for a plate girder, it is customary to add 5 to 10 per cent 'artificial' uniaxial compression to the shear stress system in order to improve numerical conditioning of the eigenequations. Owing to inherent curvature, the situation is more involved for shell structures. This could provide a possible avenue for future investigations. The order of error for

shear buckling loads was generally between 10 to 30 per cent for annular plates. With thin cylinders, the length corresponding to minimum shear buckling load for each harmonic was different from the corresponding theoretical length.

The experimental results for the static case had created some confusing impressions, namely, for eight individual stress plots, two plots consistently varied by a factor of 10 from the numerical results. The agreement of the remaining six was moderate. The candidate is concerned in case some serious experimental aspect has been overlooked.

The recorded frequencies obtained from the perspex model, helped the candidate to become briefly acquainted with some of the contemporary techniques in experimental dynamics. Furthermore, owing to the favourable agreement between numerical and experimental results, some of the misgivings due to partial success of the static tests were dispelled.

Finally owing to shortage of time only a limited number of simple examples indicating a change in the behaviour of shells due to the action of inplane stress resultants were included. The apparent success of the limited number of attempted cases was encouraging.

The development stated in the above paragraph indicates that the way is paved towards formulation leading to the attempt of the full response problem. In fact the only foreseeable difficulty is likely to be the size of the core memory and the computer time.

The extension of this work to shells in the post elastic range would only be possible for cases where the following two conditions are satisfied simultaneously:-

a) The loading conditions are such that only a finite number of Fourier terms are required to represent the load, in order to avoid uncertainty of the location of the non-linear stresses.

b) The geometrical and loading conditions must be such that only membrane forces are set up. Any deviation from this would involve integration along the thickness for a shell which was initially considered to be thin.

The candidate speculates that the solution of meridionally cracked shells might be examined by considering a reduced form of Elastic moduli with the aid of Fourier Series representation. He is quite prepared to accept the possibility of existence of a theorem in Elastomechanics which rejects the above representation.

APPENDIX 1

DERIVATION OF SHAPE FUNCTIONS

A1.1 It was pointed out in Chapter 3, that the displacements which generally associated with the internal nodes were labelled Surplus Functions. These displacements could be used, optionally as locally directed or globally directed displacements. All displacements were expressed in global coordinates prior to being used in kinematic equations.

The subroutine SHPFN, generating both types of displacements was outlined in Chapter 3. Some aspects of derivation and broad hints of subsequent codification will be highlighted in the following paragraphs. The formulation and development of these functions are due to Irons.*

A1.2 Let ξ be the basic variable and the N-th derivative with respect to ξ abbreviated in the normal manner by the operator D^N. The Surplus Function Q_N is then defined as,

where

$$\left.\begin{aligned} Q_N &= D^N u^{N+2}, \\ u &= \xi^2 - 1. \end{aligned}\right\} \qquad \ldots\ldots \text{ eqn. A1.1(a)}$$

The successive derivatives then follow as,

$$\left.\begin{aligned} Q_N' &= D^{N+1} u^{N+2}, \\ Q_N'' &= D^{N+2} u^{N+2}, \\ Q_N''' &= D^{N+3} u^{N+2}. \\ &\vdots \end{aligned}\right\} \qquad \ldots\ldots \text{ eqn. A1.1(b)}$$

---

* Reference (8) of Chapter 3.

Now consider the term u^{N+2}. For a value of n=N-1, this term is differentiated n-times using Leibnitz,

$$D^n(u^{n+1}) = D^n(u.u^n)$$
$$= uD^nu^n + nu'D^{n-1}u^n + \frac{n(n-1)}{2!}u''D^{n-2}u^n + 0. + \ldots$$
$$= uQ''_{n-2} + nu'Q'_{n-2} + \frac{n(n-2)}{2}u''Q_{n-2}$$

also

$$D^n(u^{n+1}) = D.D^{n-1}(u^{n+1})$$
$$= Q'_{n-1}$$

$$\therefore Q'_{n-1} = uQ''_{n-2} + nu'Q'_{n-2} + \frac{n(n-1)}{2}u''Q_{N-2}. \qquad \ldots\ldots \text{ eqn. A1.2}$$

By definition the following relationships hold,

$$D(u^n) = nu'u^{n-1},$$

and $$u.D(u^n) = nu'u^n.$$

Now determine the (n-1)th derivative of the term $uD(u^n)$ using Leibnitz, thus,

$$D^{n-1}uDu^n = D^{n-1}(nu'u^n) \quad \text{(from above defn.)}$$
$$= uD^{n-1}(Du^n)+(n-1)u'D^{n-2}(Du^n)$$
$$+ \frac{(n-1)(n-2)}{2!}u''D^{n-3}(Du^n)$$
$$= nu'D^{n-1}u^n + n(n-1)u''D^{n-2}u^n$$
$$\text{L.H.S.} = uD^nu^n + (n-1)u'D^{n-1}u^n + \frac{(n-1)(n-2)}{2}u''D^{n-2}u^n$$
$$= uQ''_{n-2} + (n-1)u'Q'_{n-2} + \frac{(n-1)(n-2)}{2}u''Q_{n-2}$$
$$\text{R.H.S.} = nu'Q'_{n-2} + (n)(n-1)u''Q_{n-2},$$

equating and collecting terms and substituting $u = \xi^2-1$, $u' = 2\xi$ and $u'' = 2$,

$$(\xi^2-1)Q''_{n-2}-2\xi Q'_{n-2}-(n-1)(+n+2)Q_{n-2}=0,$$

or for N=n+2,

$$(\xi^2-1)Q''_N-2\xi Q'_N-(N+1)(N+4)Q_N=0. \qquad \ldots\ldots \text{ eqn. A1.3}$$

The above equation is termed as Legendre-type polynomial in view of its apparent similarity to the Legendre polynomial given below,

$$(\xi^2-1)L''_N + 2\xi L'_N - N(N+1)L_N = 0.$$

The indicial expansion of eqn. A1.3 has been discarded, since it was feared that the solution might lead to complicated programming procedures. The recurring-type solution being simpler was thought to be more suitable and therefore adopted.

Consider the identity,

$$(n+1)P_{n+1} - (2n+1)\xi P_n + nP_{n-1} = 0$$

where the general term P_N is defined as $P_N = \frac{D^N u^N}{2^N N!}$. This identity can easily be verified using the method of induction for N=1,2,3,...,n. Now by definition,

$$Q''_{N-2} = D^N u^N = 2^N N! P_N,$$

substituting Q and its derivatives in the above identity,

$$\frac{(n+1)}{(n+1)!2^{n+1}} Q''_{n-1} - \frac{(2n+1)\xi}{n!2^n} Q''_{n-2} + \frac{n}{(n-1)!2^{n-1}} Q''_{n-3} = 0,$$

Also substituting N=n-1 in the above equation,

$$Q''_N = 2(2N+3)\xi Q''_{N-1} + 4(N+1)^2 Q''_{N-2} . \qquad \ldots\ldots \text{ eqn. A1.4}$$

The value of Q''_{n-2} is substituted from eqn. A1.2 in eqn. A1.3 which results in,

$$Q'_{n-1} = 2\xi(n+1)Q'_{n-2} + 2(n-1)(n+1)Q_{n-2}$$

Similarly for N = n-1

$$Q'_N = 2\xi(N+2)Q'_{N-1} + 2N(N+2)Q_{N-1}. \qquad \ldots\ldots \text{ eqn. A1.5}$$

Now by rearranging eqn. A1.3, the following value for Q_N results

$$Q_N = \frac{uQ''_N - 2\xi Q'_N}{(N+1)(N+4)} \quad . \qquad \ldots\ldots \text{ eqn. A1.6}$$

Calculation of the term Q'''_N is obtained by using Leibnitz as follows:

$$\begin{aligned} Q'''_N &= D^{N+3}u^{N+2} \\ &= D^{N+2}(D.u^{N+2}) \\ &= (N+2)(2\xi D^{N+2}u^{N+1} + 2(N+2)D^{N+1}u^{N+1}) \end{aligned}$$

$$\therefore \quad Q'''_N = 2(N+2)(\xi Q'''_{N-1} + (N+2)Q''_{N-1}) \qquad \ldots\ldots \text{ eqn. A1.7}$$

Equations A1.4 to A1.7 are the required equations for recurring terms. The general value of Q''_N is calculated from previous values of Q''_{N-1} and Q''_{N-2}. The first derivative Q'_N is dependant on Q'_{N-1} and Q_{N-1}. Finally Q_N is based on Q'_N and Q''_N which are already calculated. It must be borne in mind that the operator D^N is only defined for $N \geq 0$.

To initiate the calculations the following quantities are calculated,

when n = -1

$$Q'_{-1} = D^0u = u$$
$$Q''_{-1} = D^1u = 2\xi$$
$$Q'''_{-1} = D^2u = 2$$

when n = 0

$$Q_0 = u^2 = D^0u^2$$
$$Q'_0 = D^1u^2 = 4\xi u$$
$$Q''_0 = 12u+2 = D^2u^2$$
$$Q'''_0 = D^3u^2 = 24\xi$$

Now the values of Q'''_1, Q''_1, Q'_1, Q_1, Q''_2, ..., Q_n can be calculated from the above values. Unfortunately the amplitude of these polynomials tend to increase indefinitely for increasing values of N. There is

therefore a possibility of overflow occurring for large values of N.

A1.3 Normalisation - It was found necessary therefore to reorientate the above equations slightly in order to arrive at "near" unit amplitudes. The I-th derivatives of the term Q_N is expanded as follows:

$$Q^I_N = D^{N+I}u^{N+2} = (N+2)D^{(N+I-1)}(u'.u^{N+1})$$

$$= (N+2)\left[u'D^{N+I-1}u^{N+1}+(N+I-1)u''D^{N+I-2}u^{N+1}\right]$$

$$\therefore Q^I_N = 2(N+2)\left[\xi Q^I_{N-1}+(N+I-1)Q^{(I-1)}_{n-1}\right]$$

Substituting for I = 1,2 and 3 and dividing by "normalisation" factor N:

$$Q'_N = 2(N+2)\left[\xi Q'_{N-1}+NQ_{N-1}\right]/N$$

$$Q''_N = 2(N+2)\left[\xi Q''_{N-1}+(N+1)Q_{N-1}\right]/N$$

$$Q'''_N = 2(N+2)\left[\xi Q'''_{N-1}+(N+2)Q_{N-1}\right]/N$$

These equations together with eqn. A1.6 achieve "near" normalisation as can be seen from Fig. 3.12.